Robust and Fault Tolerant Control of CD-players

Ph.D. thesis

Enrique Vidal Sánchez

Department of Control Engineering
Aalborg University
Fredrik Bajers Vej 7, 9220 Aalborg East, Denmark

ISBN 87-90664-15-9
Doc. no. D-03-4663
October 2003

This thesis was typeset using LaTeX2$_\varepsilon$ in `report` document class.
MATLAB is a registered trademark of The MathWorks, Inc.

Preface

This thesis is submitted in partial fulfilment of the requirements for the European Doctor of Philosophy at the Department of Control Engineering at the Institute of Electronic Systems, Aalborg University, Denmark. The work has been carried out in the period from November 1999 to October 2003 under the supervision of Professor Jakob Stoustrup and Associate Professor Palle Andersen.

The Ph.D. project forms part of the OPTOCTRL-project which deals with nonlinear and robust control of electromechanical systems with optical sensors. The purpose was to identify control and signal processing algorithms for increasing the robustness in systems with optical sensors. The OPTOCTRL-project is supported by the Danish Technical Science Foundation (STVF) grant no. 9701481 and was initiated in collaboration with Bang & Olufsen, Denmark, who financed part of the present Ph.D. project.

Aalborg University, October 2003
Enrique Vidal Sánchez

Acknowledgments

In all the theses that I have read, the student is typically thankful or grateful to his/her supervisor for the quality of the guidance and assistance. This thesis will not be an exception. Not because I would like to stick to the rules of what it could be considered as tradition or politeness, but because he truly deserves it: Professor Jakob Stoustrup. Associate Professor Palle Andersen has also acted as a second supervisor, to whom I am also very thankful. I appreciate the support given by Associate Professor Tom S. Pedersen too. Furthermore, I would like to thank all other colleagues at the Department of Control Engineering, especially Karen Drescher who helped me in transforming the Spanish-Danish-English manuscript into a nearly plain English version. However, I am still considering whether I should thank the "colleagues" that I played Red Alert 2 with. At the beginning the recreative activity was limited to never-ending Friday afternoons but it soon developed to occupy other time slots of the week...

The thesis would not see an end, either a start, without the support, also financially, from Bang & Olufsen. Henrik F. Mikkelsen from B&O participated in the definition of the project and offered throughout the project valuable assistance. I would also like to express my gratitude to Ben L. Verbraak from B&O for his enthusiasm for the project. The exciting industrial placement in Philips Semiconductors Southampton (PSS) for a six months period in the year 2001 was made a reality thanks to B&O and Charles Limonard from PSS. In that period I was under the guidance of Pradip Sinha which I highly appreciated. A very inspiring person from PSS was Alexandre Pechev, who I spent my coffee-breaks with, having many interesting technical discussions.

I would like to thank "Er Clú" for its own special support. Warm thanks go to my family members Enrique (not me, my father...), Luisa, María, Carmela and Sergio for their moral support in one or another way. Most of all, I am indebted to Jeanette for her passion, especially reflected in the packed lunchs she prepared for me: an indispensable source of energy which allowed me to finish the thesis.

Abstract

Several new standards have emerged recently in the area of portable optical data storage media and more are on their way. In addition to the well known Compact Disc (CD), portable optical media now also feature media for video storage (DVDs) and general data storage media for computer purposes (CD-ROMs). DVDs can be two-sided with multiple layers, allowing read, write and rewrite operations. Most significantly in this context, the new media typically have much higher physical data densities. This constitutes a significant challenge in terms of *playability* (the ability to reproduce the information from non-ideal discs in non-ideal circumstances) which is the main topic this Ph.D. thesis is focused on.

There are three important contributions to the technical field of study treated in the thesis. It is known that the specific characteristics of the CD-drives vary from unit to unit. Traditionally the parameter estimation is performed in closed loop, probably because open loop estimation has been stated for being very difficult or even impossible. A novel method, which requires an additional current measurement, is presented in this work where parameter estimation is accomplished in open loop in a simple and reliable way. The second main contribution is related to robust control. Usually, the nominal and uncertainty models are assumed to be known and the designer is limited to specify the performance requirements. In a more realistic situation, the designer may only have a set of complex points in the Nyquist plane from several worst-case plants as a result of measurement experiments. In the thesis a deterministic method is proposed, which generates a nominal and uncertainty model based on the set of complex points in a less conservative way than conventional methods. Finally, the third main contribution is to be found in the fault-diagnosis and fault-tolerant control fields. One of the main challenges in the positioning control of the focus point in CD-players is to handle two types of disturbances with conflicting requirements in an effective way. While a high bandwidth is desired to better suppress shocks, a low bandwidth is preferred in the presence of surface defects. Traditionally, a simple defect detector is employed to deal with this trade-off. In this work, two fault diagnosis schemes are suggested which are able not only to detect but also to separate, to certain extent, the characteristics of the signals originated by the surface defects. Furthermore two fault-tolerant control schemes are proposed such that the mentioned trade-off is handled in a more efficient way.

Contents

List of Figures

List of Tables

Nomenclature

Acronyms

A.R.	Amplitude Ratio
AGC	Automatic Gain Controller
BLER	BLock Error Rate
BRD	Blu-Ray Disc
CD	Compact Disc
CIRC	Cross Interleaved Reed-Solomon
DPD	Differential Phase Detection
DTD	Differential Time Detection
DVD	Digital Video/Versatile Disc
EFM	Eighteen-to-Fourteen Modulation
FDI	Fault Detection and Isolation
FTC	Fault-Tolerant Control
GM	Gain Margin (specified in [dB])
HF	High Frequency
LFT	Linear Fractional Transformation
LP	Long Play
LQG	Linear Quadratic Gaussian
MIMO	Multiple Input Multiple Output
MPEG	Motion Pictures Experts Group
nX	rotation velocity factor of the disc where the CD-audio is used as the reference rotation velocity.
OPU	Optical Pickup Unit

PID	Proportional, Integral, Derivative controller
PLL	Phase Lock Loop
PM	Phase Margin (specified in [°])
SISO	Single Input Single Output
THD	Total Harmonic Distortion
TOC	Table Of Contents
WORM	Write Once Read Many

Constants/Variables

Δx[m]	Depth of focus
λ[m]	Wavelength
μ[units]	Refractive index, statistical mean or structured singular value
A_{cd}[m]	Amplitude of the vertical deviation
b[N·s/m]	Viscosity coefficient
b_1[N·s/m]	Viscosity coefficient related to the mass m_1
b_2[N·s/m]	Viscosity coefficient related to the mass m_2
Bl[N/A]	AC-sensitivity of the actuator coil
D[m]	Diameter of the readout beam entering the disc surface
d[m]	Diameter of the focus point (on the information layer)
k[N/m]	Spring modulus
k_1[N/m]	Spring modulus related to the mass m_1
k_2[N/m]	Spring modulus related to the mass m_2
K_{dc}[m/V]	DC-sensitivity of the actuator coil
K_{optFn}[units/V]	Normalized focus optical gain
K_{optF}[V/m]	Unnormalized focus optical gain
K_{optRn}[units/V]	Normalized radial optical gain
K_{optR}[V/m]	Unnormalized radial optical gain
K_{pd}[units]	Gain of the power drive
L[H]	Inductance of the actuator coil
M	Number of measurement periods
m[Kg]	Moving mass of the optical pickup
m_1[Kg]	Mass of the moving lens

m_2[Kg]	Mass of the arms which sustain the moving lens
NA[units]	Numerical aperture
q	Forward shift operator
R[Ω]	Resistance of the actuator coil
r[Ω]	Inserted measurement resistance in series with the actuator coil
T_s[s]	Sampling time

Signals

$\omega_Q(t)$[units]	Measurement quality factor
$e_x(t)$[m]	Vertical distance between the focus point and the information layer
$e_y(t)$[m]	Horizontal distance between the focus point and the track
$f_e(t)$[V]	Focus error
$f_{a1}(t)$[V]	Actuator 1 faults
$f_{a2}(t)$[N]	Actuator 2 faults
$f_{en}(t)$[units]	Normalized focus error
$f_{sd}(t)$[m]	Fault related to the surface defect disturbance
$f_{sen}(t)$[m]	Sensor faults
$r_e(t)$[V]	Radial error
$r_{en}(t)$[units]	Normalized radial error
$u(t)$[V]	Control signal
$w_{md}(t)$[N]	Mechanical disturbances
$w_{sd}(t)$[m]	Surface defect disturbances
$w_{sp}(t)$[N]	Self-pollution disturbances
$x(t)$[m]	Vertical position of the focus point
$x_{cd}(t)$[m]	Vertical position of the information layer
$y(t)$[m]	Horizontal position of the focus point
$y_{cd}(t)$[m]	Horizontal position of the track

Transfer Functions/Weights

$ACT(s)$	Dynamics of the actuator
$F_l(\cdot,\cdot)$	Lower LFT
$F_u(\cdot,\cdot)$	Upper LFT
$G(s)$	Plant to be controlled

$G_{rf}(s)$	Transfer matrix from the fault to the residual
$H_{act}(s)$	Transfer matrix related to the actuator in the residual generator
$H_{photo}(s)$	Transfer matrix related to the optics in the residual generator
$K(s)$	Stabilizing controller
$S(s)$	Sensitivity function
$T(s)$	Complementary sensitivity function
$W_p(s)$	Performance weight (model of disturbances)
$W_u(s)$	Control effort weight

1

Introduction

Compact Disc (CD) players have expanded rapidly since the beginning of the 80's and can now be found practically in every home. They are characterized by their complexity which represents the effort achieved by a multidisciplinary research. To name a few of the involved disciplines, it covers from physics, to optical, coding theory, digital electronics, audio and control engineering. The last one being the central part of this thesis, where mathematics are not the main emphasis. The problems are rather approached from an engineering point of view.

1.1 Background and Motivation

In autumn 1997 a cooperation was initiated between the Department of Control Engineering at Aalborg University and Bang & Olufsen where the master students Jesper Rasmussen, Hans C. Schøien and the author of the present thesis had the opportunity to design and implement advanced control techniques in a CD-player [Vidal *et al.*, 1998]. It was soon discovered that the number of challenges were of such size, that a large research project was defined (OPTOCTRL), including the present Ph.D. project which started in November 1999. Bang & Olufsen was interested in investigating what advanced control techniques could contribute with to the reproduction of sound in CD-players, which is also the primary objective of this thesis. Another outcome of the

OPTOCTRL research project was a large number of student projects.

Data from a CD is read by focusing a laser beam onto the surface of the CD in question and by measuring the intensity of the reflected beam. Unlike vinyl players, the absence of physical contact between the optical pickup and the disc in CD-players makes feedback control necessary in order to maintain the focus point at the correct position. The reflected beam also carries positioning information of the focus point which is fed to the positioning controllers. One of the main challenges, seen from a control perspective, is to keep the focus point at the correct position despite the existence of various classes of disturbances with conflicting requirements. While a high bandwidth is desired to better suppress shocks, a low bandwidth is preferred in the presence of surface defects. The different classes of disturbances are treated in more details in Section 2.5. The reliability of the feedback control influences directly on the ability to retrieve data from the disc, and consequently it affects as well to the overall performance of the CD-player. It is therefore desired to handle in a more efficient way the mentioned trade-off with advanced control techniques, and if possible, to eliminate it.

1.2 Overview of Previous and Related Work

Philips and Sony launched the first CD-players into the market in 1982. However, the major part of control related scientific publications are to be found one decade later. This was probably correlated with the development of simulation tools and faster and more flexible processors which made it easier to design and implement control strategies in CD-players. There has especially been an intense research on adaptive and robust controllers. See for example [Draijer *et al.*, 1992] where a self tuning controller is suggested without having to inject a probe signal as described in [Bierhoff, 1984]. In the same year, it is documented in [Steinbuch *et al.*, 1992] the first application of a μ-controller to a CD-player based on the DK-iteration algorithm. Later, an adaptive repetitive control configuration is proposed [Dötsch *et al.*, 1995] which can theoretically achieve asymptotic attenuation of periodic disturbances caused by the rotation of the disc. The scheme is adapted automatically to the rotation frequency. There exists also a large number of control techniques applied to CD-players: rejection of non/repeatable disturbances [Li and Tsao, 1999], fuzzy control algorithms [Yen *et al.*, 1992], a disturbance observer [Fujiyama *et al.*, 1998], Linear Quadratic Gaussian control [Weerasooriya and Phan, 1995] and quantitative feedback theory [Hearns and Grimble, 1999].

The advent of DVD-players has implied that attention is also paid to these applications. For example in [Zhou *et al.*, 2002] a sliding mode control is suggested which significantly improves the performance against mechanical disturbances compared to the traditional PID controller. A μ-controller based on a parametric uncertainty description is also applied to DVD-players in [Filardi *et al.*, 2003].

In spite of the increasing quantity of DVD-players in the market, the research activities are still focused on CD-players, which is corroborated by the latter Ph.D. dissertations. In [Lee, 1998] robust repetitive control is studied (applied to CD-players as a case study). System identification for control design in CD-players is investigated in [Dötsch, 1998]. And recently, LMI techniques are treated in order to solve in particular two control problems: multi-objective design and gain-scheduling [Dettori, 2001]. DVD-players have tighter performance criteria but they rely on similar optical principles than CD-players, thus the results achieved on CD-players generally apply as well to DVD-players.

In the majority of the above mentioned publications on optical disc drives it is strived towards a high controller bandwidth, typically by minimizing the disturbance channel from mechanical disturbances/disc deviations to the positioning error. However, none of them have directly addressed the other main source of disturbance, namely surface defects, which imposes in fact an upper bound on the achievable bandwidth. Traditionally, a simple defect detector is employed to deal with this trade-off combined with a PID controller. In [Akkermans, 2001] the development of the controller types used in Philips is shown from the beginning of the 90's with audio CD-players till the change of the decade with recordable DVD-players. It is interesting to observe that the main controller is still a PID-like structure, which due to the increasing rotational speed, has recently been combined with a repetitive controller. One of the given reasons is that the PID-like structure is relatively easy to adapt to different applications.

1.3 Contributions

The list presented below summarizes the main contributions of the author, most of which have been presented in conference proceedings.

- Open loop system identification is suggested in CD-players by measuring the current through the voice motor coils of the optical pickup [Vidal *et al.*, 2001d]. The method is demonstrated on 12 CD-drives where both the focus and the radial loop are estimated.
- A method for obtaining the nominal and uncertainty models appropriate for designing a robust controller is proposed [Vidal *et al.*, 2002]. It is shown how to apply the method where the designer only has a set of complex points in the Nyquist plane from several worst-case plants.
- The advantage of having two different $\mathcal{H}_\infty$-controllers in CD-players is indicated in [Vidal *et al.*, 2000]. One controller of high bandwidth, such that it can effectively attenuate disturbances of mechanical character. The second one of lower

bandwidth, which only runs on the presence of surface defects like scratches and finger prints.

- It is shown that a μ-controller can be designed and reduced to a third order (μ-PID) and still meet Compact Disc Digital Audio standard specifications for the 12 CD-drives.
- A method is proposed to reduce the sensitivity to mechanical disturbances in CD-drives [Stoustrup *et al.*, 2000]. It requires an additional current measurement and it is shown through simulations how to apply the method.
- μ-theory is applied to the design of a controller in CD-players with an uncertainty model based on a parametric description of plants where the perturbations are restricted to be real [Vidal *et al.*, 2003].
- An alternative way of analyzing the photo diode signals from the optical pickup is revealed [Vidal *et al.*, 2001a]. It permits to extract more information from the feedback signals during a faulty situation compared to traditional existing methods. It is shown how to interpret the measurements realized in different faulty situations.
- A fault diagnosis method is suggested based on an observer and a disturbance estimator, where the feedback signals are recovered in spite of the presence of surface defects.
- An fault-tolerant control approach is suggested based on the previous fault diagnosis method, where the position of the optical pickup is controlled during a surface defect by the estimated feedback error signal [Vidal *et al.*, 2001b]. It is as well demonstrated how to implement this method in practice.
- A patented method is proposed to improve reading of a digital disc [Vidal *et al.*, 2001c]. Some application examples are revealed in the already mentioned references [Vidal *et al.*, 2001a] and [Vidal *et al.*, 2001b].
- An application example is given to the approach introduced in [Stoustrup *et al.*, 1997]. It consists on the design of a robust fault diagnosis filter which removes the estimated surface defects from the feedback error signal.
- Based on the previously mentioned robust fault diagnosis filter, a fault-tolerant control strategy is suggested, such that the controller does not *advert* the presence of surface defects.

1.4 Thesis Outline

The remaining of thesis is organized as follows:

Chapter 2: Introduction to Compact Disc Players and to their Control Challenges introduces the compact disc technology to the reader. Several optical disc formats are briefly described and their common optical principles are treated. The positioning servos of the optical pickup are explained, finalizing with a discussion of the challenges in CD-players seen from a control perspective.

Part I: Modeling a Compact Disc Drive

Chapter 3: Model of Positioning Loops reviews some of the most common optical pickups employed in CD-players followed by the derivation of two SISO models of the position of the focus point suitable for control. Furthermore the developed experimental setup in the Ph.D. project is also described.

Chapter 4: Parameter Estimation on a CD-drive is devoted to the parameter estimation of 12 CD-drives. A novel approach is introduced which permits to perform open loop system identification in CD-drives in a simple yet reliable way. Closed loop system identification is performed as well and both approaches are validated through experiments.

Part II: Robust Control of Compact Disc Drives

Chapter 5: Obtaining the Nominal and Uncertainty Models describes an original method which yields a nominal and uncertainty model suitable for designing a controller in the $\mathcal{H}_\infty$-framework. The motivation for the development of such method is based on the fact that generally a nominal and uncertainty model are assumed to be available beforehand in the $\mathcal{H}_\infty$ literature. However, in a more realistic situation the opposite is usually the case. The suggested method is applied to measured data from 12 CD-drives and is compared with two other well-known methods.

Chapter 6: Robust Control Applied to a CD-drive deals with the control problem formulation in the $\mathcal{H}_\infty$-framework. A synthesis algorithm is employed, the (μ,D)-K-iteration, which is less conservative than the D-K iteration. The chapter serves also as a model validation of the identified models obtained from the previous chapter. Moreover the performed measurements are presented and discussed.

Part III: Fault Diagnosis and Fault Tolerant Control of Compact Disc Drives

Chapter 7: Fault Diagnosis on CD-drives reveals how fault detection, isolation and estimation can be applied to CD-drives. It is especially focused on the sensor part (photo diodes) of CD-drives. Some alternative approaches are described, whose aim is to extract more information from the feedback signals during a faulty situation compared to traditional existing methods. One of the approaches relies on the estimation of surface defects by means of a robust fault diagnosis filter. The other approach estimates instead the position of the information layer and the position of the optical pickup, hence the feedback signals can be recovered, to some extent, in spite of the presence of surface defects. The simulation results are documented and discussed.

Chapter 8: Fault-Tolerant Control Strategies on CD-drives presents four fault-tolerant control strategies, two of which are novel. The latter are based on the results achieved in fault diagnosis in CD-drives from the previous chapter. All the strategies belong to the *fault accommodation* class, where a μ-controller is employed. The strategies are simulated and implemented in the laboratory setup and the obtained results are compared and discussed.

Chapter 9: Conclusions and Future Work gives concluding remarks of the thesis in general and recommendations for future work.

2

Introduction to Compact Disc Players and to their Control Challenges

This chapter is devoted to the description of the challenges on control of CD-players. In order to better understand the challenges, other related and relevant topics are described as well. In Section 2.1 some of the most known optical discs are briefed followed by the construction of optical discs in Section 2.2. The structure of a general optical disc player is described in Section 2.3. The optical principles on which optical disc players are based are treated in Section 2.4. The remaining two sections are dedicated to the CD-player in specific, although the majority of the principles also apply to other optical disc players. The CD servos are described in Section 2.5 and playability, also related to CD-players, is discussed in Section 2.6.

2.1 Optical Disc Formats

In 1972 Philips announced a technique to store data on an optical disc. First in 1981 Philips and Sony proposed the Compact Disc Digital Audio standard (CD-DA) which

was coded in the so-called Red Book [Philips and Sony Corporation, 1991] . The development of this technique revolutionized the audio world by introducing truly digital technology for the first time. It was in the year 1982 that Philips and Sony launched the first players and discs on the market. The CD became the music carrier of choice by 1991, when sales exceeded those of audio-cassettes.
Another widely available optical disc technology is the Digital Video/Versatile Disc, abbreviated as DVD. While a CD holds either 650[MB] or 700[MB] of data, a DVD can hold up to 25 times more. There is even another type of optical discs, the so-called high capacity optical discs, which are characterized by offering the user storage capacities typically in the range from 20[GB] to 50[GB], (approximately between 30 to 75 times more data than a CD). At this writing, four high capacity optical discs have been announced so far: the Blu-ray disc (BRD) [Hitachi *et al.*, 2002], the advanced optical disc [Toshiba and NEC, 2002], the Blue-HD (High Density) disc [OES and AOSRA, 2002] and the HD-DVD-9 disc [Bros, 2002]. All are in principle rewritable discs, although ROM versions are being discussed.

Since the first mass replication moulded CDs were introduced on the market a confusing number of optical disc formats have been developed giving the consumer not only the possibility to read data but also to record and erase as desired. The numerous standards and formats of optical discs can be divided in three groups, the most common of which are shown in Figure 2.1.

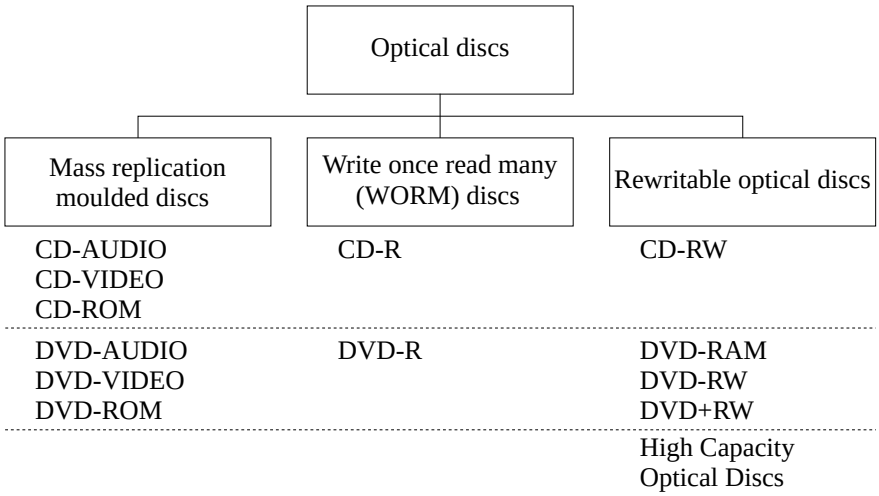

Figure 2.1: *Most common types of optical discs.*

Mass Replication Moulded Discs

This group of CDs and DVDs holds either audio, video or data consisting of prerecorded discs which are designed for mass duplication by stamping. The surface of the disc is coated with an ultra thin layer of reflective material such as aluminium, silver, gold or copper. They cannot be re-recorded.

WORM Discs

WORM discs, consisting of a recordable CD (CD-R) and a recordable DVD (DVD-R), are very similar to the first group except that they have a layer of photosensitive dye covered by a reflective metallic layer. Recording is performed by burning the photosensitive compounds in the dye by a laser. Once a recording has been made, it cannot be changed or erased.

Rewritable Optical Discs

The rewritable optical discs resemble WORM discs except that the dye layer is replaced by a special phase-change compound. The states of this compound can be altered according to the amount of applied energy by the laser. The rewritable CD and DVD (CD-RW, DVD-RW and DVD+RW) can be re-recorded around a thousand times while DVD-RAM discs can be re-recorded up to 100,000 times. MiniDiscs (MD) belong also to this group of rewritable optical discs. The principles behind a MD are based on magnetic-optic principles and are not described here. The interested reader is referred to [Watkinson, 2001].

There is a wide variety of optical discs on the market and winners in the rewritable DVD race have not yet been determined. It is even more unclear to predict the winner among the high capacity optical discs as their standards have not been completely established yet. However, optical discs, whether it be a CD, a DVD or a higher capacity optical disc, they rely in similar optical principles [Milster, 2003] which are described in the subsequent sections.

2.2 Optical Disc Construction

Common for the CD and DVD is that they are discs of 120 mm in diameter. Data is stored in the form of microscopic pits, see Figure 2.2, forming a clockwise spiral track which starts at the center of the disc. The length of the pits and the distance between them form the recorded information. The layer which holds the data, called information layer, is divided in three parts. Starting from the center of the disc, the first area is the lead-in area, which contains a table of contents (TOC). The TOC contains information on the contents of the disc, such as number of selections, the starting point of each selection

and duration. The information interesting to the user is contained in the program area. The end of the program area is defined by the lead-out area.

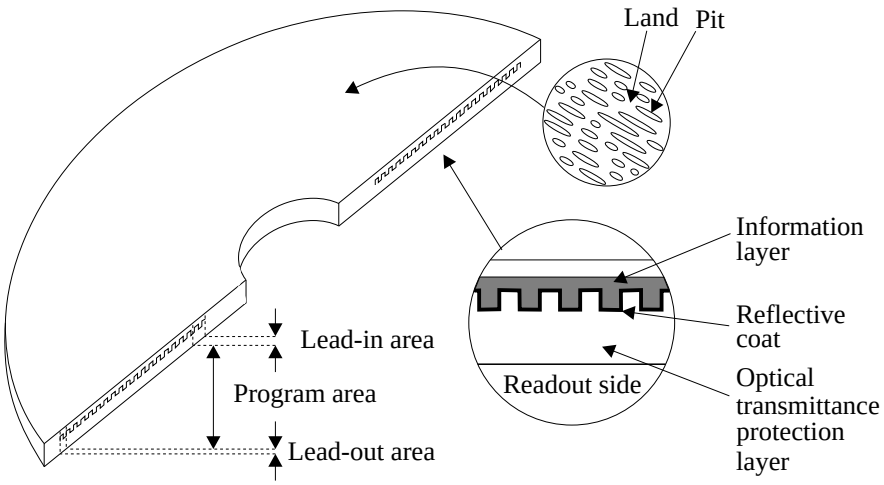

Figure 2.2: *General structure of optical discs. Only one information layer is shown in the figure, although depending on the type of optical disc, there may be several information layers.*

The optical discs are basically constituted by inexpensive polycarbonate plastic in which an information layer and a reflective coat are placed. Viewed from the readout side, the laser is focused through a layer of polycarbonate plastic. This layer is also called optical transmittance protection layer as it protects the information layer from being damaged by sharp objects or by parts of the optical disc drive such as the optical pickup. The information layer has poor reflection properties, therefore it is covered with a reflective coat such that the photo diodes (optical sensors) are able to register variations of the intensity of the reflected laser. In the case of a dual layer DVD, the first information layer (seen from the readout side) can be covered with a semi-reflective coat. The laser can focus through this layer in order to read the second information layer which has a conventional reflective coat. Data in the first layer is not as densely packed as the second layer such that the signal/noise ratio is kept to an acceptable level. The top layer is also called the label side where a label is printed on. However, on double sided discs like DVDs, if a label is printed, it should be made transparent to the laser beam, such that the relevant reflection properties of the disc remain unchanged.

The most relevant specifications of optical discs are contrasted in Table 2.1, [Philips and Sony Corporation, 1991, ECMA, 2001, Hitachi *et al.*, 2002]. The Blu-ray

disc is included as one example of the high capacity optical discs. Other standards in this group may have different specifications. In order to achieve a higher data density than the CD, the pits and track pitch have been physically reduced in the DVDs and BRDs. For optical reasons which will become clear in the next section, it has also been necessary to reduce the thickness of the optical transmittance protection layer, the numerical aperture has been increased and the laser wavelength has been shifted from infrared (CD), passing to red (DVD) up to a blue-violet wavelength (hence the name Blu-Ray Disc, BRD).

	CD	**DVD**	**BRD**(*)
Disc diameter [mm]	120	120	120
Disc thickness [mm]	1.2	1.2	1.2
Tracking pitch [μm]	1.6	0.74	0.32
Optical transmittance protection layer [mm]	1.17	0.6	0.1
Laser wavelength [nm]	780 (infrared)	650 (red)	405 (blue-violet)
Numerical aperture (NA)	0.45	0.6	0.85
Air/disc refractive index (μ)	1.55	1.55	1.55
Data layers	1	1 or 2	1 or 2
Readout sides	1	1 or 2	1 or 2
Data capacity [GBytes]	0.65 or 0.7	4.7-17.0	23.3-50

Table 2.1: Most relevant specifications for the CD, DVD and BRD standards. The BRD is included as one example of the high capacity optical disc.
(*) Specifications available at writing time.

2.3 Optical Disc Player Structure

Figure 2.3 shows a block diagram of a generalized optical disc player and illustrates the essential components. The most natural division within the block diagram is into the control/servo system and the data path. The logic unit provides the interface between the user and the servo mechanisms and performs the logic required for the correct sequence of operation.
The servo system includes the servos related to the positioning of the optical pickup. These are the sledge servo which moves the pickup for coarse radial positioning and the focus and radial servos for fine positioning of the optical pickup's focus point. Although the disc servo is not directly related to the positioning of the optical pickup, it has the important function of rotating the disc at the adequate speed. The data path consists in

broad outline of a data separator, error correction, deinterleave and data buffer module.

The optical pickup reads the self-clocking waveform data from the disc, also referred to as High Frequency (HF) signal. In CDs, data is coded by the Eight-to-Fourteen modulation (EFM) channel code where 8 bits data are represented on the disc by 14 channel bits plus 3 additional channel bits for concatenation purposes. The shortest pit/land is composed by 3 channel bits and the longest pit/land by 11. DVD uses a refinement of the modulation channel code, called EFM+, where 8 bits of data are represented by 17 channel bits. The data separator converts the HF signal into data. The separated output consists essentially of subcode bytes, data samples (whether it be audio, video or *data*), clock signal and redundancy data. The subcode bytes are an auxiliary data stream which basically assists the disc player in locating the data to be read from the disc. The sampling clock, mainly used to count the acquired samples, is regenerated by a Phase-Locked Oscillator from the self-clocking waveform. The Phase-Locked Oscillator generates the correct clock frequency thanks to a Phase-Locked Loop (PLL) which uses the HF signal as time base reference. The slicer in the data separator module uses the clock signal together with the decision level in order to detect the pits and lands. Figure 2.4 shows some results of the pit/land structure simulation. As mentioned before, the shortest pit (or land) is composed by 3 channel bits, which is equivalent to the duration of three complete clock cycles. The longest pit (or land) is consequently equivalent to 11 complete clock cycles. Once the generated clock follows the HF-signal (due to the PLL) the number of clock cycles is counted for every time the HF-signals crosses the predetermined decision level. In that way the length of the pits and lands are determined and data can be decoded.
Once the samples are separated, they are fed to the error correction module where redundancy data is used to check, and eventually correct erroneous data. Cross Interleaved Reed-Solomon code (CIRC), attributed to [Reed and Solomon, 1960], is used in CDs, capable of correcting a maximal length of about 4000 bits (2.5[mm] track length). A variant of this correction code is used in DVDs, called Reed-Solomon (RS) product code, capable of correcting a burst length of approximately 6[mm]. The deinterleave process is achieved by writing sequentially into a data buffer and reading out by means of a sequencer. The speed of the disc motor is unimportant and the system drives the spindle at whatever speed is necessary so that the data buffer neither underflows nor overflows. The size of the data buffer is a compromise between economical costs and resistance to burst errors.

2.4 Optical Principles

The microscopic pits in the information layer form simply a relief structure which is difficult to study with conventional optics. But in 1934 Zernike described a technique called phase contrast microscopy which today allows to read such a structure using optical interference [Watkinson, 2001]. The principles behind this technique applied to

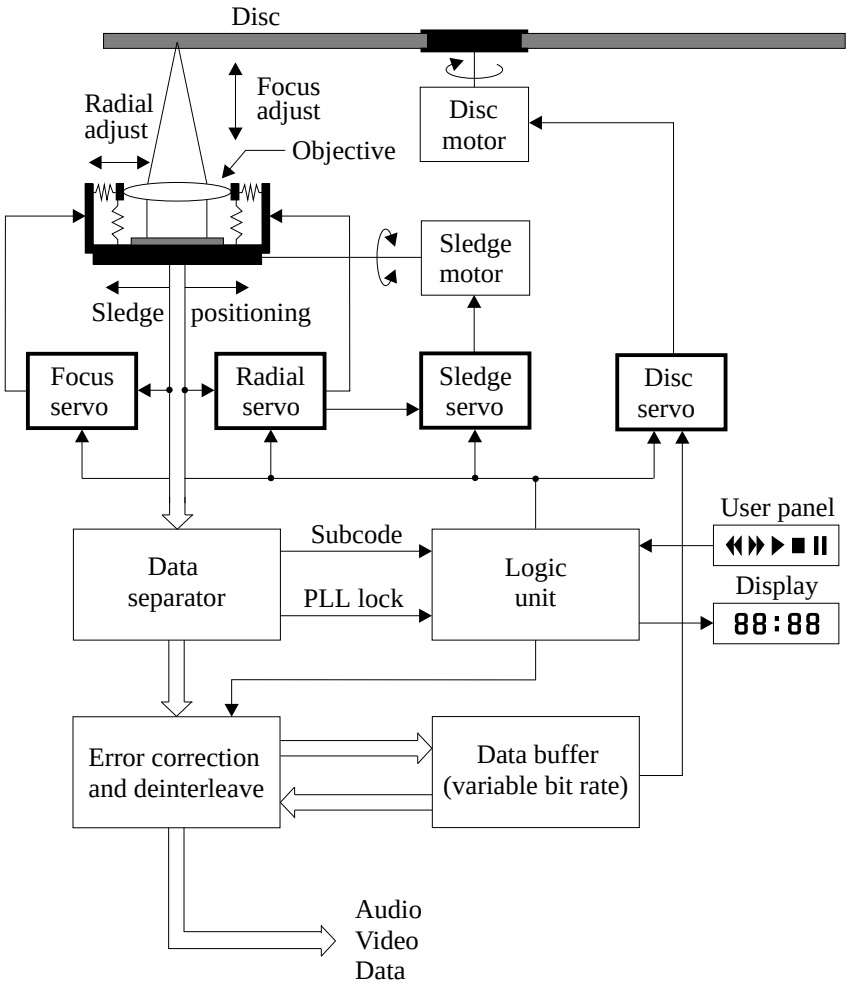

Figure 2.3: *Block diagram of the essential parts of optical disc players showing the data path (broad arrow) and control/servo systems. See text for details.*

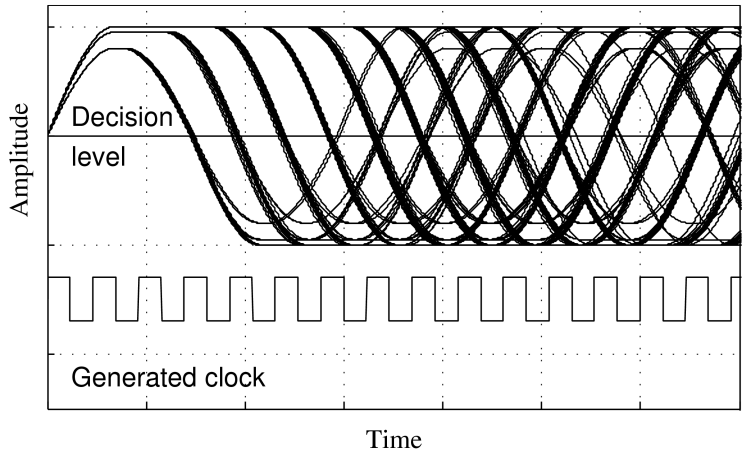

Figure 2.4: *Simulation of the pit/land structure. The HF signal is triggered on an arbitrary positive transient and so the length of the pits can be compared; this plot is commonly referred to as "eye pattern". The shortest pit is equal to a 3T period which corresponds to 3 complete clock cycles. Based on the generated clock and the decision level it can be determined whether it is a pit or a land. Variations in the pit/land length result in jitter which is especially visible along the eye pattern of the HF signal.*

optical discs are illustrated in Figure 2.5.
A laser beam (**l**ight **a**mplification by **s**timulated **e**mission of **r**adiation) is a light composed by photons which bounce synchronously resulting in a light with a well-defined wavelength λ[m]. In optical disc players such type of light is focused by means of an objective through the optical transmittance protection layer onto the information layer. For example, in the case of a CD, the laser's wavelength of the incident laser beam is 780[nm], see Table 2.1. The change of propagation medium from air to the denser medium made of polycarbonate plastic results in a reduction of the velocity of propagation. This ratio of velocity, also known as refractive index of the medium, is μ=1.55 for optical discs. That is, the wavelength is reduced from 780[nm] to approx. 500[nm]. The pit height in CDs is 0.12[μm] which is about a quarter of the laser's wavelength in the transmittance protection layer of the CD. If the laser beam hits a land in the information layer, the light will be reflected preserving the phase. However, if part of the laser beam hits a pit, the reflected light suffers a 180° phase-shift, causing optical destructive interference with the reflected light from the land level, and the intensity of the light leaving the disc is therefore drastically reduced. The information from the disc is then read by a number of photo diodes placed on the light path of the reflected light which registers

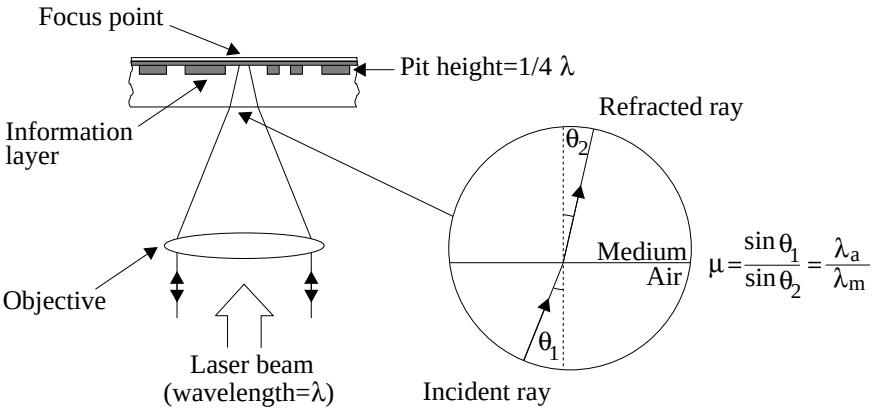

Figure 2.5: *Laser beam reflection from the disc surface. Note that due to the refractive index of $\mu = 1.55$, the diameter of the focus point on the information layer is considerably smaller than the diameter of the readout beam entering the disc surface.*

the variations of the intensity of the reflected light.

2.4.1 Rejecting Surface Contamination

Now that the principles behind the phase contrast microscopy applied to optical discs have been surveyed, it is interesting to estimate the effects of surface contamination in order to have an idea of how well optical disc players may work in practice. Some elementary calculations are needed starting by calculating the angle, θ_1, of the incident ray which enters the disc surface

$$\theta_1 = \sin^{-1} NA \ \ [^\circ] \ , \tag{2.1}$$

where NA is the numerical aperture of the objective lens of the optical pickup. As the refraction index, μ, also is known, see Table 2.1, the angle, θ_2, of the refracted ray can be calculated by

$$\theta_2 = \sin^{-1}\left(\frac{\sin\theta_1}{\mu}\right) \ \ [^\circ] \ . \tag{2.2}$$

The diameter of the spot at the focus point, d, is given by [Bouwhuis *et al.*, 1985]

$$d = \frac{\lambda}{2NA} \ \ [\mathrm{m}] \ . \tag{2.3}$$

The thickness of the optical transmittance protection layer which the laser beam has to travel through is also specified in Table 2.1. Certain trigonometric calculations reveal that the diameter of the readout beam, D, entering the disc surface is given by the following expression

$$D = \frac{2 \cdot \text{layer\_thickness}}{\tan(90^\circ - \theta_2)} + d. \tag{2.4}$$

The information density can be approximately to [Bouwhuis *et al.*, 1985]

$$\text{density} \;\; = \left(\frac{NA}{\lambda}\right)^2. \tag{2.5}$$

It can be observed from Equation 2.5 that in order to increase the information density, the numerical aperture must be increased and/or the laser's wavelength must be reduced, resulting in a reduced focus point size. The side-effect of an increased numerical aperture and a reduced wavelength is an increased optical aberration (distortion), which is compensated by reducing the thickness of the optical transmittance protection layer. A summary of the results from the above calculations is presented in Table 2.2. Note that the results are based on the ideal optical relations described above. In practice some of the figures may vary. The Blu-ray disc is included as one example of the high capacity optical discs. Other standards in this group may have different specifications.

	CD	**DVD**	**BRD**
Incident angle (θ_1) [$^\circ$]	27	37	58
Refracted angle (θ_2) [$^\circ$]	17	23	33
Readout beam size on surface (D) [mm]	0.72	0.51	0.13
Focus point size (d) [μm]	0.87	0.54	0.24

Table 2.2: Calculated optical relations in the CD, DVD and BRD.

Despite the minute size of the focus point on CDs (<1[μm] in diameter), the light enters and leaves through a 0.72[mm] diameter circle. As a result, surface debris up to a few hundred micrometers will be out of focus to the sensing mechanism and no data is missed in the reading process. For example dust particles and hair are as a thumb of rule considered to be respectively 40[μm] and 75[μm] in diameter, and therefore do not constitute an issue while reading data from the disc. In DVDs and high capacity optical discs like the BRD, the immunity against surface debris is lower according to the figures presented in Table 2.2, since the diameter of the laser beam which enters the disc is smaller.

2.4.2 Optical Pickups

Beside specifying the numerical aperture and the laser's wavelength, little else is described in the standards of optical discs on how the optical pickups should be designed.

This gives several degrees of freedom to the designers which is reflected in the wide variety of optical pickups existing in the market. For simplicity, a classical light path for CD is shown in Figure 2.6.

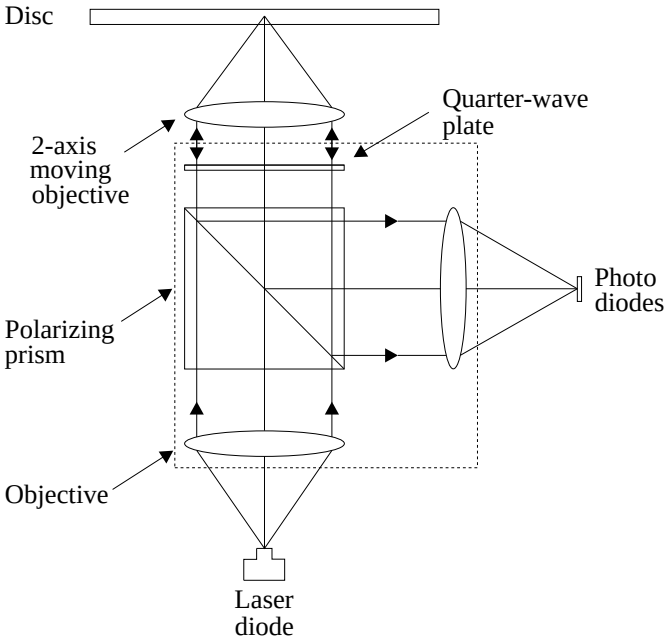

Figure 2.6: *Classical light path for CD-players based on a polarizing prism and a quarter-wave plate.*

The emitted light from the laser diode passes through an objective and a polarizing prism which has a defined transmission plane. Afterwards the light is phase-shifted 90° by the quarter-wave plate. The 2-axis moving objective focuses the light beam on the disc and the reflected light passes again through the same objective. The quarter-wave plate shifts the phase another 90°, now being shifted in total 180° with respect to the transmission plane of the polarizing prism. The light beam undergoes consequently a 90° of deviation and is reflected to an objective in charge of focusing the light beam on the photo diodes. An alternative to this construction setup is to substitute the polarizing prism and the quarter-wave plate by a semi-silvered mirror which lets pass some of the light in the forward direction and reflects some of the returning light into the photo diodes. This is however not very efficient, as half of the replay signal is lost by transmission straight on. Another preferred variant is the substitution of the optical elements in the dashed box in Figure 2.6 by a hologram. The laser diode and the photo diodes can then be placed in the same house. The attractiveness of the hologram solution is its mechanical and environmental stability.

2.4.3 Focus Error Generation

Due to the lack of physical contact between the pickup head and the disc, feedback control is necessary in order to maintain the focus point on the information layer. There is a number of ways in which the error signal suitable for feedback control can be derived, the most common of which are described here.

Single Foucault Method

The left side of Figure 2.7 shows the single Foucault method of determining focus, also known as the knife-edge method. At (b) the focus point is coincident with the knife edge, so it has little effect on the beam. At (a) the focus point is generated behind the knife edge, and descending rays are interrupted, reducing the output of the lower photo diode. At (c) the focus point is generated in front of the knife edge, and rising rays are interrupted, reducing the output of the upper photo diode. The focus error is derived by comparing the outputs of the two photo diodes. A drawback of the single Foucault method is that the lateral position of the knife edge is highly critical.

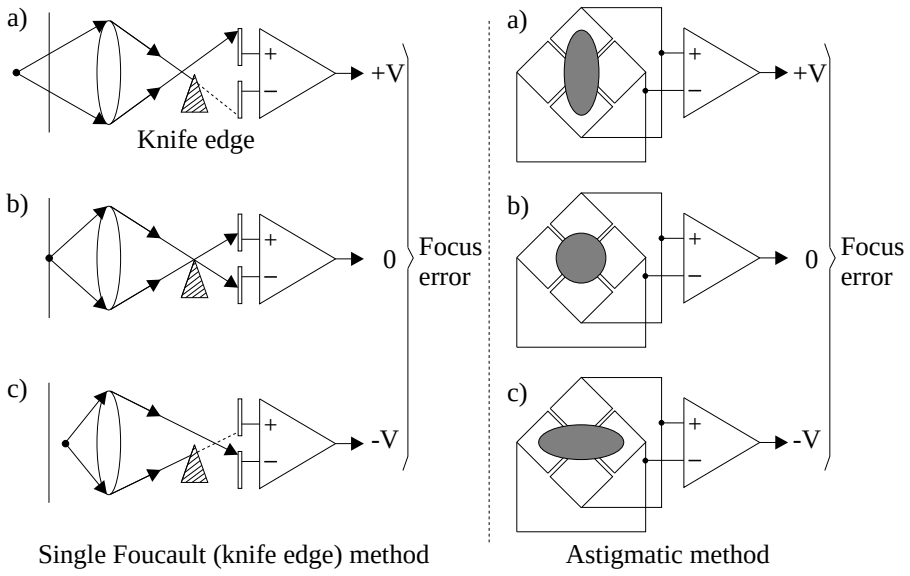

Figure 2.7: *Single Foucault and astigmatic method for focus system.*

Astigmatic Method

The right side of Figure 2.7 illustrates the astigmatic method. A cylindrical lens is installed before the photo diodes. The effect of this lens is that the beam has two foci,

but none of them on the photo diodes. The image will be an ellipse whose aspect ratio changes as a function of the state of focus. Between the two foci, the image will be circular. The aspect ratio of the ellipse, and hence the focus error, can be found by dividing the photo diodes into four quadrants. When these are connected as shown, the focus error signal is generated. The data readout signal is the sum of the quadrant outputs. The captive range of the single Foucault is compared with the astigmatic method in Figure 2.8, which shows that the astigmatic method has a much smaller capture range. A focus search mechanism will be required, which moves the focus servo over its entire operating area, looking for a zero crossing. At this time the feedback loop will be completed and the photo diodes will remain on the linear part of their characteristic. The spiral track of optical discs starts at the inside which has been deliberately arranged because there are less vertical deviations and initial focusing will be easier. One of the disadvantages of the astigmatic method is that it is particularly sensitive to birefringence (different refractive indices in different directions).

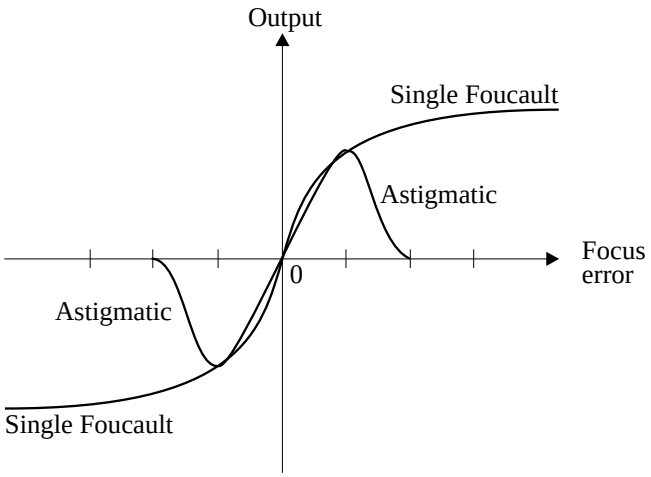

Figure 2.8: *Comparison of captive range of astigmatic and single Foucault method.*

Double Foucault Method

Apart from the two methods described herein, the focus error can also be optically generated by means of a double Foucault arrangement. This method uses a prism instead of the knife edge to split the beam along its optical axis, and two pairs of photo diodes are necessary to obtain the focus error signal. However, this method has been replaced almost entirely by its counterpart, the single Foucault method.

2.4.4 Radial Error Generation

Feedback control is also necessary in order to maintain the focus point centered on the track owing the lack of physical contact between the pickup head and the disc. There is a number of ways in which the error signal suitable for feedback control can be derived, the most common of which are described here.

Twin-spot Method

In the twin spot method, two additional light beams are focused on the disc track, one offset to each side of the track centerline. Figure 2.9 shows that when one side spot moves away from the track into the mirror area, absent of pits, there is less destructive interference and more reflection. This causes the average amplitude of the side spots to change differentially with the radial error. The laser head contains a diffraction grating which produces the side spots and two extra photo diodes onto which the reflections of the side spots will fall. The side spots feed a differential amplifier, which has a low-pass filter to reject the high frequency information of the pits and retains the average brightness difference.

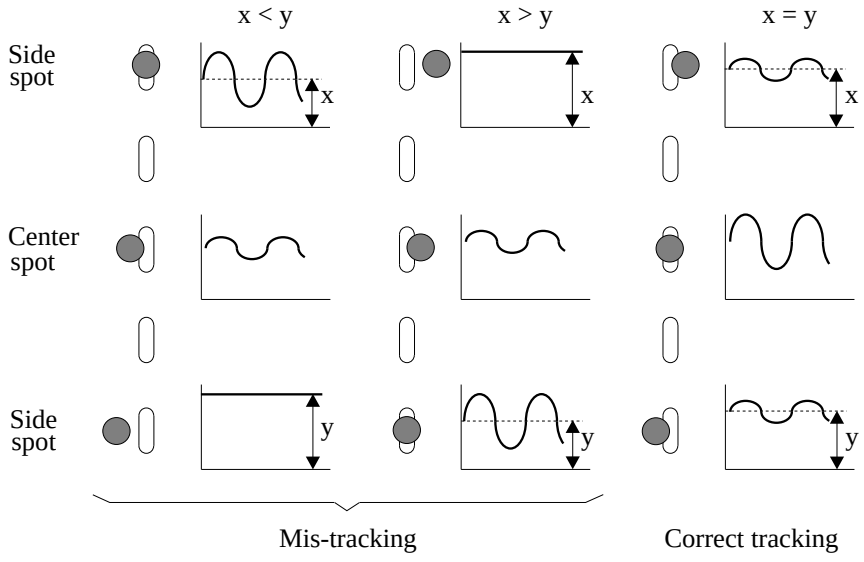

Figure 2.9: *Twin-spot method of producing tracking error compares average level of side-spot signals. Side spots are produced by a diffraction grating and require their own photo diodes.*

Push-pull Method

An alternative approach to the twin-spot method is to analyze the diffraction pattern of the reflected beam. Figure 2.10 shows that one photo diode will see greater pit/land modulation than the other when being off-track. Such system may be prone to develop an offset due either to drift or to contamination of the optics. A further tracking mechanism is often added to avoid the need for periodic adjustment.

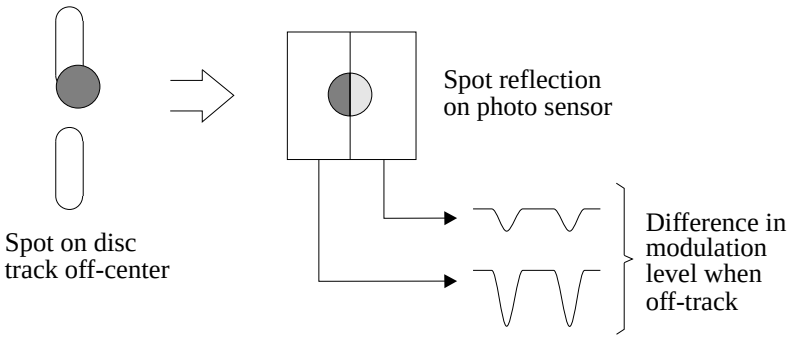

Figure 2.10: *The push-pull method of producing tracking error focuses the spot image onto the photo diodes. One photo diode will have more modulation when being off-track.*

Track Wobble Method

Another method to generate a radial error signal consists of feeding a sinusoidal signal to the radial servo as depicted in Figure 2.11, causing a radial oscillation of the spot position of few decades of nanometers. This results in modulation of the envelope of the readout signal, which can be synchronously detected to obtain the radial error signal. The dither can be obtained by oscillating the whole pickup.

Differential Phase Detection Method

The above described methods are popular in CD-players, they have however some disadvantages. The twin-spot method requires an extra grating with a rather delicate angular orientation and in the recording mode, about 20% of the optical power is spread out to the auxiliary twin spots. The push-pull method is sensitive to the phase depth of the information and does not work in the presence of pure amplitude information patterns. The track wobble method, due to its nature, consumes precious space in the radial direction and is likely to increase the cross-talk between tracks when compared to the other methods at equal information density on the discs. The Differential Phase Detection (DPD), also known as Differential Time Detection (DTD) method, is instead preferred

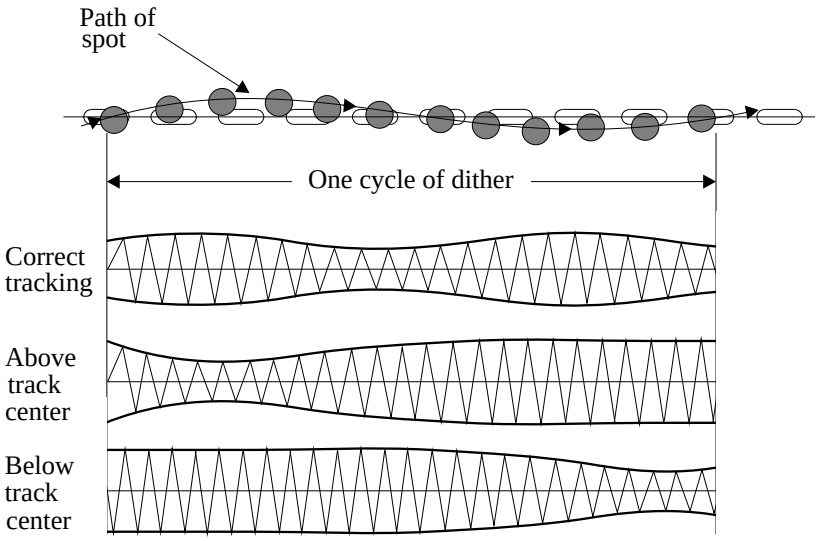

Figure 2.11: *Dither applied to readout spot modulates the readout envelope, as a result, a tracking error can be derived.*

on high-density discs like DVDs. The basic idea is to detect the phase changes of the high-frequency signal as a function of the off-track movement of the scanning spot. These phase changes arise in the four quadrants of photo diodes with different signs and after signal processing the desired tracking error signal is obtained. DPD/DTD is an involved method, not treated further in the thesis, a deeper description of is present in e.g. [Braat, 1998, Braat *et al.*, 2002].

2.5 Optical Disc Servos

Unlike in vinyl LP (Long Play) records, in optical discs there is no inherent mechanical guidance of the pickup which makes feedback control necessary to keep the spot on the information layer and centered on the track. As mentioned in Section 2.3 the servo systems include the focus, radial, sledge and disc servo. In this section the focus and radial servo loops are treated in greater detail as they are the two main feedback systems within a CD-player. Owing the similarity of the focus and radial loop, they are described in parallel and it is notified where they differ.

2.5.1 Focus and Radial Servos

The frequency response of the laser pickup and the amount of cross-talk are both a function of the spot size and care must be taken to keep the beam focused on the information layer. If the spot on the disc becomes too large, it will be unable to discern the smaller features of the track, and can also be affected by the adjacent track. Disc warp and thickness irregularities will cause focal-plane movement beyond the depth of focus of the optical system and track eccentricity will cause jumps of several tracks, therefore a focus and a radial servo system are needed. The optical pickup servos move the *moving objective*, shown in Figure 2.6, along the optical axis in order to keep the spot in focus and in the radial axis in order to keep the focus point on the center of the track. Since dynamic focus changes are largely due to warps, the focus loop must have a frequency response in excess of the rotational speed. The same applies to the radial loop mainly due to track eccentricity. A moving-coil actuator is often used owing to the small moving mass which this permits. There is a large variety of focusing and tracking mechanical systems in CD-players. Some of the most common solutions are later described in Section 3.1.

Red Book Specifications

The Compact Disc Digital Audio standard [Philips and Sony Corporation, 1991], commonly referred to as the Red Book , specifies the relevant CD related parameters such compatibility between CDs and CD-players is ensured. The worst-case vertical and horizontal deviations, according to the Red Book specifications, are shown respectively in Table 2.3 and 2.4. In the following an analysis of these deviations is performed. The vertical deviation $x_{cd}(t)$[m] is modeled as a harmonic and differentiating it twice, an expression for the acceleration $\ddot{x}_{cd}(t)$[m/s^2] is obtained

Conditions	Parameter	Specification
Below 500 [Hz]	Max. deviation	$\pm$500 [μm]
	Max. vertical acceleration	10 [m/s^2]
Above 500 [Hz]	Max. deviation	$\pm$1.0 [μm]

Table 2.3: Standardized vertical deviations from nominal position of the information layer specified at the disc scanning velocity $v_a = 1.2 \ldots 1.4$[m/s]

Conditions	Parameter	Specification
Below 500 [Hz]	Max. eccentricity of the track radius	± 70 [μm]
	Max. radial acceleration	0.4 [m/s^2]
Above 500 [Hz]	Max. tracking error(*)	± 0.03 [μm]

Table 2.4: Standardized radial deviations of the track specified at the disc scanning velocity $v_a = 1.2 \ldots 1.4$[m/s].
(*) The maximal tracking error is the measured tracking error between 500[Hz] and 10[kHz] in closed loop with a controller such that the open loop cross over frequency is 200[Hz] having an integration time of 0.02[s].

$$
\begin{aligned}
x_{cd}(t) &= A_{cd} sin(2\pi f t) \ \text{[m]} \ , \\
\dot{x}_{cd}(t) &= A_{cd} 2\pi f cos(2\pi f t) \ \text{[m/s]} \ , \\
\ddot{x}_{cd}(t) &= -A_{cd}(2\pi f)^2 sin(2\pi f t) \ \text{[m/s}^2\text{]} \ ,
\end{aligned} \tag{2.6}
$$

where A_{cd}[m] is the maximal amplitude of the vertical disturbance, which is limited by the maximal acceleration $\ddot{x}_{cd} = 10$[m/s^2]. That is, the maximal frequency below 500[Hz] where $A_{cd} = 500$[μm] is given by

$$
\frac{1}{2\pi}\sqrt{\frac{max(|\ddot{x}_{cd}|)}{max(|A_{cd}|)}} = \frac{1}{2\pi}\sqrt{\frac{10}{500 \cdot 10^{-6}}} \simeq 22 \ \text{[Hz]} \ . \tag{2.7}
$$

Above 22[Hz] the amplitude is limited by the specified maximal acceleration up to the frequency where the maximal vertical disturbance is A_{xcd} =1[μm]

$$
\frac{1}{2\pi}\sqrt{\frac{max(|\ddot{x}_{cd}|)}{max(|A_{cd}|)}} = \frac{1}{2\pi}\sqrt{\frac{10}{1 \cdot 10^{-6}}} \simeq 500 \ \text{[Hz]} \ . \tag{2.8}
$$

Above 500[Hz] the maximal vertical disturbance is A_{cd} =1[μm]. Calculations on the horizontal deviations give a lower frequency of approx. 12[Hz] and an upper frequency of approx. 580[Hz]. For clarity, the restrictions on the vertical and horizontal deviations are visualized in Figure 2.12.
The maximal specified deviations should be compared with the maximal allowed vertical and horizontal error in order to know how much control effort should be applied.
For CDs, the maximal vertical error allowed is approx. $e_x = \pm 2$[μm] and $e_y = \pm 0.2$[μm] for the radial direction [Bouwhuis *et al.*, 1985]. While the maximal vertical error allowed can be calculated theoretically, the maximal radial error allowed is calculated based on a combination of theoretical and empirical considerations. The limiting factor for the size of the maximal allowed error is especially the cross-talk due to adjacent tracks.

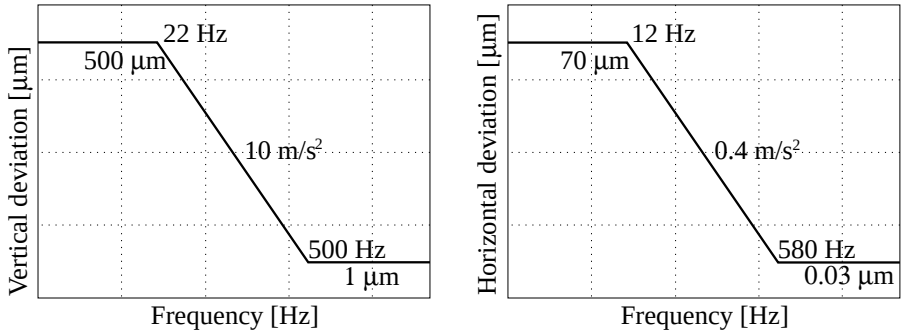

Figure 2.12: *Stylistic representation of the maximal vertical (focus) and horizontal (radial) deviation on CDs for a scanning velocity of 1.2-1.4[m/s].*

Focus and Radial Disturbances

The Red Book specifications could serve as a general guideline on the design process of the positioning servos (controllers) if no other disturbances were present. Unfortunately this is not the case, Figure 2.13 shows a block diagram with the main type of disturbances which affect the focus loop (an equivalent block diagram applies to the radial loop). The main disturbances impinging the focus and radial loop can be divided in four groups as follows:

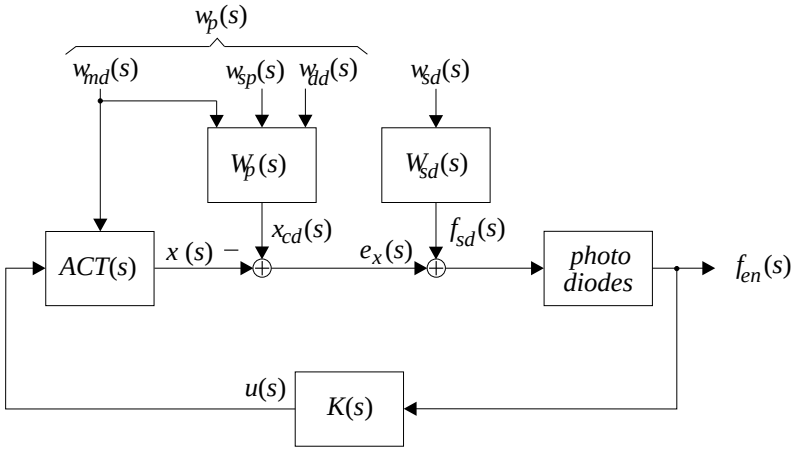

Figure 2.13: *Main disturbances which affect the focus (radial) loop.*

- *Disc deviations,* $w_{dd}(s)$[m]: This group is composed by any deformity in the

disc or CD-player which contributes to a position deviation of the information layer from the normal. Disc warp, unbalanced discs and track eccentricity are the main sources to such deviations resulting in periodic disturbances with the natural frequency given by the rotation frequency of the disc. Tables 2.3 and 2.4 specify the maximal allowed deformities of the disc. Mechanical inaccuracies in the clamping zone of CD-players add up also to the overall position deviation of the information layer.

- *Mechanical disturbances*, $w_{md}(s)$[N]: External shocks propagate through the chassis of the CD-player affecting the position of the optical pickup and the disc. The size of these shocks depends on the environment the CD-player is in. Obviously a portable disc-man or a car-mounted CD-player are more exposed to mechanical disturbances than a stationary CD-player at home, hence the bandwidth of the positioning loops in the first two types of CD-players should be higher than in the stationary CD-player. However, the disadvantage of this approach is a reduced immunity against surface defects. Furthermore portable disc-mans have limited battery power and a higher bandwidth of the positioning loops should be weighted against an increased power consumption. CD-players which are more exposed to said mechanical disturbances, are usually equipped with a large buffer in which music data is stored such that a constant stream of music can be generated in spite of severe mechanical disturbances.

- *Self-pollution*, $w_{sp}(s)$[N]: It is a result of unwanted behavior which have origin in the CD-player itself such as cross-couplings from the focus/radial, sledge and disc loop. An abrupt movement of e.g. the sledge (read Subsection 2.5.2 for an explanation of the sledge) can severely disturb the radial loop and in less extent the focus loop. Another source of self-pollution is the air flow due to the spinning of the disc. Nevertheless it is of reduced importance in audio CD-player as they spin at highest 9[Hz]. In CD-ROM applications, where rotation frequencies of 100[Hz] are not uncommon, the air flow becomes an issue. The level of self-pollution can either be accepted as it is and the positioning loops are designed such that they can cope with it, or the source of self-pollution is reduced in favour to more relaxed requirements of the positioning servos.

- *Surface defects*, $w_{sd}(s)$[m]: This category may be the most challenging from a control point of view, composed by scratches, fingerprints, dust and other surface debris, air bubbles, coating defects, birefringence due to molding problems, thickness irregularities, etc. Common to all of them is that the photo diodes *misunderstand* the reflected signals and generate erroneous feedback signals. The controllers base the generation of the control signal $u(s)$[V] upon an erroneous focus/radial error which can drive the focus point out of track and ultimately out of focus. While an off-track situation can be remediated relatively fast, loosing the focus can imply the execution of a time consuming sequence (stop spinning the CD, drive the sledge at home, start a catch-focus procedure and jump to the

last location). Virtually all CD-players are equipped with a defect detector which is based on the fact that the majority of the surface defects result in a drop of the reflected light intensity. A sudden drop triggers a logic which eventually opens the positioning loops. Still the bandwidth of the focus and radial loop should be low to better cope with this kind of disturbances. Besides disturbing the positioning servos, surface defects also affect the integrity of the data. According to the Red Book a burst error up to 2.5[mm] of track length can be fully corrected. It is generally more than the positioning servos can cope with in a satisfactory way, especially the radial servo. Therefore the immunity against surface defects is usually limited by the positioning servos. A challenge in CD-players is that there is a certain overlap in the frequency range of mechanical disturbances and surface defects, hence it is not trivial how the controller should behave given that both kind of disturbances coincide in time and frequency domain.

In Figure 2.13, the dynamics related to the movements of the objective are described in $ACT(s)$[m/V], where $x(s)$[m] is the position of the focus point. The weight $W_{sd}(s)$ describes the frequency content of the surface defects and $W_p(s)$ is the weight which describes how the different classes of disturbances affect the position of the information layer $x_{cd}(s)$[m]. The photo diodes generate a signal $f_{en}(s)$[V], as described in Subsection 2.4.3, suitable for feedback control. This feedback error signal is given by the following expression (taking the focus loop as an example)

$$f_{en}(s) = K_{optFn}(-x(s) + x_{cd}(s) + f_{sd}(s)), \tag{2.9}$$

where $f_{sd}(s)$ represents the surface defects and K_{optFn} is the normalized optical gain of the photo diodes treated in Section 3.6. The task of the controller is therefore to generate a control signal $u(s)$[V] such that f_{en}[V] is minimized.
In the ideal case, where there is no surface defect, the minimization of f_{en}[V] would indirectly imply the minimization of $e_x(s) = -x(s) + x_{cd}(s)$[m]. However, when the surface defects $f_{sd}(s)$ are present, a minimization of the sensed focus error $f_{en}(s)$ does not necessarily imply a minimization of the actual focus error $e_x(s)$. As previously mentioned, virtually all CD-players are equipped with a defect detector, whose purpose is in fact to better deal with the trade-off between disturbances of conflicting requirements like mechanical disturbances and surface defects. The defect detector increases, to some extent, the ability to cope with surface defects without deteriorating the ability to cope with for example mechanical disturbances. Figure 2.14 shows a measurement example of how this approach works.
The upper plot shows the sensed focus error, see Equation 2.9. As discussed before, the task of the controller is to generate a control signal $u(s)$ (shown in the lower plot) that minimizes the focus error. Thus, ideally, the focus error should be a straight line with zero DC-offset. However, at time 1.584[s] a surface defect is present and the defect detector triggers a logic which results in a zeroing of the focus error fed to the controller. Consequently the controller remains passive throughout the surface defect, and is re-engaged immediately afterwards. Unfortunately, the focus point $x(s)$ has moved from

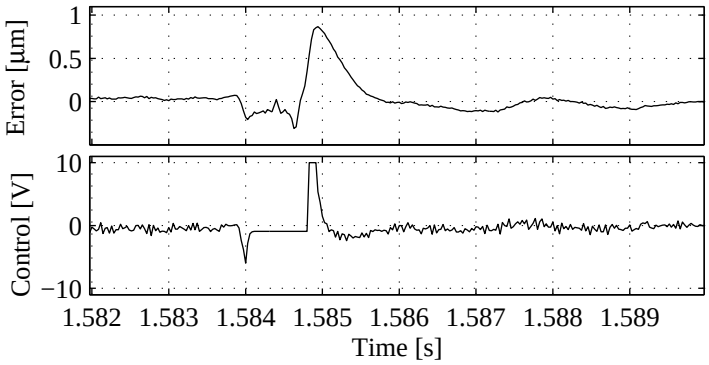

Figure 2.14: *Measurement example of how the defect detector works. In the upper plot the focus error is shown, whereas the control effort is shown in the lower plot.*

the position of the information layer $x_{cd}(s)$ during the surface defect as a result of the controller inactivity, and once the controller is re-engaged, a strong response is observed. The response is obviously an unwanted side-effect as it may prevent the optical pickup from reading data from the disc correctly. Eventually the response may be of such size that focus and/or radial tracking is lost. This topic is studied in greater details in the thesis and strategies on how to reduce the negative effects after a surface defects has been passed will be discussed.

2.5.2 Sledge Servo

The majority of the optical pickups in CD-players are mounted on a linear tracking sledge driven by a motorized gear worm which permits the access of different location on the disc. The working area of the radial moving coil is limited to a few hundred tracks and therefore it cannot access all data in the disc. The main purpose of the sledge is to permit this access. It also serves as a coarse radial positioning when a disc is played continuously. The cross-coupling between the sledge and radial servo loop is logically higher than the cross-coupling between the sledge and focus servo loop. Ideally, the sledge moves slowly but continuously while the radial servo is in charge of the higher frequency deviations which the sledge cannot track, and any perturbation originated by the sledge would be effectively damped by the radial servo. Unfortunately this is not always the case as imperfections in the sledge mechanics may create abrupt movements of the sledge, causing severe disturbances in the radial servo which may result in a loss of track situation. Two projects dedicated to this topic are found in [Aangenent, 2002, Dzanovic and Lauritsen, 2003]. An alternative mechanical solution to the sledge, but not longer present in recent commercial applications, consists on a coil driven arm that

swings an arc across the disc (see for example these Ph.D. dissertations [Dettori, 2001, Dötsch, 1998]). The principle of the coil driven arm is sketched in Figure 3.3 in Section 3.1.

2.5.3 Disc Servo

Data in optical discs is recorded using a constant channel clock. The disc servo should therefore decrease the rotation speed linearly such that a Constant Linear Velocity (CLV) of 1.3[m/s] is achieved feeding the data separator module described in Section 2.3 with a constant data throughput of 150[KB/sec] (also referred to as 1X speed). With CLV the rotation frequency decreases gradually from approx. 9[Hz] to 3[Hz]. In practice, since CD-players have a data buffer, the speed of the disc motor is unimportant and the disc rotates at whatever speed is necessary such that the data buffer neither underflows nor overflows. However, the average speed should lie between 1.2 and 1.4[m/s] which are the defined limits in the Red Book. In CD-ROMs and DVD-ROMs a constant data throughput is not relevant. The user is interested in acquiring data as fast as possible and 50X speed is nowadays common. For that purpose Constant Angular Velocity (CAV) is used or a combination of CLV and CAV resulting in other velocity profiles such as P-CAV (Partial-Constant Angular Velocity) or Z-CLV (Zone-Constant Linear Velocity). The consequences of acquiring data as fast as possible necessarily means that an upper limit is met, imposed either by the channel electronics or by the focus and radial servo-mechanics [Stan, 1998].

2.6 Playability

The Red Book specifies the maximal physical tolerances of CDs, which are meant to be followed by CD producers. In principle, CD-drive manufacturers know therefore what kind of discs to expect and CD-drives are designed such that they at least can cope with the Red Book specifications. In that way compatibility between CDs and CD-players is ensured, an important factor which contributed to the expansion of the CD technology. The Red Book not only specifies the maximal physical tolerances of CDs but also specifies some characteristics of the HF signal. It specifies moreover some parameters concerning the integrity of the decoded data. An acceptable playability is therefore ensured as long as the Red Book requirements are fulfilled, where *playability* can be defined in this context as

> *the ability to reproduce the information from non-ideal discs in non-ideal circumstances.*

Some companies like Philips and Almedio have designed test discs which contain a wide variety of intentional defects so that drive manufacturers can stress their pickups and

servo designs. The tests to be performed by the CD-drive manufacturers can generally be categorized under three headings:

- *Data channel test* is concerned with the integrity of the decoded data from the disc in terms of the amount of and severity of errors on the disc. Typically the discs analyzed in this test are the previously mentioned test discs and those returned from the market. The Block Error Rate (BLER) indicates the amount of errors, which over one second must be less than 220 according to the Red Book. This is a good overall indication of disc quality, however, when there are underlying problems causing high error rate the root of the problem can be found by looking at other tests.

- *Servo tests* generally indicate the ability to track on the disc. The feedback error and the control effort are measured in this test, which may indicate whether there are any problems with the overall track geometry or with the servos.

- *HF signal test* examines the read signals from the optical pickup. A large quantity of parameters are measured like reflectivity, cross-talk, jitter, eye pattern and others which indicate the overall pit structure on the disc. An unacceptable HF signal may indicate a poor servo performance, problems with the track geometry or an unsatisfactory pit structure.

Unfortunately not all discs meet the Red Book specifications due to either fabrication errors or maltreatment of the media by the user and the CD-player may eventually fail to reproduce the information recorded on the disc. If there is a visible error like a scratch, the user may accept that the CD-player fails to reproduce the contents of the disc. However, track eccentricity which does not meet the Red Book specifications is not visible to the user, and he/she may think that the CD-player does not work as intended and tries with another CD-player, which by chance, is able to reproduce the disc. The disc does not meet the Red Book specifications but the user believes that the first CD-player is not working properly. Thus CD-drive producers have the dilemma of whether to improve the playability of CD-drives, despite the fact that they already meet the Red Book specifications, or to accept that the CD-drive will not be able to play such kind of CDs. Given the case they decide to improve it, the challenge is to find the bottleneck, to optimize the module in question without deteriorating the performance of the other modules, to find the next bottleneck and so forth. Playability is a unitless, non directly measurable quantity which popularly speaking can be understood as a balloon, see Figure 2.15.
The ideal (and utopian) case would be a single point where no parameter results in the degradation of playability. However, in practice, certain parameters influence the playability negatively, which is depicted by the length of the arrows. The longer the arrow, the more negative the playability is influenced by the parameter in question. In stationary applications, where the CD-players are located at home, the bandwidth of the controller should generally be lower than in portable solutions like a disc-man. It corresponds to a translation and/or change of shape of the playability balloon, but its

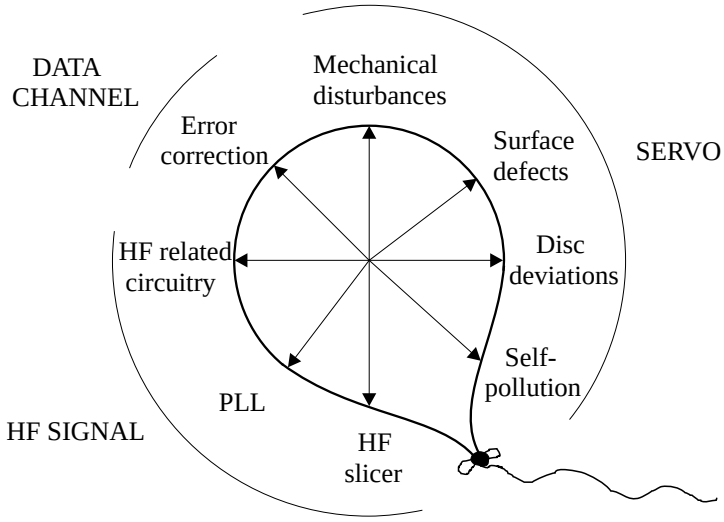

Figure 2.15: *Stylistic representation of playability constraints with a non exhaustive list of influencing parameters. Read text for details.*

volume is kept constant. One may perform better than the other, depending on the situation, but a playability test where all possible parameters are tested, would show that they may perform equally. That is, both of them have a playability balloon of identical volume but different shape. The increased ability to cope with mechanical disturbances is somewhat compensated with the performance degradation to cope with surface defects. Exactly this trade-off is desired to be handled in a more efficient way, and if possible, to eliminate it. The constraints are better explained with an example. It is desired to improve the performance against mechanical disturbances. A straight forward solution is to increase the bandwidth of the servos. The side effect is a reduced immunity against surface defects like scratches, which results in a longer settling time of the HF signal once a scratch is passed. The levels of the HF slicer could then be lowered to compensate for the added settling time of the signal. As a consequence of lowered levels, jitter increases perturbing the PLL causing more data errors. Although it is a simplified example, it can be seen that the interconnection complexity is highly elevated. Pressing the playability balloon in one direction may result in a pop-up effect in another place of the balloon. The aim is to shrink the size of the balloon, avoiding pop-up effects and avoiding balloon translations.

Naturally, an important issue is how to determine the size of the balloon. That is, how to measure the playability in CD-players. Although the Red Book specifies the regions in which certain parameters should be, no specific directions are given to exactly determine

the playability. The companies have therefore developed their own heuristic approaches to determine it. They know generally from experience which parameters influence the playability and in which regions they should be. Any CD and CD-player returned from the market, due to a customer complain, is valuable material which is involved in the process of achieving a better estimation of the playability of CD-players. One of the main drawbacks of these heuristic methods is that they do not permit to estimate the playability of competitor's CD-players accurately. Company A only receives defective CDs and CD-players related to their own products. If they want to estimate the playability of company B (their competitors), such estimation will clearly be biased since the products from company B will not necessarily fail to play the returned CDs to company A.

2.7 Summary

This chapter focused on the description of the challenges on control of CD-players. The most common optical disc formats were described in Section 2.1. It could be observed that the trend is towards higher density data disc which implies a more detailed structure of the information layer and some changes in the optical pickup. In Section 2.2 the physical characteristics of the optical discs were treated and in Section 2.3 the structure of a general optical disc player was revealed. Unlike in vinyl LP records, in optical discs players there is no inherent mechanical guidance of the pickup which makes feedback control necessary to keep the focus point on the information layer and centered on the track. Different methods of generating the feedback control signals were surveyed in Section 2.4. The CD-servos, together with the disturbances they are exposed to, were described in Section 2.5. An important topic is the conflicting requirements the servos must deal with. On the one hand the bandwidth of the positioning controllers should be high in order to better damp mechanical disturbances for example, whilst on the other hand a low bandwidth would be preferable in order to better cope with surface defects such as scratches. This topic is studied in greater details in the thesis. Not only the servos have influence in the overall performance of CD-players, as explained in Section 2.6. Playability defined as *the ability to reproduce the information from non-ideal discs in non-ideal circumstances* can be considered as a balloon where the optimization of a module in the CD-player may cause a pop-up effect in the other side of the balloon and at the end playability may be not improved. Due to the lack of a standard which gives specific directions on how to measure playability, companies have developed their own heuristic approaches primary based on returned products from the market. A main drawback of the heuristic approaches is that they do not allow the companies to accurately estimate playability of the competitor's products.

Part I

Modeling a Compact Disc Drive

3

Model of Positioning Loops

The aim of this chapter is to derive two SISO models suitable for control of the position of the focus point. However, a natural question arises: what is a suitable model for control? A general answer is that the model should be such that the controller design based on this model gives a satisfactory performance when applied to the modeled system. The model has usually to be good around the cross-over frequency. For example, the heuristical approach by Ziegler and Nichols determines the parameters of a PID controller based on one single Nyquist point, namely the cross-over frequency point. While this approach may be sufficient for some control systems, others ask for a more detailed knowledge of the system to control. With respect to CD-players, the typical closed loop bandwidths of focus and radial loops lie in the interval 0.5-2[kHz] (see for example [Chait *et al.*, 1994, Dettori *et al.*, 1999, Moon *et al.*, 1996, Steinbuch *et al.*, 1994a, Huang *et al.*, 1999, Yokoyama *et al.*, 1994]) and apparently a detailed model of the positioning loops outside this interval should not be necessary. However, as suggested in Chapter 8, it is desired to have a controller strategy which permits to reduce the bandwidth of the closed loop, eventually down to 0[Hz] in the case of serious surface defects. With that need in mind, it is also chosen to model the dynamics below 500[Hz]. There are basically two ways of modeling the behavior of a system. The first way is the theoretical or deductive method also called white-box modeling (or first principle modeling). All parameters and variables can be interpreted in terms of physical entities and all constants are known a priori. Knowledge of how the system behaves is of course needed,

however, such knowledge is not always available. The system may also be governed by complicated laws which lead to a model appropriate for simulations but not suitable for control purposes. At the other end of the modeling scale the experimental or inductive methods are found, also called black-box modeling, which are based on input/output measurements of the system. The parameters of the model have no physical interpretation, they just serve as tuning knobs. In this sequel only white-box modeling is employed to derive the model of the positioning loops.
The chapter starts giving a review in Section 3.1 of some of the most common 2-axis devices employed in CD-players. In Sections 3.2 and 3.3 a general model is given for respectively the actuator and the optical position transfer. Section 3.4 presents the obtained general model and some considerations regarding the cross-couplings between the focus and radial loop are briefed in Section 3.5. The developed experimental setup in the Ph.D. project is described in Section 3.6, where a model of the parts constituting the CD-drive in question is derived. Finally, in Section 3.7 a specific model is derived valid for the focus and radial loops described in the experimental setup.

3.1 Types of 2-axis Devices

Due to the absence of any physical contact between the disc and the pickup device, CD-players contain auto-focus and auto-tracking functions. These functions are performed by the focus and radial servo circuits via a 2-axis device, enabling a movement of the objective in two axis: vertically for focus correction and horizontally for track following. Figure 3.1 shows one type of such 2-axis device construction, used in early CD- and DVD-players.
The principle of operation is that of the moving coil in a magnetic field. Two coils, the focus and radial coil, are suspended between magnets creating two magnetic fields. A current through either coil, due to the magnetic field, will cause the coil to be subjected to a force, moving the coil in the corresponding direction. While a guidance axis permits straight vertical movements for focus correction, movements for radial correction describe an arc as the objective assembly rotates around the axis. However, the radial movement can be approximated to a linear movement due to the reduced arc of rotation.
Another suitable 2-axis device, which is the most common among existing CD-players, consists of the suspension of the objective assembly on four parallel rigid arms, see Figure 3.2. The extremes of the arms are made of a flexible compound which acts as a spring. Here both the focus and radial displacement trajectory describe an arc but again, due to the limited working area of the coils, the trajectory can be considered to be linear. A variant of this device is the substitution of the rigid arms by flexible rods, coated with a damping material such as rubber for better dynamic properties.
An alternative 2-axis device is the CD rotatable arm shown in Figure 3.3. While the pickups shown in Figure 3.1 and 3.2 need to be mounted on a sledge in order to access different locations on the disc, the advantage of the CD rotatable arm is that a sledge is not necessary. They exhibit also a remarkable performance against surface defects

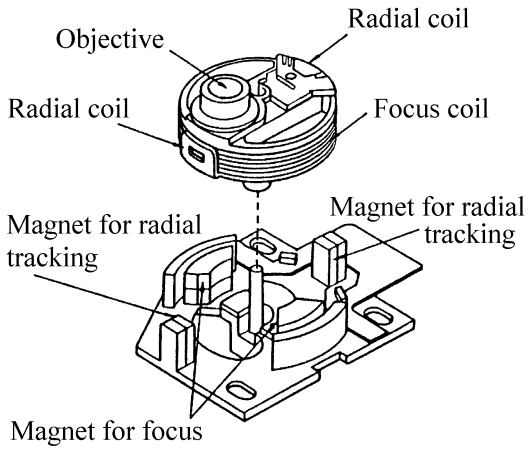

Figure 3.1: Type I: *Construction of a 2-axis device where the objective assembly is suspended on magnets.*

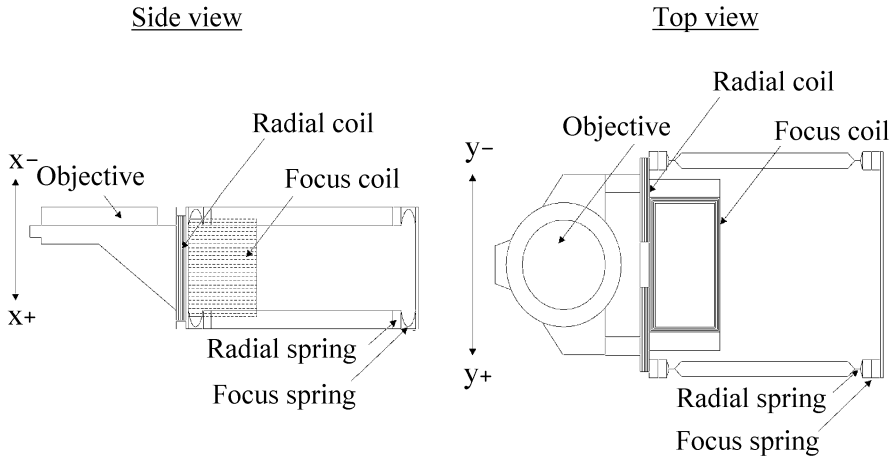

Figure 3.2: Type II: *2-axis device suspended on four parallel arms.*

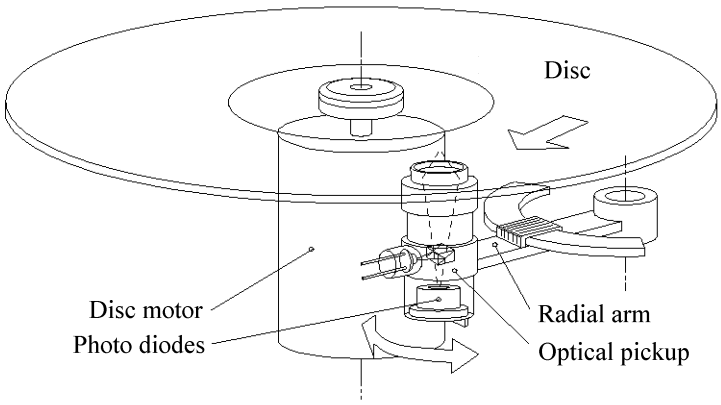

Figure 3.3: Type III: *2-axis device with rotatable arm.*

such as scratches. However, the disadvantage of oblong constructions as this one is that they are restricted to low bandwidths and are not suitable for e.g. high-speed CD-ROM players. The increasing rotation speeds of optical disc applications has implied that this pickup is in disuse.
Independently of which of the above presented 2-axis device is considered, the transfer from the control signal to the error signal can be represented as shown in Figure 3.4. A voltage $u(s)$[V] is applied to the actuator which is transformed in the *driver transfer* module into a force $F(s)$[N]. This force acts on the objective assembly resulting in a displacement $x(s)$[m] of the objective assembly and consequently also an equal displacement of the focus point. $e_x(s)$[m] is the distance between the position of the information layer and the position of the focus point. This distance is indirectly measured by the photo diodes resulting in the positioning error signal $f_{en}(s)$[V] suitable for feedback control.

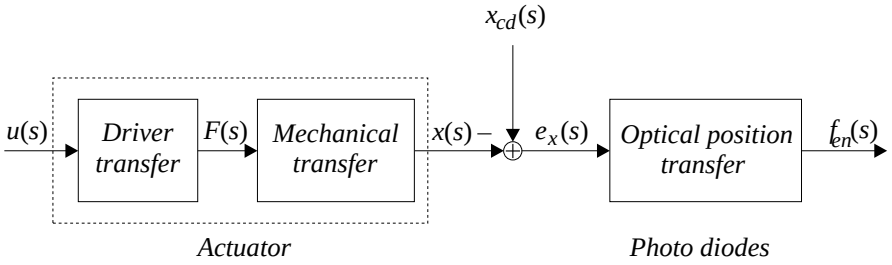

Figure 3.4: *Focus optical pickup transfer, (an equivalent diagram applies to the radial transfer).*

3.2 Actuator Model

The focus point displacements necessary for tracking are obtained using an electromagnetic device, the actuator. In CD-players, such actuator is a two-dimensional (2-D) actuator and, as shown in Figure 3.4, it is composed by a driver transfer and a mechanical transfer, which are described in more details in the following two subsections.

3.2.1 Driver Transfer

The conversion between the applied control voltage $u(s)$[m] into force acting on the objective assembly, $F(s)$[N], takes place in the driver transfer. Figure 3.5 depicts such device. The coil in the actuator is driven by current, therefore the input voltage is converted to current in the *power driver* module with gain K_{pd}, which results in a different voltage across the coil, namely $v_{coil}(s)$[V].

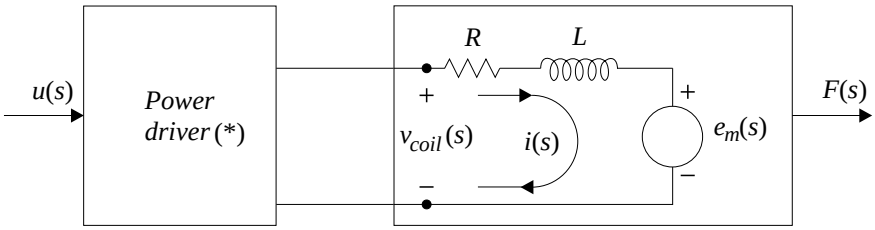

Figure 3.5: *Driver transfer where the applied control signal $u(s)$[V], is converted into a current $i(s)$[A]. This current runs through a coil, which in a magnetic field, results in the generation of a force $F(s)$[N].*
(*) Although the power driver *module is not physically located in the pickup device, it is considered to belong to the driver transfer and forms also consequently a part of the actuator.*

The actuator is based on a voice-motor coil which behaves for restricted displacements like a direct-current (dc) motor. The equivalent electrical diagram is therefore as shown in Figure 3.5 composed by a resistance R[Ω], an inductance L[H] and an induced voltage source $e_m(s)$[V]. According to *Kirchhoff's voltage law*, the voltage across the coil is given by the sum of the voltages across the elements

$$u(s)K_{pd} = v_{coil}(s) = Ri(s) + Lsi(s) + e_m(s) \ \text{[V]} \ . \tag{3.1}$$

The induced voltage $e_m(s)$ is the result of the coil movements relative to the magnetic field. The principle illustrated in the left part of Figure 3.6 is described by the following relationship

$$e_m = (\dot{\mathbf{x}} \times \mathbf{B}) \cdot \mathbf{l} \ \text{[V]} \ . \tag{3.2}$$

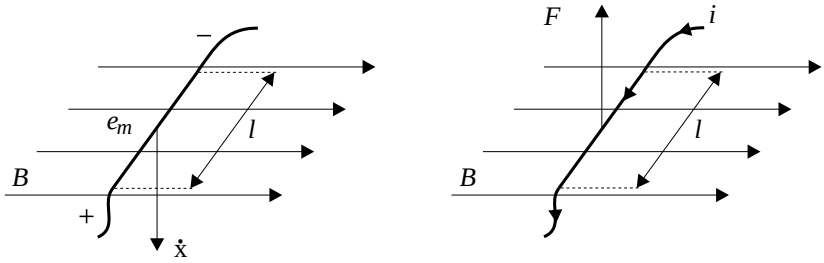

Induced voltage in a moving conductor *Electrical induced force*

Figure 3.6: *Graphical representation of the induced voltage in a moving conductor and electrical induced force.*

where $\dot{\mathbf{x}}$[m/s] is the velocity of the coil, **B**[Wb] the flux density of the magnetic field and **l**[m] the length of the moving coil. The cross represents the vector cross product and the dot denotes the scalar product. In practice, the three vectors in Equation 3.2 are mutually perpendicular, so the relationship can be simplified to $e_m = Blv$[V]. The current through the coil can be calculated by substituting the induced voltage e_m[V] from the simplified version of Equation 3.2 into Equation 3.1

$$i(s) = \frac{v(s)K_{pd} - Blsx(s)}{R + Ls} \text{ [A] .} \tag{3.3}$$

A different physical law governs the electrical induced force. Now the conductor is assumed to be fixed for the sake of simplicity and the interaction between the magnetic field and the current through the conductor generates a force on it. The principle is shown in the right part of Figure 3.6 which is described by the following relationship

$$\mathbf{F} = i(\mathbf{B} \times \mathbf{l}) \text{ [N] .} \tag{3.4}$$

Again, in practice the vectors are mutually perpendicular and the induced force can be calculated by $F = Bli$[N]. By substituting the current $i(s)$[A] from Equation 3.3 into the simplified version of Equation 3.4, the induced force is described by

$$F(s) = Bl\frac{v(s)K_{pd} - Blsx(s)}{R + Ls} \text{ [N] ,} \tag{3.5}$$

which finalizes the calculations for the driver transfer.

3.2.2 Mechanical Transfer

The generated force, $F(s)$[N], by the driver transfer is applied to the objective assembly of mass m[Kg]. In the absence of effects such as friction, elasticity, etc. this subsystem

acts as a double integrator which is described by *Newton's second law*, $F = m\ddot{x}$[N], where $\ddot{x}$[m/s^2] is the acceleration of the objective assembly. The position follows by integrating the acceleration twice, and the force-to-position transfer function is therefore given in the *Laplace*-domain by

$$\frac{x(s)}{F(s)} = \frac{1}{ms^2} \text{ [m/N] .} \tag{3.6}$$

As a result of this double integration, the transfer function decreases with frequency as $|\frac{1}{s^2}| = \frac{1}{\omega^2}$, resulting in a slope of -40[dB/dec] in the amplitude of the bode plot. In principle all position control systems in use in optical discs belong to this category of second order control systems [Bouwhuis *et al.*, 1985]. The above calculations considered the objective assembly to be floating. Alternatively, the objective mass may be suspended on leaf-springs. In that case the transfer function is no longer a double integrator over the whole frequency scale.

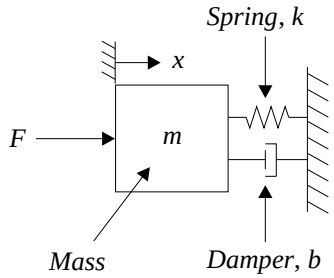

Figure 3.7: *Translational diagram of the mechanical transfer, (spring-mass damper system).*

Figure 3.7 shows the translational diagram for such system, where m[Kg] is the mass of the moving objective assembly and x[m] represents its displacement. b[N·s/m] and k[N/m] are respectively the spring constant and the damping, and F[N] is the applied force. The force-to-position transfer function is now given by

$$\frac{x(s)}{F(s)} = \frac{1}{ms^2 + bs + k} \text{ [m/N] .} \tag{3.7}$$

The bode plot of the spring-mass damper system given in Equation 3.7 is shown in Figure 3.8 for various values of the damping ratio $\zeta = \frac{b}{2\sqrt{mk}}$.
For high frequencies both transfer functions given in Equations 3.6 and 3.7 are equal. At low frequencies the transfer function in Equation 3.7 is dominated by the spring constant k[N/m]. For intermediate frequencies, there is a resonance behavior. The quality factor Q of the resonance, defined as $\frac{1}{2\zeta}$, gives the height of the peak relative to the low frequency level. In optical disc drives the quality factor typically lies between 10 and 100, depending on the choice of the spring material [Bouwhuis *et al.*, 1985].

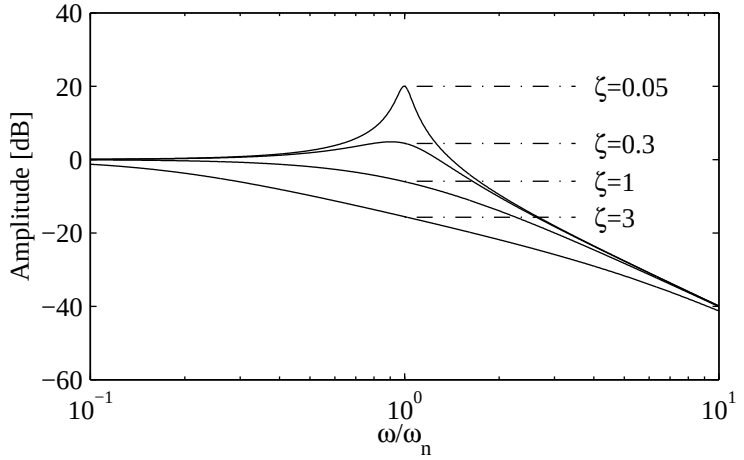

Figure 3.8: *Bode plot of the spring-mass damper system. Frequency axis is normalized with respect to the natural frequency ω_n of the system.*

3.3 Optical Position Transfer

The position of the focus point is not measured directly, instead the distance between the position of the focus point and the center of the track in the information layer is measured using photo diodes. The task of the photo diodes is therefore to provide a feedback signal to the positioning controllers. See Figure 3.4 for a visualization of the focus optical pickup transfer. The relationship between the magnitude of the feedback signal and the distance to be measured in optical disc players is nonlinear and the characteristics vary depending on the optical method used to generate such feedback signals. Usually this relationship can be considered to be linear as long as the feedback error is kept within some defined limits. Under these assumptions the feedback error is then given by

$$f_e(s) = K_{optF} e_x(s) = K_{optF}(-x(s) + x_{cd}(s)) \text{ [V]} , \tag{3.8}$$

for the focus loop and

$$r_e(s) = K_{optR} e_y(s) = K_{optR}(-y(s) + y_{cd}(s)) \text{ [V]} , \tag{3.9}$$

for the radial loop, where K_{optF}[V/m] and K_{optR}[V/m] are respectively the focus and radial optical linearized gains.

3.4 General Model of Positioning Loops

After having determined the actuator transfer together with the optical position transfer a general model of the CD-drive can be derived. The total actuator transfer function from the applied voltage $u(s)$[V] to the position of the focus point $x(s)$[m] is obtained by substituting the calculated force from the driver transfer in Equation 3.5 into the force-to-position transfer function given in Equation 3.7. After a proper isolation of the variables, the following expression is obtained

$$\frac{x(s)}{u(s)} = K_{pd} \cdot \frac{\frac{Bl}{mR}}{\frac{L}{R}s\left(s^2 + \frac{b}{m}s + \frac{k}{m}\right) + \left(s^2 + \left(\frac{(Bl)^2}{mR} + \frac{b}{m}\right)s + \frac{k}{m}\right)} \text{ [m/V] .} \quad (3.10)$$

By taking the optical position transfer into account the transfer function from the control voltage $u(s)$[V] to the focus positioning error is obtained

$$\frac{f_e(s)}{v(s)} = K_{optF}K_{pd} \cdot \frac{\frac{Bl}{mR}}{\frac{L}{R}s\left(s^2 + \frac{b}{m}s + \frac{k}{m}\right) + \left(s^2 + \left(\frac{(Bl)^2}{mR} + \frac{b}{m}\right)s + \frac{k}{m}\right)} \text{ [V/V] .} \quad (3.11)$$

A similar transfer function applies to the radial loop.

3.5 Cross-couplings

The focus and radial coils are placed orthogonal to each other such that the cross-coupling is minimized. There is, however, a certain amount of cross-coupling from focus to radial loop and from radial to focus loop due to different natures. These are listed below:

- *Electrical:* Its origin is mainly from the hardware. Signals in one control loop may produce unwanted variations in the other loop due to e.g. same shared electronic components and physical proximity of the signal paths. Therefore care should be taken especially at the stage of designing the Printed Circuit Board (PCB) layout.
- *Magnetic:* The magnetic fields of both actuators cross and will therefore cause interaction. Current through either the focus or radial coil will generate a magnetic field which is captured by the other coil. As shown in the right part of Figure 3.6, a force is induced causing a displacement of the corresponding coil.
- *Mechanic:* The nature of this cross-coupling has its origin in mechanical imperfections. Differences in for example the spring coefficients, see Figure 3.2, will result in a torque force which perturbs both loops. As another side effect it can be mentioned that the laser beam will not be projected perpendicularly onto the information layer, limiting the linear working area of the photo diodes.

- *Optical:* A poor performance of the focus controller results in changes of the amplitude of the reflected light, which obviously will perturb the radial loop. A worse scenario is the case where the focus point goes out of focus, then no valid feedback measurement will be available to the radial controller. However, a poor performance of the radial controller has not such a severe impact in the focus loop. The pits of the track are detected due to their lower reflection compared to the lands. If the radial controller has a poor performance, the movement of the focus point will describe a zig-zag trajectory centered around the track in question. As no pits are encountered to either side of the track, the result of this zig-zag trajectory is a higher reflection of the laser beam which also affects the focus loop. The optical cross-coupling is the only one which can be assumed to be static, however, it is highly nonlinear due to the construction of the optics.

While the mechanical cross-coupling is significant in the CD rotatable pickup device, the optical cross-coupling is the most significant in the other presented pickup devices [Bouwhuis *et al.*, 1985]. On the other hand, if the feedback errors are kept in the linear area, the optical cross-coupling is reduced, therefore it is chosen in the thesis to neglect the cross-couplings. An ongoing Ph.D. project is partially dedicated to the description of the mentioned optical cross-coupling [Odgaard, to be submitted in 2004] where, based on a detailed model of the optics, it is intended to recover the positioning information from the corrupted feedback error signals due to surface defects.

3.6 Experimental Setup

A stereo music system together with 12 CD-drives are confined to research purposes. The internal focus and radial PID controllers are implemented in a digital servo of fixed structure in the stereo music system, where only the parameters can be changed (the order of the controllers and the control strategy are fixed). These limitations can be circumvented by having a PC-based experimental setup, as shown in Figure 3.9 which is based on a previous design documented in [Vidal *et al.*, 1998, Andersen and Karlsson, 2000]. The original CD-drive is separated from the stereo music system but the communication link is preserved such that it is still possible to operate the stereo music system as usual. The PID controllers in the CD-drive receive as input the photo diode signals $d_1(s)$[V], $d_2(s)$[V], $s_1(s)$[V] and $s_2(s)$[V]. The control signals u_F[V] and u_R[V], which are the output of the controllers, are conducted through the PC-controlled switches back to the CD-drive so that the control loops are closed. Alternatively the position of the focus point can be controlled by two controllers implemented in the PC. The photo diode signals are amplified, low pass filtered, discretized by the PCI 9118-DG I/O card and fed to the PC. In the PC the photo diode signals are processed and two control signals are generated and pass afterwards through an attenuator stage. Finally the PC-controlled switches are in charge of directing the control signals to the CD-drive. The control signals u_F[V] and u_R[V] and the current through the focus and radial coils c_F[V] and

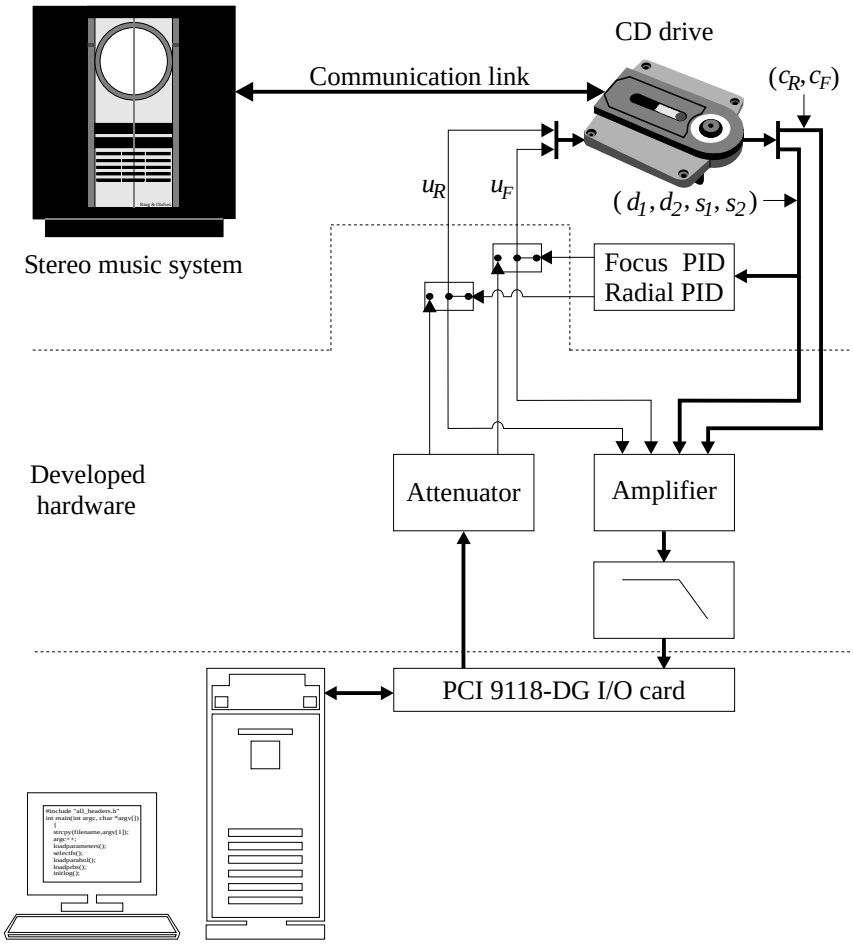

Figure 3.9: *Overview of the experimental setup. The CD-drive of a stereo stereo system is connected through the developed hardware to a PC. The position of the focus point can either be controlled by the internal PID controllers or by the external controllers implemented in the PC.*

c_R[V] (converted to voltage) are also sampled for system identification purposes, explained in Chapter 4. The current is indirectly measured by inserting a small resistance $r[\Omega]$ (approx 5% of the coil's resistance) and measuring its voltage drop. Below there is a list with the relevant specifications of the experimental setup. The selection of sampling frequency together with the bandwidth of the anti aliasing filter is a trade-off between the desired closed loop bandwidth, reduction of aliasing artifacts and PC's calculation power. The given figures are an acceptable trade-off for the present application.

- *Amplifier gain:* Photo diode signals gain: 60[dB]. Coil current signals gain: 38[dB]. Control signals gain: 40[dB].
- *Anti aliasing filter:* First order low pass filter with a 8[kHz] bandwidth.
- *Attenuation factor:* -54[dB].
- *PCI 9118-DG I/O card:* 8 12-bit $\pm$5[V] analog inputs with on chip sample-and-hold. 2 12-bit $\pm$10[V] analog outputs. 35[kHz] sampling frequency for each channel. Direct Memory Access (DMA) data transfer.
- *Personal Computer:* AMD Athlon PC 1100MHz with DOS 6.1 operating system installed and C-compiler.

The amplifier is the most critical stage of the experimental setup. The optical pickup generates current signals below 12[μA] which obviously cannot be directly sampled by the PCI 9118-DG I/O card. A conversion to voltage and an amplification are necessary. It is of outmost importance to keep the wire lengths between the generated photo diode signals and the hardware responsible for this operation as short as possible. The photo diode signals are extremely sensitive and any disturbance results in a deterioration of playability.

3.6.1 Limitations

An on-the-fly change from the internal to the external controller is only possible in the focus loop. At the time of switching, any difference between the internal and the external controller's output produces a step on the control signal applied to the moving coil. The focus loop accepts large errors ($\pm$ 6[μm]) before loosing focus and has shown in practice to be robust against the produced steps. However, the radial loop is more sensitive to steps on the control signal, and a radial error generally greater than $\pm$ 0.8[μm] will result in a jump to the contiguous track. The in-built logic in the stereo music system detects this jump and gives orders to the radial controller to jump back to the previous track but since the output of the internal controller is disabled due to the position of the switch, it will fail jumping to the previous track. Therefore the in-built logic generates an error which stops the CD-drive immediately. A work-around to this problem is the implementation of external radial controllers when the stereo music

system is set in test mode, where no actions are taken in the presence of tracking errors. The sledge servo is however disabled and the radial controller can consequently work for a few seconds before reaching the saturation limits of the moving coil in the radial direction.

Another limitation is imposed by the low-budget PCI 9118-DG I/O card. It is a data sampling card intended to be used in applications where data is sampled in a row and turn-around delay is not critical. In closed loop control applications delays lead to instability and therefore such delays are not desired. An involved software code was created to reduce spurious delays and to limit the turn-around delay between one and two sampling periods. A better alternative is to base the experimental setup on dSPACE, which offers a powerful development tool for control but at an elevated price. In [Dettori, 2001] an example is given on how to control the position of the focus point of a CD-drive based on a dSPACE control solution. In that reference it is moreover suggested a hardware-software based solution where the radial controller can be changed on-the-fly without having the limitations imposed by the experimental setup of the present Ph.D. work.

3.6.2 CD-drive

The previously mentioned CD-drive is based on some specific principles listed below:

- Optic arrangement: Holographic
- Focus error generation: Single Foucault method
- Radial error generation: Twin-spot method
- 2-axis device: Type II (mounted on a sledge)

These principles have been described in Chapter 2 and in the present chapter. The derived model presented in Section 3.4 (Equation 3.11) is of general character. Based on the available knowledge of the specific CD-drive, a more specific model can be obtained in order to better describe the focus and radial loops. The changes apply to the actuator (both the driver and mechanical transfer) and the optical transfer.

Driver Transfer adapted to the specific CD-drive

In Subsection 3.2.1 it is explained that the equivalent diagram of the voice-motor coil is composed by a resistance $R[\Omega]$, an inductance L[H] and an induced voltage source $e_m(s)$[V], see Figure 3.5. In the derived transfer function of the general model given in Equation 3.11 it can be observed that the inductance introduces a pole (in the left part of the denominator) with a time constant which can be approximated to $\tau \simeq \frac{L}{R}$[s]. However, measurements of τ[s] of the focus and radial coil revealed that the pole lied in both cases above 10[kHz], see Table A.1 and A.2 in Appendix A.1. Given the fact that the

typical closed loop bandwidth of focus and radial loops in CD-players are in the interval 0.5-2[kHz] (see for example [Chait *et al.*, 1994, Dettori *et al.*, 1999, Moon *et al.*, 1996, Steinbuch *et al.*, 1994a, Huang *et al.*, 1999, Yokoyama *et al.*, 1994]) it is chosen not to model the effects of the inductance. The inserted resistance $r[\Omega]$, in series with the coil to measure the current is also taken into account in the model by considering a total resistance of $(R + r)[\Omega]$.

Mechanical Transfer adapted to the specific CD-drive

At the beginning of Section 3.2 it is assumed that the objective assembly is freely suspended neglecting the effects of the leaf-spring. Afterwards the model is extended to include these effects, still being general for the presented pickups. However, the connections and transmissions on mechanical constructions show in practice a certain amount of elasticity resulting in parasitic mass-spring subsystems which decrease the bandwidth of the actuators. In the case of the optical pickup in the specific CD-drive there is a parasitic mass-spring subsystem, illustrated in Figure 3.10, having the following physical interpretation. If the arms are fixed, it is still possible to move the rest of the objective assembly, although the elasticity properties are very poor. This extra degree of freedom in the movement of the objective assembly implies that the acceleration of m_1 is not necessarily equal to m_2's acceleration.

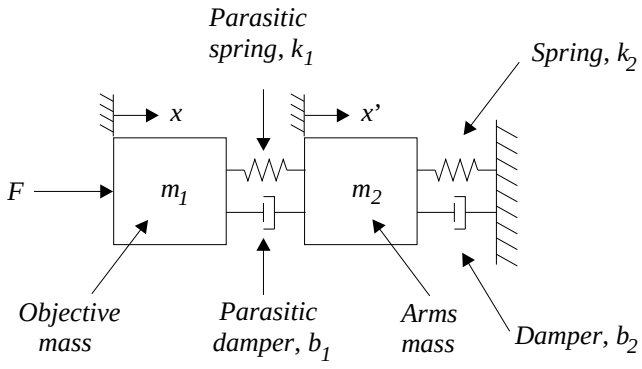

Figure 3.10: *Parasitic spring-mass system in the* type II *2-axis pickup device.*

From the translational diagram, following relationships can be derived

$$m_1 s^2 x(s) = F(s) - b_2\big(sx(s) - sx'(s)\big) - k_2\big(x(s) - x'(s)\big), \tag{3.12}$$

$$m_2 s^2 x'(s) = b_2\big(sx(s) - sx'(s)\big) + k_2\big(x(s) - x'(s)\big) - b_1 sx'(s) - k_1 x'(s). \tag{3.13}$$

The parasitic mass-spring subsystem adds a complex conjugate zero pair followed by a complex conjugate pole pair to the transfer function. Since it is only desired to determine the relationship between the applied force $F(s)$[N] and the position of the objective assembly $x(s)$[m], $x'(s)$[m] is of no importance and is therefore eliminated. This is for example achieved by isolating $x'(s)$[m] in Equation 3.13 and substituting it in Equation 3.12. By rearranging the terms, following expression is obtained

$$\frac{x(s)}{F(s)} = \frac{m_2 s^2 + (b_1 + b_2)s + k_1 + k_2}{(P + Q)} \text{ [m/N] ,} \tag{3.14}$$

where P and Q are

$$P = [m_1 m_2 s^4 + (m_1(b_1 + b_2) + m_2 b_2)s^3],$$
$$Q = [(m_1(k_1 + k_2) + m_2 k_2 + b_1 b_2)s^2 + (k_1 b_2 + k_2 b_1)s + k_1 k_2].$$

This concludes the calculations concerning the mechanical transfer extended to model the parasitic mass-spring subsystem.

Optical Transfer adapted to the specific CD-drive

As explained before, the CD-drive's optical pickup uses the single Foucault method to generate the focus error signal and the twin-spot method to generate the radial error signal. The photo diodes which generate these signals are depicted in Figure 3.11, see [Sharp, 2003] for a general information about laser diodes and hologram lasers.

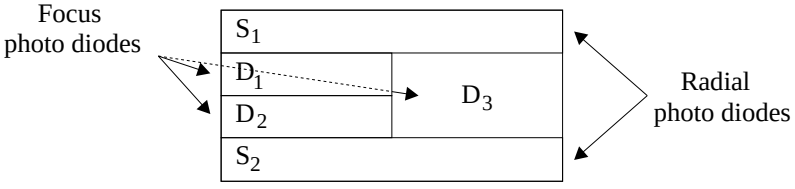

Figure 3.11: *Physical arrangement of the photo diodes of the CD-drive. S_1 and S_2 generate the radial error signal. D_1, D_2 together with D_3 are in charge of generating the HF signal and the focus error signal.*

While S_1 and S_2 are only used for tracking purposes, D_1, D_2 and D_3 are used to generate the focus error signal and the HF signal (the sum of the generated signals from the photo diodes D_1, D_2 and D_3 form the HF signal). The feedback error signals can be generated by the mutual subtraction of the photo diode signals

$$f_e(s) = K_{optF} e_x(s) = K_{optF}(-x(s) + x_{cd}(s)) = d_1(s) - d_2(s) \text{ [V] ,}$$
$$r_e(s) = K_{optR} e_y(s) = K_{optR}(-y(s) + y_{cd}(s)) = s_1(s) - s_2(s) \text{ [V] .} \tag{3.15}$$

It is recalled that $x(s)$[m] and and $y(s)$[m] are respectively the vertical and horizontal position of the focus point and that $x_{cd}(s)$[m] and $y_{cd}(s)$[m] represent the position of the center of the track to be followed by the controllers. K_{optF}[V/m] and K_{optR}[V/m] are the linearized optical gains. These optical gains have the unfortunate consequence of being dependent on the reflection coefficient of the disc. The unwanted dependency is removed by normalizing the feedback error signals[1]

$$f_{en}(s) = K_{optFn} e_x(s) = \frac{d_1(s) - d_2(s)}{d_1(s) + d_2(s)} \text{ [units] ,} \tag{3.16}$$

$$r_{en}(s) = K_{optRn} e_x(s) = \frac{s_1(s) - s_2(s)}{s_1(s) + s_2(s)} \text{ [units] .} \tag{3.17}$$

$d_3(s)$[V] can also be used to normalize the focus error signal. Figure 3.12 illustrates the generation of the normalized focus error $f_{en}(s)$[units], an equivalent illustration applies to the normalized radial error generation. The photo diodes D_1 and D_2 receive the reflected light and generate in the linear area a current proportional to the distance $e_x(s)$[m] between the focus point $x(s)$[m] and the information layer $x_{cd}(s)$[m]. These current signals are converted to voltage signals and are subtracted to generate the focus error $f_e(s)$[V] and added to generate the focus sum $f_s(s)$[V]. The optical gain K_{optF}[V/m] is the visualized slope with a dotted line. The normalization of the error is performed by dividing the focus/radial error by the focus/radial sum. The normalized optical gain K_{optFn}[units/m] is as well visualized with a dotted line where the abscissa still has [m] as units while the ordinate is unitless. The vertical dividing line in the figure indicates that the generation of the diode signals is performed in the hardware platform while the generation of the focus error, focus sum and normalized focus error takes place in a microprocessor. In practice, the controllers implemented in the microprocessor have as well access to each of the diode signals, but for simplicity, throughout the thesis only the normalized focus/radial error is depicted as the output of the photo diodes.
Normalizing the error signals has also the advantage that the mentioned optical cross-couplings in Section 3.5 are reduced. However, there are some side effects. Imperfections of the disc's surface, such as scratches or dust, cause the reflected light to fall drastically. As a consequence, the denominators in Equations 3.16 and 3.17 become very small, resulting in a large and misleading feedback error. Misleading because neither the position of the focus point nor the position of the center of the track have necessarily changed. Therefore the controllers generate a control signal based on a faulty feedback error signal which may result in an unwanted movement behavior. Nevertheless this side effect of the error normalization is reduced by including a detector which prevents the control loops to react against surface defects.

[1] In practice, such normalization occurs in a microprocessor where $f_{en}[k] = \frac{d_1[k]-d_2[k]}{d_1[k]+d_2[k]}$ and $r_{en}[k] = \frac{s_1[k]-s_2[k]}{s_1[k]+s_2[k]}$. The author is aware of the abuse of the notation but for simplicity reasons it has been chosen to show the operations in the Laplace-domain.

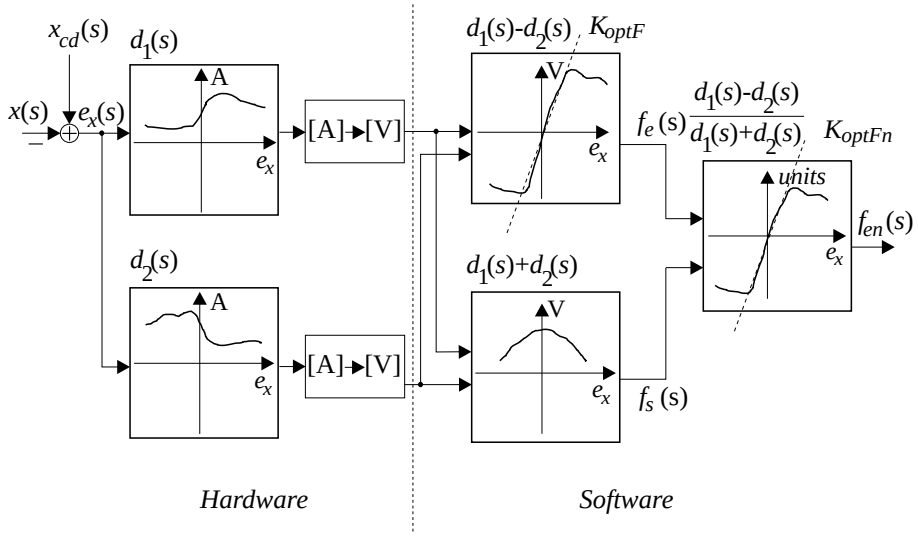

Figure 3.12: *Illustration of the optical characteristics of the photo diodes, which generate the focus feedback signal.*

3.7 Specific Models of the Positioning Loops in the Experimental Setup

In Section 3.4 a general model was derived, valid for the three types of the presented pickup devices. However, given the fact that in the experimental setup specific knowledge is available concerning the CD-drives of the laboratory setup, it is natural to derive a model which better describes the transfer from the control to the feedback error signal. Table 3.1 gives an overview of the equations which describe both the general and the specific model for focus (a similar model applies in this section to the radial loop).

	General model	**Specific model**
Driver transfer	Equation 3.5	Effects of the inductance removed from Equation 3.5
Mechanical transfer	Equation 3.7	Equation 3.14
Optical transfer	Equation 3.8	Equation 3.16

Table 3.1: General and specific model equations of the CD-drive.

Moreover, there are three stages from the experimental setup which must be taken into account to complete the specific model, namely the attenuator, amplifier and anti aliasing

filter stages. While the first two stages can be described with two gains, the anti aliasing filter is modeled with a pole. By adequately joining the driver, mechanical and optical transfers of the specific model and the three stages from the experimental setup, a final expression of the transfer function from the control to the error signal is obtained, see Equation 3.18

$$\frac{f_{en}(s)}{u(s)} = K_{total}\frac{num_0 s^2 + num_1 s + num_2}{den_0 s^4 + den_1 s^3 + den_2 s^2 + den_3 s + den_4} \cdot \frac{\omega_a}{s+\omega_a} \text{ [units/V] ,} \tag{3.18}$$

where ω_a is the bandwidth of the anti aliasing filter and $Ktotal = K_{at}K_{amp}K_{optFn}$[units/V] composed by respectively the gain of the attenuation and amplification stages and by the normalized optical gain. Table 3.2 shows the coefficients of the polynomials.

num_0	$m_2 Bl$
num_1	$Bl(b_1 + b_2)$
num_2	$Bl(k_1 + k_2)$
den_0	$(R+r)m_1 m_2$
den_1	$(Bl)^2 m_2 + (R+r)m_1(b_1+b_2) + (R+r)m_2 b_2$
den_2	$(Bl)^2(b_1+b_2) + (R+r)m_1(k_1+k_2) + (R+r)m_2 k_2 + (R+r)b_1 b_2$
den_3	$(Bl)^2(k_1+k_2) + (R+r)k_1 b_2 + (R+r)k_2 b_1$
den_4	$(R+r)k_1 k_2$

Table 3.2: Coefficients of the focus/radial transfer functions.

Some of the relevant parameters are specified in the CD-drive's data sheet. However, not all the parameters in the data sheet can be related directly to the parameters in the model given by Equation 3.18 and some calculations are therefore necessary. The AC-sensitivity of the coils is equal to Bl[N/A]. The spring constant is given by

$$k = \frac{\text{AC-sensitivty}}{k_{DC}(R+r)} \text{ [N/m] ,} \tag{3.19}$$

where k_{DC}[m/V] is the DC-sensitivity. Since the effects of the parasitic mass-spring subsystem also are modeled, the spring constant k[N/m] is distributed between k_1[N/m] and k_2[N/m], such that $k = \frac{k_1 \cdot k_2}{k_1 + k_2}$[N/m]. Finally, for second order systems, the second coefficient of the denominator is equal to $2\zeta\omega_n$, where $\zeta = \frac{1}{2Q}$. The damping factor can be calculated by isolating b[N·s/m] in the following equality

$$\left(\frac{(Bl)^2}{mR} + \frac{b}{m}\right) = \frac{\omega_n}{Q} \text{ [rad/s] ,} \tag{3.20}$$

and therefore b is given by

$$b = \frac{m\omega_n R - Q(Bl)^2}{QR} = \frac{m\omega_n}{Q} - \frac{(Bl)^2}{R} \text{ [N·s/m] .} \tag{3.21}$$

The damping factor is distributed between b_1[N·s/m] and b_2[N·s/m] such that $b = b_1 + b_2$[N·s/m].

Most of the values are known in the model, except the optical gains and the distributions between k_1[N/m], k_2[N/m], b_1[N·s/m] and b_2[N·s/m], therefore system identification is performed in Chapter 4 to estimate the unknown parameters.

3.8 Summary

This chapter has been devoted to the derivation of a model of the positioning loops of a CD-player. Three types of optical pickup devices were described in Section 3.1. A general model of the actuator and optical position transfer was derived respectively in Sections 3.2 and 3.3 and the entire model of the positioning loops was given in Section 3.4. The most common factors which contribute to the cross-coupling between the focus and radial loops were briefed in Section 3.5. A stereo music system together with 12 CD-drives were available during the Ph.D. project. Since the internal controllers and the controller strategy which are implemented in the CD-drives are of fixed structure, an experimental setup was developed to circumvent these limitations, described in Section 3.6. The internal and external focus controllers can be changed on-the-fly, while the external radial controller can only be implemented in test mode where the sledge controller is disabled. Finally a specific model was presented in Section 3.7 which takes into account the developed hardware and the specific characteristics of the CD-drives in question.

4

Parameter Estimation on a CD-drive

This chapter is devoted to the parameter estimation of 12 CD-drives. The results of this chapter are intended to be used in a $\mathcal{H}_\infty$-framework in Chapters 5 and 6 where a nominal and an uncertainty model is necessary to design a $\mathcal{H}_\infty$-controller. A brief introduction to parametric identification is given in Section 4.1 where some of the most common parametric and nonparametric methods are shortly described. In [Schoukens *et al.*, 1997] an error-in-variables least-squares method is suggested to identify the parameter of a system. Section 4.2 is inspired by this method in that periodic excitation is employed and that the noise characteristics and the nonparametric model are separately estimated.

In CD-players, the focus point should be in the working area of the photo diodes in order to retrieve meaningful information from the generated feedback signals. Perhaps that might be the reason why system identification in CD-players is traditionally performed in closed loop. The challenges of performing open loop system identification in CD-players are surveyed in Section 4.3. Here a method to perform open and closed loop identification in CD-players is revealed, allowing to identify the parameters which constitute the derived fourth order model from the previous chapter. A simple procedure is given in Section 4.4 to estimate both the focus and radial optical gain. In Section 4.5 it is

described how to analyze whether the open and closed loop experiments are performed in the linear area. The results of the parameter estimation are presented in Section 4.6 and in Section 4.7 some concluding remarks are given.

4.1 Brief Introduction to System Identification

In the 1960's system identification started to develop, mainly with the work realized by Åström. An important driving force for this development was the increased interest in model based control stimulated by Kalman's work on optimal control. Since then, the system identification field has experienced a rapid growth and is today a well established research area, (see for example [Forssell, 1999] for a recent source of references to system identification).

System identification can be defined as the parametric modeling of dynamic systems by means of experimental data. The key elements of system identification are the selection of the model structure, experiment design, parameter estimation and validation. Selection of model structure and parameterization are fundamental issues. The experiment design is also crucial for successful system identification, which in control problems is reduced to a proper selection of the input signal. Knowledge of the system and the intended use of the model are also consequently essential.

In terms of how input/output data are translated into a mathematical relation, the field of identification can broadly be divided into two groups: parametric identification and nonparametric identification. While in parametric identification the structure of the model is parameterized a priori and the parameters of the structure are fitted to the data, in nonparametric identification, no (or very little) assumption is made with respect to the model structure.

In order to give a basic understanding on the essence of parameter estimation, some of the most common methods are shortly described in the following. More material can be found in the text books [Ljung, 1987, Åström and Wittenmark, 1995, Stark and Woods, 1994]. Some nonparametric methods are also explained to give a feeling of how they work.

4.1.1 Parametric Identification

- *Least Squares (LS)*: In general the parameter estimation problem of linear parameter models can be treated as a linear regression problem. It is based on the minimization of the following loss function

$$V(\theta, t) = \frac{1}{2}\sum_{i=1}^{t}(y(i) - \varphi^T(i)\theta)^2. \tag{4.1}$$

$y(i)$ is the output of the physical model obtained from experiments. $\varphi(i)$ are the regressors and θ are the parameters of the model to be determined.

- *Prediction Error Methods (PEM)*: The prediction error methods predict the output based on the previous data and the identified model, and then minimize the error between the predicted and real output. To define the PEM the user has to make a choice of model structure, of predictor and criterion. In general terms, many methods of parameter estimation can be considered as minimization of errors of some predictions from measured data.

- *Instrumental Variables (IV)*: In the presence of correlated noise the IV method is an alternative, which estimates the system dynamics without providing a noise model. The basic idea of the method is to modify the model equation by introducing so-called *instruments* in order to cancel the effect of correlated noise. That is, given that the real parameters θ_0 are used, the prediction error $\epsilon(t, \theta)$, becomes independent of previous measurements Z^{t-1} as shown in Equation 4.2

$$E[\epsilon(t, \theta)Z^{t-1}] = 0 \Leftrightarrow \theta = \theta_0. \tag{4.2}$$

- *Maximum Likelihood (ML)*: The basic idea is to construct a function of the data and the unknown parameters called *likelihood* function, $L(\theta) = f_y(\theta; Y)$, where f_y is the probability density function of the measurements Y which are dependent on the parameters θ. The estimate is then obtained as the parameter value which minimizes the function $\frac{\partial l}{\partial \theta} = 0$. That is, the parameters θ, which make the given observations most probable, are selected.

4.1.2 Nonparametric Identification

In reality, the dividing line between parametric and nonparametric identification is somewhat blurred. In nonparametric identification, some assumptions are always made about the system structure (e.g., a finite length impulse response, smoothness of the frequency response) to obtain a well-posed estimation problem. In addition, in parametric identification, a proper choice of the model order is often determined by examining the residuals from fitting models of various orders. In the following three nonparametric methods are shortly explained:

- *Step Response Method*: The system is excited with a step at the input and the output is registered. It works reasonably well for first and second order systems,

eventually with time-delay, provided that there is no appreciable noise on the signals. Noise in the input logically leads to significant uncertainty on the parameter estimation. Impulse response may also be applied to discrete systems.

- *Frequency Response (Periodic Excitation) Method*: It consists on employing a sinusoidal signal as input and to measure the amplitude and phase-shift between the output and input signals. Each time the experiment is repeated for each frequency, a new point is generated in the bode plot of the transfer function. A large number of measurements is necessary and the method is therefore not suitable for plants with a large settling time such as distillation columns. Nevertheless periodic excitation is suitable to reveal the degree of nonlinearity of the system in question.

- *Spectral Method*: It is based on the relationship between the spectrum of the input Φ_u and the cross-spectrum between the input and output Φ_{yu} as presented in Equation 4.3

$$\hat{G}(e^{j\omega}) = \frac{\hat{\Phi}_{yu}(j\omega)}{\hat{\Phi}_u(j\omega)}. \tag{4.3}$$

  However the estimated model $\hat{G}$ depends on how the spectra are estimated.

There is a wide range of methods available to estimate the parameters, with their own strengths and weaknesses. The use of periodic excitation signals in identification is an often overlooked possibility, [Forssell, 1999]. With periodic excitation a number of things are gained, it is possible to separate the *signal* from the *noise* and hence the noise properties can be estimated separately. This information can be used to improve the quality of the estimates or to construct identification methods that can handle special situations, for example when both the input and the output are corrupted by noise. This is called an *errors-in-variables* problem which is solved in e.g. [Schoukens *et al.*, 1997] involving a least-squares minimization where the nonparametric noise model is estimated from the data set. Although the method is characterized by its simplicity, the expressions in the minimization step involving least-squares are rather involved. In the next section the problem statement is formalized and a more pragmatic approach is employed where once the nonparametric model is obtained by means of averaging the measurements, the model of fixed order is fitted using the MATLAB script `fitsys.m` provided by the *μ-Analysis and Synthesis Toolbox*. In the previous chapter a parametric model of the positioning loops was derived, therefore it is not necessary to go through every step of the system identification. The main purpose is consequently the *parameter estimation*, understood as a sub-task of system identification, consisting on the determination of the parameters in a dynamic system of a given structure by means of experimental data [Knudsen, 1993].

4.2 Periodic Excitation in Parameter Estimation

Consider the setup depicted in Figure 4.1 where the model of known structure is given by $G(q) = \frac{B(q)}{A(q)}$, q being the forward shift operator and $A(q)$ and $B(q)$ are the polynomials

$$A(q) = q^r + a_1 q^{r-1} + \ldots + a_r \tag{4.4}$$

$$B(q) = b_1 q^{t-1} + b_2 q^{t-2} + \ldots + b_t. \tag{4.5}$$

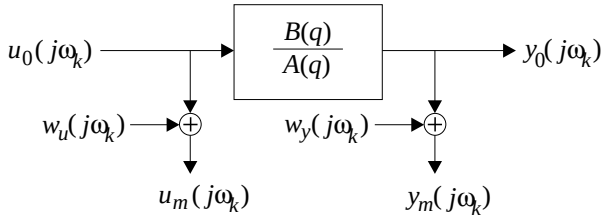

Figure 4.1: *Measurement setup to identify the parameters of $B(q)$ and $A(q)$.*

The problem to study is how to identify the model parameters $\{a_i\}$ and $\{b_i\}$ using the measurements $u_m(j\omega_k)$ and $y_m(j\omega_k)$ obtained at angular frequencies $j\omega_k, k = 1, \ldots, N$, corrupted by the noise $w_u(j\omega_k)$ and $w_y(j\omega_k)$. The measured data can be described by

$$u_m(j\omega_k) = \{u_m(j\omega_1), \ldots, u_m(j\omega_N)\}, \tag{4.6}$$

$$y_m(j\omega_k) = \{y_m(j\omega_1), \ldots, y_m(j\omega_N)\}, \tag{4.7}$$

$$u_m(j\omega_k) = u_0(j\omega_k) + w_u(j\omega_k) \qquad y_m(j\omega_k) = y_0(j\omega_k) + w_y(j\omega_k). \tag{4.8}$$

It is assumed that the input $u_0(j\omega_k)$ is periodic and that an integer number of periods M, are measured. It is further assumed that the noise $w_u(j\omega_k)$ and $w_y(j\omega_k)$ are zero mean signals and uncorrelated with $u_0(j\omega_k)$ and $y_0(j\omega_k)$.

4.2.1 Nonparametric Model

Once the measurements have been acquired, the input and output measurements, $u_m(j\omega_k)$ and $y_m(j\omega_k)$ are averaged over M periods

$$\overline{u}(j\omega_k) = \frac{1}{M} \sum_{m=1}^{M} u_m(j\omega_k) \qquad k \in [1, \ldots, N], \tag{4.9}$$

$$\overline{y}(j\omega_k) = \frac{1}{M}\sum_{m=1}^{M} y_m(j\omega_k) \qquad k \in [1,\ldots,N]. \tag{4.10}$$

The amount of measured periods should be such that an unbiased estimation of the mean can be obtained. [Schoukens *et al.*, 1997] proves that $M = 4$ is sufficient. There are also other practical aspects which should not be overlooked. In order to avoid transients effects, the measurements can only start when the transients become negligible compared with the steady-state response. Leakage problems are avoided by measuring an integer number of periods and the sampling rate is selected such that the Nyquist sampling criterion is not violated. Obviously the signals also need to be filter with an anti-aliasing filter.
Each frequency point of the bode plot is estimated by dividing the averaged output by the averaged input

$$\hat{G}(j\omega_k) = \frac{\overline{y}(j\omega_k)}{\overline{u}(j\omega_k)}. \tag{4.11}$$

The amplitude ratio (in [dB]) and phase angle are calculated as shown in respectively Equations 4.12 and 4.13

$$\text{A.R.}(j\omega_k) = 20\cdot\log_{10}\cdot|\hat{G}(j\omega_k)| = 20\cdot\log_{10}\cdot\sqrt{\text{Re}\,\{\hat{G}(j\omega_k)\}^2 + \text{Im}\,\{\hat{G}(j\omega_k)\}^2}, \tag{4.12}$$

$$\phi(j\omega_k) = \tan^{-1}\left[\frac{\text{Im}\,\{\hat{G}(j\omega_k)\}}{\text{Re}\,\{\hat{G}(j\omega_k)\}}\right]\cdot\frac{180^\circ}{\pi}. \tag{4.13}$$

4.2.2 Confidence Intervals

So far, a bode plot (of the system shown in Figure 4.1) has been estimated. However, without a statement about its quality, the obtained bode plot is virtually useless. The statistical way to deal with this is to provide estimated standard deviations or alternatively confidence intervals. In this way, regions can be established where the true bode plot can be found with a certain probability. These regions can then be translated to corresponding confidence regions for the estimated parameters. Nevertheless, given the fact that the estimated parameters are intended to be used in the $\mathcal{H}_\infty$-framework, *hard bounds* are required, not *soft bounds* as provided by statistics analysis. One of the main characteristics of $\mathcal{H}_\infty$-controllers is that the control errors can be maintained within some predefined hard bounds for all perturbed plants about the nominal model up to the worst-case model uncertainty. Clearly, the model uncertainties must also be hard bounded. However, as pointed out in [Wahlberg and Ljung, 1992], given only measured data, one can never be 100% positive about the uncertainty bounds. Some assumptions are needed in order to be able to provide explicit hard bounds. In the following it is assumed that the system to identify can be described with a rational

transfer function. Furthermore given that the statistical assumptions are realistic, the calculated confidence intervals will have a certain degree of conservatism since no assumptions are made on the model. A 99% confidence interval is therefore considered as sufficient to provide hard bounds.

Let $X_m(j\omega_k)$ be a two-dimensional array containing all the M complex points, measured at angular frequencies $\omega_k, k = 1, \ldots, N$. Suppose that $X_m(j\omega_k)$ is composed by samples that are normally distributed with unknown mean μ and unknown variance σ^2. Moreover assume that the real and imaginary parts of $X_m(j\omega_k)$ have equal variance, that is $\sigma_r^2 = \sigma_c^2$, and also that they are independently distributed. It is now desired to construct a $100(1-\alpha)$ percent confidence interval for μ. By letting

$$S_k^2 = \sum_{m=1}^{M} \frac{[X_m(j\omega_k) - \overline{X}(j\omega_k)][X_m(j\omega_k) - \overline{X}(j\omega_k)]^*}{M-1} \qquad k \in [1, \ldots, N], \quad (4.14)$$

denote the sample variance then $\sqrt{n}\frac{(\overline{X}_m(j\omega_k)-\mu)}{S}$ has a t distribution, also known as *Student's distribution*, with $n-1$ degrees of freedom. Hence, for any $\alpha \in [0, \frac{1}{2}]$ (see for example [Ross, 1987]), it can be said with $100(1-\alpha)$ percent confidence that the mean lies in the interval given below

$$\mu_k \in \Big(\overline{X}(j\omega_k) - t_{\alpha/2,n-1}\frac{S_k}{\sqrt{n}}, \quad \overline{X}(j\omega_k) + t_{\alpha/2,n-1}\frac{S_k}{\sqrt{n}}\Big). \qquad (4.15)$$

4.2.3 Estimation of Parameters

To recapitulate, the system was excited by sinusoidal signals and the amplitude ratio and phase have been averaged over M periods measured at N frequency points. The averaging process led to the estimated nonparametric model and a confidence interval has been calculated. The estimated nonparametric model is now fitted using the MATLAB script `fitsys.m` provided by the *μ-Analysis and Synthesis Toolbox*. `fitsys.m` yields the coefficients $\{a_i\}$ and $\{b_i\}$ of the polynomial $A(q)$ and $B(q)$ depicted in Figure 4.1. By allowing small changes in the parameters, the region described by the confidence interval is covered and the uncertainty of the bode plot is therefore translated to the corresponding confidence interval for the parameters. The specific issues of parameter estimation related to CD-players are treated in the following section.

4.3 Periodic Excitation Applied to a CD-drive

The method of periodic excitation to estimate the parameters can be performed both in open loop and closed loop. Even for low signal/noise ratio the estimate will converge to the true value ($\overline{u} \to u_0$ and $\overline{y} \to y_0$ for $M \to \infty$) in closed loop as long

as the system is persistently excited [Schoukens *et al.*, 1997]. That is, the estimates converge to the bode plot of the finite dimensional system $\frac{B(q)}{A(q)}$, which is the system to be estimated. While it is of important theoretical value to ensure convergence in closed loop for poor signal/noise ratios, in practice convergence alone may not be enough. Exciting the system with a few periods and a fixed amplitude results in a large statistical variance and results consequently also in large confidence intervals but the experiment is realized fast and only few data need to be logged. On the other hand, if the system is excited with a large number of periods and a fixed amplitude, the statistical variance can be kept small but the experiment would take a long time, with large quantities of data to be logged as a consequence. Another trade-off is found in the amplitude of the excitation signal. As the focus and radial plants are basically a double integrator, it implies that there is a frequency region where the periodic excitation method will render an optimal performance. Below that region, a small excitation amplitude results in a large amplitude at the output with the risk of loosing focus/track (poor signal/noise ratio). And above that region a large excitation amplitude only results in a small amplitude at the output with the risk of saturating the input with no margin to the control signal (again poor signal/noise ratio). Besides the mentioned trade-offs there is also the unwanted presence of disturbances in closed loop. In [Dötsch, 1998], a Ph.D. dissertation concerning the identification for control design with application to a CD-drive, it was pointed out in the recommendations for further research that "*As we have observed in the estimation of model error bounds based on closed loop measurement data, a controller that achieves a higher bandwidth may lead to larger error bounds, resulting from an increased effect of disturbances on the signals in the closed loop.*" Irregularities in the track such as eccentricity and surface defects clearly constitute a challenge when it comes to system identification.

The above exposed arguments suggest that identification in closed loop in CD-players is not without expenses. In [de Callafon *et al.*, 1993] (and references therein) it is stated that the best model for control design cannot be derived from open loop experiments alone, with a CD-player as control example. A nominal model is estimated and the uncertainty bounds are provided. It is mentioned that these uncertainties are kept small in the closed loop frequency domain of interest, namely around the cross-over frequency. However, since it is desired in the present Ph.D. dissertation to have a controller strategy, which permits to reduce the bandwidth of the controller eventually down to 0[Hz] in the case of serious surface defects as suggested in Chapter 8, open loop identification should also be considered. Nevertheless system identification (and parameter estimation) has traditionally been performed in closed loop in CD-players (see for example [Steinbuch and Norg, 1998, Pintelon *et al.*, 1992, van Donkelaar *et al.*, 1995] and two Ph.D dissertations [Dötsch, 1998, Dettori, 2001]) and recently also in DVD-players [Filardi *et al.*, 2002]. While some stated prudently that the dynamics were very hard to measure in open loop, others claimed that it was not possible to perform open loop measurements of the dynamics. A peculiarity of the CD-players is that the focus

point should be in the working area of the photo diodes in order to retrieve meaningful information from the generated feedback signals. Without a focus and a radial controller, it is a difficult task to maintain the focus point in the working area of the photo diodes, since the slightest perturbation will bring the focus point out of said working area. In [Vidal *et al.*, 1998] the dynamics are measured in open loop by means of periodic excitation but the employed method was cumbersome and not highly reliable. A more reliable alternative, but certainly technically more complicated, is performed in [Yeh and Pan, 2000] where the open loop characteristics are measured by using a laser Doppler vibrometer. In the following, it is explained how parameter estimation can be performed in a combined open loop (in a simple and reliable way) and closed loop method with periodic excitations.

4.3.1 Parameter Estimation in Open Loop

The operating range of the photo diodes is limited to a few micrometers, beyond that limit, the signals from the photo diodes are virtually useless, therefore without feedback control, parameter estimation is not feasible based on the feedback error signals. However, by inserting a known resistance, r, in series connection with the coil of the actuator, the current through the coil can be indirectly measured, as depicted in Figure 4.2 ([Vidal *et al.*, 2001d]).
$u(s)$[V] is the input signal to the actuator and $x'(s)$[m] and $x(s)$[m] are the positions of respectively the arms and the lens. It is desired to estimate the parameters of the transfer function,

$$\frac{x(s)}{u(s)} = \frac{\frac{Bl}{m(R+r)}}{s^2 + (\frac{b}{m} + \frac{(Bl)^2}{m(R+r)})s + \frac{k}{m}} \text{ [m/V] .} \tag{4.16}$$

If instead $\frac{v_r(s)}{u(s)}$ is identified, information of all the parameters can be retrieved thanks to the provided feedback by Bl[N/A] (also known as *back emf*). Whether it can be applied to other optical disc drives, like DVD-drives, depends on the specific dynamic characteristics of the $\frac{v_r(s)}{u(s)}$ transfer function. In the case of the CD-drives used in the work of this Ph.D. dissertation, it is found that only the parameters involved in the dynamics of the first resonance peak can reliably be identified and not the parameters concerning the parasitic mass-spring subsystem. The frequency response of $\frac{v_r(s)}{u(s)}$ in the focus actuator is basically flat with one significant peak at around 30[Hz] (50[Hz] in the radial case). The parasitic subsystem is highly damped and the manifestation in $\frac{v_r(s)}{u(s)}$ is virtually non existent. Therefore the parasitic subsystem around 500[Hz] for focus (and 800[Hz] in the radial case) is identified in closed loop.
The transfer function $\frac{v_r(s)}{u(s)}$ is consequently reduced to

$$\frac{v_r(s)}{u(s)} = \frac{\frac{r}{R+r}(s^2 + \frac{b}{m}s + \frac{k}{m})}{s^2 + (\frac{c}{m} + \frac{(Bl)^2}{m(R+r)})s + \frac{k}{m}} \tag{4.17}$$

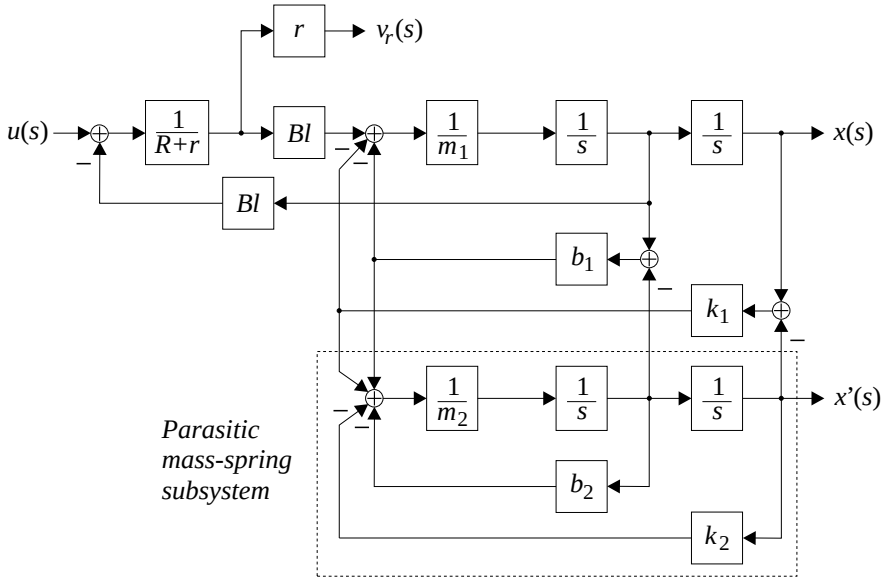

Figure 4.2: *State space diagram of the positioning loop. See Figure 3.10 for the corresponding translational system. The inserted resistance r, in series with the moving coil, allows to perform open loop system identification in CD-drives.*

which is equivalent to merging the two masses m_1[Kg] and m_2[Kg] into one, m[Kg]. Following substitutions are then made

$$m = m_1 + m_2 \qquad k = \frac{k_1 + k_2}{k_1 \cdot k_2} \qquad b = b_1 + b_2. \tag{4.18}$$

The corresponding translational diagram is shown in Figure 3.7 in the previous chapter. $\frac{v_r(s)}{u(s)}$ has consequently the following rational structure

$$A \cdot \frac{s^2 + a_1 s + a_2}{s^2 + b_1 s + b_2}. \tag{4.19}$$

It is now assumed that the mass of the optical pickup does not have an appreciable variation during production and along the life-time of the CD-player and that the measurement resistance, $r[\Omega]$, is well-known. Moreover, it is assumed that $a_2 = b_2$, which implies that $\frac{v_r(j\omega=0)}{u(j\omega=0)} = \frac{v_r(j\omega=\infty)}{u(j\omega=\infty)}$. Under these assumptions, the physical parameters, $R[\Omega]$, b[N·s/m], k[N/m] and Bl[N/A], which are subjected to both variation in production and change along the life-time of the CD-drive, can be estimated by the following expressions

$$R = \frac{r \cdot (1 - A)}{A} \ [\Omega] \ , \tag{4.20}$$

$$b = m \cdot a_1 \ [\text{N·s/m}] \ , \tag{4.21}$$

$$k = m \cdot a_2 \ [\text{N/m}] \ , \tag{4.22}$$

$$Bl = \sqrt{m \frac{r}{A}(b_1 - a_1)} \ [\text{N/A}] \ . \tag{4.23}$$

Thus the parameters of Equation 4.16 has been indirectly estimated.

4.3.2 Parameter Estimation in Closed Loop

While in open loop the only input to the system to be estimated is the excitation signal, in a closed loop configuration, the excitation signal is superimposed with the control signal. The principle is depicted in Figure 4.3.

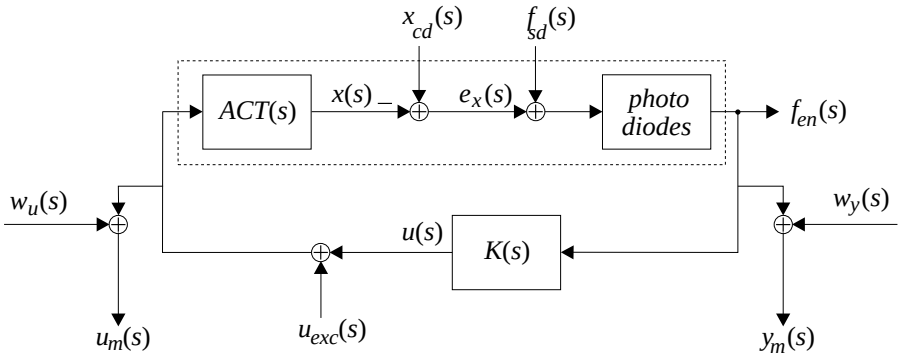

Figure 4.3: *Periodic excitation in the focus closed loop of a CD-player (the same principle applies to the radial closed loop).*

The controller $K(s)$ is in charge of generating a control signal $u(s)$[V] such that the feedback error signal $f_{en}(s)$[V] is minimized. Supposing that there are no surface defects, $f_{sd}(s)$=0[m], it necessarily implies that the position of the focus point $x(s)$[m] matches the position of the information layer $x_{cd}(s)$[m] in the focus direction. For identification purposes, an excitation signal $u_{exc}(s)$[V] is superimposed with the control signal and the closed loop is therefore excited with the frequency of the excitation signal. In order to estimate the gain and phase of the dynamics in $ACT(s)$ at the excitation frequency, the amplitude ratio and phase-shift between the measured output $y_m(s)$[V] and the measured input $u_m(s)$[V] are determined. A direct consequence of performing the identification in closed loop is that the measured signals have certain unwanted

components compared to the open loop identification, as shown in Equations 4.24 and 4.25

$$u_m(s) = u_{exc}(s) + w_u(s) + u(s) \ \text{[V]} \ , \tag{4.24}$$

$$y_m(s) = w_y(s) + f_{en}(s) \ \text{[V]} \ . \tag{4.25}$$

The presence of the control signal $u(s)$[V] and the feedback error signal $f_{en}(s)$[V] is namely not desired in the measured signals. Furthermore, there are two other disturbances impinging the closed loop, the position of the information layer in the focus direction, $x_{cd}(s)$[m] and surface defects $f_{sd}(s)$[m]. Hence the reliability of the identification in closed loop in terms of parameter estimation accuracy is diminished compared to the open loop identification given that the same excitation signals are employed. With this approach it should also be clear that the identified system is composed by the dynamics of the actuator, described by $ACT(s)$, plus the optical gain of the photo diodes. In order to estimate only $ACT(s)$, the optical gain must be estimated separately, a procedure which is explained in the next section.

It is known from Subsection 3.6.2 that the dynamics of the actuator around 500[Hz] in focus (800[Hz] in the radial case) can be approximated to a complex conjugate pole pair and a complex conjugate zero pair. After having identified the parameters R[Ω], Bl[N/A], k[N/m] and b[N·s/m] with the open loop method, the task to do now is to distribute m_1[Kg], m_2[Kg], k_1[N/m], k_2[N/m], b_1[N·s/m] and b_2[N·s/m] such that the identified parasitic dynamics in closed loop are fitted. In that way the parameters which describe the parasitic dynamics can be estimated.

4.4 Estimation of Optical Gain

In simple control loop configurations in CD-players, the optical gain alone has little practical value. Instead it is more important to know the gain around the cross-over frequency. In the start-up sequence a wobble signal is injected, centered at the cross-over frequency, which serves as input signal to the automatic gain controller (AGC) [Bierhoff, 1984]. The purpose of the AGC is therefore to compensate for different disc reflection gains and hardware tolerances in the focus and radial loop. However, the optical gain alone has a value for the designer at the time of analyzing the feedback error signals. While volts or amperes may say little about how far the focus point is from the track, micrometers have a straightforward physical interpretation in this case. The normalized and unnormalized optical gains are calculated by analyzing the linear slope of the photo diodes characteristics.

4.4.1 Focus Optical Gain Estimation

In Figure 2.8 of Subsection 2.4.3 the optical characteristics of the astigmatic and single Foucault methods are sketched. Although theoretically they have certainly a different appearance, in practice the characteristics of the single Foucault method approach the astigmatic's. The characteristics of the generated focus error by this kind of hologram lasers are commonly referred to as the "s-curve" and the distance between the lowest and the highest spike is specified by the optical pickup manufacturers (in this case the distance from the lowest to the highest spike is specified to 12[μm]). By applying a ramp signal to the focus coil and measuring the photo diode signals, the s-curve can be registered and the optical gain in the linear area can be calculated. The experiment must be realized with a fixed disc.

4.4.2 Radial Optical Gain Estimation

From Section 2.4 it is known that when the focus point is centered on the track, the amount of reflected light to the radial diodes is lower than in an off-track situation. As virtually all CDs have a certain degree of eccentricity, the following experiment can be carried out to estimate the radial optical gain. The focus loop is activated while the CD is spinning. The radial loop is not engaged. Due to the eccentricity, the optical pickup will register the tracks passing sideways. The photo diodes in the radial loop generate as a consequence a sinusoidal signal where the positive zero-crossings correspond to the center of the track and the negative zero-crossings correspond to the center between two adjacent tracks. Since the tracking-pitch is specified to 1.6[μm] (see Table 2.1), the radial optical gain can be calculated in a similar way as the focus optical gain.

4.5 Linearity Analysis

Before proceeding with the identification experiments it is necessary to establish whether the system can be considered linear across the desired operating range. One of the simplest techniques to establish the linearity of a system is to inject a series of single sine waves of increasing amplitudes and analyze for signs of distortion on the output signal as commented in [Evans *et al.*, 1994]. Another method commented in the same reference, which is more involved but faster, relies on the excitation of the system by using a wide-band multisine and by analyzing the degree of distortion of the frequency response function. The sources of nonlinearities in CD-drives are mainly mechanical, due to the construction characteristics of the 2-axis devices, and optical, caused by the characteristics of the photo diodes. In the case of the treated CD-drives in this thesis, the optical nonlinearities are far more dominant, therefore the dynamic model of such CD-drives can be considered to be a Wiener type model, where the nonlinearity from the optics follows the linear subsystem which describes the movement of the pickup. As explained in the previous section, the photo diode characteristics can easily be identified

by the suggested methods, so the nonlinearities can be considered as well-known. Hence the aim in the sequel is to determine whether the identification experiments are performed in the linear area, and not to find the limits of the linear operating range.

One of the advantages of frequency domain identification is that the effects of nonlinearities can be detected by the presence of output harmonics in addition to those present in the input signal, thus the proposed periodic excitation method to identify the parameters in the CD-drives is well-suited to perform such linear analysis. A widely known measure to establish the degree of nonlinear distortion in the music field is the Total Harmonic Distortion (THD). The THD is the percentage ratio of the root mean square (rms) voltage of all harmonics components above the fundamental frequency to the rms voltage of the fundamental

$$\text{THD} = \sqrt{\frac{\sum_{n=1}^{\infty} V_n^2}{V_1^2}} \cdot 100[\%]. \tag{4.26}$$

In practice, the first few harmonics are sufficient to calculate the THD. In the experiments it will only be used to give a qualitative evaluation: if the input and output have approximately the same level of THD, the identification experiments on the system will be considered to be performed in the linear operating range.

4.6 Experimental Results

The above presented methods have been applied in the laboratory to the focus and radial loop of the 12 CD-drives. The results can be divided in four parts: Open loop, closed loop, optical gain and linearity analysis results, described in the following subsections. It is anticipated that the methods worked properly in all the CD-drives. Only the results of specific drives are included in this section in order to better illustrate determined characteristics.

4.6.1 Open Loop Results

According to the data sheet of the CD-drives, the resonance frequency in the focus actuator is around 30[Hz] and in the radial case around 50[Hz]. A frequency range from 10[Hz] to 50[Hz] in focus (10[Hz] to 100[Hz] in the radial case) is therefore considered as sufficient in order to capture the relevant dynamics with a linear frequency step of 0.1[Hz] to give fine resolution. The measurement resistance, $r[\Omega]$, is inserted in series with the actuator coil and is used to indirectly measure the current through the coil. A low measurement impedance results in a poor signal/noise ratio, whereas a high impedance gives a high signal/noise ratio and biases the parameter estimation. $r = 1[\Omega]$ was chosen to be an acceptable value, which in practice, after soldering resulted in a total added resistance of approx. $r = 1.25[\Omega]$. As a consequence of the added resistances in

the focus and radial moving coils, their resonance frequencies were respectively shifted with -1[Hz] and -2[Hz]. At the time of control, the appropriate is therefore to keep the measurement resistance $r[\Omega]$ soldered since the estimated parameters have been slightly biased by the insertion of $r[\Omega]$.

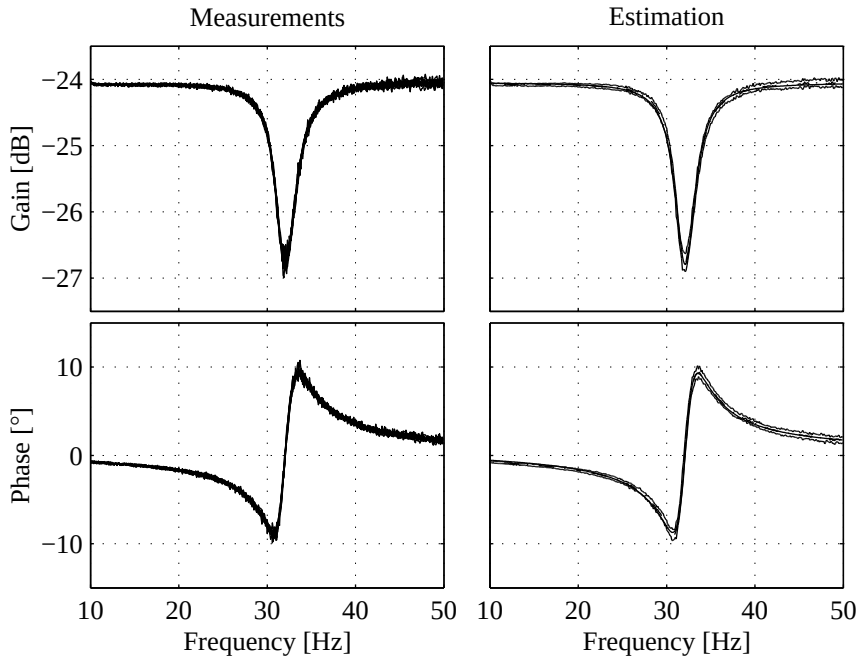

Figure 4.4: *Measurements of the bode plot of CD1-drive to the left. 10 measurement points are shown in the figure for every 0.1[Hz]. The estimated bode plot together with the 99% confidence interval is shown to the right.*

24 bode plots were obtained in the experiments, 12 focus and 12 radial bode plots and Figure 4.4 shows the bode plot of the focus CD1-drive. The measured bode plot is shown at the left part, where for each frequency step, 20 periodic excitations were injected. Only the last 10 periods were employed to estimate the steady-state response in order to let the transients die out. The plots have been corrected with the gains of the power drive, the attenuation and the amplification stages such that the shown bode plots correspond to the transfer function presented in Equation 4.17. The right part of Figure 4.4 shows the estimated bode plot together with its 99% confidence interval. In Section 4.2, in relation with the estimation of the confidence interval, it was assumed that $\sigma_r^2 = \sigma_c^2$ and that they were independently distributed. These assumptions were checked and it could be concluded that they were realistic.

In order to calculate the parameters of the system, the estimated transfer function is fitted using the MATLAB script `fitsys.m` provided by the *μ-Analysis and Synthesis Toolbox*. The fitted bode plot is not shown as it is not discernable from the estimated bode plot. From the fitted bode plot, the parameters can be calculated and by allowing small variations in the parameters, the 99% confidence interval shown in the figure can be covered. This procedure has been performed for all CD-drives and the estimated parameters are shown in Table A.1 and A.2 in Appendix A.1. The tables are divided in three parts for each drive, where the estimated parameters from the open loop method are shown in the second part of the tables. For example, the estimated resistance $R[\Omega]$ of the focus actuator of CD1-drive is $R = 18.7[\Omega](1\%)$, where the percentage value in brackets gives the estimation accuracy with a 99% confidence interval. That is, it is 99% likely that the true value lies in an interval of 1% with respect to $R = 18.7[\Omega]$. The estimated values showed to have a high degree of accuracy. The only parameter which could easily be measured was the resistance, which is also included in the the first part of the tables denoted as $R_{meas}[\Omega]$. The difference between the estimated and measured resistances is in all 24 cases below 2%. Taking into account that the temperature in the room changes, the estimates of the resistance can be considered as highly accurate. In general, reliable results from the open loop method were achieved, the only parameter which showed to have a lower accuracy is the viscosity coefficient b[N·s/m] with an interval with respect to the estimated value of 5% accuracy in a 99% confidence interval. It must also be pointed out that the estimated AC-sensitivity Bl[N/A] of the radial actuator has been consistently below the minimum value specified by the data sheet of the CD-drives and the estimated AC-sensitivity of the focus actuator is generally in the lower end on the specified range. A low AC-sensitivity is manifested in the bode plot as a lower resonance frequency. As mentioned before, this is the expected consequence of adding a measurement resistance in series with the actuator coil.

4.6.2 Closed Loop Results

Both focus and radial loop were excited, not at the same time, with periodic signals from 100[Hz] to 2000[Hz] and with a linear frequency step of 2[Hz]. As in open loop, out of 20 periodic excitations only 10 are employed to estimate the steady-state response. Figure 4.5 shows the estimated and fitted bode plot of the radial loop of CD1-drive to the left, and the bode plot of the focus loop of CD12-drive is shown to the right.
It can be observed that the estimated and fitted radial bode plot have a high degree of similarity, except for a minor phase inconsistency at frequencies above the parasitic resonance. However, some estimated bode plots showed to have two and even three parasitic resonances. For example, the bode plot to the right, in Figure 4.5, shows two parasitic resonances very close to each other. In Subsection 3.6.2 of the previous chapter the moving mass of the optical pickup was considered to be divided in two: the mass of the objective m_1[Kg] and the total mass of the four arms m_2[Kg] which the

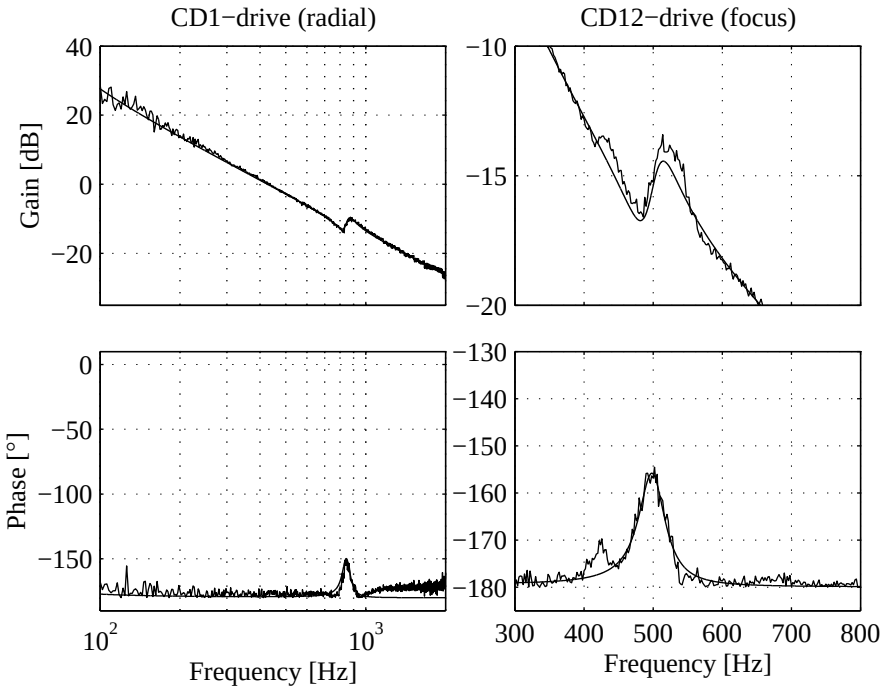

Figure 4.5: *Measurements of the open loop realized with the described closed loop method.*

objective is suspended on. If the flexible compound at the extremes of each arm exhibits different flexible characteristics, the proper would be to split m_2[Kg] into four masses, one of each arm. This mass split increases the order model from 4 to 10. Although for accurate simulation purposes it may be relevant, at the time of control the benefits of such detailed model would be questionable. In order to keep the model simple, it is chosen to model only one parasitic resonance. Generally, when there were multiple parasitic resonances encountered in the CD-drives, there was one which was dominant over the rest, and that is the one which is fitted. A side effect of the reduced order model is the difficulty of calculating the confidence intervals, since the fitted model should have the same order model as the model to be fitted. A visual check of the raw data from the experiments together with the 24 estimated and fitted bode plots revealed that the estimated parameters had a *reasonable* accuracy.

4.6.3 Optical Gain Results

Two experiments were performed, one to estimate the focus optical gain and the other to estimate the radial optical gain. The characteristics of the photo diodes related to the focus error generation can be obtained by applying a ramp signal to the actuator while keeping the disc fixed. Figure 4.6 shows the results of such experiment where the focus and radial sum have been scaled for the sake of clarity.

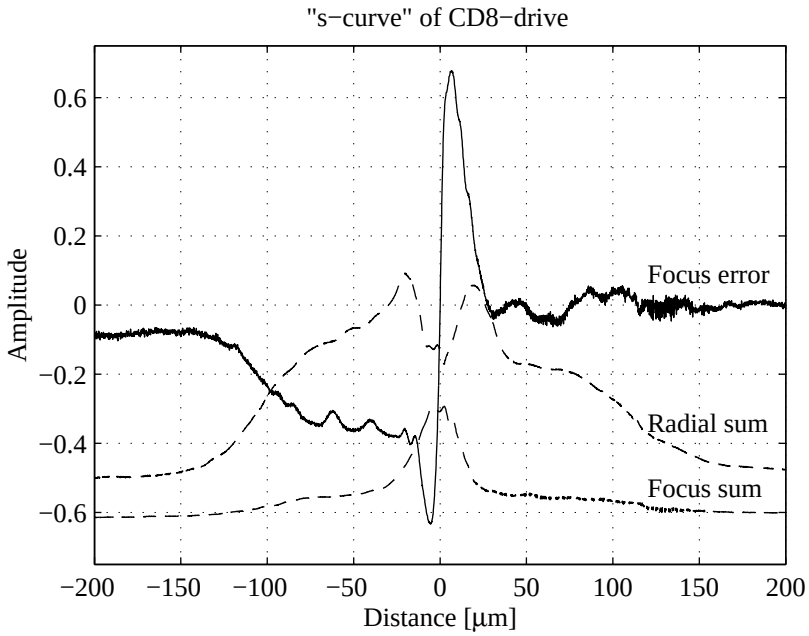

Figure 4.6: *Characteristics of the measured focus error versus distance (also referred to as "s-curve").*

It can be seen that the normalized focus error resembles the shape of an "s" as explained in Section 4.4. The distance from peak-to-peak according to the data sheet is specified to 12[μm] and the optical gain can therefore be calculated. The focus sum peaks approximately where the focus error is nearly zero, as expected. However, this is not the case for the radial sum, it experiences a sudden increase in magnitude and decreases afterwards as the objective moves gradually up to $\pm$150[μm]. The nature of this optical cross-coupling is found by a closer inspection of the physical arrangement of the photo diodes. Any focus error perturbs the radial sum, but not the radial error. As the radial sum is approximately constant in the linear area of the focus error, it is not chosen to take into account such optical cross-coupling. The estimated optical gains are presented in Table A.3 in Appendix A.1. By taking the lowest and highest optical gains

along the 12 CD-drives and calculating the average, the tolerance can be calculated. The maximum tolerance with respect to the average of the unnormalized gain K_{optF}[V/m] was calculated to be above 50%, whereas the maximum tolerance for the normalized gain K_{optFn}[units/m] was calculated to be below 20%. It explains why the normalized optical gain is preferred as the time of control: the optical tolerances are reduced.

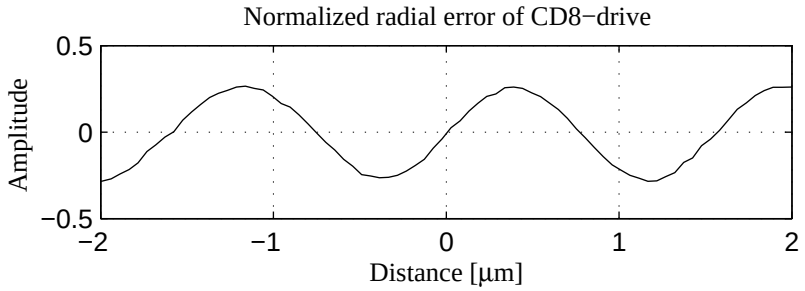

Figure 4.7: *Characteristics of the measured radial error. Note that the space between two adjacent tracks is approx. 1.6[μm], as specified in the Red Book.*

Figure 4.7 shows a sideways scan of three tracks of the disc as a result of the eccentricity of the disc while the radial loop is open and the focus loop is closed. Every positive zero-cross indicates the centre of each track. According to the Red Book, the distance between two adjacent tracks is 1.6[μm] and consequently the optical gain can be calculated. The estimated optical gains are presented in Table A.3 in Appendix A.1. As regards the unnormalized gain K_{optR}[V/m] the tolerance over the 12 CD-drives is nearly 30% while for the normalized gain K_{optRn}[units/m], the tolerance is around 10%, again it can be understood why the normalized optical gain is preferred. All the relevant parameters have now been estimated with respect to the fourth order model given in Equation 3.18 in Section 3.7 of the previous chapter. Figure 4.8 shows the resulting Nyquist plots of the 12 CD-drives where the parasitic resonances can be appreciated at the lower plots. The large oval shapes of the upper plots correspond to the resonance of the focus and radial loop respectively at 30[Hz] and 50[Hz].

4.6.4 Linearity Analysis Results

The open and closed loop experiments should be realized in the linear area along the frequency range such that reliable parameter estimates can be given. Figure 4.9 shows the results of the linearity analysis of CD1-drive, the other drives exhibited similar characteristics. In each quadrant two traces are showed: the THD level of the input signal is represented by a dashed line and the THD level of the output signal is represented by a solid line. Only the fundamental frequency and the first four harmonics are involved

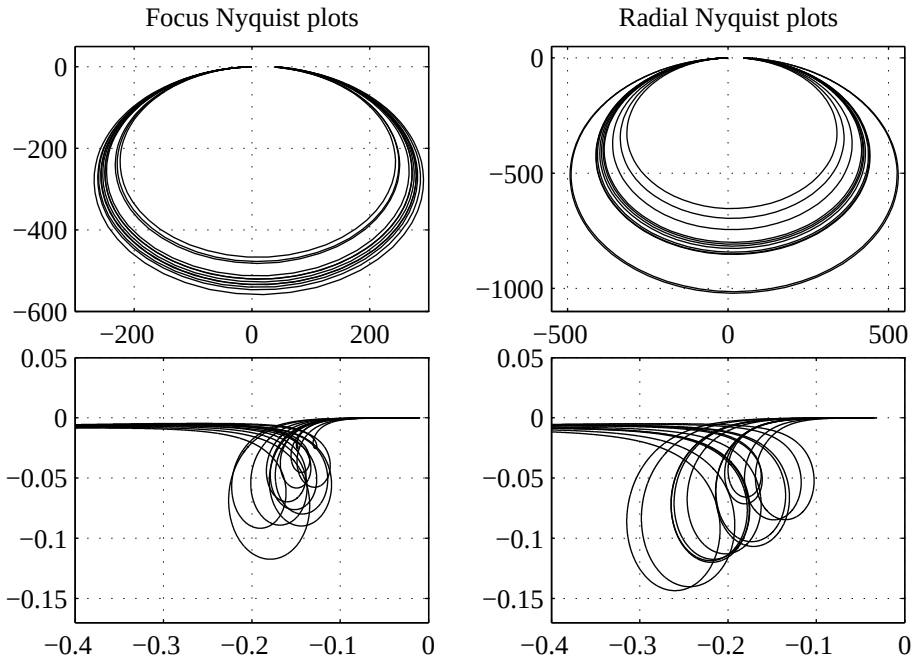

Figure 4.8: *Nyquist plots of the focus and radial loop. The two lower plots show a zoom-in of the parasitic resonances of the focus and radial actuators respectively at approx. 500[Hz] and 800[Hz].*

in the calculation of the THD. The amplitude of the harmonics decayed fast and above the fourth harmonic the contribution to the total THD level was not appreciable. As previously explained in Section 4.5, the aim of this analysis is to compare the THD between the input and output of the realized experiments. Note that there is basically no difference between the input and output THD level of the open loop experiments, shown in the two upper quadrants, which indicates that the dynamics of the CD-drive has been measured in the linear area.
The linearity results of the experiments performed in closed loop are shown in the two lower quadrants of the figure. While the THD level of the output signal is kept around 5%, the THD level of the input starts from approx. 100% and gradually decreases to the same level as the THD level of the output . Since the experiment is performed in closed loop, the periodic excitation signal is superimposed with the control signal which implies that even though the excitation signal itself does not lead to higher-order harmonics, the control signal has a contribution. As the THD level of the output is low (around 5%) the experiments are considered to be performed in the linear area of the CD-drives.

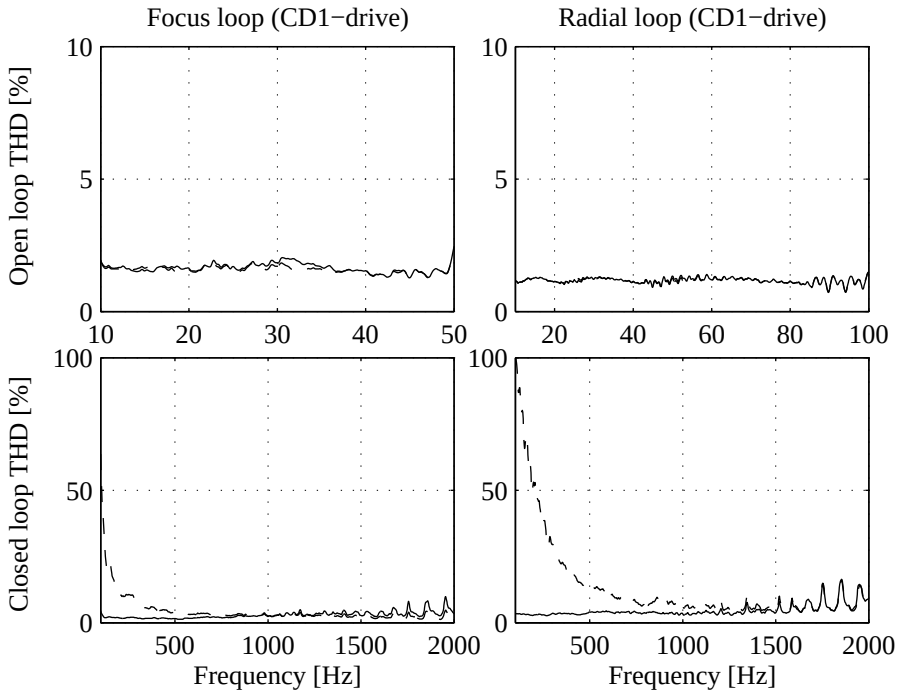

Figure 4.9: *Linearity analysis of the focus and radial THD level in open and closed loop of CD1-drive. The dashed line represents the THD level of the input while the solid line represents the THD level of the output.*

4.7 Conclusion

The main purpose of Chapter 4 was to identify the parameters (and dynamic characteristics) of the 12 CD-drives. Inspired by the method proposed in [Schoukens *et al.*, 1997], periodic excitation is also used in this chapter and it is showed how to apply it to CD-players. A novel method is suggested which makes it possible to identify certain parameters of CD-drives in open loop. A known resistance is inserted in series connection with the coil of the actuator such that the current through the coil can be measured indirectly and parametric identification can be performed [Vidal *et al.*, 2001d]. The estimated confidence intervals indicate that parameter estimates are highly reliable. Closed loop identification is performed as well to estimate the parameters related to the parasitic resonance. *Reasonable* estimates were achieved but no explicit confidence intervals were given since the chosen model to describe the parasitic resonance only could model one but not two or even three parasitic resonances present in the CD-drives. The optical gains were estimated too and showed the immediate advantage of the normalized optical gain

which significantly reduces the optical tolerances. The experiments unveiled also that there is a certain static optical cross-coupling between the focus and radial loop, but not of considerable magnitude. Finally a linearity analysis revealed that the experiments in open and closed loop were performed in the linear area of the CD-drives.

4.8 Summary

This chapter treated the parameter estimation of 12 CD-drives. A brief introduction to parametric identification was given in Section 4.1 where some of the most common parametric and nonparametric methods were shortly described. In Section 4.2 some essential characteristics of the periodic excitation method were explained and in 4.3 it was described how to apply the method to CD-drives in open and closed loop. The estimation of the optical gain was treated in Section 4.4 and in Section 4.5 it is suggested how to determine whether the periodic excitation method was realized in the linear area. The results of the optical gain estimation and the estimation of the CD-drive's parameters based on the periodic estimation method were presented in Section 4.6 and in Section 4.7 a conclusion was given.

Part II

Robust Control of Compact Disc Drives

5

Obtaining the Nominal and Uncertainty Models

Most control designs are based on the use of a design model which is simple enough to facilitate design, yet complex enough to give the designer confidence that the designed control, based on such model, will work on the true plant. The differences between the model and the modeled reality are often referred to as *uncertainty*. Obviously, uncertainties on the model are not desired and should be addressed in the design process to ensure certain immunity against their presence when the controller is implemented on the true plant. Mainly during the last two decades a wide range of design control methods have been developed, which provide such immunity against uncertainties. These methods are commonly known as *robust control* methods, which generally rely on complex mathematics. In a recent Ph.D. dissertation [Schønhoff, 2002] it is pointed out that the available literature and software related to robust control focuses almost completely on the mathematical controller synthesis, and when applied to practice, difficulties of numerical and methodical nature occur. Being aware of that problem, a continuous chain of tools making robust controller synthesis practically applicable is established in order to unburden the engineer. In the same reference, the modeling part is reduced to identifying the nominal model, the uncertainty model is assumed to be known. In a more realistic situation, the designer may not even have the uncertainty model available. In [Tøffner-Claussen, 1995] the *stochastic embedding approach* is suggested where, based

on certain stochastic assumptions, the nominal and the uncertainty models are generated. In the following, a different starting point is taken, namely that the designer only has a set of complex points in the Nyquist plane from several worst-case plants. Having a limited knowledge of the plant, it might not be trivial how to obtain a nominal and an uncertainty model suited for the $\mathcal{H}_\infty$-framework. In this chapter a method for obtaining such nominal and uncertainty models is presented. The $\mathcal{H}_\infty$-control concepts relevant to this chapter are introduced in Section 5.1. It should not be regarded as a self-contained introduction to $\mathcal{H}_\infty$-control. Interested readers are referred to [Zhou *et al.*, 1996] where the $\mathcal{H}_\infty$-control theory is treated, and [Skogestad and Postlethwaite, 1997] where the practical aspects of $\mathcal{H}_\infty$-control are covered. Three methods of obtaining the nominal and the uncertainty models are described in Sections 5.2, 5.3 and 5.4, which are based on different uncertainty representations. It is stressed that in this work, parametric uncertainty representation is referred to as uncertainty in the *physical* parameters of the plant. In Section 5.2 it is therefore assumed that the structure of the model and the uncertainty regions for each parameter is given. In Section 5.3 it is assumed that the nominal and the uncertainty models can be described by a rational transfer function and that the uncertainties are bounded. The uncertainties are based on a disc-shape representation (circles), thus only complex uncertainties are treated. In Section 5.4 an alternative and potentially less conservative method compared to the disc-shape representation is suggested, where the uncertainties are based on a "olympic stadium"-shape representation, also referred to as a mixed representation, since it requires both a complex and a real entity. The three methods are applied to the data from the 12 CD-drives obtained from Chapter 4 and the results are documented in Section 5.5 and discussed in Section 5.6. Finally a summary is given in Section 5.7.

5.1 Introduction to $\mathcal{H}_\infty$-control

During the 60's and 70's great attention was paid to uncertainty on the signals, represented as additive noise. LQG (Linear Quadratic Gaussian) optimal control is an approach based on such uncertainty representation. However, given a stable plant, additive noise cannot lead to instability, whereas e.g. parameter uncertainty can. Since LQG optimal control did not address uncertainty adequately, the focus was moved to other techniques which offered a more reliable representation of the uncertainties. It started in the 80's with the $\mathcal{H}_\infty$-optimization and led until today to different *robust control* methods, the most common of which are shown in Table 5.1. It should also be mentioned that many $\mathcal{H}_\infty$ control problems can be formulated in other frameworks, such as for example in terms of linear matrix inequalities (LMI). In [Dettori, 2001] it is shown how to apply LMIs to CD-players.

Before introducing the methods presented in Table 5.1 it is convenient to define four important concepts [Skogestad and Postlethwaite, 1997] and to describe the different types of disturbance representation:

- *Nominal stability (NS)*: the system is stable with no model uncertainty.
- *Nominal performance (NP)*: the system satisfies the performance specifications with no model uncertainty.
- *Robust stability (RS)*: The system is stable for all perturbed plants about the nominal model up to the worst-case model uncertainty.
- *Robust performance (RP)*: The system satisfies the performance specifications for all perturbed plants about the nominal model up to the worst-case model uncertainty.

				Structured uncertainty		
	Nominal performance	Robust performance	Unstructured uncertainty	Complex	Real	Repeated
Standard $\mathcal{H}_\infty$-optimization						
mixed-sensitivity $\mathcal{H}_\infty$-control	✓	(✓)	✓			
$\mathcal{H}_\infty$ loop shaping design	✓	(✓)	✓			
Non-standard $\mathcal{H}_\infty$-optimization (μ-synthesis)						
D-K-iteration	✓	✓	✓	✓		✓
(D,G)-K-iteration	✓	✓	✓	✓	✓	✓
(μ,D)-K-iteration	✓	✓	✓	✓	✓	✓

Table 5.1: Characteristics of certain controller synthesis methods in the $\mathcal{H}_\infty$-framework. The check marks in parenthesis indicate that robust performance can be achieved based on a rather conservative approach. μ-synthesis is taken as an example of non-standard $\mathcal{H}_\infty$-optimization.

5.1.1 Uncertainty Representation in $\mathcal{H}_\infty$-control

There are several factors which contribute to the uncertainty in the model due to e.g. linear approximation, neglected dynamics, inaccurate measurements, high frequency uncertainty, etc. The different sources of uncertainty can be divided in three groups:

- *Parametric uncertainty*: The structure of the model is known but some of the parameters are uncertain. It is assumed that each uncertain parameter is uncertain within some region $[\alpha_{\min}, \alpha_{\max}]$. The uncertain parameters can therefore be expressed as,

$$\alpha_p = \overline{\alpha}(1 + r_\alpha \delta) \qquad -1 \leq \delta \leq 1, \tag{5.1}$$

  where $\overline{\alpha}$ is the mean parameter value and $r_\alpha = \frac{\alpha_{\max} - \alpha_{\min}}{\alpha_{\max} + \alpha_{\min}}$ is the relative uncertainty in the parameter. δ is any real bounded scalar. Parametric uncertainty representation is a suitable choice if the parameter tolerances of a product are known. However, they are difficult to deal with mathematically and numerically, especially when it comes to controller synthesis. Often the real perturbation $-1 \leq \delta \leq 1$ is replaced by a complex perturbation $|\Delta(j\omega)| \leq 1$ which in the Nyquist plot describes a circle with center at $\overline{\alpha}$ and radius r_α. Obviously this is conservative since it introduces possible plants which are not present in the original set.

- *Neglected/unmodeled dynamics uncertainty*: The main source of uncertainty is the model itself which is a simplified description of the plant. The quantification of this kind of uncertainty is more difficult and is represented with complex perturbations such that the largest gain for any input direction in Δ is 1, $\|\Delta\|_\infty \leq 1$.

- *Lumped uncertainty*: It is a combination of the above mentioned uncertainty classes. The uncertainty description represents one or several sources of parametric and/or unmodeled dynamics uncertainty combined into a single lumped perturbation of a chosen structure. The frequency domain is also well suited for describing lumped uncertainty. There are several ways of describing these uncertainties, the most common of which is the multiplicative and additive uncertainty.

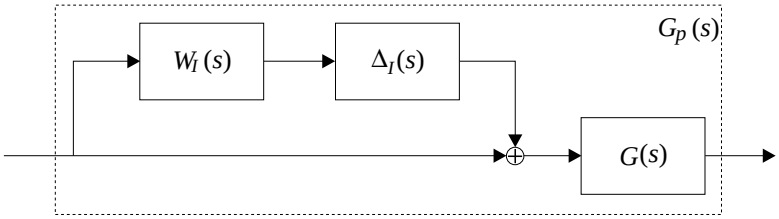

Figure 5.1: *Plant $G(s)$ with input multiplicative uncertainty $W_I(s)\Delta_I(s)$.*

Figure 5.1 shows the first case. The weight $W_I(s)$, usually chosen as a stable minimum phase transfer function, describes the uncertainty level along frequency. The perturbed plant is given by

$$\Pi_I: \quad G_p(s) = G(s)(1 + W_I(s)\Delta_I(s)); \quad \|\Delta_I\|_\infty \leq 1, \tag{5.2}$$

where $\Delta_I(s)$ is any stable transfer function with bounded $\mathcal{H}_\infty$-norm. Alternatively, if the uncertainty is desired to be expressed as additive uncertainty, the perturbed plant is described by

$$\Pi_A : \quad G_p(s) = G(s) + W_A(s)\Delta_A(s); \quad \|\Delta_A\|_\infty \leq 1, \tag{5.3}$$

where $\Delta_A(s)$ is again any stable transfer function with bounded $\mathcal{H}_\infty$-norm. Multiplicative weights are however preferred because their numerical value is more informative.

Once the uncertainties of the plant have been identified, they are *pulled out* into a block diagonal matrix

$$\Delta = diag\{\Delta_i\} = \begin{bmatrix} \Delta_1 & & & \\ & \ddots & & \\ & & \Delta_i & \\ & & & \ddots \end{bmatrix},$$

where each Δ_i represents a specific source of uncertainty, e.g. input uncertainty or parametric uncertainty.

Unstructured uncertainties

If the diagonal structure of the matrix Δ is ignored, then the uncertainty is considered to be an unstructured uncertainty where Δ is a *full* complex perturbation matrix. It is a way of getting a simple uncertainty model but it is potentially conservative particularly since non-physical couplings across the perturbation channels are introduced.

Structured uncertainties

Diagonal uncertainty usually arises from a consideration of uncertainty in the individual input channels like actuators or in the individual output channels like sensors. This type of diagonal uncertainty is always present and should be taken into account to reduce conservatism at the time of stability analysis (and controller synthesis). However, the mathematical tools necessary to handle structured uncertainties are more involved than those to handle unstructured uncertainties. Stability analysis is performed by means of a real non-negative function denoted μ (structured singular value), explained in Subsection 5.1.3.

5.1.2 Standard $\mathcal{H}_\infty$-optimization

The formulation of the standard $\mathcal{H}_\infty$ optimal control problem, see [Doyle *et al.*, 1989], makes use of the general control configuration in Figure 5.2, without uncertainties. The

exogenous inputs w, can be commands, disturbances and noise and the exogenous outputs z are the error signals to be minimized.

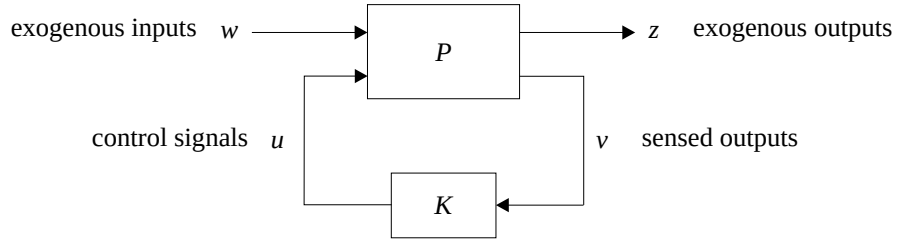

Figure 5.2: *General control configuration (without uncertainties).*

The overall control objective is to design a controller K which based on the sensed outputs v generates the control signals u such that some norm of the transfer function from w to z is minimized. In the case of the standard $\mathcal{H}_\infty$ optimal control problem, the selected norm to minimize is the $\mathcal{H}_\infty$-norm, see Equation 5.4

$$\|F_l(P,K)\|_\infty = \max_\omega \overline{\sigma}(F_l(P,K)(j\omega)), \tag{5.4}$$

where $F_l(\cdot,\cdot)$ stands for the lower LFT (Linear Fractional Transformation) and yields the transfer function from w to z as a result from wrapping K around the lower part of P. The standard $\mathcal{H}_\infty$ optimal control problem therefore minimizes the peak of the maximum singular value $\overline{\sigma}$ of $F_l(P(j\omega),K(j\omega))$, (for SISO systems it corresponds to the highest peak of the bode plot). In practice, it is usually not possible (and desirable) to obtain such optimal controller and a suboptimal is instead calculated [Doyle *et al.*, 1989]. Let $\gamma_{\min}$ be the minimum value of $\| F_l(P,K) \|_\infty$ over all stabilizing controllers K. Then the $\mathcal{H}_\infty$ sub-optimal control problem is to find all the stabilizing controllers K, such that

$$\|F_l(P,K)\|_\infty < \gamma \qquad \text{where } \gamma > \gamma_{\min} . \tag{5.5}$$

The synthesis of the controllers K involves the solution of two algebraic Riccati equations combined with the iterative reduction of γ. Mixed-sensitivity $\mathcal{H}_\infty$-control offers the possibility of specifying the desired sensitivity function $S = (I + GK)^{-1}$ together with other closed-loop transfer functions such as KS or the complementary sensitivity function $T = I - S$. In that way the designer can choose a suitable trade-off between e.g. the maximum allowed error at the output, weighted against the maximum allowed control effort such that the nominal performance is achieved. The expression to minimize would then be

$$\left\| \begin{bmatrix} W_1 S \\ W_2 K S \end{bmatrix} \right\|_\infty , \tag{5.6}$$

where $W_1(s)$ and $W_2(s)$ are the performance weights chosen by the designer. An alternative approach is the $\mathcal{H}_\infty$ loop shaping design where the singular values of the plant P are shaped to give a desired open-loop shape. In the first step a pre- and postcompensator W_1 and W_2 are combined to form the plant $P_s = W_2 P W_1$. Then the resulting shaped plant P_s is robustly stabilized using $\mathcal{H}_\infty$-optimization. The final feedback controller K is then constructed by combining the $\mathcal{H}_\infty$-controller K_∞ with the shaping functions W_1 and W_2 such that

$$K = W_1 K_\infty W_2. \tag{5.7}$$

The advantage of this method is that no uncertainty modeling or weight selection is required in the second step.

All the above mentioned methods ensure nominal performance and can only handle unstructured uncertainties. Robust performance can also be guaranteed in a rather conservative way. For complex problems, where it is desired that the synthesized controller meets certain robust performance requirements and where at the same time uncertainties are handled in a less conservative fashion, more advanced techniques are necessary, described in the following subsection.

5.1.3 Non-standard $\mathcal{H}_\infty$-optimization (μ-synthesis)

Figure 5.3 shows the general control configuration with the controller K, the plant P and the uncertainty Δ. However, controller synthesis based on this configuration is still an unsolved problem, instead certain approaches are employed to synthesize a robust controller, described later this section.

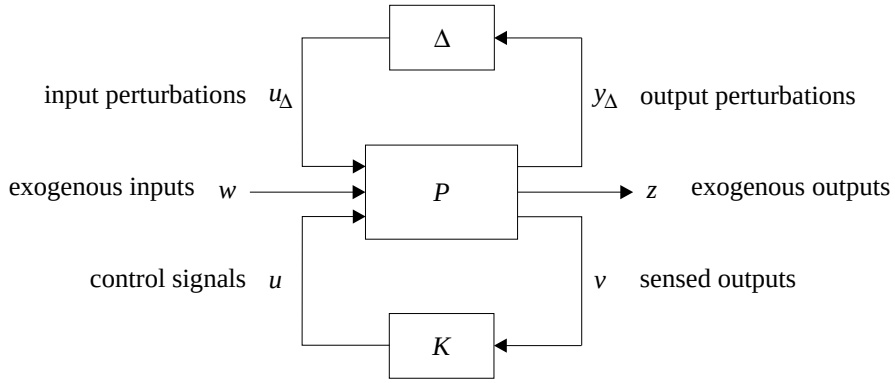

Figure 5.3: *General control configuration (for controller synthesis).*

The nominal closed loop system is given by the following lower LFT

$$N = F_l(P, K) \triangleq P_{11} + P_{12}K(I - P_{22}K)^{-1}P_{21}. \tag{5.8}$$

The lower LFT yields the closed loop transfer function of the generalized plant P and the generalized controller K. To analyze robust stability, the system is rearranged into the $M\Delta$-structure shown in Figure 5.4, where $M = N_{11}$ is the transfer function from the output to the input of the perturbations which are assumed to be bounded satisfying $\|\Delta\|_\infty \leq 1$. According to the *small gain theorem* (see for example [Zhou *et al.*, 1996]), robust stability of the $M\Delta$-structure is guaranteed if $\overline{\sigma}(M(j\omega)) < 1 \quad \forall\omega$, equivalent to requiring that $\|M\|_\infty \leq 1$.

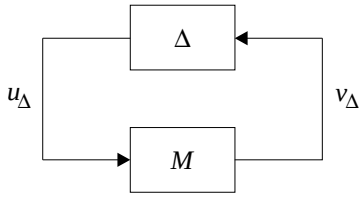

Figure 5.4: *$M\Delta$-structure for robust stability analysis.*

The question is whether some advantage can be taken given the fact that $\Delta = \text{diag } \{\Delta_i\}$ is structured to obtain a tighter RS-condition. The structured singular value μ is part of the answer to that question. μ is defined as

$$\mu(M)^{-1} \triangleq \min_{\Delta}\{\bar{\sigma}(\Delta) | det(I - M\Delta) = 0 \text{ for structured } \Delta\}.$$

That is, first the smallest structured Δ is found, measured in terms of $\overline{\sigma}(\Delta)$, which makes $det(I - M\Delta) = 0$, then $\mu(M) = 1/\overline{\sigma}(\Delta)$. In other words, μ is the reciprocal of the smallest perturbation which makes the system unstable. The value of μ is restricted by the following two bounds

$$\rho(M) \leq \mu(M) \leq \overline{\sigma}(M). \tag{5.9}$$

The lower bound, $\rho(M)$ (the largest of the absolute values of the eigenvalue in M, also called *spectral radius*) is achieved in the case of repeated scalar complex perturbations, whereas for *full* block complex perturbations μ attains the upper bound, $\overline{\sigma}(M)$. Obviously these bounds alone are not sufficient to provide a less conservative analysis because the gap between ρ and $\overline{\sigma}$ can be arbitrarily large. Unfortunately the calculation of μ with either pure real or mixed real/complex uncertainties is proved to be a NP (Nondeterministic Polynomial-time)-hard problem [Braatz *et al.*, 1994]. Only in a few cases the upper bound is guaranteed to be equal to μ [Balas *et al.*, 1993]. To calculate μ exactly it is required an exhaustive examination of all possibilities, also known as "brute force" method. In order to provide tighter bounds than the shown in Equation 5.9, both M and Δ can be pre- and postmultiplied by block-diagonal scaling matrices

$D = diag\{d_i I_i\}$ which do not affect $\mu(M)$ but which do affect ρ and $\overline{\sigma}$. Therefore the new matrices are $M = DMD^{-1}$ and $\Delta = D\Delta D^{-1}$. The *μ-Analysis and Synthesis Toolbox* of MATLAB provides a script `mu.m` which, with the default setup, computes the lower bound using the power method [Packard *et al.*, 1988, Young and Doyle, 1990a] and the upper bound is computed based on a balance technique [Fan *et al.*, 1991].

The machinery to handle structured uncertainties (non-standard $\mathcal{H}_\infty$-optimization) is far more complicated than the one needed to handle unstructured uncertainties (standard $\mathcal{H}_\infty$-optimization) but the conservatism is reduced, implying higher controller performance. μ-synthesis methods are developed to synthesize robust $\mathcal{H}_\infty$ performance controllers under consideration of structured uncertainties. At present, there is no direct method to synthesize a μ-optimal controller based on Figure 5.3.

The DK-iteration is an established technique which considers complex uncertainties. It combines $\mathcal{H}_\infty$-synthesis and μ-analysis. The idea is to find the controller that minimizes the peak value over frequency of the upper bound

$$\min_K(\min_{D\in\mathcal{D}} \|DN(K)D^{-1}\|_\infty),$$

by alternating between minimizing $\| DN(K)D^{-1} \|_\infty$ with respect to either K or D (while holding the other fixed), hence the name DK-iteration. Although the minimization steps are convex, joint convexity is not guaranteed and therefore the iterations may converge to a local minimum. However, practical experience suggests that the method is numerically efficient and reliable. In the case of dealing with a combination of complex and real uncertainties, or just real uncertainties, the DK-iteration is conservative in that real perturbations $-1 \leq \Delta \leq 1$, are replaced by complex perturbations $|\Delta(j\omega)| \leq 1$, thus possible plants which are not present in the original set are introduced. The (D,G)-K-iteration exploits not only the block-diagonal structure of the perturbations with D-matrices but also exploits the structure of the real perturbations with G-matrices. The D-scalings only need to be fit in magnitude whereas the G-scalings need to be fit both in magnitude and phase, which ask for high order filter structures. As the order of the filter, which fits the G-scalings, adds to the order of the controller K, the final controller is usually of elevated order. An alternative approach involving a series of scaled DK-iterations is the (μ,D)-K-iteration method *which sacrifices some of the guaranteed convergence properties of the (D,G)-K-iteration, but which on the other hand only requires that scalings are fitted in magnitude*, [Tøffner-Claussen, 1995].

5.2 Uncertainty Representation: Parametric

Changes in the material properties employed in the systems to be produced create evidently variations of the parameters over the different systems. Assuming that the structure of the mathematical model, which describes the system in a reliable way is known

and that the information of the parameter uncertainties is available, the formulation of the parametric uncertainty representation is relatively easy. Although it is not sure which values of the parameters better describe the nominal model, a common approach is to take the average of the extrema of the uncertainty region as the nominal parameter [Skogestad and Postlethwaite, 1997]. A natural way of formulating the parametric uncertainty representation in the μ-framework is by means of LFTs. In the following example it is assumed that there are two uncertain parameters α and $1/\beta$, each lies within its corresponding uncertainty region $[\alpha_{\min}, \alpha_{\max}]$ and $[\beta_{\min}, \beta_{\max}]$. The uncertain (perturbed) parameters can be expressed as

$$\alpha_p = \overline{\alpha}(1 + r_\alpha \delta_\alpha) \qquad -1 \leq \delta_\alpha \leq 1, \tag{5.10}$$

$$\frac{1}{\beta_p} = \frac{1}{\overline{\beta}(1 + r_\beta \delta_\beta)} \qquad -1 \leq \delta_\beta \leq 1, \tag{5.11}$$

where $\overline{\alpha}$ and $\overline{\beta}$ are the mean parameter values and $r_\alpha = \frac{\alpha_{\max} - \alpha_{\min}}{\alpha_{\max} + \alpha_{\min}}$ and $r_\beta = \frac{\beta_{\max} - \beta_{\min}}{\beta_{\max} + \beta_{\min}}$ are the relative uncertainties in the parameters.
The LFT representation is achieved by a rearrangement of the terms

$$\alpha_p = \overline{\alpha}(1 + r_\alpha \delta_\alpha) = \overline{\alpha} + \overline{\alpha}\delta_\alpha r_\alpha = F_u(M_\alpha, \delta_\alpha), \tag{5.12}$$

$$\frac{1}{\beta_p} = \frac{1}{\overline{\beta}(1 + r_\beta \delta_\beta)} = \frac{1}{\overline{\beta}} - \frac{r_\beta}{\overline{\beta}} \delta_\beta (1 + r_\beta \delta_\beta)^{-1} = F_l(M_\beta, \delta_\beta), \tag{5.13}$$

implying that M_α and M_β are equal to

$$M_\alpha = \begin{bmatrix} 0 & r_\alpha \\ \overline{\alpha} & \overline{\alpha} \end{bmatrix} \qquad M_\beta = \begin{bmatrix} \frac{1}{\overline{\beta}} & -\frac{r_\beta}{\overline{\beta}} \\ 1 & -r_\beta \end{bmatrix}. \tag{5.14}$$

Figure 5.5 gives a graphical representation of these two LFTs. The uncertainties are *pulled out* into the block diagonal matrix Δ and the modules M_α and M_β are connected to the proper locations of the system which α and $\frac{1}{\beta}$ belong to.
One of the main disadvantages of dealing with real uncertainties is the numerical reliability problems which they cause when computing μ. The function μ is not guaranteed to be continuous and the upper bound may not even converge to the true value of μ [Packard and Pandey, 1993]. In the same reference, the continuity of μ is recovered by adding small complex quantities to the real uncertainties. However, in practice, real uncertainties do not appear alone. In the μ-framework, complex uncertain blocks also arise for problems of robust performance, and thus practical applications on μ always involve at least one complex block and the function μ will be continuous at the problem data.

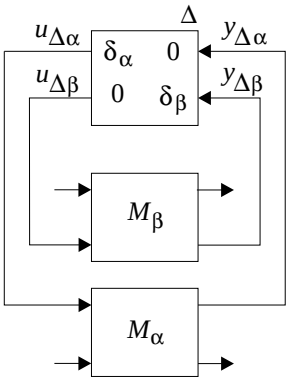

Figure 5.5: *LFT representation of parametric uncertainties.*

5.3 Uncertainty Representation: Complex

Extensive literature can be found explaining how to formulate multivariable robustness problems but usually the nominal and the uncertainty models are assumed to be known. In a more realistic situation, the designer may only have measurement data composed by a set of complex points in the Nyquist plane from several worst-case plants. Having a limited knowledge of the plant, it might not be trivial how to obtain a nominal and a uncertainty model suited for the robust control framework.

5.3.1 Finding the First Set of Circles

A possibility to obtain the nominal and the uncertainty models, the one studied in this section, is to circumscribe the set of complex points of the different plants with minimal area circles at each frequency point, (the MATLAB script `circumscribe.m` which finds such minimal area circles given a set of points is developed by J. Stoustrup). The nominal model is obtained by fitting a rational transfer function to the center of the circles. Figure 5.6 gives a schematic representation of the steps necessary to calculate the minimal area circles which circumscribe all the measurement points at each frequency point. First the geometric center C_1 is found, and a circle with radius given by the most distant point P_1, in the set from the current center, is computed (see upper left quadrant of Figure 5.6). A fictitious line is now traced from the center C_1 to the most distant point P_1 and the circle is shrunk by moving its center along the fictive line towards the point P_1 until another point P_2 is met (see upper right quadrant). A new circle is obtained with center at C_2. The algorithm enters now in the main loop with P_1 and P_2 as the original points . The perpendicular bisector of the points P_1 and P_2 is calculated, which has the property of containing the center C_2 and it intersects the line P_1P_2 at the midpoint B_1. Another fictive line is traced from the center C_2 to the midpoint B_1 and the circle is

shrunk by moving its center along the fictive line towards the point B_1 until another point P_3 is met (see lower left quadrant). Now it is necessary to analyze whether the circle in question is the minimal area circle. Having a triangle described by the points P_1, P_2 and P_3, there is a unique circle that passes through each of the vertices of the triangle, namely the *circumcircle*. Its center, also called *circumcenter* has the property of being the intersection of the three perpendicular bisectors. This is checked by calculating the line-line angles $\angle P_2P_1 - P_3P_1$ and $\angle P_1P_2 - P_3P_2$. If any of the points P_1 and P_2 does not form an acute angle with the two other points, then that point (P_1 or P_2) is discarded in favour of the new point P_3. The main loop starts again, now with the original points P_1 or P_2 and P_3. The loop continues until a valid circumcenter is found (see lower right quadrant). The loop will also stop if the line P_1P_2, in the process of shrinking the circle, becomes the diameter of the circle.

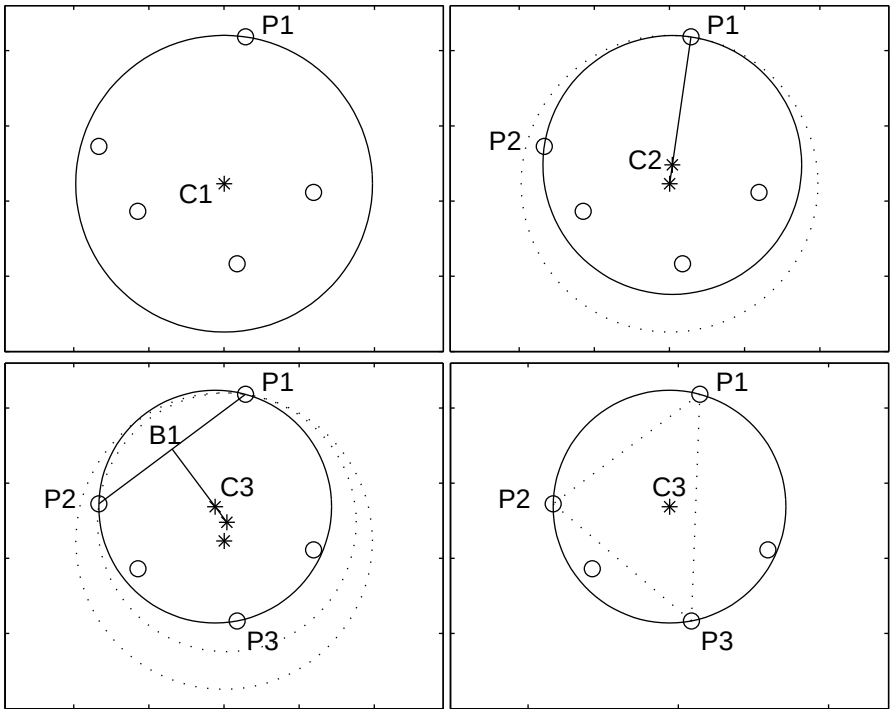

Figure 5.6: *Finding the first set of circles which describe the nominal model. Read text for the explanation of the algorithm.*

5.3.2 Finding the Second Set of Circles

Once the first set of circles is found by means of the described method, a rational transfer function is fitted to the center of the circles. As a result of the fit, the center of the circles will not necessarily coincide with the nominal model and therefore a second set of circles must be found. Since the center is given by the nominal model, the second set of circles is now found by expanding the circles until the most distant point is met. From this set of circles, the additive and multiplicative uncertainty models can be derived. The multiplicative uncertainty models are obtained by "dividing" the second set of circles by the nominal model frequency point by frequency point, (the additive uncertainty can be obtained by subtracting the nominal model from the second set of circles). In order to find the multiplicative complex uncertainty weight, $W_c(s)$, a rational transfer function is fitted to the radii of the circles. Only magnitude is fitted as the phase is not relevant for complex uncertainties.

Method based on Circles

To summarize, the method for obtaining the nominal and the uncertainty models by means of choosing the smallest circles is given below:

1. Find the 1st set of smallest circles at each frequency point which contains all the Nyquist points from the measurement set.
2. Fit a rational transfer function to the center of the 1st set of circles yielding the nominal model $G(s)$.
3. Find the 2nd set of smallest circles with center described by $G(s)$, containing at the same time all the obtained points at the corresponding frequency point.
4. To derive the multiplicative uncertainty, "divide" the set of circles by the nominal model (the additive uncertainty can be obtained by subtracting the nominal model from the set of circles).
5. Fit a rational transfer function to the radii of the second set of circles yielding the multiplicative complex uncertainty description $W_c(s)$, (only the magnitude is fitted).

5.4 Uncertainty Representation: Mixed

Still assuming that the designer has only a set of complex points in the Nyquist plane from several worst-case plants, a potentially less conservative uncertainty model can be obtained by considering an alternative geometric convex figure, composed by a rectangle and two semicircles, one at each end of the smallest side of the rectangle, see Figure 5.7.

This geometric figure has also been used in [Tøffner-Claussen, 1995]. As a result of performing system identification, an ellipsoid confidence interval was calculated for every frequency point. The geometric figure shown in Figure 5.7 was employed to encapsulate these ellipsoids such that they could be used in connection with the μ-framework.

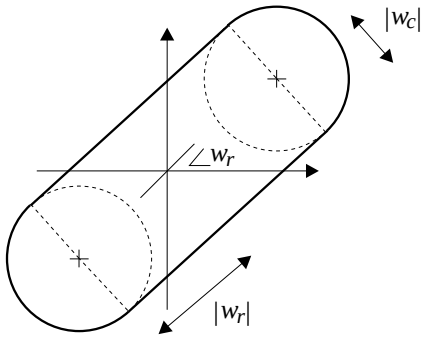

Figure 5.7: *Uncertainty representation of the perturbation set with the alternative geometric figure, named "olympic stadium" (OS).*

This geometric figure can mathematically be described by a real and a complex multiplicative perturbation

$$\begin{aligned} G_p(s) &= G(s)(1 + W_c(s)\delta_c + W_r(s)\delta_r), \\ \delta_c \in \mathbf{C}, \delta_r \in \mathbf{R}, &\quad |\delta_c| \leq 1, -1 \leq \delta_r \leq 1, \end{aligned} \tag{5.15}$$

where $W_c(s)$ and $W_r(s)$ are respectively the complex and real multiplicative perturbation weights. For convenience, the geometric figure is named "olympic stadium" (OS). Two main relevant criteria can be distinguished in order to determine the OS's shape. One consists of choosing minimal area OSs and the other one consists of choosing the narrowest OSs, treated in this sequel. As it was pointed out before, the D-K iteration handles complex but not real nor mixed uncertainties, which implies that the orientation of the OSs are not taken into account, instead the D-K iteration addresses them as circles with radius $W_r + W_c$. In this case the criteria of minimal area OSs should be preferred. It is known however that the (μ,D)-K-iteration (and the (D,G)-K-iteration) handles real and mixed uncertainties in a less conservative way than D-K iteration, where the orientation of the OSs also are taken into account. In view of that fact, the OSs should be chosen according to the criteria which yields the narrowest OSs and not necessarily the minimal area in the Nyquist plane.

5.4.1 Finding the First Set of OS

In order to calculate the narrowest OS, first the convex hull of the set of Nyquist points for each frequency point is determined. This convex hull is a convex polygon with a

subset of all the Nyquist points observed as its vertices. As an example, it is shown in upper quadrants in Figure 5.8 the vertices of the convex polygon. Once the polygon is determined, the distance between every side and its *most distant* point is calculated. A parallel line to the side in question containing its *most distant* point is traced. The remaining vertices must lie in between, in order to ensure that the OS will contain all the points. If not all the vertices lie in between, the *most distant* point in question is not valid. The side with its closest valid *most distant* point is chosen and a parallel line to the chosen side is traced, which contains its closest valid *most distant* point. The sides of the OS are then found, see lower left quadrant of Figure 5.8. The half of the distance between the two parallel lines determines the radius of the semicircles, W_c. These semicircles are moved in the same direction as the parallel lines towards the polygon until a vertex of the polygon is contained by the semicircles, see lower right quadrant of Figure 5.8. The half of the distance between the radii of the semicircles is W_r, and $\angle W_r$ is the angle between the principal axis of the OS and the coordinate system given by the quadrant axes.

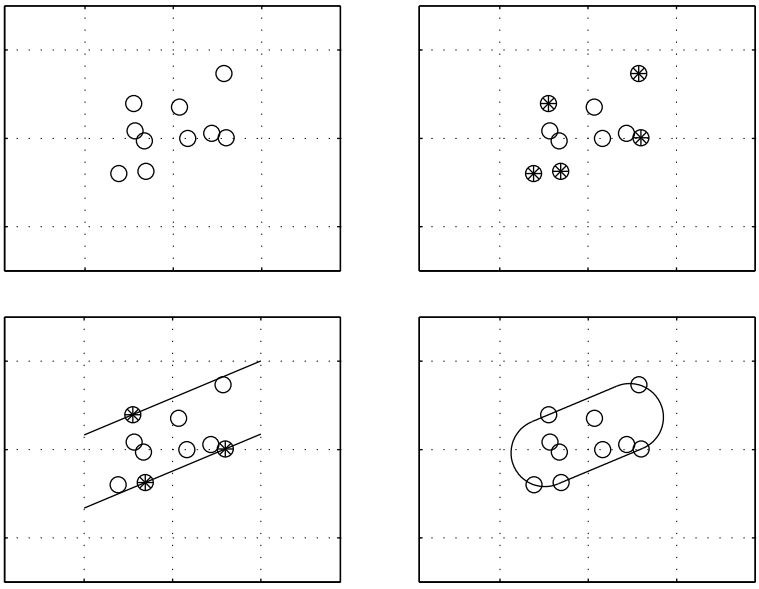

Figure 5.8: *Calculating the first set of narrowest OSs.*

Once the first set of OSs is found, a rational transfer function is fitted (only in magnitude) to the center of the OSs yielding the nominal model. As a result of the fit, the center of the OSs will not necessarily coincide with the nominal model and therefore a second set of OS must be found in order to center it according to the nominal model.

5.4.2 Finding the Second Set of OS

Finding the second set of minimal area circles which circumscribe the vertices of the polygon when the center is given, is a trivial task. However, the algorithm to find the second set of OS is by far more involved. First the convex polygon must be determined, which in fact is the same polygon as for the first set of OSs, (a translation of the Nyquist points, as a result of the fit, does not alter the shape of the polygon). There are now two candidates which yield the narrowest OS. The first candidate is given in the case where one side of the polygon is coincident with one side of the OS. The other candidate is given in the case where each side of the OS contains one vertex of the polygon. For the sake of clarity, the two candidates are illustrated in Figure 5.9.

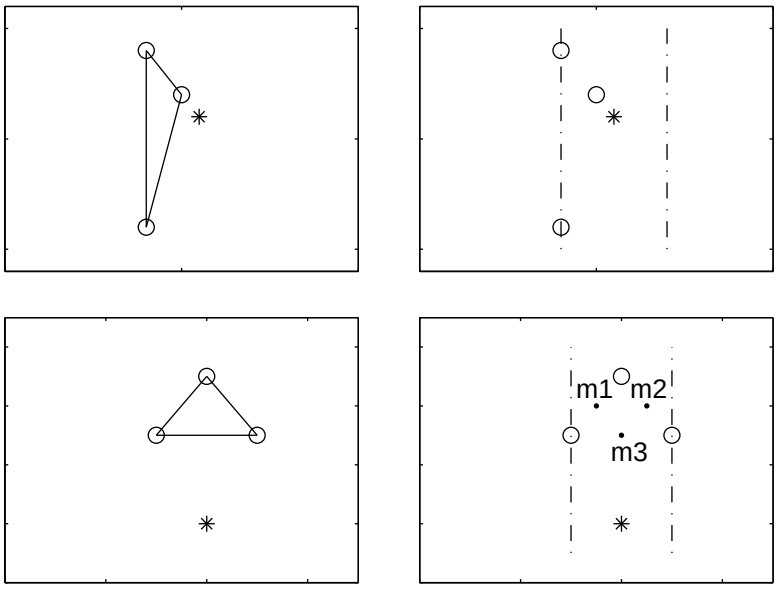

Figure 5.9: *Calculating the second set of narrowest OSs.*

The first case is shown in the two upper quadrants. Consider a polygon given by 3 vertices where the given center (without loss of generality) lies outside, see the upper left quadrant. With respect to the given center, the distance for each side is calculated and the side where the given center is the closest valid *most distant* point is selected. A parallel line to the selected side is traced such that the given center is exactly in the middle, see the upper right quadrant. In the second case, shown in the two lower quadrants, where the center is also outside the polygon, it is clear that if the same method is applied as in the first case, it will not yield the narrowest OS. Instead all the median points of the polygon must be calculated, represented as dots

(m_1, m_2 and m_3) in the right lower quadrant. A fictitious line from the given center to a median point is traced. If the *most distant* point to the fictitious line is one of the two vertices which determine the median point in question, then this median point is valid (in order to ensure that the OS will contain all the points). This procedure is repeated for all median points. The median point which has the closest *most distant* vertices is then selected yielding the narrowest OS. In the lower right quadrant, m_3 is selected according to the described procedure, and as a result, the narrowest OS is found.

As it can be seen, finding the narrowest OS where the center is given, implies the investigation of both cases and the narrowest OS among both cases is selected. Once the sides of the OS are found, the two semicircles can be found as described in the method for finding the first set of OSs.

5.4.3 Finding the Third Set of OS

The orientation of the second set of OSs in the Nyquist plan depends on how the Nyquist points are distributed. If the orientation of the OSs along the frequency axis seems aleatory, it indicates that the OSs should be discarded as geometric figure in favour of circles. However, given a set of measurement data consisting of complex points in the Nyquist plane from several worst-case plants, the orientation of certain OS may vary with respect to the rest due to e.g. measurement noise. In this case it may be convenient to restrict the orientation of these "erratic" OSs to some defined limits to ease the process of fitting the uncertainty weights in both magnitude and weight. Therefore finding the third set of OS consists of determining the orientation of the OS, $\angle W_r$, and comparing it to a given nominal orientation, $\angle W_{r-nom}$. If $\angle W_r$ exceeds the specified limits, a new OS is constructed with a forced angle given by $\angle W_{r-nom}$. Constructing the narrowest OS where the center and the orientation are given is therefore a trivial task.

5.4.4 Determining the Uncertainty Weights

Once the third set of OS is found the uncertainties must be formulated such that they can be handled by the algorithms in the μ-framework. First the set of OS is "divided" by the nominal model frequency point by frequency point to obtain the multiplicative uncertainties, (the additive uncertainty can be obtained by subtracting the nominal model from the set of OS). In order to find the multiplicative complex uncertainty weight, $W_c(s)$, a rational transfer function is fitted to the radii of the semicircles constituting the OSs. Only magnitude is fitted as the phase is not relevant for complex uncertainties. Finding the multiplicative real uncertainty weight implies fitting a rational, stable, minimum phase in both magnitude and phase, which is not always trivial. The *μ-Analysis and Synthesis Toolbox* of MATLAB provides a script `fitsys.m` which performs such fit. The accuracy of the fit should be weighted against the order of the weights. When it comes to the controller synthesis, the uncertainty weights should generally be fitted to a low order transfer function.

Method based on OS

To recapitulate, the method for obtaining the nominal and the uncertainty models by means of choosing the narrowest OS can be summarized as follows:

1. Find the 1st set of narrowest OSs at each frequency point which contains all the Nyquist points from the measurement set.
2. Fit a rational transfer function to the center of the 1st set of OS yielding the nominal model $G(s)$.
3. Find the 2nd set of narrowest OSs with the center described by $G(s)$, containing at the same time all the obtained points at the corresponding frequency point.
4. Eventually erratic orientations in the 2nd set of OS are corrected yielding the 3rd and final set of OSs.
5. To derive the multiplicative uncertainty, "divide" the 3rd set of OS by the nominal model (the additive uncertainty can be obtained by subtracting the nominal model from the 3rd set of OS).
6. Fit a rational transfer function to the OS's width from the 3rd set of OS, yielding the multiplicative complex uncertainty description $W_c(s)$, (only the magnitude is fitted).
7. Fit a rational stable and minimum phase transfer function to OS's length from the 3rd set, yielding the multiplicative real uncertainty description $W_r(s)$.

5.5 Results

The three kinds of uncertainty presentations explained above were applied to the data achieved from the identification results from Chapter 4. While in the parametric uncertainty representation, the structure of the model and the uncertainty region for each parameter were assumed to be known, in the complex (circle) and mixed ("olympic stadium") uncertainty representation the only available data assumed to be known was the Nyquist plots (and bode plots) of the CD-drives. In view of the fact that the dynamic deviations in between plants overshadows the confidence intervals of the estimated parameters and estimated Nyquist plots, the estimated confidence intervals are considered to be small enough to be neglected. The complexity of the algorithms which yield the nominal and the uncertainty models of the plants is consequently reduced.

Nominal Bode Plots

Figure 5.10 shows the obtained focus nominal models (all of them being of fourth order) based on the parametric, complex and mixed uncertainty representations. As it can be

observed, it is hard to discern the bode plots from each other. The same observations can be made concerning the radial nominal bode plots shown in Figure 5.11.

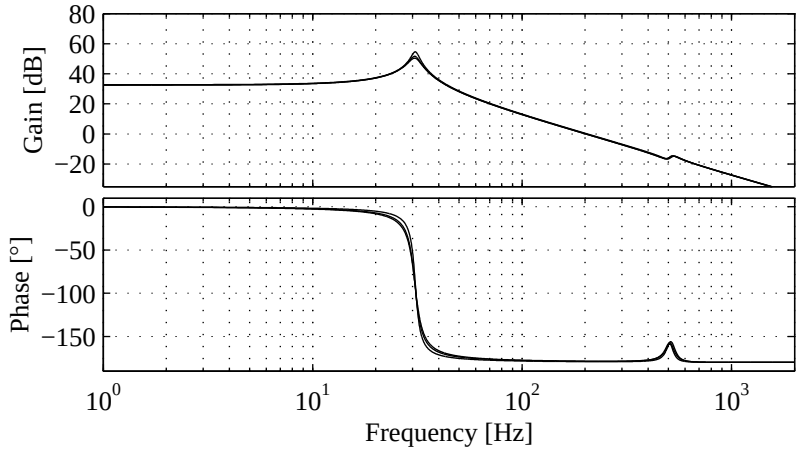

Figure 5.10: *Obtained focus nominal models based on parametric, complex and mixed uncertainty representations.*

Parametric Uncertainty Representation

Table 5.2 shows the uncertainty in the parameters of the focus and radial plants. The nominal mass of the focus and radial plant should be the same since they are suspended in the same mechanical device, but as it can be appreciated, there is only a minor discrepancy of 1e-6[Kg].

Complex Uncertainty Representation

The radii of the second set of circles result in the uncertainty weight which only has to be fitted in magnitude. The script `fitmag.m` provided by the *μ-Analysis and Synthesis Toolbox* of MATLAB performs such a fit. The upper part of Figure 5.12 shows the calculated (dotted) and fitted (solid) multiplicative uncertainty weight of the focus plant. The radial multiplicative uncertainty weight is show in the lower part of the figure. Both weights could be described by a fourth order transfer function.

Mixed Uncertainty Representation

The "olympic stadiums" must be fitted both in length (magnitude and phase) and width (magnitude). While the fit of the width was performed by the MATLAB script

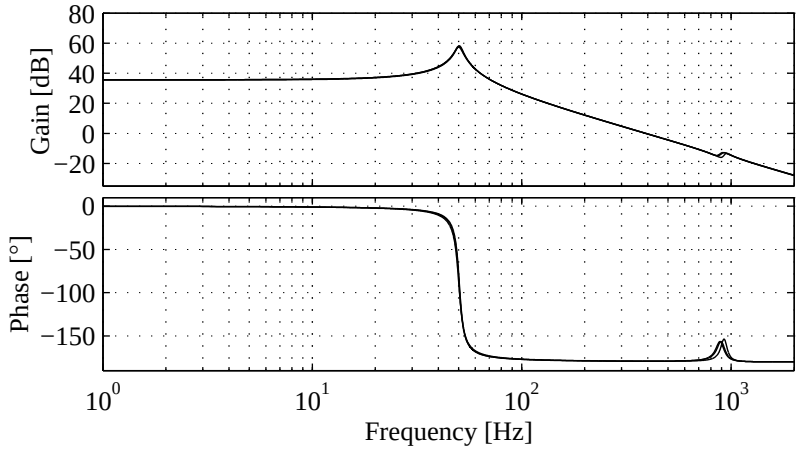

Figure 5.11: *Obtained radial nominal models based on parametric, complex and mixed uncertainty representations.*

Parameters	**Focus (nom.)**	**Focus (Δ)**	**Radial (nom.)**	**Radial (Δ)**
DC_{gain}	76000	7.9%	300000	20%
R	17.5 [Ω]	6.9%	17.1 [Ω]	2.7%
Bl	0.22 [N/A]	7.6%	0.20 [N/A]	5.1%
k_1	23.2 [N/m]	17.4%	60.3 [N/m]	5.8%
k_2	221.3 [N/m]	28.9%	778.6 [N/m]	21.4%
b_1	7.3e-3 [N·s/m]	9.1%	12.1e-3 [N·s/m]	5.9%
b_2	0.38e-3 [N·s/m]	9.1%	0.64e-3 [N·s/m]	5.9%
m_1	0.536e-3 [Kg]	1.4%	0.535e-3 [Kg]	0.05%
m_2	0.024e-3 [Kg]	31.0%	0.025e-3 [Kg]	11.1%

Table 5.2: Nominal and uncertainty parametric values of focus and radial plants.

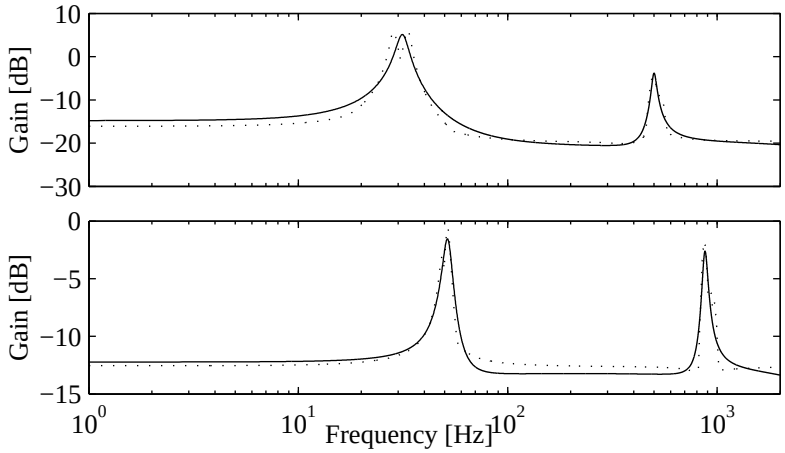

Figure 5.12: *Calculated (dotted) and fitted (solid) multiplicative complex uncertainty models based on circles. The focus uncertainty weight is shown in the upper graph, while the radial uncertainty weight is show in the lower graph.*

`fitmag.m`, the length was fitted manually, since it resulted difficult to achieve an acceptable trade-off between accuracy and order of the filter with the script `fitsys.m` which fits both in magnitude and phase. The upper part of Figure 5.13 shows the calculated and fitted focus multiplicative uncertainty weight and the lower part shows the weight related to the radial plant.
Figures 5.14 and 5.15 show the calculated and the fitted multiplicative real uncertainty weights of the respectively focus and radial plants.

Graphical Comparison of the Uncertainty Representation Methods

In order to obtain a bode plot which shows the worst-case multiplicative parameter uncertainty, the nine parameters were changed between the minimum, the nominal and the maximum allowed values. This results in $3^9 = 19683$ bode plots. However, it is not guaranteed to yield the worst-case as the worst-case may be at the interior of the intervals. Adding two interior points, symmetric to the nominal values, would result in 5^9 bode plots, nearly 2 millions. Analyzing only the minimum, nominal and maximum allowed values gives nevertheless an approximate uncertainty. The magnitude of 19683 bode plots is then subtracted the nominal magnitude and the resultant magnitude is divided by the nominal magnitude $|(G_p - G_{nom})/G_{nom}|$, yielding the (relative) multiplicative uncertainty. Some of the uncertainties can however be lumped, still preserving a similar worst-case plant, and simplicity is gained. The uncertainties on the parameters

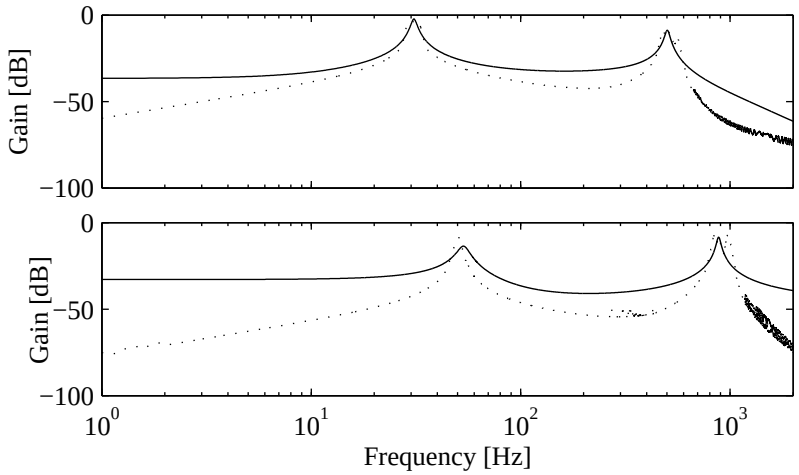

Figure 5.13: *Calculated (dotted) and fitted (solid) multiplicative complex uncertainty models based on OS. The focus uncertainty weight is shown in the upper graph, while the radial uncertainty weight is show in the lower graph.*

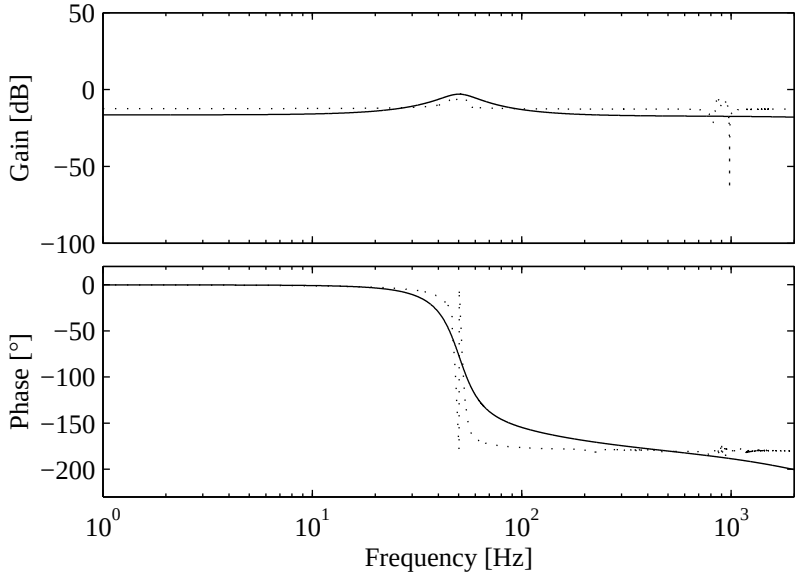

Figure 5.14: *Calculated (dotted) and fitted (solid) focus multiplicative real uncertainty models based on OS.*

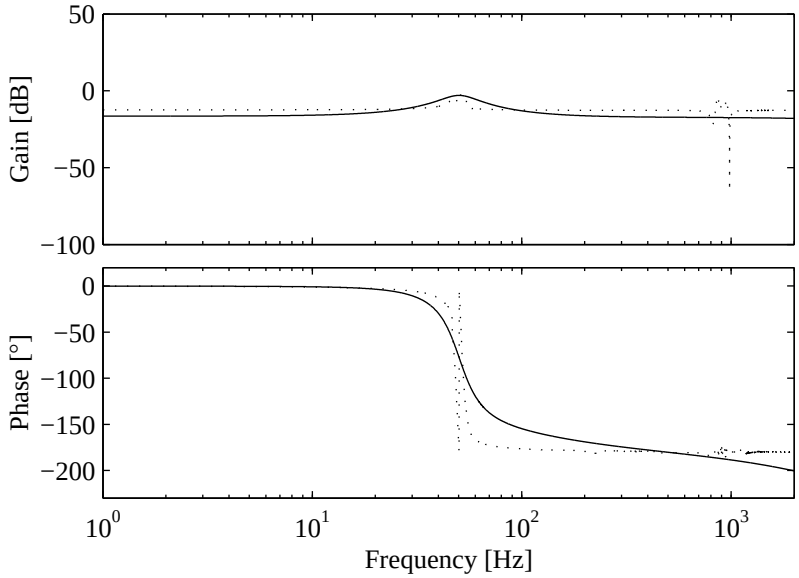

Figure 5.15: *Calculated (dotted) and fitted (solid) radial multiplicative real uncertainty models based on OS.*

Bl, m_1, m_2, b_1 and b_2 were therefore removed and instead it was compensated for them by increasing the uncertainty in R. Another parameter uncertainty which can be eliminated (however yielding a more optimistic overall worst-case parameter uncertainty of the plant) is the DC_{gain}. As mentioned in Section 4.4 there is an AGC in the CD-drives which is in charge of compensating for possible gain deviations around the cross-over frequency. Having that in mind, the DC_{gain} uncertainty can be neglected. Table 5.3 shows after these considerations that three parameters are therefore enough to describe the uncertainties in the plants.

Parameters	**Focus (Δ)**	**Radial (Δ)**
R	$6.9\%\cdot 2 = 13.8\%$	$2.7\%\cdot 2.5 = 6.8\%$
k_1	17.4%	5.8%
k_2	28.9%	21.4%

Table 5.3: Reduced number of uncertain parameters in focus and radial plants.

In Figure 5.16 the treated uncertainty representations are contrasted. After the modifications in the parametric uncertainty, it can be observed that the parametric (dashed

trace) and the complex (dotted trace) representations are comparable in sizes, whereas the mixed (solid trace) uncertainty representation results in the least conservative uncertainty.

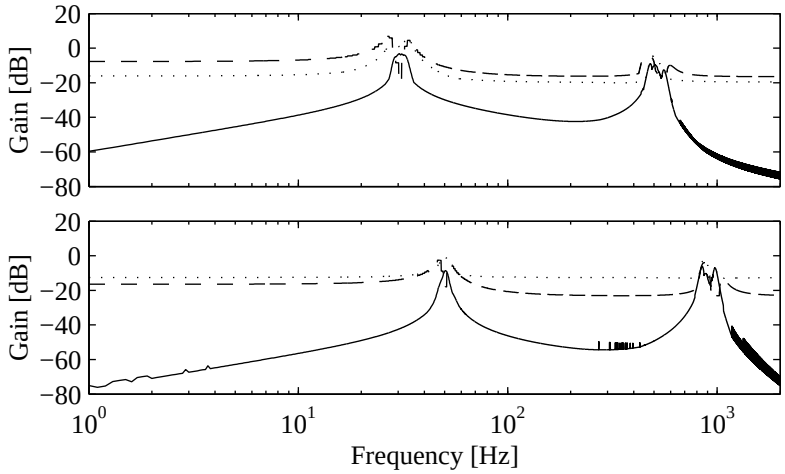

Figure 5.16: *Graphical comparison of the uncertainty representation methods. The dashed trace represents the parametric uncertainty, the dotted trace represents the complex uncertainty and the solid trace represents the mixed (width of the OS) uncertainty. The upper graph applies to the focus plant, whereas the lower graphs applies to the radial plant.*

5.6 Discussion

Whether the parametric, complex or mixed uncertainty representation was employed, the obtained nominal models had high degree of similarity. Not surprisingly the complex and mixed uncertainty representation resulted in nearly the same nominal models since both methods are based on the minimization (in size or width) of a convex geometric figure. What it is worth to notice it that by taking the average of each uncertainty region of the parameters, basically the same nominal models were achieved. This fact indicates that even given the situation where limited knowledge of the plants is available (only the measurement set of Nyquist points) it is still possible to obtain a nominal model which could be obtained if specific knowledge of the plants is available (uncertainty regions of the parameters). However, no specific guidelines are given in the methods to which order the models should be fitted. These considerations should be made by the designer where accuracy and complexity should be weighted against each other.

A deceiving aspect of the parametric uncertainty description is that they provide a detailed description of each parameter but not all combinations may be present in the physical plant, yielding consequently in a conservative uncertainty description. It was necessary to make two kinds of reductions in the parametric uncertainties, the first was to reduce the complexity, still preserving a similar worst-case, and the second consisted on achieving a more *realistic* multiplicative uncertainty. Even though the DC_{gain} uncertainty was removed, comparable results were achieved by encapsulating the Nyquist point at each frequency by circles, being an acceptable alternative to obtain the uncertainty model when only the Nyquist plots are available.

Although hard to see from Figure 5.16, the mixed uncertainty plot never exceeds in magnitude the complex uncertainty. This is due to the fact that with the OS method, the narrowest OS set is chosen, which in the worst-case yields a minimal area circle set. It should be reminded that only the width of the mixed uncertainty representation is shown, which is the uncertainty the controller "looks into" as long as it rotates the OS in the convenient directions such that they are furthest away from the instability point. That is, OSs are potentially less conservative than the circles, however, the OSs require control synthesis methods which address the mixed uncertainties in a less conservative way than the D-K iteration, such as the (μ,D)-K-iteration and (D,G)-K-iteration.

5.7 Summary

The chapter starts giving an introduction in Section 5.1 to the $\mathcal{H}_\infty$-control concepts relevant to this work. Generally it is assumed that the nominal and the uncertainty models are available. In this chapter a more realistic approach is taken and it is assumed that no nominal and no uncertainty models are given beforehand. Two methods are explained known from robust control literature, one based on a parametric uncertainty representation in Section 5.2 and the other based on complex uncertainty representation in Section 5.3. A method is described in Section 5.4 where an alternative convex geometric figure is suggested, the "olympic stadium". The three methods are applied to the data from 12 CD-drives obtained from Chapter 4 and through the results in Section 5.5 it is verified that the conservatism is potentially reduced with the "olympic stadiums" as uncertainty representation. As pointed out in the discussion (Section 5.6) control synthesis methods which address the mixed uncertainties in a less conservative way than the D-K iteration, such as the (D,G)-K and (μ,D)-K-iteration are required, such that the geometric properties of the OS are better exploited.

6

Robust Control Applied to a CD-drive

As explained in Section 2.5 the disturbances in CD-players (and other optical disc players) can roughly be classified in two groups. On the one hand the bandwidth of the positioning controllers should be high in order to better damp mechanical disturbances for example, whilst on the other hand a low bandwidth would be preferable in order to better cope with surface defects such as scratches. Besides the disturbances impinging the control loop, the controller must be able to cope with loop changes caused by e.g. the aging of the actuators, parameter variations along the production of CD-players and variations in the disc properties like the optical gain. The primary specification in the design problem of CD-players is to guarantee a hard bound on the time-domain amplitude of the error signals in the presence of model uncertainties. The design of such controller can be formulated as a $\mathcal{H}_\infty$-control problem where norm-bounded uncertainties are assumed, although other techniques can be successfully applied to CD-players as well. The Ph.D. dissertation [Lee, 1998] is dedicated to the study of robust repetitive control, (applied to CD-players as a case study). Provided that the rotational frequency of the disc is known, the periodic disturbances generated as a result of such rotation, can be effectively attenuated using the concept of repetitive control. Basically it consists of adding infinity gain to the loop transfer at the rotation frequency and at its sub-harmonics. In [Dötsch *et al.*, 1995] an adaptive repetitive scheme is proposed where

the frequency is estimated on-line based on the feedback error signal. However, as mentioned in the reference, *once the periodic components are sufficiently suppressed in the error signal, excitation of the estimation algorithm is lost, resulting in a bad estimate of the period*. In [Vidal *et al.*, 1998] such estimation is based on the control signal of a PID-like controller. Any low-frequency disturbance will to some extent be attenuated by the controller, and as a consequence, the control signal will contain that periodicity which can be fed to the adaptive algorithm. Another recent Ph.D. dissertation where the CD-player is chosen as a case study is [Dettori, 2001]. LMI techniques are treated to solve in particular two control problems: multi-objective design and gain-scheduling. Positive results were documented with gain-scheduling, however, *multi-objective techniques did not lead to better controllers for the CD-players than standard $\mathcal{H}_\infty$ design*. It is pointed out that one of the reasons is the elevated conservatism of the employed multi-objective techniques, however μ-synthesis is potentially less conservative. Numerous publications can be found on this subject applied to CD-players, see for example [Steinbuch *et al.*, 1992, Steinbuch *et al.*, 1994b, van Groos *et al.*, 1994] where the D-K iteration algorithm was used to synthesize the controllers.

Based on part of the available research literature on control applied to CD-players, it can be appreciated that $\mathcal{H}_\infty$-control is well represented. This fact indicates that $\mathcal{H}_\infty$-control is a suitable approach to synthesize controllers to CD-players, which is also supported by the considerable parameter variations observed in Chapter 4. However, the main controllers used in commercial CD-players are still based on a PID-like structure [Akkermans, 2001]. The objective of the present chapter is two-fold. It is investigated whether a controller with a PID-like structure is sufficient to offer robust performance. In that respect, a μ-synthesis technique less conservative than the D-K iteration is employed, the (μ,D)-K-iteration, described in the Ph.D. dissertation [Tøffner-Claussen, 1995]. Higher order controller structures are also investigated. The other objective of this chapter is to assess whether the "olympic stadiums" suggested in Chapter 5 offer any significant advantage over the parametric and especially the complex uncertainty representation in the $\mathcal{H}_\infty$-framework.

The chapter starts formulating the general control problem in Section 6.1, followed by the specification of the performance requirements in Section 6.2. In Sections 6.3 and 6.4 the extensive results are documented and discussed. A summary is given at the end in Section 6.5.

6.1 General Control Problem Formulation

There are many ways in which feedback design problems can be cast as $\mathcal{H}_\infty$-optimization problems. One widely known approach explained in Section 5.1 is the mixed-sensitivity $\mathcal{H}_\infty$-control, consisting on the minimization of the weighted sensitivity function $S = (I + GK)^{-1}$ together with other closed-loop transfer functions such

as KS or the complementary sensitivity function $T = I - S$. In the case the sensitivity and control effort weights are specified, the aim of the $\mathcal{H}_\infty$-control synthesis algorithm is to find a controller such that the following inequality holds

$$\left\| \begin{bmatrix} W_p S \\ W_u K S \end{bmatrix} \right\|_\infty < 1. \tag{6.1}$$

However, with this $\mathcal{H}_\infty$-design formulation, nominal performance and robust stability can only be guaranteed by the controller. Robust performance can also be guaranteed although in a rather conservative fashion. A better alternative to design for robust performance is to consider the design formulation in a non-standard $\mathcal{H}_\infty$-optimization framework such as the μ-synthesis.

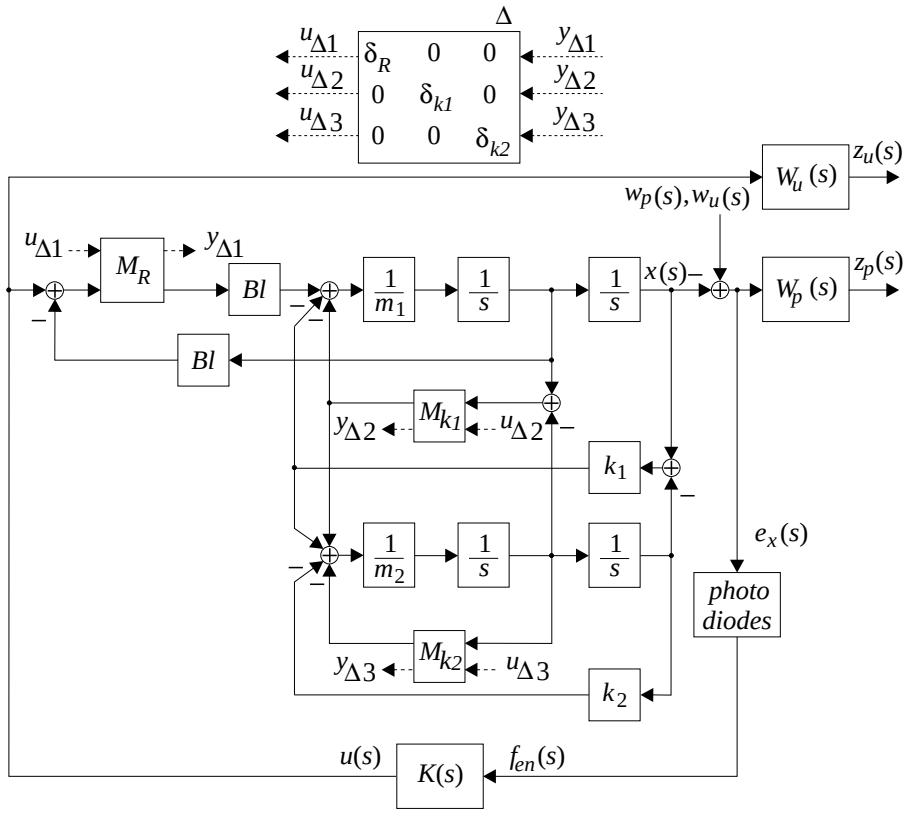

Figure 6.1: *Generalized focus plant with parametric uncertainties including the performance weight $W_p(s)$ and control effort weight $W_u(s)$. An equivalent plant applies to the radial loop as well.*

The addressed uncertainty types of the previous chapter were the parametric, the complex (circles), and the mixed ("olympic stadiums") uncertainties. Figure 6.1 shows the generalized plant with multiplicative parametric uncertainties and the controller. The uncertainty of the resistance R, and the spring moduli k_1 and k_2 are described by the corresponding LFT as explained in the last chapter. The uncertainties are *pulled out* into a block-diagonal matrix, Δ, where each parametric uncertainty δ_i is real. The plant together with the weights $W_u(s)$ and $W_p(s)$ constitute the generalized plant.

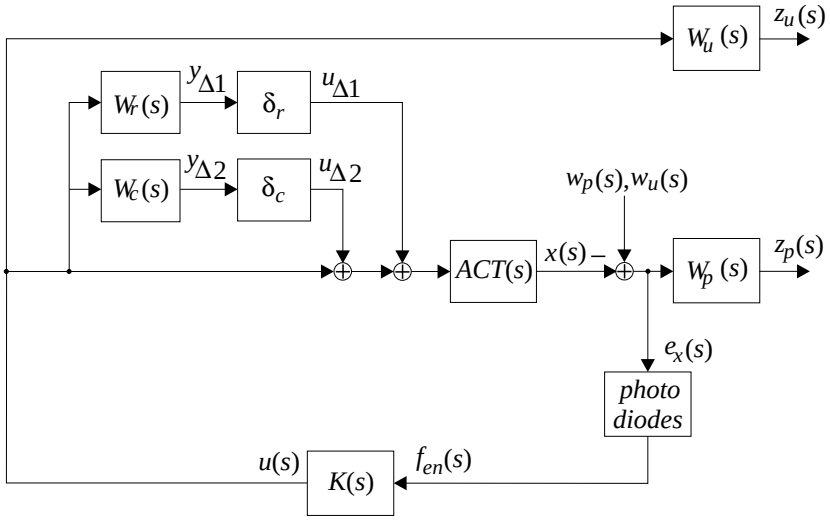

Figure 6.2: *Generalized plant with mixed uncertainties including the performance weight $W_p(s)$ and control effort weight $W_u(s)$.*

In the case of dealing with mixed uncertainties, the generalized plant has a different look, see Figure 6.2. The nominal plant is described by a transfer function, $G(s)$, and two types of uncertainties are present. The complex one, where the weight $W_c(s)$ specifies the width of the "olympic stadiums" along the frequency axis, and the real uncertainty, where the weight $W_r(s)$ specifies the length and orientation of the "olympic stadiums". The uncertainties δ_c and δ_r are as well *pulled-out* into a block-diagonal matrix Δ. Note that only the weight $W_c(s)$ is necessary if the circles are chosen instead of the "olympic stadiums" since the orientation of the former is not relevant in the context.
Independently on which uncertainty representation is chosen, the control objectives are similar. Two disturbance channels can be distinguished, from w_p to z_p and from w_u to z_u. Common to the CD-players is that the position of the information layer (the position of the track in the radial case) can be considered as a disturbance, w_p, impinging the control loop, which must be effectively attenuated by the controller $K(s)$ such that the position of the focus point $x(s)$ follows the position of the information layer. That is,

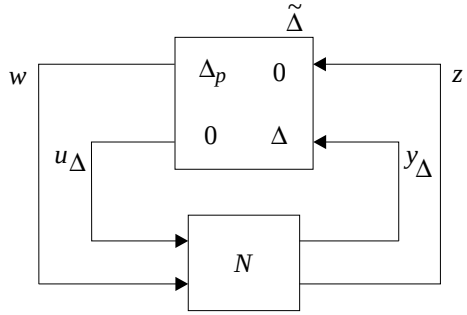

Figure 6.3: *Structure for robust stability analysis.*

$e_x(s) = -x(s) + w_p(s) = 0$ (the reference signal is zero). Therefore $K(s)$ minimizes the disturbance channel $w_p \rightarrow z_p$. Generally, the higher the gain and bandwidth of $K(s)$, the more the disturbance channel $w_p \rightarrow z_p$ is minimized. However, there are in practice some physical constraints on the size of the control signal. Therefore it is important to include a mechanism which limits the size and bandwidth of the controller. In this case, this is achieved by minimizing the other disturbance channel at the same time, namely, $w_u \rightarrow z_u$.
The control objective presented in Equation 6.1 can be rephrased into the μ-framework in order to permit designing the controller for robust performance

$$\mu_{\tilde{\Delta}}(N) < 1, \qquad \text{where} \qquad N = F_l(P, K). \tag{6.2}$$

The generalized plant P is partitioned such that it is compatible with K. $\mu_{\tilde{\Delta}}(N)$ is computed with respect to the structured uncertainty block $\tilde{\Delta} = \text{ diag } \{\Delta, \Delta_p\}$, see Figure 6.3, where Δ represents the uncertainty of the plant and Δ_p is a fictitious 2×2 performance block which connects the exogenous outputs, z_p and z_u, with the exogenous inputs, w_p and w_u. In Section 5.2 it was pointed out that real uncertainties do not appear alone in practice, hence the function μ is continuous at the problem data. Δ_p is in fact the complex block which ensures such continuity on μ.

6.2 Performance Specifications

In the analysis of the disturbances in optical disc servos described in Section 2.5 it was found that the disturbances could broadly be classified in two groups of conflicting requirements: the first group composed by disturbances, such as disc deviations, self-pollution and mechanical shocks where a high bandwidth is preferred, and the second group, mainly composed by surface defects where a low bandwidth should be selected. However, independently on the CD application (e.g. stationary, car-mounted or portable CD-player) the controller should at least be able to cope with the disc

deviations specified by the Red Book as described in Section 2.5. The specifications given in Table 2.3 can be formulated in a natural way as the requirements for the output sensitivity function of the focus loop $S = (I + GK)^{-1}$. The focus error, $e_x(s)$, should not be higher than 2[μm] [Bouwhuis *et al.*, 1985], that is, $z_p = Sw_p < 2$ [μm], which imposes the following requirement to the sensitivity function: $S \leq w_p^{-1}2 = W_p$. W_p is the performance weight given by the "inverse" of the vertical deviation of the disc. Since it is desired to eliminate constant steady-state errors, an integrator should be added, slightly moved to the left half plane, otherwise it becomes an uncontrollable pole of the feedback system and the $\mathcal{H}_\infty$ assumptions are violated [Zhou *et al.*, 1996]. In the same reference a reformulation of the control problem is given if it is desired to have a pole in the imaginary axis.

The specifications on the sensitivity function determine a lower bound on the bandwidth but not an upper one. This is solved by including the mentioned mechanism which imposes at the same time a bound on the control effort. In [Skogestad and Postlethwaite, 1997] it is suggested to choose $W_u = I$ given that the plant has been previously scaled. In the presence of different disturbance channels it is essential to scale the plant such that the norms of the channels are comparable in size. Choosing the correct weights is also of paramount importance so that a proper trade-off is obtained between the conflicting performance and robustness specifications. The shape of the weights are naturally application-dependent but in CD-players it can be recommended to start with $W_u = (K_{optFn})^{-1}$ (the inverse of the optical gain) and to perform a μ-analysis with a known controller. Then the weight may be modified such that the norms of the perturbation channels $w_p \rightarrow z_p$ and $w_u \rightarrow z_u$ are comparable.

The performance weights, previously described, are also included in the generalized plant P. Taking Figure 6.2 as an example, P can be obtained by inspection,

$$\left[\begin{array}{c} \begin{bmatrix} y_{\Delta 1} \\ y_{\Delta 2} \end{bmatrix} \\ \hline \begin{bmatrix} z_p \\ z_u \end{bmatrix} \\ \hline f_{en} \end{array}\right] = P \left[\begin{array}{c} \begin{bmatrix} u_{\Delta 1} \\ u_{\Delta 2} \end{bmatrix} \\ \hline \begin{bmatrix} w_p \\ w_u \end{bmatrix} \\ \hline u \end{array}\right], \tag{6.3}$$

where P is given by

$$P = \left[\begin{array}{cc|cc|c} \begin{bmatrix} 0 & 0 \\ 0 & 0 \end{bmatrix} & & \begin{bmatrix} 0 & 0 \\ 0 & 0 \end{bmatrix} & & \begin{bmatrix} W_r \\ W_c \end{bmatrix} \\ \begin{bmatrix} -W_pACT & -W_pACT \\ 0 & 0 \end{bmatrix} & & \begin{bmatrix} W_p & W_p \\ 0 & 0 \end{bmatrix} & & \begin{bmatrix} -W_pACT \\ W_u \end{bmatrix} \\ \hline \begin{bmatrix} -K_{optFn}ACT & -K_{optFn}ACT \end{bmatrix} & & \begin{bmatrix} K_{optFn} & K_{optFn} \end{bmatrix} & & -K_{optFn}ACT \end{array}\right] \tag{6.4}$$

The closed loop between the plant P and the controller K is given by the following lower LFT

$$N = F_l(P, K) = P_{11} + P_{12}K(I - P_{22}K)^{-1}P_{21}, \tag{6.5}$$

that is,

$$\begin{bmatrix} y_\Delta \\ z \end{bmatrix} = \begin{bmatrix} N_{11} & N_{12} \\ N_{21} & N_{22} \end{bmatrix} \begin{bmatrix} u_\Delta \\ w \end{bmatrix}. \tag{6.6}$$

By performing the necessary algebraic calculations, the four partitions of N can be calculated to be

$$N_{11} = \begin{bmatrix} -W_rKSK_{optFn}ACT & -W_rKSK_{optFn}ACT \\ -W_cKSK_{optFn}ACT & -W_cKSK_{optFn}ACT \end{bmatrix}, \tag{6.7}$$

$$N_{12} = \begin{bmatrix} -W_rKSK_{optFn} & -W_rKSK_{optFn} \\ -W_cKSK_{optFn} & -W_cKSK_{optFn} \end{bmatrix}, \tag{6.8}$$

$$N_{21} = \begin{bmatrix} W_pACT(KSK_{optFn}ACT - I) & W_pACT(KSK_{optFn}ACT - I) \\ -W_uKSK_{optFn}ACT & -W_uKSK_{optFn}ACT \end{bmatrix}, \tag{6.9}$$

$$N_{22} = \begin{bmatrix} W_p(I - ACTKSK_{optFn}) & W_p(I - ACTKSK_{optFn}) \\ -W_uKSK_{optFn} & -W_uKSK_{optFn} \end{bmatrix}. \tag{6.10}$$

To recall, K_{optFn} is the normalized optical gain of the focus loop. The same principles apply however to the radial loop as well. All the existing algorithms for μ-synthesis are based on $\mathcal{H}_\infty$-synthesis, see e.g. [Doyle *et al.*, 1989]. Examples of algorithms for mixed μ-synthesis are [Young and Doyle, 1990b, Young *et al.*, 1992] and [Tøffner-Clausen *et al.*, 1995]. In [Tøffner-Claussen, 1995] the algorithms are described and compared. In this work the algorithm described in [Tøffner-Clausen *et al.*, 1995] ((μ,D)-K-iteration) is chosen, although the (D,G)-K-iteration would also be a suitable choice. Nevertheless common to all of them is that they target to find a controller, K, such that the following conditions are met

$$
\begin{aligned}
NS: &\quad \text{nominal internal stability ,} \\
NP: &\quad \overline{\sigma}(N_{22}) = \mu_{\Delta_P} < 1, \quad \forall\omega, \quad and \quad NS, \\
RS: &\quad \mu_{\Delta}(N_{11}) < 1, \quad \forall\omega, \quad and \quad NS, \\
RP: &\quad \mu_{\hat{\Delta}}(N) < 1, \quad \forall\omega, \hat{\Delta} = \begin{bmatrix} \Delta_P & 0 \\ 0 & \Delta \end{bmatrix} \quad and \quad NS.
\end{aligned}
$$

It can be appreciated that the uncertainty weights $W_r(s)$ and $W_c(s)$ form part of N_{11}, which is the partition matrix related to the robust stability analysis. The nominal performance is analyzed by calculating the μ value of N_{22} where the performance weights ($W_p(s)$ and $W_u(s)$) are taken into account without the uncertainties. The uncertainty weight are not involved in such analysis since they are not relevant for the nominal case. However all the partitions are involved in the analysis of robust performance.

6.3 Results

Only the focus loop is treated in this section, however, equivalent results apply to the radial loop. The obtained results can be divided into five parts, shortly briefed in the following:

- *Comparison of the uncertainty models at 1X-speed*: A μ-PID is synthesized and the found parametric, complex and mixed uncertainty models from the previous chapter are evaluated through a robust performance analysis. The controller is referred to as μ-PID in the sequel since it was synthesized in the μ-framework and could be reduced to a PID structure without altering its characteristics significantly.

- *Robust performance analysis at 5X-speed*: A robust performance analysis is performed at 5X with the μ-PID and with a higher order structure μ-controller. It should be mentioned that the specifications of the Red Book do not go beyond 2X. However, being aware of that fact, 5X is chosen in order to better give a picture of what are the effects of an increase of the rotation speed of the disc.

- *Sensitivity and gain margins of the μ-PID controller*: The sensitivity plot of the μ-PID controller is simulated and measured in the 12 CD-drives. The gain margins are as well measured in the 12 CD-drives. The sensitivity analysis is also performed while the gain of controller has been reduced by 3 (approx. -9.5[dB]). The gain reduction of -9.5[dB] is performed in order to show the trade-off between mechanical disturbances and surface defects. A controller which does not necessarily meet the Red Book specifications may have a greater immunity against surface defects.

- *Closed loop measurements with the μ-PID controller*: The μ-PID of nominal and reduced gain (-9.5[dB]) are compared by means of closed loop measurements where the focus loop is affected by periodical vertical deviations and by surface defects.
- *Nyquist plots based on OS and circles*: A graphical comparison is made between two different uncertainty representations, namely the OSs and the circles. The comparison is performed based on the Nyquist plots of the open loop (the μ-PID with the nominal plant) together with the OSs and the circles as uncertainty representation.

The algorithm used to synthesize the controllers is the mixed-μ algorithm described in [Tøffner-Clausen *et al.*, 1995]. The employed performance weights are the same in all the analysis and synthesis of the controllers. $W_p(s)$ is given by

$$W_p(s) = \frac{(s/M^{1/3} + Xw_B)^3}{(s + Xw_B A^{1/3})^3} \cdot \frac{(s + w_I)}{(s + 0.001)}, \tag{6.11}$$

where M=2, A=0.004 and w_B=2π·230 [rad/sec]. The speed factor X specifies the linear disc scan velocity where $X = 1$ corresponds to the nominal velocity of audio CDs, 1.3[m/s]. The steady-state errors are eliminated by an integrator , slightly moved to the left half plan, as explained in Section 6.2. w_I=2π ·10[rad/sec] is in charge of removing the integral action. It should be noticed that the maximum allowed vertical acceleration according to the Table 2.3 is 10[m/s] which is equivalent to -40[dB/dec]. However, a slope of -60[dB/dec] was preferred since it yields a better fit at the frequency corners. Several performance analysis and experiments were realized and the weight $W_u = (100 \cdot K_{optFn})^{-1}$ was found to be acceptable.

6.3.1 Comparison of the Uncertainty Models at 1X-speed

A μ controller based on the parametric uncertainties was synthesized. The synthesized order controller had an elevated order (94th) and was reduced to a third order controller without noticeably deteriorating its properties [Vidal *et al.*, 2003]. The reduced controller is referred to as μ-PID, shown in Equation 6.12

$$\mu{-}PID(s) = \underbrace{12.9{\cdot}10^6}_{P-part} \cdot \underbrace{\frac{(2\pi 31s + 1)}{(2\pi 1.6{\cdot}10^{-4}s + 1)}}_{I-part} \cdot \underbrace{\frac{(2\pi 230 + 1)}{(2\pi 9820 + 1)}}_{lead-part} \cdot \underbrace{\frac{1}{(2\pi 14130 + 1)}}_{HF-pole}. \tag{6.12}$$

The μ-PID controller and the previously explained performance weights were used in the robust analysis with the three different uncertainty representations. Figure 6.4 shows the robust performance μ-analysis of the disturbance channel $w_p \rightarrow z_p$. The robust

performance of the other disturbance channel ($w_u \rightarrow z_u$) was satisfied for all the uncertainty representations. From the figure it can be observed that the robust performance for parametric uncertainties (dashed line) is satisfied. A μ value lower than 1 indicates that there is room for larger uncertainties and/or more elevated performance requirements. A property of the $\mathcal{H}_\infty$-synthesis algorithms is that the synthesized controller tends to ensure equal robust performance along frequency, resulting in a *flat* robust performance plot. That applies to the 94th order controller, but after the order reduction, the robust performance changed slightly, though still meeting the robust performance requirements. The robust performance for mixed uncertainties (solid line) meets also the requirements. However, the robust performance requirements for the complex uncertainties (dotted line) are not met around 30[Hz], which is the resonance frequency of the focus loop. Robust analysis based on complex uncertainties is clearly more conservative than the two other uncertainty representations.

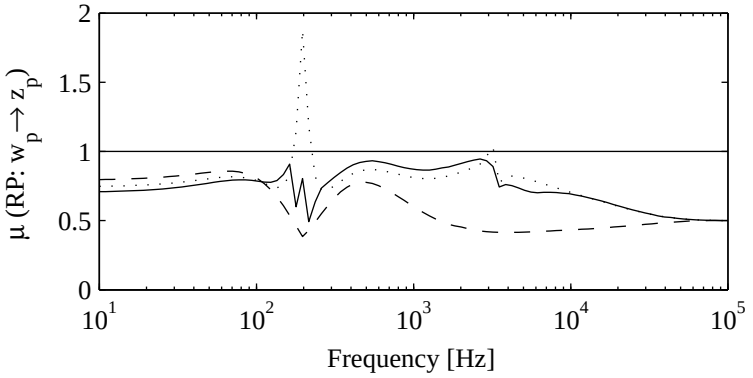

Figure 6.4: *μ-analysis of robust performance of disturbance channel $w_p \rightarrow z_p$ for three different uncertainty representations at normal scan velocity (1X). The dashed line represents the parametric uncertainty, the dotted line represents the complex (circle) uncertainty and the solid line represents the mixed ("olympic stadiums") uncertainty. Robust performance is attained for μ values below 1.*

6.3.2 Robust Performance Analysis at 5X-speed

In the following, the linear disc scan velocity is increased to $X = 5$ and it is investigated whether the robust performance requirements are still satisfied. Moreover, another μ-controller is synthesized based on the mixed uncertainties with the increased performance weight W_p. W_u remains unchanged. The robust performance of both disturbance channels for mixed uncertainties is analyzed with both controllers, see Figure 6.5.

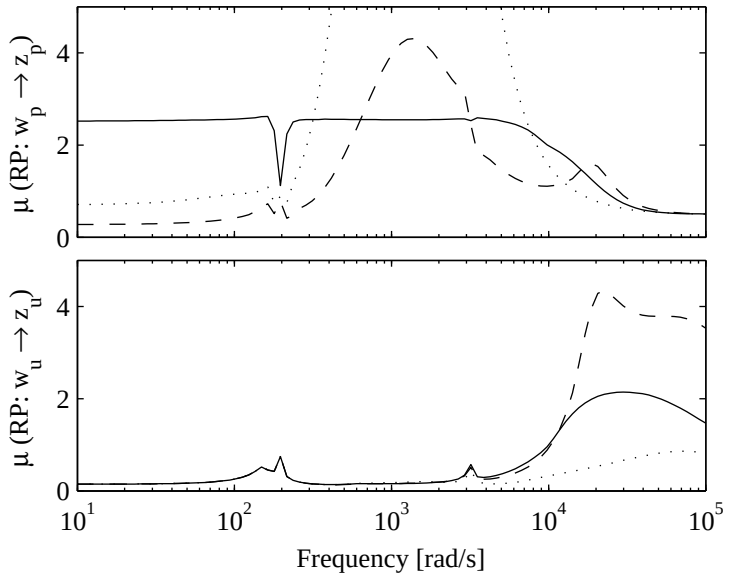

Figure 6.5: *μ-analysis of robust performance of disturbance channels $w_p \rightarrow z_p$ (upper graph) and $w_u \rightarrow z_u$ (lower graph) at increased velocity scan (5X). The dotted lines show the μ-analysis for a μ-PID controller, the dashed lines show the μ-analysis for the μ-PID controller with adjusted gain and the solid lines show the μ-analysis for a μ-controller of higher order.*

The dotted line shows the robust performance analysis of the μ-PID controller. While the disturbance channel $w_u \rightarrow z_u$ meets the requirements (μ is below 1), the same does not apply for the other channel. It reaches a value of 20. In practice, if that controller had to be used, the gain should be increased such that the μ value of both channels is comparable. The results of this gain increase are visualized in the figure with the dashed line. The solid line shows the μ-analysis of the μ-controller synthesized with the increased performance weight, (the order was reduced from 74th down to 9th). The flat robust performance can be appreciated in this plot and at the same time it can be seen that the robust performance requirements are not fulfilled. This is due to the size of the uncertainties and especially to the severe performance requirements.

6.3.3 Sensitivity and Gain Margins of the μ-PID Controller

The output sensitivity functions of the 12 CD-drives were simulated with the obtained nominal models from system identification of Chapter 4. Moreover, the output sensitivity functions were also measured in order to verify whether the performance require-

ments dictated by $W_p(s)$ at $1X$ were fulfilled. A periodic excitation signal $e_{exc}(s)$ was injected in closed loop before the controller and the sensitivity was measured by determining the amplitude ratio between the produced focus error and the excitation signal. The procedure is similar to the one employed to identify the bode plot of the plant dynamics in open loop, described in Section 4.2. The dashed line in Figure 6.6 represents the Red Book requirements described by $W_p(s)$. In the left plots the μ-PID controller with nominal gain was used, while in the right plots the gain of the μ-PID controller was reduced by a factor of 3 (approx. -9.5[dB]). It can be appreciated that the μ-PID controller with nominal gain satisfies the performance requirements for all plants, whereas the μ-PID controller with reduced gain fails to meet the requirements for frequencies below 500[Hz].

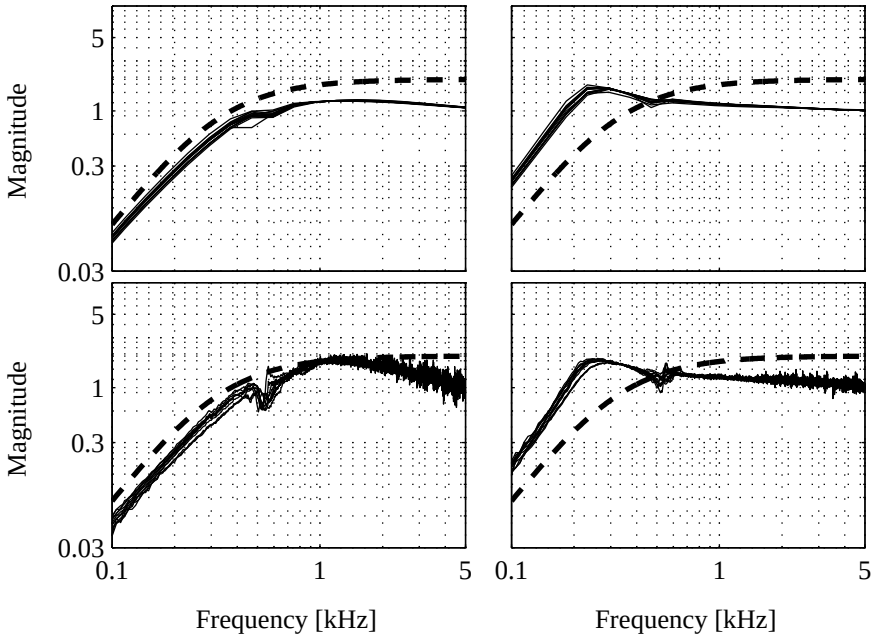

Figure 6.6: *Simulated and measured focus output sensitivity plots with two different controller gains. The upper graphs are the simulated sensitivities while the measured sensitivities are shown in the lower graphs. The graphs to the left show the sensitivities with the nominal controller while the controller used to obtain the graphs to the right has been divided by 3 (approx. -9.5[dB]). The dashed line represents the Red Book requirements described by $W_p(s)$.*

Table A.4 in Appendix A.2 shows the results of the gain margin measurements with the nominal gain μ-PID controller for each CD-drive, being the smallest gain margin

13.1[dB] measured in CD6-drive. The *gain margin* is understood in the sequel as the absolute value of the minimum allowable gain increase/decrease of the controller with respect to its nominal gain before instability is met. In practice, the focus loop was closed with the μ-PID controller and, after two seconds, the gain was gradually de/increased with 2[dB/sec] until the vicinity of instability was reached or until the saturation limits of the control signal was reached. Simulations of the focus loop revealed that a closed loop bandwidth of 1330[Hz] was achieved with the μ-PID controller and that the cross-over frequency could be moved (as a consequence of the gain de/increase of the controller) down to approx. 100[Hz] and up to approx. 4000[Hz] before meeting the instability limits. In the measurements, oscillations of 100[Hz] in the closed loop signals were appreciated, as expected, just before loosing focus when the gain was reduced. The increase of the gain did not result in oscillations of approx. 4000[Hz] since the control signal reached the saturation limits. Only oscillations of approx. 2000[Hz] were registered.

6.3.4 Closed Loop Measurements with the μ-PID Controller

Figure 6.7 shows the closed loop measurements of the error and the control signals of two experiments. In the first one, shown in the upper graphs, the μ-PID controller with nominal gain was used and in the other, in the lower graphs, the gain of the μ-PID controller was reduced by a factor of 3. It can be observed from the plots that the μ-PID with the nominal gain attenuates more efficiently the low frequent disturbances originated from the vertical disc deviation. However, the reactions against the scratch of approx. $1e^{-3}$[m] are more violent with the μ-PID controller with nominal gain.

6.3.5 Nyquist plots based on OS and circles

Figure 6.8 shows the Nyquist plot of the open loop (the μ-PID controller together with the plant) using two different uncertainty representations. The uncertainty representation of the Nyquist plots to the left are based on OSs while the Nyquist plots to the right are based on circles. It can be appreciated that the uncertainty representation based on circles at the first resonance peak (at around 30[Hz]) is more conservative than the uncertainty representation based on OSs. At higher frequencies (between 200-2000[Hz]), see lower plots, it can also be observed that the OSs are less conservative than the circles, since the former are furthest away from the Nyquist instability point, -1.

6.4 Discussion

It could be seen from the μ-analysis results of the different uncertainty models at 1X-speed that the mixed uncertainty description with "olympic stadiums" was significantly less conservative around 30[Hz] than the complex uncertainty description with circles. It suggests that the "olympic stadiums" are a better alternative, compared

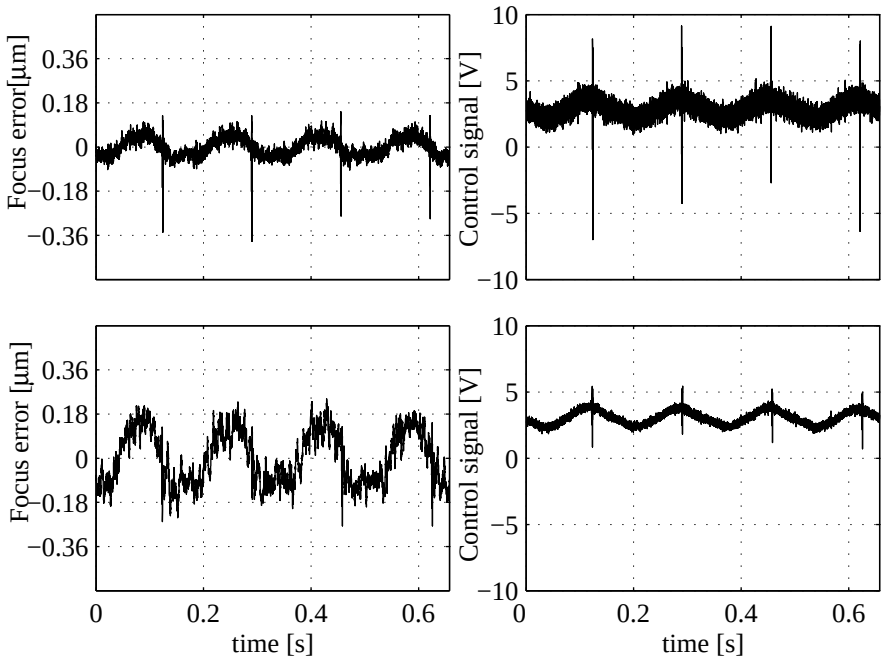

Figure 6.7: *Focus closed loop measurements with the μ-PID controller with two different gains. In the upper graphs the nominal μ-PID controller was employed while in the lower graphs the gain of the μ-PID controller was reduced by a factor of 3 (approx. -9.5[dB]). The CD rotated at 6[Hz] and had a scratch of approx.* $1e^{-3}[m]$.

to the circles, to describe the uncertainties in resonant systems, like those found in the CD-drives. As pointed out in [Vidal *et al.*, 2003], perhaps the most interesting result concerning this μ-analysis is the employed controller. The μ-PID is able to offer robust performance with still some room to adjust the gain of the controller because this model allows less conservative design at the critical frequencies . This fact may explain why a relatively simple controller has been and is widely used in commercial CD-players. The challenges are in finding a controller which is able to cope with disturbances of conflictive requirements. One possibility is the strategy suggested in [Vidal *et al.*, 2000], where two $\mathcal{H}_\infty$-controllers are designed. The plant is closed by a controller which specifically attenuates the disturbance channel $w_p \rightarrow z_p$, and it is temporary replaced on-line by a lower bandwidth $\mathcal{H}_\infty$-controller in the presence of surface defects.

Figure 6.7 clearly showed the trade-off in the controllers of CD-players where a μ-PID

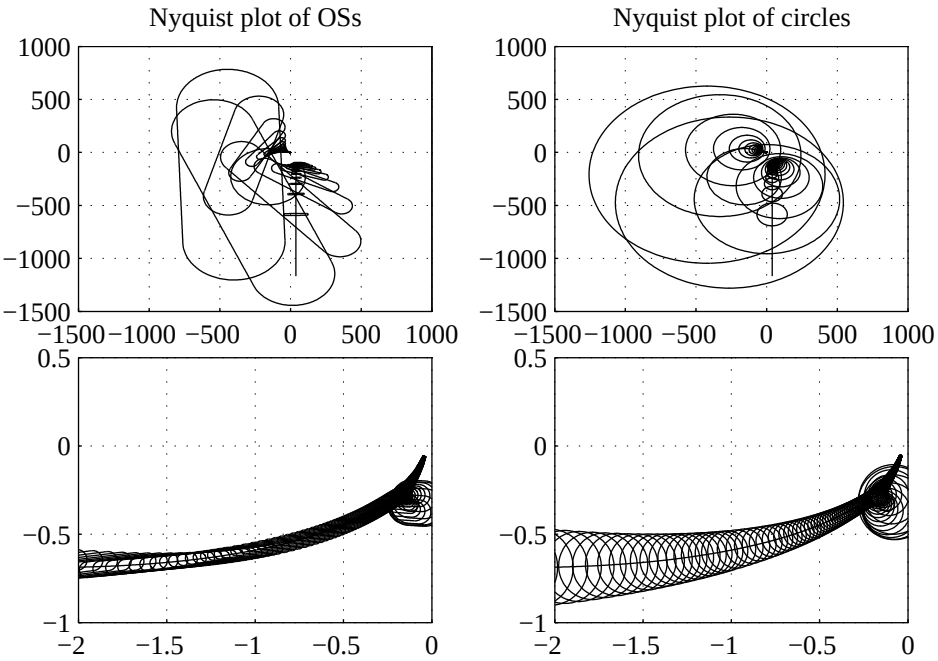

Figure 6.8: *Nyquist plots of the open loop (the controller together with the plant) using two different uncertainty representations, namely the OSs and the circles. While the upper graphs show the complete Nyquist plot, the lower graphs show the zoomed version near the instability Nyquist point, -1.*

controller, which did not meet the robust performance requirements of the disturbance channel $w_p \rightarrow z_p$, could cope better with surface defects like scratches. In more demanding optical applications like CD-ROM or DVD-players, where the scan velocity is considerably higher than 1X, the trade-off is more severe and higher order structure controllers should be considered since they offer the possibility to achieve greater robust performance that the PID controllers. An analysis at 5X revealed that a PID controller did not show a satisfactory robust performance. Robust performance with a higher order controller could not be achieved either, an issue which is specific to the utilized laboratory setup. Nevertheless, it indicates that not only the controller but also the hardware should be revisited if a 1X platform is attempted to be upgraded to handle higher scan velocities.

The high similarity between the simulated and measured output sensitivities suggests that the method used to identify the parameters of the plants, described in Chapter 4, is

reliable for simulation and control design purposes.

In the last chapter it was argued that the OS offer a potentially less conservative mathematical representation of the uncertainty in resonant systems such as the treated CD-drives in the present thesis. The advantage of OS is evident based on the Nyquist plots shown in Figure 6.8. While the circles contain the Nyquist instability point, it can be observed that the OSs remain outside that point. It is also clear from this case that the appropriate is to choose the narrowest OSs and not the OSs which yield the smallest area. At higher frequencies the OSs also result in a less conservative uncertainty representation.

6.5 Summary

This chapter was dedicated to the application of robust control techniques to CD-players. In Section 6.1 insight was given on how to include the uncertainty representations in the control problem formulation treated in Chapter 5. Besides specifying the nominal model together with the related uncertainties, some minimization criteria must be given to the control synthesizing algorithms. Two different disturbance channels were distinguished, the first one, $w_p \rightarrow z_p$, related to the disc deviation of the disc and external disturbances such as mechanical shocks and the other one, $w_u \rightarrow z_u$, related to the control effort. It is shown that the disc deviations described in the Red Book can be formulated in a natural way as the requirements to the output sensitivity function, associated with the $w_p \rightarrow z_p$ disturbance channel. The weight to the other disturbance channel is application dependent but it is recommended to use the inverse of the optical gain as an initial weight. In Sections 6.3 and 6.4 the results are presented and discussed. Furthermore, it is shown for resonant systems, through CD-players as example, that the suggested mixed uncertainty representation from the previous chapter is less conservative than the complex representation. A μ-analysis of a PID controller revealed that it can meet relevant robust performance requirements in CD-players. However, for more demanding applications like CD-ROM or DVD-players, higher order controllers are preferred. Though the challenge is still to design a controller which is able to cope with the disturbances of conflictive requirements in a satisfactory way. The output sensitivity of the CD-drives are simulated and measured and their similarity suggest that the identification method described in Chapter 4 is reliable. Finally, it was shown by means of a graphical comparison of the Nyquist plots of the open loop, that the OSs yield a less conservative uncertainty representation than the circles.

Part III

Fault Diagnosis and Fault Tolerant Control in Compact Disc Drives

7

Fault Diagnosis on CD-drives

In safety-critical systems such as nuclear reactors, ships, aircraft and chemical plants the consequences of faults can be paid at an elevated price in terms of environmental impact, human mortality and economic loss. Similar consequences apply to smaller-scale safety-critical systems like cars and trains. Common to all of them is the growing need for on-line supervision and fault diagnosis to increase the reliability. While a CD-player cannot be considered to belong to the safety-critical systems category, a fault during the process of reading music from the disc may result in audible drop-outs causing inconvenience for the listener. In CD-ROM applications it may imply that the entire information stored in the disc is useless. On-line fault diagnosis techniques can be used for this kind of systems to improve plant efficiency and reliability.

A large number of control techniques have been applied to CD-players: adaptive control [Draijer *et al.*, 1992], adaptive repetitive control [Dötsch *et al.*, 1995], robust control [Steinbuch *et al.*, 1992], robust repetitive control [Lee, 1998], rejection of non/repeatable disturbances [Li and Tsao, 1999], LMI techniques [Dettori, 2001], fuzzy control algorithms [Yen *et al.*, 1992], a disturbance observer [Fujiyama *et al.*, 1998], Linear Quadratic Gaussian control [Weerasooriya and Phan, 1995] and quantitative feedback theory [Hearns and Grimble, 1999]. The majority of them strive towards a high controller bandwidth by minimizing the disturbance channel $w_p \rightarrow z_p$ in order to attenuate

mechanical disturbances $w_{md}(s)$, self-pollution $w_{sp}(s)$ and disc deviations $w_{cd}(s)$, shown in Figure 2.13 in Chapter 2. However, none of them have directly addressed the other main source of disturbance, namely surface defects $w_{sd}(s)$, which in fact imposes an upper bound on the achievable bandwidth. A simple but essential form for fault diagnosis is used in commercial CD-players. This fact indicates that some advantages can be obtained from fault diagnosis. Unfortunately, for unclear reasons, it does not seem to capture the attention of the control research community, judged on the amount of publications concerned the application of fault diagnosis to CD-players.

It is the purpose of this chapter to reveal how fault diagnosis can be applied to CD-players. Furthermore, the potential benefits are pointed out, assuming that fault diagnosis is integrated in a fault-tolerant control strategy. Section 7.1 starts introducing the terminology and concepts concerning fault diagnosis and how it relates to CD-players. A more general treatment of the concepts and methods can be obtained in [Chen and Patton, 1999]. In Section 7.2 two fault diagnosis strategies are presented. They are verified through simulations documented in Section 7.3 and discussed in Section 7.4. Finally a summary of the chapter is given in Section 7.5.

7.1 Fault Diagnosis

In fault diagnosis, a fault is understood as an unexpected change of system function, although it may not represent physical failure or breakdown [Chen and Patton, 1999]. An alternative definition attributed to [Isermann, 1984], which may be more suitable to CD-players, is "a non permitted deviation of a characteristic property which leads to the inability to fulfil the intended purpose". As later argued in the chapter, surface defects which are viewed as faults, are considered as a *non permitted deviation* rather than an *unexpected change of system function*. The term *fault* is used to indicate that a malfunction may be tolerable at its present stage. Logically, a fault should be diagnosed as early as possible before it develops and leads to serious consequences. For that purpose a fault diagnosis system is utilized, divided into the following tasks:

- *Fault detection*: to make a binary decision. Either it works properly or it does not work properly.
- *Fault isolation*: to determine the location of the fault. It could for example be a malfunctioning sensor or actuator.
- *Fault estimation*: to estimate the size and type of the fault.

While fault detection and isolation are essential in a fault diagnosis system, commonly referred to as FDI, fault estimation is not strictly necessary. However the latter becomes more important in a fault-tolerant control system, characterized for being able to continue operating to fulfil specified functions despite the presence of faults. Fault diagnosis

plays obviously an important role in fault-tolerant control systems. Before any control law reconfiguration is possible, the fault must be detected, isolated and eventually estimated such that the supervision mechanism can make a suitable decision. In the next chapter, fault-tolerant control is treated, making use of the achieved results in fault diagnosis of the present chapter.

There are two conceptual different approaches to fault diagnosis. The first one is based on hardware redundancy methods, being its major disadvantage the increased cost due to the duplication of e.g. sensors and actuators. The other alternative is based on analytical redundancy which makes use of a mathematical model of the monitored process and is therefore usually referred to as the *model-based approach* to fault diagnosis [Chen and Patton, 1999]. In the same reference *model-based approach* is defined as *the determination of faults of a system from the comparison of available system measurements with a priori information represented by the system's mathematical model, through generation of residual quantities and their analysis*, where a residual is understood as a fault indicator. The advantage of the analytical redundancy is that no extra hardware components are added which may lead to additional faults.

The idea of replacing hardware by analytical redundancy is attributed to [Beard, 1971]. Since then, a wide diversity of model-based fault diagnosis approaches have been suggested. To name a few, the observer-based FDI approach attributed to [Clark *et al.*, 1975] where Luenberger observers were used for fault detection, frequency domain design for model-based FDI where μ synthesis was applied to robustfy the FDI problem attributed to [Mangoubi *et al.*, 1992] and two-stages model-based FDI structure attributed to [Chow and Willsky, 1980]. The last is accepted as a standard procedure for model-based FDI, illustrated in Figure 7.1.

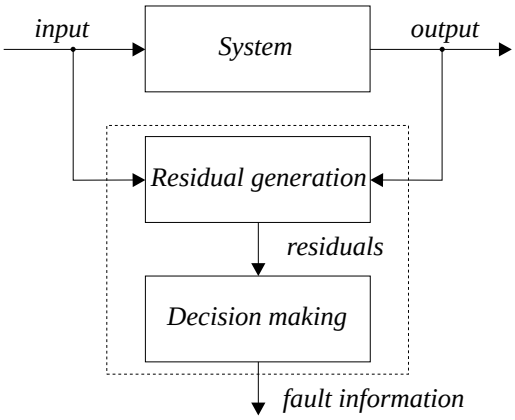

Figure 7.1: *Conceptual structure of model-based fault diagnosis.*

The purpose of the residual generation stage is to generate a fault indicating signal, also called residual. The residual should ideally carry only fault information and should be

independent on the characteristics of the system input and output. In other words, the residual should be approx. zero when no fault is present but distinguishable different from zero when a fault occurs. In the decision-making stage the residuals are examined for the likelihood of faults based on a decision rule which can rely on statistical decision theory or just as simple as a threshold test. Generally, if a reliable residual generation is designed, the task of decision making is relatively easy.

The choice of FDI method is a complicated problem and it is hard to say whether a particular method is better than another method because one may be good in one aspect but bad in others. Hence the choice of FDI method is dependent on the problem to be solved [Chen and Patton, 1999]. In the next subsection an analysis of the faults that may occur in a CD-player is performed and the remaining of the chapter is dedicated to describe how they can be detected, isolated and estimated and how they can be integrated in a suitable FDI strategy.

7.1.1 Fault Analysis of a CD-drive

In the general case, a system can have faults in the actuators, in the plant to be controlled and in the sensors. However, in the case of the CD-player, the plant to be controlled is the actuator itself, as illustrated in Figure 7.2 which shows the focus loop with possible faults. It is important to recall that the signals available are not only the focus normalized error but also $d_1(s)$, $d_2(s)$, $f_e(s)$ and $f_s(s)$ as shown in Figure 3.12 in Section 3.6. An equivalent figure applies to the radial loop as well. In the thesis only the focus and radial loops are considered. However, it is known from Section 2.5 that the sledge have certain influence, especially on the radial loop, [Aangenent, 2002, Dzanovic and Lauritsen, 2003]. Fault diagnosis (and fault-tolerant control) could also be beneficial to handle faults in the sledge loop.

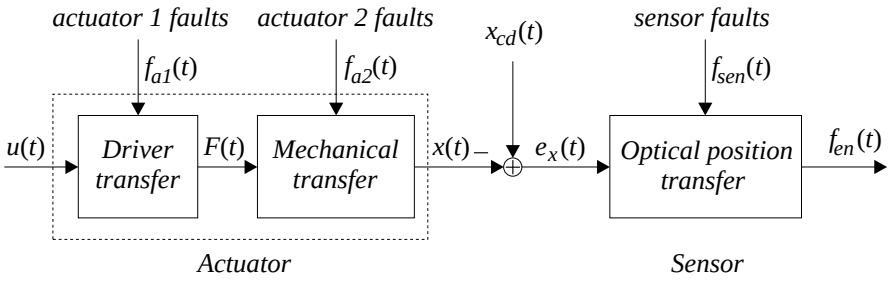

Figure 7.2: *Focus transfer diagram with its possible related faults.*

Three types of faults can be distinguished in Figure 7.2. Those which may occur in the first and in the second part of the actuator, denoted respectively *actuator 1* and *actuator 2 faults* and those which may occur in the photo diodes, denoted *sensor faults*.

Actuator 1 faults: Driver transfer

There are basically three parts which constitute the driver transfer. These are the power driver, the coil and the permanent magnet. The dynamic equations which describe the possible faults in the driver transfer can be described by

$$\begin{aligned} \dot{x}_{a1}(t) &= A_{a1}x_{a1}(t) + B_{a1}u(t) + f_{a1}(t) \\ F(t) &= C_{a1}x_{a1}(t) + D_{a1}u(t), \end{aligned} \tag{7.1}$$

where $f_{a1}(t)$ is the actuator fault which may occur in linear system. In some cases, the faults could be expressed as a change in the parameters of the system [Chen and Patton, 1999], hence the dynamic equation of the actuator can be described as

$$\dot{x}(t) = Ax(t) + B_{a1}u(t) + I_i\Delta a_{ij}x_j(t), \tag{7.2}$$

where $x_j(t)$ is the j_{th} element of the vector $x(t)$ and I_i is a n-dimensional vector with all zero elements except a 1 in the i_{th} element.

In general the power drivers are designed with a short circuit and a thermal protection. They also have an internal feedback circuitry which ensures a constant gain. It can be said that they are tolerant to faults up to some limits. However, serious faults which result in a damaged power driver implies that the position of the pickup cannot be controlled and consequently the CD-player will no work. Some of the effects due to changes in the resistance of the coil can be compensated by the internal feedback circuitry of the power drivers, but a damaged coil which results in an open circuit will again imply that the CD-player cannot work. The third and last part constituting the driver transfer is the permanent magnet which is practically not exposed to faults. This brief analysis suggests that marginal improvements can be done on the driver transfer function to avoid a defective CD-player if any of the parts is damaged. Therefore, the benefits of fault diagnosis integrated in a fault-tolerant control strategy on this part of the actuator are rather limited.

Actuator 2 faults: Mechanical transfer

The second part of the actuator can be understood as the device in which the lens is suspended, that moves as a result of the interaction between the permanent magnet and the created magnetic field by the coil. As for the first part of the actuator, similar equations can be set up for the possible faults in the mechanical transfer

$$\begin{aligned} \dot{x}_{a2}(t) &= A_{a2}x_{a2}(t) + B_{a2}F(t) + f_{a2}(t) \\ x(t) &= C_{a2}x_{a2}(t) + D_{a2}F(t). \end{aligned} \tag{7.3}$$

The exposed element to faults is the flexible compound which permits a vertical and horizontal movement of the lens. Especially aging of the pickup leads to a weaker flexible compound giving different dynamic characteristics of the actuator. These changes in the actuator can be considered as slow faults, also denoted as *incipient faults*, described in more details in Subsection 7.1.2. Given the case that the flexible compound breaks, nothing can be done to prevent the CD-player stop working. Nevertheless, any controller should have a certain degree of robustness which accounts for the slow variations of the actuator dynamics due to the aging process. Performance of the controller could, however, be improved by relaxing the robustness requirements provided the inclusion of fault diagnosis in a fault-tolerant strategy. This strategy could be based on the estimation of the parameters at the start-up sequence of the CD-player which takes proper decisions that adjust the control strategy. In practice there is an AGC in the CD-players, described in Section 4.4 which also compensates within some margins for the effects of the aging process and as a consequence the robustness requirements of the controller are reduced. Due to the presence of the AGC in CD-players, the advantages, as a result of the addition of fault diagnosis in a fault-tolerant strategy, are also reduced.

Sensor faults: Optical position transfer

The optical position transfer is not only composed by the photo diodes but also by the laser, the lenses and the surface of the disc where the laser beam is focused on. Any anomaly of the listed elements may lead to a sensor fault which can be described as

$$f_{en}(t) = K_{optFn}(e_x(t) + f_{sen}(t)), \tag{7.4}$$

where $f_{sen}(t)$ is the sensor fault and $e_x(t)$ is the actual focus error. These two signals are amplified by the optical gain K_{optFn}, yielding the focus error $f_{en}(t)$ suitable for feedback control. The dynamics of the sensor can be neglected since its bandwidth is considerably larger than the frequencies of interest. All the sensor faults can be described by choosing a proper value of the fault $f_{sen}(t)$. Given the hypothetical case that the photo diodes delivered a constant focus error, e.g. $f_{en}(t) = 0$, the fault would then be given by $f_{sen}(t) = -e_x(t)$. Multiplicative faults can also be generated by the above sensor fault description.

Fault diagnosis may not provide direct advantages when the faults occur in the laser, lenses or photodiodes. The laser diode delivers a constant emission of photons thanks to an internal feedback. Aging of the laser diode typically causes that a higher level of current is necessary to ensure the constant emission of photons. However, at a certain point of its life cycle, the constant emission cannot be guaranteed due to physical constraints (e.g. the source current reaches a maximum value). Hence the CD-player will be more prone to fail, which typically results in an increasing number of music drop-outs, until the CD-player eventually stops working. Dirt or scratches in the lenses

will generally result in a lower transparency, but owing to the AGC, the effect of these faults can be corrected up to certain extent. The last part to mention are the photo diodes, which normally work correct along the life cycle of the CD-player.

From a control point of view, surface defects can be considered as sensor faults which mask the position information of the focus point. Fault diagnosis alone does not enhance the playability of CD-players, although it is necessary in order to detect such faults. Fault diagnosis should instead be integrated in a fault-tolerant control strategy which gives the possibility to react to the detected faults. Hence the playability of CD-players can potentially be improved. The system model for CD-players which includes all possible faults can be described as

$$\begin{aligned} \dot{x}(t) &= Ax(t) + Bu(t) + R_1 f(t) \\ f_{en}(t) &= Cx(t) + Du(t) + R_2 f(t), \end{aligned} \tag{7.5}$$

where $f(t)$ is a fault vector with R_1 and R_2 as fault entry matrices which represent the effect of faults on the system. However, since it has been argued that the advantages of a fault diagnosis integrated in a fault-tolerant control strategy primary rely on the sensor side, in specific *surface defects*, the system output can be described as follows, where only sensor faults due to surface defects are considered,

$$f_{en}(s) = K_{optFn}(ACT(s)u(s) + f_{sd}(s) + e_x(s)). \tag{7.6}$$

In order to detect the faults, a residual generator is needed. Figure 7.3 shows the structure for such residual generator, which can be expressed mathematically as

$$r(s) = \begin{bmatrix} H_{act}(s) & H_{photo}(s) \end{bmatrix} \begin{bmatrix} u(s) \\ f_{en}(s) \end{bmatrix} = H_{act}(s)u(s) + H_{photo}(s)f_{en}(s), \tag{7.7}$$

where $H_{act}(s)$ and $H_{photo}(s)$ are stable and linear transfer matrices and $ACT(s)$ describes the dynamics of the plant. $w_{sd}(s)$ is an imaginary signal with flat power spectrum (white noise) which generates sensor faults $f_{sd}(s)$ with frequency content dictated by $W_{sd}(s)$. The residual $r(s)$ is designed such that it only becomes zero for a fault-free case ($f_{sd}(s) = 0$). It should be noticed that the vertical position of the track $x_{cd}(t)$ is not included in the figure since it is considered as a disturbance, which is treated later in this section.
From Figure 7.3 it can be inferred that this condition is satisfied if the transfer matrices $H_{act}(s)$ and $H_{photo}(s)$ are chosen such that

$$H_{act}(s) - H_{photo}(s)K_{optFn}ACT(s) = 0. \tag{7.8}$$

As suggested in [Chen and Patton, 1999], a fault can be detected by comparing the residual evaluation function $J(r(t))$ with a threshold function $T(s)$ according to the following test

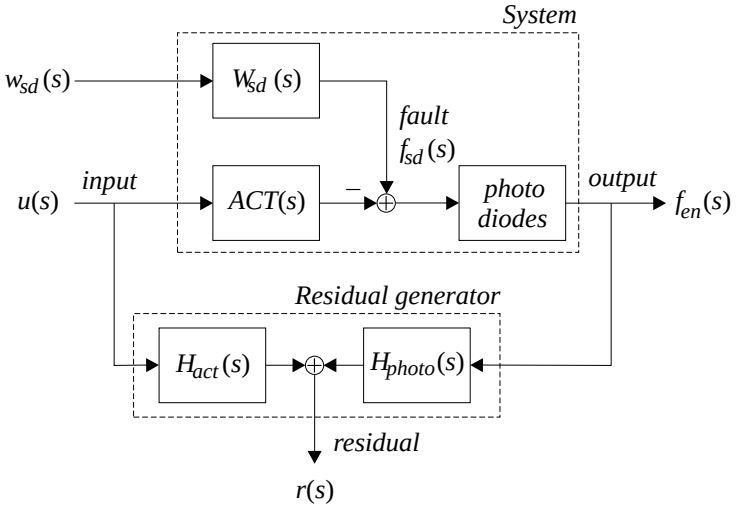

Figure 7.3: *Structure of a residual generator in CD-players ($photo\ diodes$ block added at the output of $ACT(s)$) based on the general structure attributed to [Patton and Chen, 1991]. Note that the vertical position of the track $x_{cd}(t)$ is not included here since it is considered as a disturbance, which is treated later in this section.*

$$\begin{cases} J(r(t)) \leq T(t) & \text{for} \quad f_{sd}(t) = 0 \\ J(r(t)) > T(t) & \text{for} \quad f_{sd}(t) \neq 0. \end{cases} \tag{7.9}$$

where $J(\cdot)$ basically is the logic which determines whether the residual is above or below the determined threshold.

7.1.2 Fault Detection

Before going into details on how to detect sensor faults in CD-players it is convenient to establish which type of sensor faults to detect. Faults can be classified in two groups according to the velocity they develop:

- *Incipient faults*: They have a small effect on the residuals and can be hidden as a consequence of modeling uncertainty. However, they may develop slowly, and the can eventually cause serious consequences. In CD-players a typical sensor fault of this kind could be the gradually decrease of the emission of photons by the laser diode. As another example it can be mentioned the increase/decrease of the optical gain in a CD along the tracks.

- *Abrupt faults*: As the name indicates these faults develop fast. They are relatively easy to detect because their effects on the fault diagnosis system are larger than modeling uncertainty. A threshold on the residual is usually sufficient to detect abrupt faults. There is a wide group of these sensor faults in CD-player, the majority of which were briefed in Section 2.5. Scratches, finger prints and dust are some examples.

Abrupt faults are the most common of these two groups in the daily use of a CD-player and are also the most challenging from a control point of view since they require that the correct action is taken fast. It is also important to note that the defined abrupt faults remain on the disc, and given the case that the information stored on the disc must be retrieved at all costs, little can help a replacement of the CD-drive. A technique which can handle abrupt faults is therefore imperative.

When a fault occurs, the output of the residual generator in accordance with Figure 7.3 is given by

$$r(s) = G_{rf}(s)f_{sd}(s), \tag{7.10}$$

where $G_{rf}(s) = H_{photo}(s)K_{optFn}$ is defined as the fault transfer matrix. In order to detect the faults, $G_{rf}(s)$ must satisfy the fault detectability condition of the residual $r(s)$ for a given fault $f_{sd}(s)$

$$\left[G_{rf}(s)\right] \neq 0. \tag{7.11}$$

This condition is not always sufficient since the residual might be positive at the flanks of a fault but it might go back to zero during the period of the fault. Therefore in some cases it is not clear to determine whether the fault disappeared by its own or whether the fault is still present but the effect on the residual just disappeared. Reliable fault detection is guaranteed by the *strong fault detectability condition*

$$\left[G_{rf}(0)\right] \neq 0, \tag{7.12}$$

which ensures a positive value of the residual along the entire period of the fault. In practice, the detection of surface defects in CD-players can be performed by monitoring the intensity of the reflected light, as explained in Section 2.5. If the actual intensity of the reflected light drops rapidly to a predetermined threshold, a fault is considered to be detected. The detection method is characterized by its simplicity and reliability.
Figure 7.4 shows an example of such surface defects. In the normalized error signal in the upper left plot some spikes can be discerned going both upwards and downwards. As mentioned in Section 2.5, when the laser beam encounters a surface defect, in the majority of the cases, little light is reflected back to the photo diodes resulting in a drop of the registered intensity. The detection of surface defects is not based on the focus error signal since it changes of sign. Basically it corresponds to say that the focus error

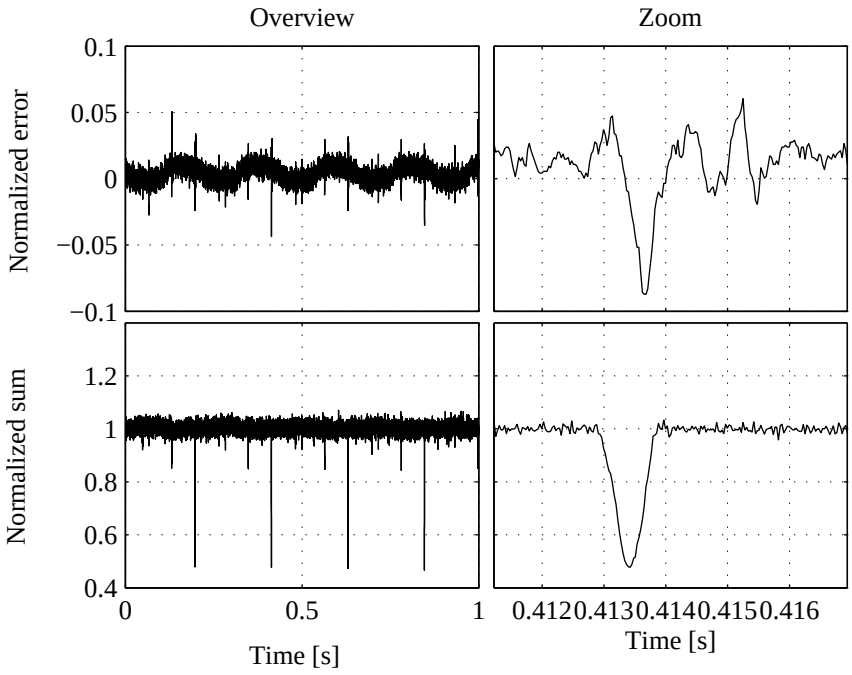

Figure 7.4: *Example of abrupt sensor faults caused by surface defects in the disc. The normalized focus error signal is shown in the upper left plot while the respective sum signal is shown in the lower left plot. The right plots show a zoomed version of the signals where the effects of a surface defected are present.*

signal satisfies the fault detectability condition in Equation 7.11 but not the strong fault detectability condition in Equation 7.12, if no further signal processing is performed. However, the focus sum signal can be straightforward employed to yield a reliable fault detection since it can be said that it satisfies both detectability conditions. Note also that once the surface defect is passed, there are still visible effects in the focus error but not in the focus sum. A more reliable fault detection is therefore clearly achieved by monitoring the focus sum.

Three known approaches of generating the focus error signal in CD-players were explained in Section 2.4, having in common that the actual focus error is approximately proportional to the generated feedback error signal. In Section 4.6 a measurement of the s-curve for the single Foucault method was presented in Figure 4.6, (the photo diode signals $d_1(t) - d_2(t)$ were plotted versus the displacement of the focus point). The con-

troller must keep the focus point in the linear area of the s-curve otherwise the focus is lost. An alternative method to detect and characterize the sensor faults in a CD-player is to consider the photo diode signals $d_1(t)$ versus $d_2(t)$ [Vidal *et al.*, 2001a]. All the possible measurements of the diode signals are contained in the triangle, illustrated in Figure 7.5.

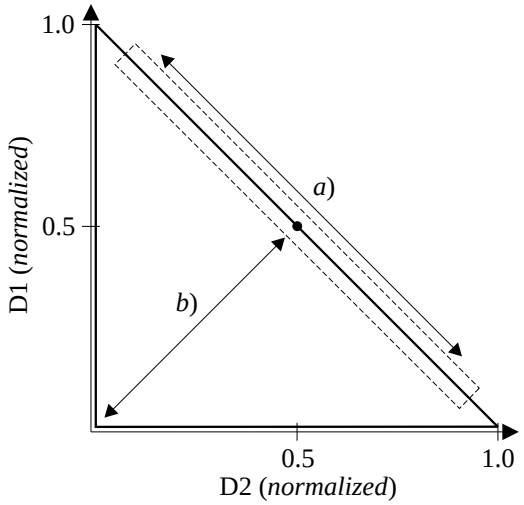

Figure 7.5: *Space spanned by the diode signals d_1 and d_2. See text for an explanation.*

It is another way of interpreting the photo diode signals, where the dotted rectangle indicates the mentioned linear area of the s-curve. The position of the focus point (and consequently the position measurements) should remain in the dotted rectangle. Ideally the focus point should be at the dot with the normalized coordinates $d_1 = 0.5,\ d_2 = 0.5$, that is, the focus error is zero. However, defects on the disc surface change the reflection properties of the disc resulting in a drop of the intensity of the reflected light, shown in case $b)$. The position measurements are not longer in accordance with the actual position of the focus point. Instead of the traditional binary decision in fault detection strategies, where there is either a fault or every thing works properly, following approach can be proposed [Vidal *et al.*, 2001b]:

$$\omega_Q = \begin{cases} 1 & \text{for} \quad dist \leq dist_{min}, \\ \left(\frac{dist_{max} - dist}{dist_{max} - dist_{min}} \right)^{\alpha} & \text{for} \quad dist_{min} < dist < dist_{max}, \\ 0 & \text{for} \quad dist \geq dist_{max}. \end{cases} \tag{7.13}$$

$dist$ is the distance between the actual measurement and the linear area, given by the expression below

$$dist = \frac{|1 - d_{1n} - d_{2n}|}{\sqrt{2}}, \tag{7.14}$$

where d_{1n} and d_{2n} are the normalized focus photo diode signals. Movements of the focus point along the linear area are fully weighted, $\omega_Q = 1$, where $dist \approx 0$. $dist_{min}$ is a security margin constant which depends on the measurement noise level. In the case of a surface defect, d_{1n} versus d_{2n} will move towards origo and are weighted with the exponent α. $dist_{max}$ is the limit where d_{1n} versus d_{2n} is not weighted at all as the actual surface defect is considered too severe. The essence is that measurements lying in the linear area are considered to be an accurate estimate of the position of the focus point, whereas measurements lying outside that area are not regarded as fully valid measurements.

7.1.3 Fault Isolation

If a fault is distinguishable from other faults using one residual or several residuals, also referred to as *residual set*, it can be said that this fault is isolable using this residual set. There are basically two schemes to isolate faults. In the first scheme each residual $r_i(t)$ is sensitive to only one fault $f_i(t)$. If the residual is positive, then its related fault is considered to be present in the system. The other approach consists in making each residual sensitive to all except one fault. It involves consequently an analysis of all the residuals but yields a higher reliability than the former approach.

Going back to the sensor faults in a CD-player, assuming that there are no disturbances, $w_p(s) = 0$, the system output is given by

$$f_{en}(s) = K_{optFn}(ACT(s)u(s) + f_{sd}(s)). \tag{7.15}$$

In the previous subsection the aim was to detect sensor faults, in particular surface defects, but nothing was mentioned on how to discern the different kinds of sensor faults. It could be a scratch, a finger print, dust, etc. Equation 7.15 can be decomposed as an example into

$$f^1_{en}(s) = K_{optFn}(ACT(s)u(s) + f^1_{sd}(s)) \tag{7.16}$$

$$f^2_{en}(s) = K_{optFn}(ACT(s)u(s) + f^2_{sd}(s)) \tag{7.17}$$

such that the residual signal is sensitive to the fault group $f^1_{sd}(s)$ and insensitive to the other fault group $f^2_{sd}(s)$. The residual generator for $f^1_{sd}(s)$ is then given by

$$r^1(s) = H^1_{act}(s)u(s) + H^1_{photo}(s)f^1_{en}(s), \tag{7.18}$$

analogous to the one presented in Equation 7.7. By substituting $f^1_{en}(s)$ from Equation 7.16 into Equation 7.18 the following residual generator is obtained

$$r^1(s) = \left[H^1_{act}(s) + H^1_{photo}(s)K_{optFn}ACT(s)\right] u(s) + H^1_{photo}(s)K_{optFn}f^1_{sd}(s). \tag{7.19}$$

In order that the residual is only sensitive to the first group of faults, $f^1_{sd}(s)$, the conditions given below must be satisfied

$$\begin{cases} H^1_{act}(s) = H^1_{photo}(s)K_{optFn}ACT(s) \\ H^1_{photo}(s) \neq 0. \end{cases} \tag{7.20}$$

provided that the frequency spectra of $f^1_{sd}(s)$ and $f^2_{sd}(s)$ do not overlap. The first condition ensures that the residual is zero in a fault-free case whereas the second condition implies that the residual is different from zero when a fault occurs. The only constraint on $H^1_{photo}(s)$ is that it should be stable and realizable. In the study documented in [Vidal *et al.*, 2001a] it is pointed out that a subspace (of the space spanned by d_{1n} and d_{2n}) can be constructed based on the possible combinations of d_{1n} and d_{2n} where no faults are assumed to be present. Other subspaces can be defined, each being characteristic for a type of sensor fault. Hence by analyzing the subspace which the actual measurement of d_{1n} and d_{2n} belongs to, fault isolation is possible. Measurements of finger prints, scratches and black dots realized with the laboratory setup support the possibility of fault isolation.

In a recent report [van Helvoirt, 2002], it is in fact demonstrated that different types of sensor faults can be distinguished from each other. First a cluster is assigned for each fault desired to be isolated. Then by analyzing the shape of the sum signal, it is identified which cluster it belongs to, and the fault in question is consequently isolated. "White dots" which have the property of resulting in an increase of focus sum were also studied. A large number of measurements were performed with the laboratory setup described in Section 3.6 but it was not possible to find a surface defect with higher reflection properties as observed in [van Helvoirt, 2002]. It may indicate that the "white dot" effect may occur rarely in practice. Only an increased reflection in the focus sum was observed with the laboratory setup when mechanical disturbances were of such magnitude that several tracks were jumped. The space between the tracks has a higher reflection coefficient and it results consequently in a focus sum increase. This forms part of the optical cross-coupling explained in Section 3.5.

7.1.4 Residual Generation

The generation of residual signals is a central issue in model-based fault diagnosis, (the most common approaches can be found in [Chen and Patton, 1999]). Inappropriate

residual signals may result in an excess number of missed and/or false alarms, which are obviously not desirable. So far, only sensor faults impinging the system have been treated, but in practice modeling errors and disturbances are inevitable and the residual generation should therefore be designed to be robust. The task in the design of a robust FDI system is thus to generate residuals which are insensitive to uncertainty and disturbances, and at the same time being sensitive to faults. The transfer function of the CD-player with modeling errors, disturbances and faults (surface defects) can be described by

$$f_{en}(s) = K_{optFn}(ACT(s)(1 + w_I(s)\Delta_I(s))u(s) + W_p(s)w_p(s) + W_{sd}(s)w_{sd}(s)), \tag{7.21}$$

where $w_I(s)$ is the multiplicative uncertainty weight which specifies the uncertainty level along frequency, see Section 5.1 for more details. Other uncertainty representations are also possible. $w_{sd}(s)$ and $w_p(s)$ are imaginary signals with a different physical interpretation, where $w_{sd}(s)$ represents the surface defects. $w_p(s)$ includes the disturbances $w_{md}(s)$, $w_{sp}(s)$, $w_{dd}(s)$ which are respectively mechanical disturbances, self-pollution and disc deviations, described in more details in Section 2.5. They are all characterized by having a flat power spectrum (white noise) which affect the system output through the filters $W_p(s)$ and $W_{sd}(s)$. The filters are therefore in charge of giving the signals the proper frequency content. The effect of the disturbances on the residual signals is logically unwanted and the residual generator should be designed to satisfy

$$H_{photo}(s)W_p(s) = 0. \tag{7.22}$$

This is called the principle of disturbance decoupling for robust residual generation [Chen and Patton, 1999]. Unfortunately, totally decoupling is not always possible. The reason why it is not possible in CD-players is that the spectra of the disturbances and faults overlap as mentioned in Section 2.5. In practice, fault detection and isolation in CD-players is relatively simple since the focus sum signal can be considered as the necessary residual which is already decoupled from disturbances. This property is illustrated in Figure 7.4 (and in Figure 7.5). In spite of the sinusoidal movement of the focus point caused the disc deviations, it can be appreciated that the sum level is constant and that it only falls drastically when a surface defect is present. Disturbances like mechanical ones, move the optical pickup from its actual position, and consequently the position of the focus point is also displaced. As long as the effects of the disturbances can be handled by the positioning controllers, the position of the focus point will remain in the linear area, shown as case $a)$ in Figure 7.5. On the other hand, surface defects change the reflection properties of the disc resulting in a decrease of the total reflected light, as shown in case $b)$. Measurements in [Vidal *et al.*, 2001a] also support the fact that the focus sum has a high degree of decoupling from external mechanical disturbances.

7.1.5 Fault Estimation

It has been explained that the existing fault detection and isolation in commercial CD-players can be achieved by a simple technique, which in practice boils down to monitoring the level of the focus sum. An alternative method that estimates the quality of the disc surface which can give a more detailed characterization of the faults in CD-players has been suggested. However, in a fault tolerant control strategy it could be convenient not only to know when and which fault has occurred but also to estimate its size and the effect faults have in the feedback signals. The advantage of estimating the shape of surface defects is that the caused effects, in theory, can be removed from the feedback signal, such that the controller only reacts on feedback signals which contain disturbances generated by $W_p(s)$ but which are not corrupted by surface defects generated by $W_{sd}(s)$. While simple techniques are sufficient to detect and isolate the faults, the degree of challenge increases considerably when it comes to fault estimation. By only having knowledge of the expected frequency content of the faults, it may be difficult to identify the contribution level of the disturbances and the faults from the feedback signals. Especially, when they coincide in the frequency and time domain, hence totally decoupling of disturbances from faults is not achievable. If the condition described in Equation 7.22 is not achievable, the following performance index is suggested [Ding and Frank, 1991]

$$I = \frac{\|H_{photo}(j\omega)W_p(j\omega)\|}{\|H_{act}(j\omega)W_{sd}(j\omega)\|}, \tag{7.23}$$

where I is minimized over a specified frequency range. The design of the filter to estimate the faults can also be formulated in the $\mathcal{H}_\infty$-framework, described in Section 5.1. It should be pointed out that the term *robust* has two different acceptions. In the $\mathcal{H}_\infty$-framework, *robust* is related to the *immunity against model uncertainties* whereas in the FDI terminology it is related to the *insensitiveness to disturbances*. Thus the aim of a $\mathcal{H}_\infty$-robust fault diagnosis filter design is to find a stable filter that minimizes effects of disturbances on the residual in the $\mathcal{H}_\infty$-norm sense while maximizing the effects of faults on the residual. It leads to the following two requirements [Sadrnia *et al.*, 1996]

$$\|G_{rw_p}(j\omega)\|_\infty < \gamma \tag{7.24}$$

$$\|G_{rw_{sd}}(j\omega)\|_\infty > \beta. \tag{7.25}$$

where $\gamma < \beta$. $G_{rw_p}(j\omega)$ and $G_{rw_{sd}}(j\omega)$ describe respectively the transfer function from the disturbances to the residual and from the faults to the residual. While condition 7.24 represents the worst-case robustness of the residual to disturbances, condition 7.25 guarantees a worst-case sensitivity of the residual to faults.

The effects of the controller in the loop should not be ignored. In [Chen and Patton, 1999] it is indicated that a robust controller may desensitize fault effects and make the fault diagnosis rather difficult and the best solution is to design the fault diagnosis scheme and the controller simultaneously, as suggested by e.g.

[Stoustrup *et al.*, 1997]. In this reference it is shown that the quality of control and the quality of detection will not improve by using the integrated design but it will be more beneficial in terms of implementation and reliability where both the controller and the diagnosis filter share the same observer. Also six possible design classes are suggested and the necessary formulae are provided. These classes are divided in two categories, nominal and robust performance of the diagnosis filter, and in each category, the controller can be designed for nominal performance, robust stability or robust performance. The simplest case is to design both the controller and the diagnosis filter for nominal performance and it can be cast as two separated standard $\mathcal{H}_\infty$-optimization problems. The other extreme of complexity is where both the controller and the diagnosis filter are designed for robust performance. It requires μ-optimization and the designs are coupled. There are still two possibilities in the latter case. Both the controller and the diagnosis filter can be designed in a single step, such that they share the same observer. Alternatively, the robust controller can be designed first. Then the diagnosis filter is designed, where the previously synthesized robust controller forms part of the solution to the filter. Note that there is an advantage in the last case. Once a robust controller is designed, the fault diagnosis filter can be redesigned without having to make changes in the controller, which is an appealing property. Assuming that the robust controller is designed as explained in Chapter 6, the diagnosis filter can be designed as follows [Stoustrup *et al.*, 1997]. First a model of the faults is necessary, which can be described with a frequency weight, as shown before

$$f_{sd} = W_{sd}(s) w_{sd}, \tag{7.26}$$

where $w_{sd}(s)$ is an imaginary signal which has a flat power spectrum. The filter $W_{sd}(s)$ generates the faults related to surface defects $f_{sd}(s)$ which affect the system output. In order to estimate these faults, it is necessary to define a fault estimation error z_f, given by

$$z_f = f_{sd} - u_f, \tag{7.27}$$

where u_f is the output of the diagnosis filter. The conditions given in Equation 7.24 and 7.25 can be rewritten to

$$\|G_{z_f w_p}(j\omega)\|_\infty < \gamma, \tag{7.28}$$

$$\|G_{z_f w_{sd}}(j\omega)\|_\infty < \beta. \tag{7.29}$$

The fulfilment of condition in Equation 7.28 ensures robustness of the fault estimation to disturbances, whereas the fulfilment of condition in Equation 7.29 guarantees the necessary sensitivity to achieve a reliable estimate of the faults. The design of such fault estimator can be cast in the μ-framework where plant uncertainties also are taken into account, see Figure 7.6.

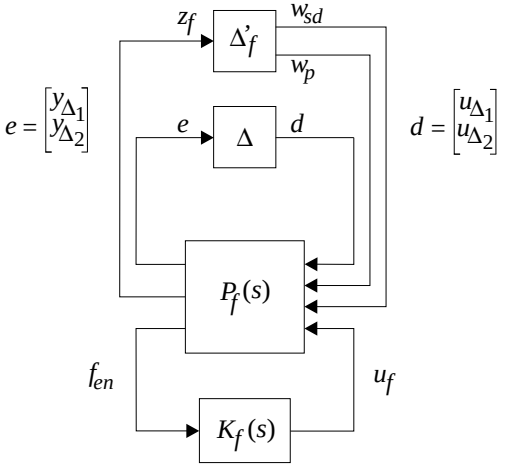

Figure 7.6: *Setup for the design of a robust fault detection filter suggested in [Stoustrup* et al.*, 1997] adapted here to CD-players.*

$P_f(s)$ is the generalized plant, which includes the plant to be controlled, the designed controller (in this case described in Chapter 6) and the uncertainty and performance weights. $K_f(s)$ is the fault estimator to be designed, which based on the sensed focus error f_{en}, generates a fault estimate u_f. The uncertainty block, Δ'_f, is related to the conditions given in Equations 7.28 and 7.29, where z_f is the defined fault estimation error and w_p and w_{sd} are respectively the disturbances and sensor faults. The uncertainties in the plant are also taken into account, modeled with the described method in Section 5.4 ("olympic stadiums"). Other types of uncertainty representations are possible too.

7.2 Suggested Fault Diagnosis Strategies

It is important to stress that the choice of FDI method is a complicated problem where it is difficult to say whether a particular method is better than another method. Experience has shown in CD-players that it is decisive to detect surface defects as soon as possible. Once these defects are detected, the challenge is how to separate the effects of the surface defects from the positioning information of the focus point such that the controller remains passive against surface defects. The feedback error is given by

$$f_{en}(s) = K_{optFn}(-x(s) + x_{cd}(s) + f_{sd}(s)), \tag{7.30}$$

visualized in block diagram form in Figure 7.7.
Two relevant approaches can be distinguished in fault diagnosis applied to CD-players whose common aim is to end up with an estimate of the disturbances to be suppressed by

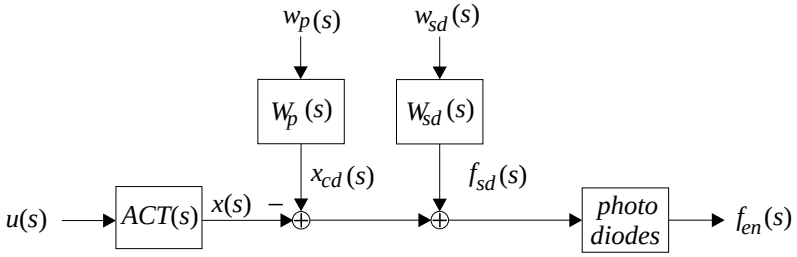

Figure 7.7: *Signals constituting the feedback error.*

the controller. The first one consists on estimating the surface defects $f_{sd}(s)$ such that these can be removed from the focus error $f_{en}(s)$. The focus error would therefore only contain the disturbances to be suppressed. Obviously, a model of the surface defects, $W_{sd}(s)$, is required. Alternatively, the focus error can be estimated based on the measurements previous to the surface defects. In this case, a model of the plant to control $ACT(s)$ and a model of the disturbances $W_p(s)$ impinging the loop are necessary. A combination of both methods is also a possibility, not treated here.

7.2.1 Estimation of the Surface Defects

The estimation of the surface defects can be based on the method suggested by [Stoustrup *et al.*, 1997], depicted in Figure 7.6. A more detailed and concrete setup for the design of the fault diagnosis filter is given in Figure 7.8.
Some similarities to Figure 6.2 from Chapter 6 are evident. The closed loop formed by the actuator $ACT(s)$, the photo diodes and the controller $K(s)$ is identical. The same uncertainty representation is present, where the weight $W_r(s)$ specifies the length and orientation of the "olympic stadiums". Their width is described by the weight $W_c(s)$. The weight $W_p(s)$, which describes the worst-case disturbances from a disc, is designed according to the Red Book specifications, as well as in Chapter 6. However in portable solutions it would be convenient to also include a model of the mechanical disturbances. The main difference between the two figures is that in Figure 7.8, the surfaces defects are modeled with the weight $W_{sd}(s)$ and are estimated by the fault diagnosis filter $K_f(s)$. The generated estimation error $z_f(s)$ is in practice duplicated where the roll of the two-rows vector $\varepsilon = \begin{bmatrix} \varepsilon_1 \\ \varepsilon_2 \end{bmatrix}$ is to scale the disturbance channel $w_p \rightarrow z_f$ and the fault channel $w_{sd} \rightarrow z_f$ such that μ-synthesis algorithm minimizes both channels adequately. While $u_f(s)$ is an estimate of the surface defect, $\omega_Q(s)$ is an estimate of the surface quality (or quality of the photo diodes measurements), as described in Equation 7.13.

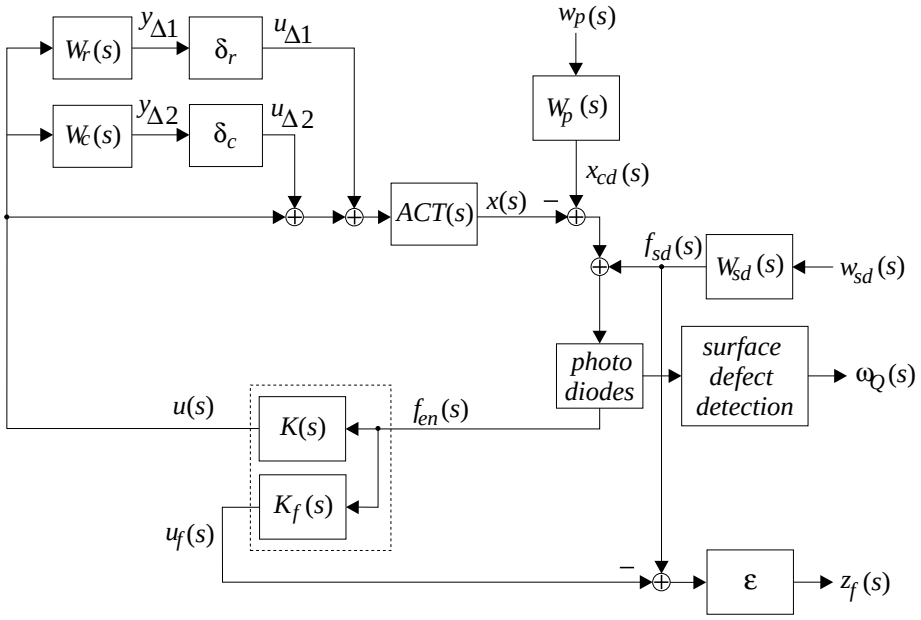

Figure 7.8: *Generalized setup for the design of a robust fault diagnosis filter.*

7.2.2 Estimation of the Positions of the Focus Point and the Information Layer

The presented strategy in Figure 7.9 (also described in [Vidal *et al.*, 2001b]) is a conceptually different solution to tackle the same problem. Again, the closed loop is formed by the actuator $ACT(s)$, the photo diodes and the controller $K(s)$. The quality of the surface, $\omega_Q(s)$, is also estimated in the *surface defect detection* block. For simplicity the uncertainties in $ACT(s)$ are not considered.
The main difference is to be found in the replacement of the fault diagnosis filter $K_f(s)$ by the position and disturbance estimators. The position estimator is composed by a model of the actuator, denoted $\widehat{ACT}(s)$, a model of the photo diodes, $\widehat{photo\ diodes}$, and a feedback gain matrix $K_{obs}(\omega_Q)$ which determines the bandwidth of the estimator. In order to compute K_{obs} such that the desired bandwidth of the estimator is achieved, some prototype filters like *ITAE* or *Bessel* can be used for this purpose [Franklin *et al.*, 1990].

Ideally, the surface of the disc is flawless, no disturbance is present and consequently the position of the information layer $x_{cd}(s)$ is constant. In this case the presence of a controller is obsolete and the estimated position of the focus point $\hat{x}(s)$ would match the

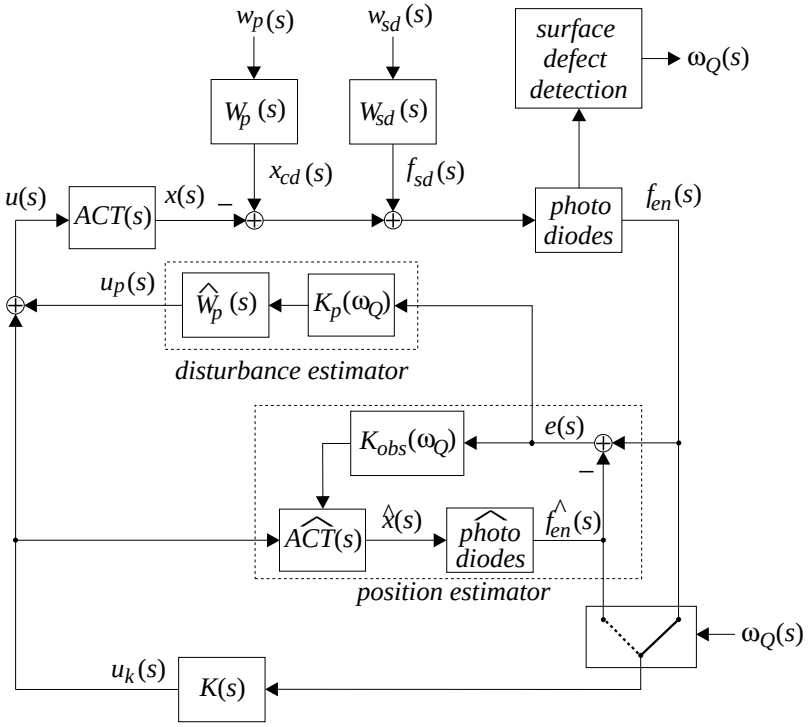

Figure 7.9: *Strategy based on the estimation of position of the focus point $x(s)$ and the position of the information layer $x_{cd}(s)$. Unlike the strategy presented in Figure 7.8, the present strategy cannot be implemented alone and needs to be integrated in a fault-tolerant control strategy in order to work properly. Therefore the details concerning the switch are explained in Section 8.4.*

actual position $x(s)$. Nevertheless, the disturbances modeled by $W_p(s)$ affect the position of the information layer $x_{cd}(s)$ and a mismatch is created between the measured and the estimated focus error, $f_{en}(s) \neq \widehat{f_{en}}(s)$. The position estimator is not able to track this mismatch, since only the dynamics of the actuator are included in the estimator. The disturbance estimator receives this mismatch as input and generates an estimation signal $u_p(s)$, such that it attenuates the effects of the disturbance originated by $W_p(s)$. Since the main source of contribution to the considered mismatch is originated due to the disc warp and track eccentricity, it is generally sufficient to model the fundamental rotation frequency with a few additional harmonics. The bandwidth of the presented estimators is adjusted according to the surface quality. In the case where a severe surface defect is detected, the estimators would run in open loop. It is therefore important to include

an adaptive scheme such that $\widehat{W}_p(s)$ follows the rotation frequency, as suggested in e.g. [Dötsch *et al.*, 1995]. The properties of this strategy are exploited in a fault tolerant control configuration described in the next chapter, where in the case of a surface defect, the controller bases the generation of the control signal only on the estimated signals. In normal conditions, where $\omega_Q \approx 1.0$, the bandwidth is limited by the feedback gain matrices, and in the presence of a surface defect, $\omega_Q \approx 0.0$, the bandwidth of the estimated signals is eventually reduced to zero. Hence in the case where there is no surface defect, the bandwidth of the observer should be such that it does not affect the bandwidth of the controller in the closed loop.

7.3 Results

The results of the present chapter can be divided into three parts with the following outline:

- *Surface defect detection*: The reliability of the fault detection is assessed based on the measurements of the diode signals $d_1(t)$ and $d_2(t)$ and the analysis of the generated quality signal ω_Q.
- *Surface defect estimation*: In order to verify its reliability it would be convenient to measure the real surface and compare it with its corresponding estimation. The optical pickup alone cannot be used to this purpose since it only measures the difference between the position of the focus point and the surface. An involved laboratory setup is required in order to have independent measurements of the position of the focus point and the position of the surface. Instead the *surface defect estimation* analysis is limited to simulations in this chapter. However, in the next chapter, when the fault tolerant strategies are implemented, it will be possible to evaluate the complete strategy where the surface defect estimation is included.
- *Position and disturbance estimation*: For the same reasons given above, the evaluation of the estimation of the focus point position, together with the disturbances affecting the loop, is only based on simulations and in the following chapter the performance will be indirectly evaluated through measurements of the related fault tolerant strategy.

In the following simulations, the position of the information layer has been chosen to be

$$x_{cd}(t) = A_{cd}\sin(\omega_{rot}\cdot t) + n(t), \tag{7.31}$$

where $A_{cd} = 500[\mu\text{m}]$ is the vertical deviation of the CD, which is the maximum value according to the Red Book. ω_{rot} determines the rotation frequency of the CD, chosen to be $\omega_{rot} = 2\pi 5.5$[rad/s], being approx. the average rotation frequency of a CD. $n(t)$ is the colored noise present in the system, which depends on the specific setup. Based

on comparisons between the simulations and the experiments, it was found that white noise, limited to a bandwidth of 1750[Hz] with an amplitude of $0.15[\mu\text{m}]$, was adequate.

7.3.1 Surface Defect Detection

Figure 7.10 shows the effects of a scratch on a disc subjected to vertical disc deviations. In ideal conditions, the measurements should all be located at point $d_1 = 0.5, d_2 = 0.5$ where the focus error is zero. Due to the presence of noise and mechanical disturbances, the obtained shape is instead elliptical, which in this case roughly occupies the region given by the bounds $0.4 \leq d_1 \leq 0.6$ and $0.4 \leq d_2 \leq 0.6$. The periodical effects of the scratch can easily be appreciated since they result in a drastic drop of the reflected intensity of light returning afterwards to the linear area. For each revolution of the CD, a new trace approaching the point $d_1 = d_2 = 0.0$ is registered.

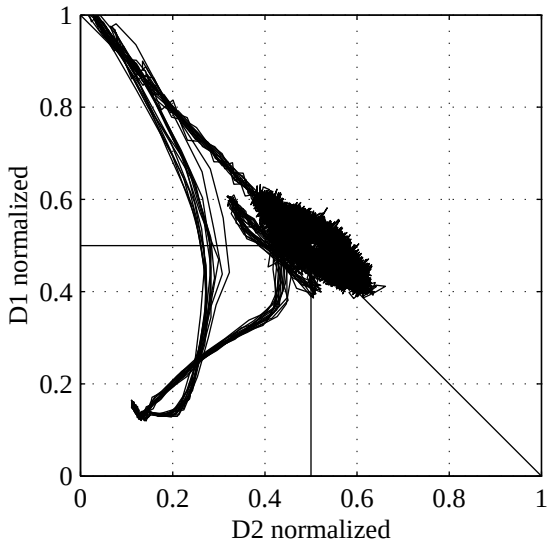

Figure 7.10: *Measurement of the focus diodes signals presented in the d_1-d_2 plane where the effects of a scratch and vertical disc deviations can be observed.*

A surface defect detection was performed on the same disc, giving the results shown in Figure 7.11. It can be observed that the scratch is detected periodically in the upper graph, which is in accordance with the rotation frequency of the CD. The lower graph zooms at one of the spikes and shows that the quality signal ω_Q changes gradually from 1 to 0 and back again to 1 as expected.

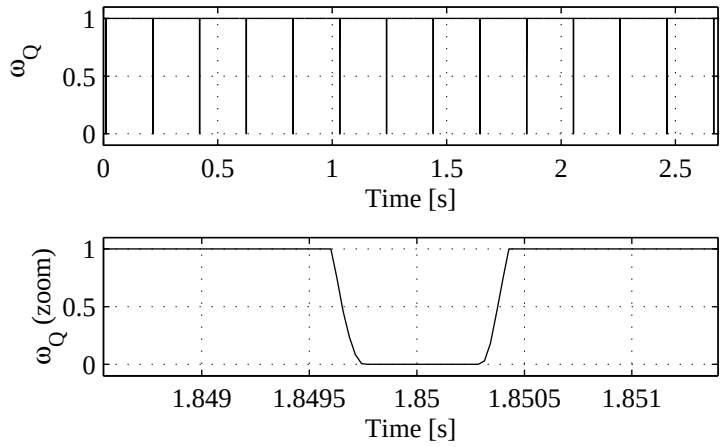

Figure 7.11: *Surface quality measurement of a disc rotating at approx. 5[Hz]. The upper graph shows that ω_Q falls down to 0.0 for each time the scratch is encountered. The lower graph gives a more detailed description of ω_Q when a scratch is detected. Note that the steepness of ω_Q it dictated by the exponent α shown in Equation 7.13.*

7.3.2 Surface Defect Estimation

There are certain similarities in the generalized plant used to design the robust fault diagnosis filter $K_f(s)$ compared to the generalized plant used to design the robust controller $K(s)$ in the previous chapter. The uncertainty representation based on the "olympic stadiums" and the performance weight $W_p(s)$ are the same. However, in the design of $K_f(s)$, a weight $W_{sd}(s)$, which describes the frequency content of the surface defects, is included.

$$W_{sd}(s) = \frac{(s + Xw_B A^{1/3})^3}{(s/M^{1/3} + Xw_B)^3}, \tag{7.32}$$

where M=250, A=0.001, $X = 3$ and w_B=2π·230[rad/sec] allowing an estimation of surface defects up to $1.6 \cdot 10^{-3}$[m]. It can be observed that it resembles $W_p(s)$ but inverted, which corresponds to say that what it is not a mechanical disturbance, it is a surface defect. However, $W_{sd}(s)$ has been shifted to a higher frequency ($X = 3$) so that the imposed requirements to the controller are feasible. The two channels to be minimized by the μ-synthesis algorithm are $w_p \rightarrow z_f$ and $w_{sd} \rightarrow z_f$ which are scaled respectively with the values $\varepsilon_1 = 5 \cdot 10^{-3}$ and $\varepsilon_1 = 2 \cdot 10^{-5}$. The design of the weights together with the suitable scales appeared to be the most difficult aspect in the filter design, an experience which is also shared by [van Groos *et al.*, 1994] where a μ-controller to a CD-player is designed. The μ-synthesis algorithm was stopped when

all the relevant μ-bounds were below magnitude 1, resulting in the filter presented in Figure 7.12.

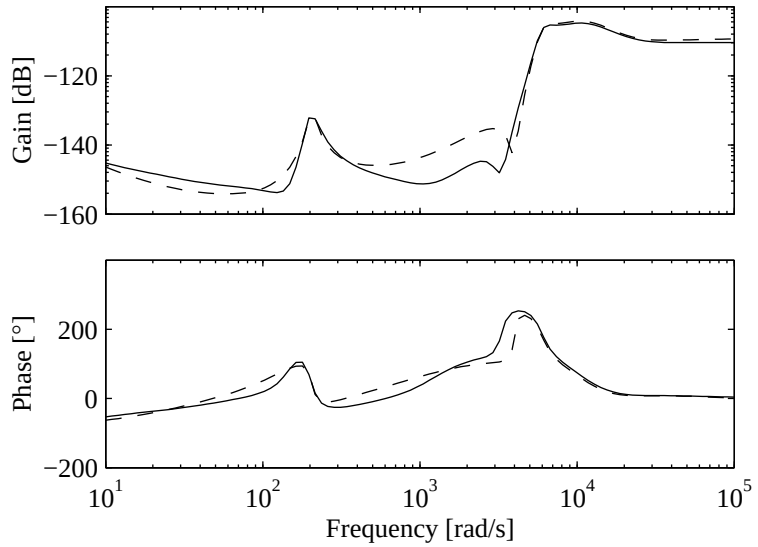

Figure 7.12: *Bode plot of the robust fault diagnosis filter. The solid trace shows the frequency response of the synthesized filter of 104th order in the continuous domain and the dashed trace shows the frequency response of the 10th order reduced filter in the discrete domain.*

The bode plot with the solid trace corresponds to the synthesized filter of 104th order in the continuous domain. The dashed trace corresponds to the filter of 10th order in the discrete domain (still meeting the performance requirements where the μ-bounds were below magnitude 1). The filter has a reasonable shape since it attenuates the low frequencies where the controller activity is elevated, and lets pass the high frequencies as described by the surface defect weight $W_{sd}(s)$. The gain at high frequency is approx. -110[dB] which is in line with the inverse of the optical gain. The reduced order filter has been tested with several simulated surface defects, two of which are shown in Figure 7.13.
It can be appreciated that the estimation of the first surface defect shown in the upper graph resembles the simulated surface defect. The estimation of the other surface defect, shown in the lower graph, is slightly poorer since it contains lower frequencies which are not able to be tracked by the filter.

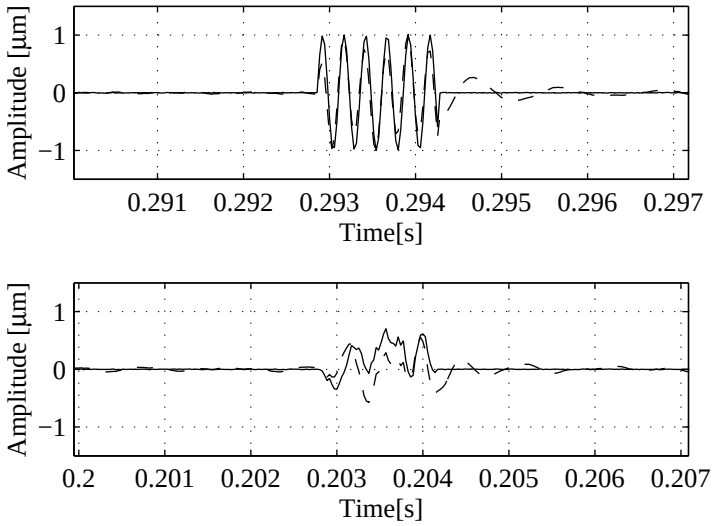

Figure 7.13: *Estimation of two simulated surface defects. The solid trace represents the simulated surface defect $f_{sd}(t)$ whereas the dashed trace represents the estimated surface defects $u_f(t)$.*

7.3.3 Position Estimations

The necessary design steps for this strategy are considerably less involved than those for the previous one. Only the feedback gain matrices K_{obs} and K_p must be calculated (the design of the adaptive weight $w_p(s)$ to the rotation frequency is not implemented). The actuator model $ACT(s)$, together with the anti-aliasing filter, form a 5th order system. The *ITAE* poles for such system are given by

$$(\frac{1}{obs_{bw}} + 0.8955)(\frac{1}{obs_{bw}} + 0.3764 \pm 1.2920j)(\frac{1}{obs_{bw}} + 0.5758 \pm 0.5339j), \quad (7.33)$$

where obs_{bw} is the bandwidth constituted by the closed loop poles. The bandwidth is selected to be $obs_{bw} = 2 \cdot \pi \cdot 5000$[rad/s] so it does not affect noticeably the bandwidth of the closed loop achieved by the robust controller $K(s)$. The resulting values of K_{obs} are

$$K_{obs} = 1 \cdot 10^{+8} \begin{bmatrix} 4.9312 \\ 4.0959 \\ 3.2174 \\ 2.3024 \\ 1.3581 \end{bmatrix}. \quad (7.34)$$

The values of K_p were found by trial and error

$$K_p = \begin{bmatrix} 45 \\ 45 \end{bmatrix}. \tag{7.35}$$

The higher the gain, the higher the ability to track the disturbance at the expense of a more noisy estimate. Figure 7.14 shows the estimation result of $x_{cd}(t)$. The amplitude given in volts, should be understood as the necessary control effort to attenuate the periodic oscillations such that the position of the focus point $x(t)$ follows $x_{cd}(t)$. The spikes are the effects of simulated surface defects. In the lower graphs, the effects of a surface defect are shown in more details. The value of ω_Q changes from 1.0 to 0.0, letting the estimator run in open loop. It can be appreciated that in this elapse of time the estimator is able to generate the missing position information of the information layer. Once the surface defect is passed, a spike arises due to inconsistencies between the simulated and the estimated signals. Such inconsistencies must therefore be minimized as much as possible.

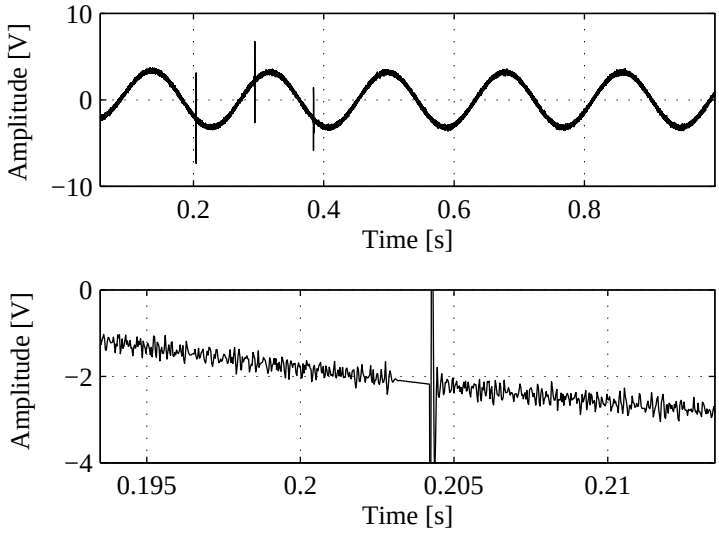

Figure 7.14: *Estimation of the position of the information layer $x_{cd}(t)$. The upper graph shows the generated control signal $u_p(t)$ which attenuates the periodic disturbances. The lower graphs shows a more detailed sequence of the same signal where it can be observed that the periodicity of the disturbance is followed in spite of the presence of a surface defect. Once the surface defect is passed, some unwanted oscillations appear.*

Figure 7.15 shows the estimation of the position of the focus point. The upper graph shows the simulated position $x(t)$ corrupted by a surface defect $f_{sd}(t)$ and the lower

graph shows the estimated position $\hat{x}(t)$. The effects of the surface defect in the estimate are substantially removed. The value of ω_Q also changes in this case from 1.0 to 0.0, letting the estimator run in open loop.
Once the surface defect is passed, ω_Q goes back to 1.0, the observer runs in closed loop and a spike of approx. 1[μm] is generated as a result of the mismatch between the simulated and the estimated states of the system. Although the effects of the surface defect are not completely eliminated, they are at least significantly reduced.

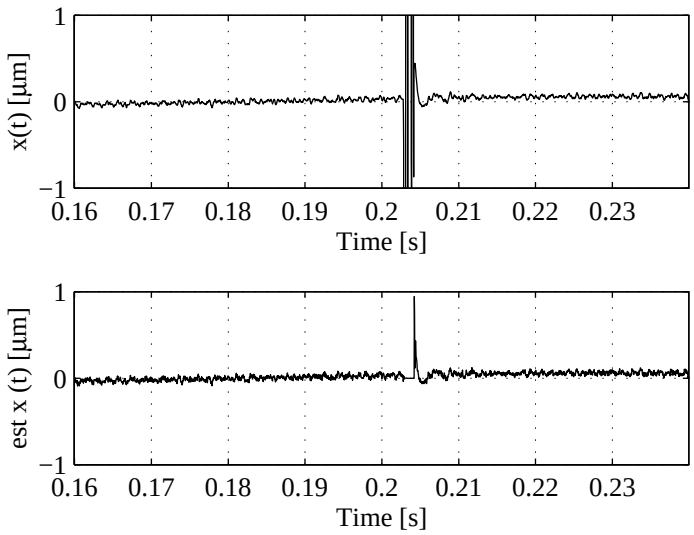

Figure 7.15: *The upper graph shows the simulated position of the information layer $x(t)$ corrupted by a surface defect $f_{sd}(t)$. The lower graph shows the estimate of the position of the focus point $\hat{x}(t)$ ($est\ x(t)$), where the effects of the surface defect are significantly reduced.*

7.4 Discussion

An alternative method to detect surface defects has been suggested. Instead of making a binary statement of whether a surface defect has been detected, a quality signal ω_Q monitors the credibility of the measured feedback error signals. In the proposed fault diagnosis strategies it is shown how the quality signal can be integrated in the design. In practice, whether ω_Q or its binary version is used might not cause notorious differences, since the transition between a flawless surface to the surface with a fault happens fast. Typically within a few samples. The important point to remark is the fact that the spanned space by the diode signals $d_1(t)$ and $d_2(t)$ can be extended to a four

dimensional space where the radial signals $s_1(t)$ and $s_2(t)$ are included too. A subspace can be determined where the measurements of the diode signals should be located in the case of a flawless surface. Depending on the surface defect, the diode signals may move from one to another subspace. In order to reconstruct the lost information of the position, a function could be defined such that the different subspaces related to the surface defects are mapped to the fault-free subspace. In [Odgaard *et al.*, 2003] a static nonlinear model of the optical pickup is derived, suitable for the suggested fault detection.

The designed robust fault diagnosis filter is not a trivial task, due to the four requirements to be satisfied. First of all it should give an appropriate estimate of the surface defects $f_{sd}(s)$. Secondly it should be able to reject at the same time the disturbances originated from the position of the information layer $x_{cd}(s)$. Thirdly the synthesized filter should exhibit certain immunity against the uncertainties of the plant and, finally, the transfer function between $f_{sd}(s)$ and $u_f(s)$ must be open loop stable. The last condition is also necessary since a surface defect should not lead to instability of the fault diagnosis strategy. Still the frequency response of the synthesized filter is in the line with the intuitive sense. At high frequencies the gain matches the inverse of the gain of the photo diodes and at lower frequencies, the input is attenuated as a consequence of the increase of disturbances. The simulation results showed that a surface defect of high frequency content can easily be tracked whereas surface defects of lower frequency content are more problematic. An alternative to this strategy is basically to do the contrary. That is, to consider the surface defects $f_{sd}(s)$ as the dominant disturbance in the loop and to estimate the position of the information layer $x_{cd}(s)$ and the focus point $x(s)$. The latter strategy is accompanied with a quality signal ω_Q in order to alleviate the requirements of the observers. The simulations indicate though that a fully match of the states of the plant and the estimated states is hard to achieve. Nevertheless, a clearer picture of the performance of these two different approaches can be achieved by means of simulations and experiments in a fault tolerant configuration, a subject to be treated in the next chapter. At the same time the benefits of fault diagnosis in CD-players will be enlightened.

7.5 Summary

This chapter has been devoted to the application of fault diagnosis to CD-players, a topic which has not received great attention in the control community. In section 7.1 an analysis of CD-players is made and it is pointed out that the advantages of a fault diagnosis configuration are specially to be found in the sensor part, where the feedback error signals are generated. Sensor faults are understood in this context as "*a non permitted deviation of a characteristic property which leads to the inability to fulfil the intended purpose*" (attributed to [Isermann, 1984]). Such faults in CD-players are anomalies of the disc surface like scratches, finger prints and dust particles. Based on this kind of

faults, two different strategies are suggested in Section 7.2. The first strategy attempts to estimate the surface defects whereas the second strategy attempts to estimate the position of the information layer and focus point. However, both have in common that the disturbances to be attenuated by the controller are (directly or indirectly) estimated. The strategies are validated through simulations described in Section 7.3, and the measurements also corroborate that the surface detection performs as intended.

8

Fault-Tolerant Control Strategies on CD-drives

The previous chapter was dedicated to fault diagnosis of CD-players which involved the detection, isolation and the estimation of faults. Fault diagnosis can form part of a supervision system where the person in charge of the vigilance has to make appropriate decisions based on the presented information concerning the system. In systems where the reaction time to a fault is critical, the vigilant can be substituted by a processor which can shorten the reaction time significantly. In some applications, there is not even the possibility for the human-machine interaction, like in satellites. Such systems should therefore be equipped with certain degree of "intelligence" which can be provided by means of fault-tolerant control. As for fault diagnosis, publications concerning fault-tolerant control applied to CD-players are virtually nonexistent, although approaches reminiscent to fault-tolerant control are in fact used in commercial CD-applications. It is the objective to investigate alternative strategies to the one existing in commercial products, referred to as *reference strategy*. First the idea and concepts behind fault-tolerant control are introduced in Section 8.1. A more detailed introduction with updated references can be obtained in [Blanke *et al.*, 2003]. In Section 8.2 the *reference strategy* is presented and in Section 8.3 a strategy based on repetitive control is introduced. The latter is known in CD applications, see for example [Dötsch *et al.*, 1995], but faults like surface defects have not been investigated. Two other original strategies are described in

Sections 8.4 and 8.5, which are based on the two approaches treated in Section 7.2. All the strategies are verified through simulations (included in Appendix A.3) and experiments presented in Section 8.6. The results are discussed in Section 8.7 and a summary is given in Section 8.8.

8.1 Introduction to Fault-Tolerant Control

A fault-tolerant control system is characterized by being able to continue operating to fulfil specified functions despite the presence of faults. The aim is consequently to make the system tolerant to faults, hence the name *fault-tolerant control*. Typical applications are aircraft, vehicles and industrial installations where fault-tolerant control increases the availability of the system and reduces the risk of safety hazards. The architecture of fault-tolerant control is depicted in Figure 8.1 [Blanke *et al.*, 2003].

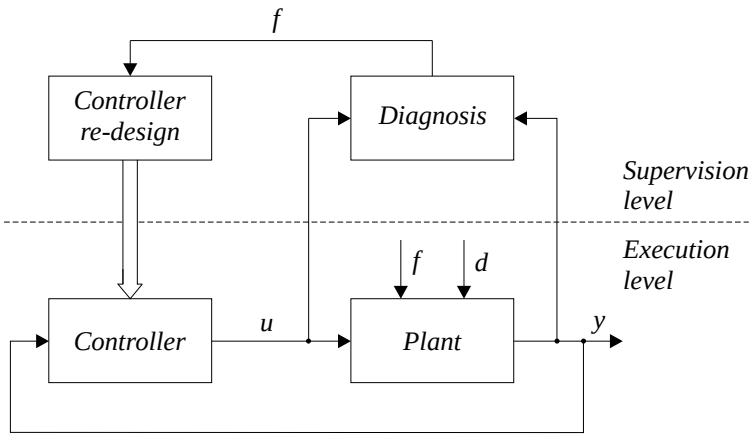

Figure 8.1: *Architecture of fault-tolerant control.*

A typical control loop is composed by a *controller* which generates a control signal u such that the output of the plant y meets certain specifications in spite of the presence of disturbances d. In fault-tolerant control, possible faults in the plant f are also taken into account and two more functions are necessary: the *diagnosis* and the *controller redesign*. The *diagnosis* module uses the measured input and output signals and tests their consistency with the plant model. The faults are therefore detected, isolated and eventually estimated. The *controller redesign* module uses the fault information, provided by the *diagnosis* module, and adjusts the controller to the faulty situation. A wide arrow between the *controller redesign* and the *controller* is drawn to indicate that this connection represents an information link in a more general sense. Depending on the faults, the parameters of the controller can be changed, but also a new control configuration can be

designed. As mentioned in Chapter 7 fault diagnosis plays an important role in fault-tolerant control, as before any control law reconfiguration is possible, the fault must be detected, isolated and eventually estimated such that the supervision mechanism can make a suitable decision. Two main ways of controller redesign can be distinguished:

- *Fault accommodation*: The controller is adapted to the effects caused by the present fault. A common and simple strategy to achieve this adaption is to design different classes of controllers off-line. Then the controller redesign consists into switching between the already designed control laws, depending on the detected fault. Naturally, the classes of controllers should cover all the possible detectable faults.
- *Control reconfiguration*: Given the case that fault accommodation is not possible, the entire control loop has to be reconfigured. Obviously, it is a more involved task since apart of having certain real-time requirements, the methods used for control reconfiguration have to guarantee a solution to the design problem.

It should be said that there are also alternatives to the structure given in Figure 8.1 in order to achieve certain tolerance to faults [Blanke *et al.*, 2003]:

- Robust control: A fixed controller is designed to tolerate a defined class of changes of the plant dynamics. The controlled system satisfies its goals under all faulty conditions. It should stay clear from Chapters 5 and 6 that fault tolerance is obtained without changing the controller parameters. Unfortunately there is a trade-off between performance and robustness/fault tolerance. This trade-off is in fact demonstrated in Chapter 6 through the realized measurements presented in Figure 6.7, where immunity against surface defects is increased at the expenses of reduced performance.
- Adaptive control: The parameters of the controller are gradually adapted to the plant parameters. If the changes are caused by faults, adaptive control can provide active fault tolerance at the contrary to robust control. However, the theory of adaptive control shows that this principle is particularly efficient only for plants that are described by linear models with slowly varying parameters.

In the following, four strategies to handle surface defects are introduced, having all in common to belong to the *fault accommodation* class of fault-tolerant control. *Control reconfiguration* in CD-players is also possible, however, due to the elevated real-time constraints, an entire reconfiguration of the control loop may not be feasible.

8.2 Reference Strategy

It has been explained in the previous chapter that in the presence of surface defects, the feedback error signal does not longer represent an accurate estimate of the positioning

error of the focus point. Therefore the corrupted signals should not be directly fed to the controller since there are limited chances that the focus point will remain on focus once the surface defect in question is passed. A simple approach is to zero the feedback error signal as long as the surface defect persists, as explained in Section 2.5. It is based on the assumption that the probability to remain on focus, once the surface defect is passed, is higher if the controller stays passive. The control loop is consequently open in the presence of a surface defect. Figure 8.2 illustrates such strategy where it can be appreciated that the surface quality signal ω_Q is in series connection with the control loop. In normal operating conditions, ω_Q is equal to one but in the presence of a surface defect, it changes to zero such that the control loop is left open. The μ-PID controller designed in Chapter 6 can be used with the present strategy.

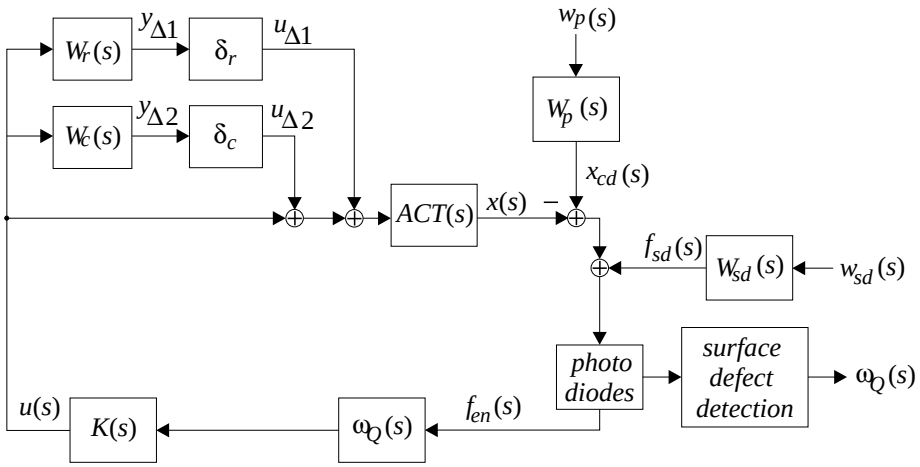

Figure 8.2: *Reference strategy where the loop is opened in the presence of surface defects, (read Section 7.2 for an explanation of the individual parts).*

Following analysis can be made for the focus loop in order to evaluate the effects of a surface defect with the *reference strategy*. A similar analysis applies to the radial loop. According to the Red Book, the rotation frequency can go up to 9[Hz] and the vertical deviation of the disc can reach the value of 500[μm]. The largest quantity of data which can be recovered by the error correction algorithm is equivalent to an elapsed time of $\Delta t = 1.9{\cdot}10^{-3}$[s]. Assuming a scanning linear velocity of 1.4[m/s] and that the feedback error signal f_{en} is set to zero in the presence of a surface defect, the excursion of the focus point after the surface defect is passed can be calculated with respect to the position of the information layer

$$e_x(\Delta t) = A_{xd} \cdot sin(\omega_0 \cdot \Delta t + \theta) \quad [\mu m], \tag{8.1}$$

where A_{xd} is the amplitude of the vertical deviation, ω_0 is the rotation frequency of the CD and Δt the corresponding elapsed time of the surface defect. The value of the phase θ is an important parameter in the calculations. If the surface defect is exactly at the top (or bottom) of the sinus, the excursion of the focus point would theoretically be zero and the focus controller will not advert the presence of such surface defect. On the other hand, is the surface defect is placed symmetrically around $\theta = 0$[rad] or $\theta = \pi$[rad], the excursion of the focus point can be up to 53.7[μm]. Since the linear area of the photo diodes is ± 6[μm], the focus point will be clearly out of focus which obviously is not desired. However, zeroing the feedback error signal does not stop the optical pickup immediately because it has a certain amount of kinetic energy which may keep the pickup moving in the same direction as the fundamental frequency as the position of the information layer, $X_d(s)$ (also considered as a disturbance), which explains why such strategy is effective to certain extent.

8.3 Strategy A

The dominant disturbance in the focus loop is caused by vertical deviations of the CD with the fundamental frequency given by the rotation frequency of the CD. Based on that fact, it could be advantageous to include a model of such disturbance in order to achieve a better focusing. For that purpose *repetitive control* has been used in several industrial applications, whose aim is to asymptotically track/reject periodic references/disturbances. It is well-known that repetitive control improves rejection of periodical disturbances in CD-players, see e.g [Dötsch *et al.*, 1995, Doh *et al.*, 2002, Vidal *et al.*, 1998]. In the Ph.D. dissertation [Lee, 1998] the trade-off between rejection of periodical disturbances and robustness is treated. While asymptotic rejection can be achieved for frequencies where the plant gain is large (in CD-players typically below 100[Hz]), at higher frequencies the asymptotic rejection is compromised in a higher degree with robustness. To achieve asymptotic rejection, the open loop has a crest of infinity gain at the fundamental and harmonic frequencies. In practice, this crest is low-pass filtered such that the effect of repetitive control at higher frequencies is reduced in favour to robustness.

It is interesting to observe that the literature where repetitive control is applied to CD-players only focuses on the asymptotic rejection of periodic disturbance caused by vertical deviations of the CD but surface defects are not treated. Figure 8.3 shows how repetitive control can be combined with the *reference strategy*.
The main difference is the presence of the filter $REP(s)$ where the crest of (theoretically) infinity gain is modeled. The advantage of this strategy, compared to the *reference*

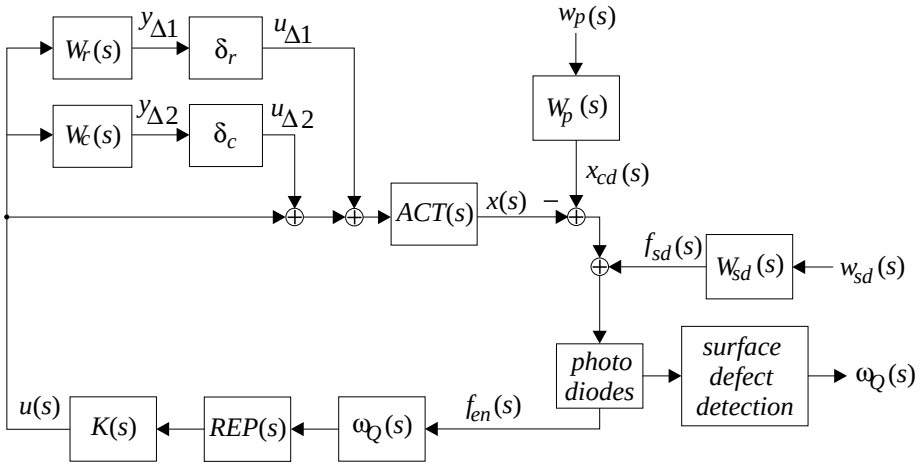

Figure 8.3: *Strategy A: As for the reference strategy, the loop with the μ-PID controller is opened in the presence of surface defects. The important difference here is that a filter $REP(s)$ is added, in charge of achieving asymptotic rejection of periodic disturbances due to e.g. track eccentricity and unbalanced discs.*

strategy, is that the focus point should be able to better follow the position of the information layer while a surface defect is present.

8.4 Strategy B

The essential part in *strategy A* is based on a simplified model of the disturbances, which have a large influence in the position of the information layer $x_{cd}(s)$. However, in the presence of surface defects the bandwidth of the controller is set to zero. This imposes a limitation on how effective the disturbance can be suppressed. A sound approach would be to recover the feedback error signal such that the controller does not advert the presence of surface defects as discussed in Section 7.2. The position of the information layer $x_{cd}(s)$ and the position of the focus point $x(s)$ are therefore estimated. The strategy illustrated in Figure 8.4 relies on the mentioned principle.
In normal operation, where there is no fault in the surface of the disc, the software switch controlled by $\omega_Q(s)$ feeds the controller with the sensed normalized focus error $f_{en}(s)$. The position estimator module includes a model of the actuator $ACT(s)$ and a model of the photo diodes which permit to estimate the focus error $f_{en}(s)$. Since the disturbances $w_p(s)$ are not modeled in the position estimator, there will be an estimation error $e(s)$ mainly originated by the inability to track these disturbances. For that purpose, a disturbance estimator is included which basically works as the repetitive filter presented

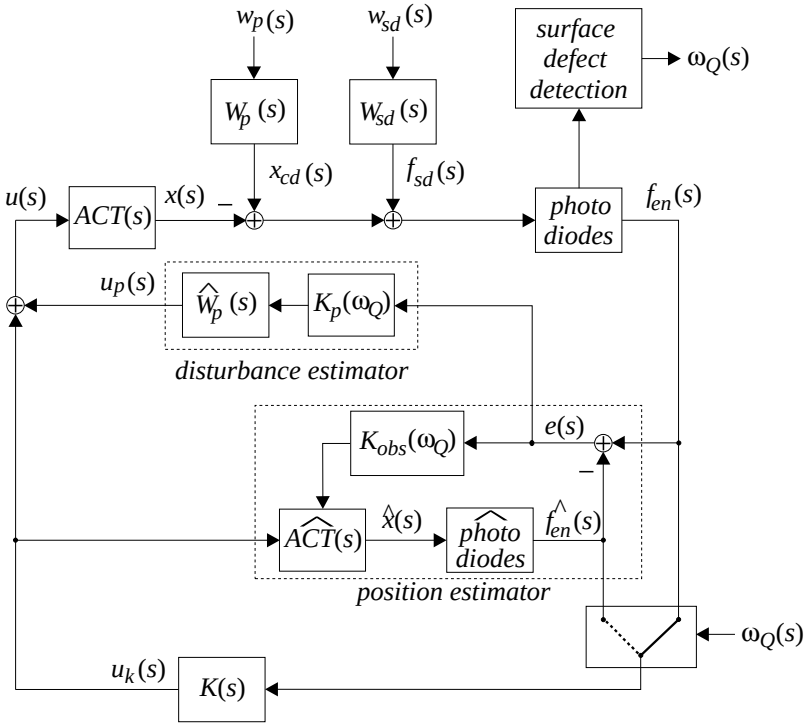

Figure 8.4: *Strategy B: In flawless disc surfaces the generated control signal is based on the sensed feedback error signal $f_{en}(s)$. Whereas during a surface defect the estimated and fault-free feedback error signals $\hat{f_{en}}(s)$ is employed. The disturbance estimator is in charge of attenuating the sinusoidal vertical deviations of the disc which have impact on the position of the information layer $x_{cd}(s)$.*

in *strategy A* and attenuates the mentioned periodic disturbances. $\widehat{W_p}(s)$ is fixed for simplicity reasons, but should be made adaptive such that it follows the actual changes of the rotation frequency in the plant, see for example [Dötsch *et al.*, 1995]. In the case that a surface defect is present, the state of $\omega_Q(s)$ changes to zero such that now the generation of $u_k(s)$ is based on the estimated focus error $\widehat{f_{en}}(s)$. The bandwidth of the estimators are accordingly set to zero such that their estimate is not influenced by the surface defects. Perhaps a more elegant solution would be to replace the controller and the switch with a state feedback controller which always generates the control signal based on the estimated focus error. For comparison purposes with the other strategies, the configuration illustrated in Figure 8.4 is selected where the $K(s)$ is the μ-PID controller.

8.5 Strategy C

A different approach to the previously mentioned is to estimate the surface defects $f_{sd}(s)$ as already treated in Section 7.2, (see Figure 7.8). The estimated surface defects $u_f(s)$ can consequently be removed from the focus error $f_{en}(s)$ such that the controller does not *advert* the presence of the surface defects. This strategy is illustrated in Figure 8.5.

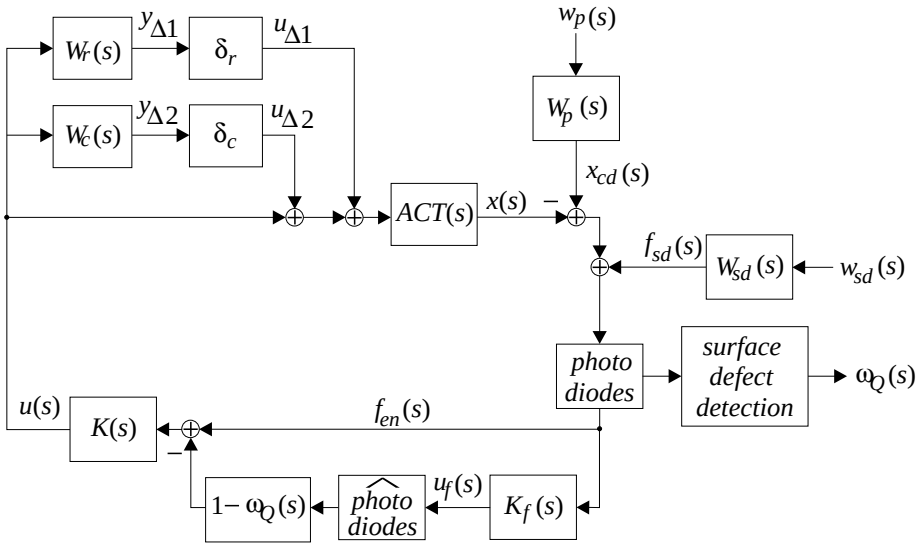

Figure 8.5: *Strategy C: The effects of the surface defects are estimated on-line and are subtracted from the normalized focus error $f_{en}(s)$. Such subtraction takes only place in the presence of surface defects, being ensured by the module $1-\omega_Q(s)$.*

According to [Stoustrup *et al.*, 1997], the controller $K(s)$ can be designed first, followed by the design of the fault diagnosis filter $K_f(s)$. Both are designed to be robust against parameter uncertainties. However, if the diagnosis filter is used in a fault-tolerant configuration like the one shown above, $K_f(s)$ alters the shape of the open loop, which implies that stability and consequently robustness are not longer guaranteed. Mainly, there are two possible ways in order to ensure stability and robustness. The first one is to make an analysis of the open loop when the fault diagnosis filter $K_f(s)$ has been designed. If the requirements are not fulfilled, the weight which describes the surface defects $W_{sd}(s)$, should be modified until the μ-synthesis algorithm returns a fault diagnosis filter which satisfies the requirements. Hence the designer deals with a trial and error process. The other alternative is to consider the configuration visualized in Figure 8.6 as a single controller. What $K_f(s)$ basically does is to reduce the high frequency gain of the open loop, which results in another controller $K'(s)$ of reduced bandwidth.

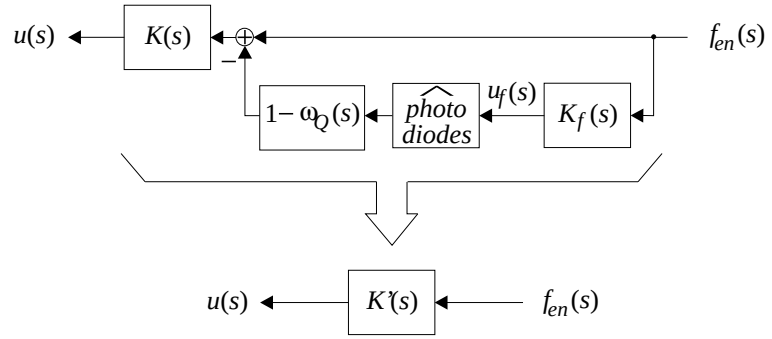

Figure 8.6: *Controller $K(s)$ and filter $K_f(s)$ reduced to the equivalent controller $K'(s)$, of lower bandwidth than $K(s)$.*

$K'(s)$ can directly be designed in the μ-framework for stability and robustness, avoiding the trial and error process previously described. The strategy would therefore consist of running with the normal controller $K(s)$ and to substitute it with $K'(s)$ in the case that a surface defect is present.

8.6 Results of the Fault-Tolerant Control Strategies

In the following, the *reference strategy* is compared with the the other strategies, namely strategy *A*, *B* and *C*. Due to the high degree of similarity between the simulations and the experiments, the former are omitted from the chapter but can be found in Appendix A.3. All the experiments are structured in the same way. In the first 1.43[s] the *reference strategy* is active whilst either strategy *A*, *B* or *C* is posteriorly engaged. The disc was notoriously unbalanced and had two scratches, one of approx. $1.2{\cdot}10^3$[m] and a minor one not relevant in the context.
The upper left plot of Figure 8.7 shows the control signal $u(t)$ where it can be appreciated that the spikes due to the scratches are reduced when the *strategy A* is engaged. The upper right plot shows the corresponding measured focus error. Here it is clear the effect of the repetitive filter $REP(s)$, which effectively suppresses the periodical disturbance. The spikes in the focus error are also reduced. The two lower plots show a zoom of the focus error before (to the left) and after (to the right) activating *strategy A*. The square signal indicates the period where the surface defect is detected, and for a better comparison of the focus error, their DC-offset has been removed. Once the surface defect is passed, the controller is again enabled, and as it can be observed in the left plot with the *reference strategy*, the amplitude of the focus error experiences a sudden increase and decrease of its amplitude, followed by some oscillations. The spike on the focus error is reduced significantly with *strategy A*, which indicates that the excursion of the focus point from the information layer during the surface defect has been restricted. As

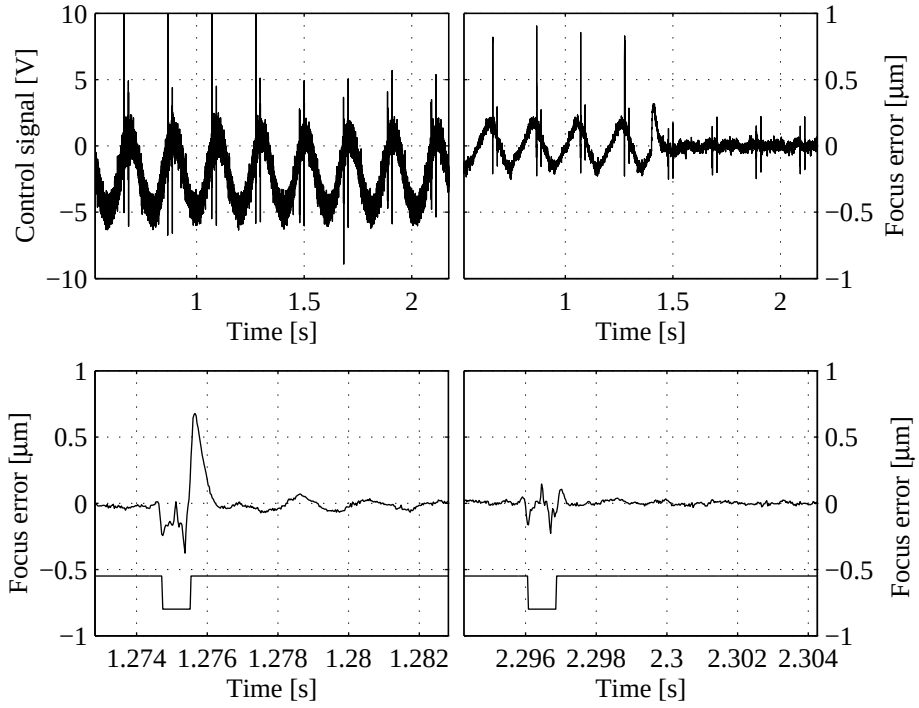

Figure 8.7: *Experiment where the* reference strategy *is compared with* strategy A.

a consequence, no oscillations are present after the surface defect.
The measurements realized with *strategy B*, shown in Figure 8.8, resemble those previously presented in Figure 8.7 with *strategy A*. *Strategy B* is also able to suppress the periodical disturbance and limits the excursion of the focus point during the surface defects, which results in a reduced spike of the focus error with no posterior oscillations.
Figure 8.9 shows the measurement results with the *strategy C*. The performance against the periodical disturbance is equal to that of the *reference strategy* since they both have the same open loop shape. However, *strategy C* has a superior ability to deal with surface defects due to the reduced bandwidth provided by $K_f(s)$ while the surface defects are present.
In order to analyze the stability of *strategy C* the frequency response of the open loops was calculated with the nominal controller $K(s)$ and with the controller of reduced bandwidth $K'(s)$. Figure 8.10 shows the frequency response of both open loops. With $K(s)$, a gain margin of approx. 20[dB] and phase margin of approach. 55[°] was obtained, whereas with $K'(s)$ a gain margin of approx. 3[dB] and a phase margin of

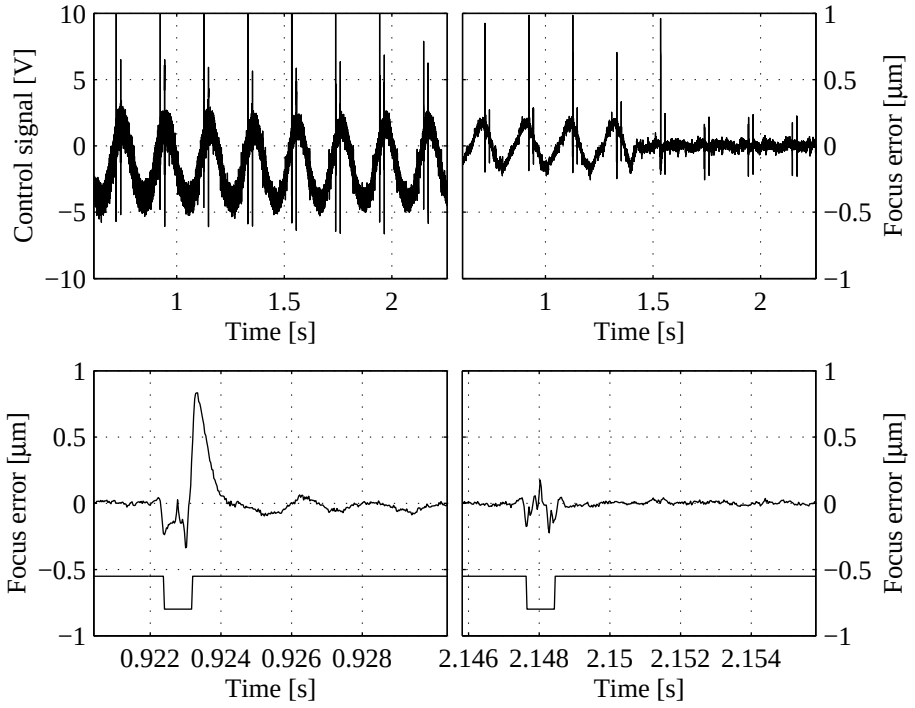

Figure 8.8: *Experiment where the* reference strategy *is compared with* strategy B.

approx. 8[°] was obtained, which is not enough to satisfy the robustness stability requirements.

8.7 Discussion

Four different strategies to handle surface defects were compared, and based on the realized measurements it could be observed that the *reference strategy* exhibited the poorest performance. It suggests that the performance of the positioning loops can be enhanced with fault diagnosis and fault-tolerant control. Only the focus loop has been tested, although comparable results are expected in the radial loop. The most similar strategies based on the achieved results were *strategy A* and *B*. This fact indicates that the position estimator of the focus point in *strategy B* does not contribute to further improvements, which again indicates that it may be enough to estimate the low frequent periodic disturbance since high frequency disturbances do not move the focus point noticeably from the information layer during surface defects. It should be noted that

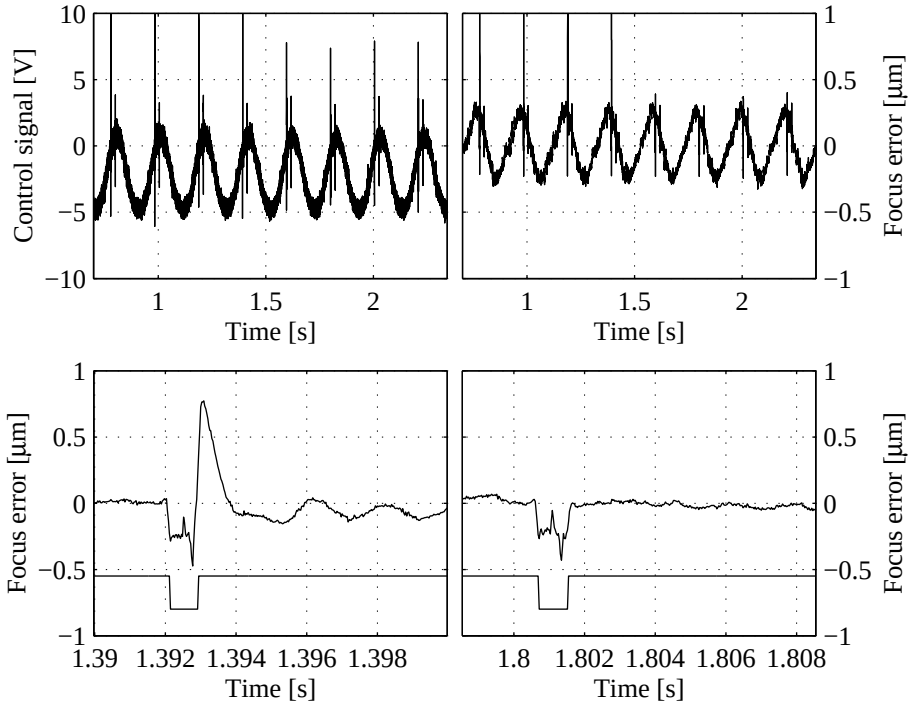

Figure 8.9: *Experiment where the* reference strategy *is compared with* strategy C.

in *strategy A* the controller is disabled during surface defects, which is not the case in *strategy B*. Alone the ability to follow the low frequent periodic disturbance appears though to be sufficient to handle surface defects appropriately. *Strategy C* uses a different approach, based on the estimation and removal of the surface defects from the sensed focus error, and its performance against surface defects also proves to be satisfactory. In practice, during the surface defects, the controller is fed with a low-pass filtered version of the focus error which makes it possible to follow low frequency disturbances. Even though *strategy C* is not able to suppress the low frequent periodic disturbance as effective as in *strategy A* and *B*, it is able to suppress the disturbances enough such that the excursion of the focus point is restricted during the surface defects. A fact which is supported by the corresponding simulations in Appendix A.3.

A topic which should be analyzed in more details is the closed loop stability of the *strategy C* during surface defects. Instability in the loop results in a divergence of the signals from their normal trend. If such divergence is slow, it may be acceptable during

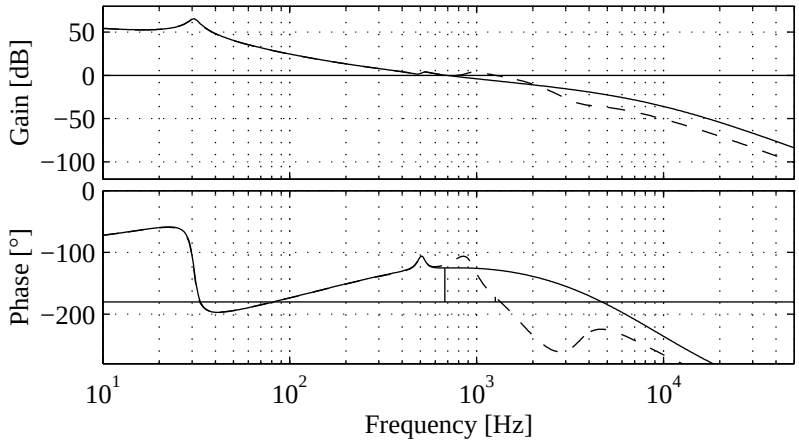

Figure 8.10: *Frequency response of the open loop with the nominal controller $K(s)$, solid trace, and with the controller of reduced bandwidth $K'(s)$, dashed line.*

the short time the surface defects are present.

The purpose of the experiments has been to indicate which strategies may have an improved performance against surface defects compared to the *reference strategy*. Experiments were also realized with different orientation angles θ (see Equation 8.1). It was possible since the vertical deviation was artificially created. The strategies *A, B* and *C* showed to have at least equal performance to the *reference strategy*. However, it was observed that the correct rotation frequency in the disturbance estimator of *strategy B* was important, otherwise it could perform worse than the *reference strategy*. In the presence of a surface defect, $u_p(s)$ is generated in open loop (see Figure 8.4), which explains the importance that the rotation frequency in the disturbance estimator matches the actual rotation frequency in the plant. This issue can be avoided if the strategy is adapted automatically to the actual rotation frequency, as for example described in [Dötsch *et al.*, 1995]. Obviously, thorough playability tests should be realized in order to better assess the performance of the strategies, before they eventually are implemented in commercial products. It is a time-consuming activity beyond the scope the present work, where primarily the data channel, the control loops and the HF signal should be tested, see Section 2.6.

8.8 Summary

This chapter has been devoted to fault-tolerant control applied to CD-players. The concepts were introduced in Section 8.1 and two different types of fault-tolerant control schemes were identified according to their complexity: *fault accommodation*, where different classes of controllers are calculated beforehand, and *control reconfiguration* where the controller is designed on-line. The four presented strategies belonged to the first type. The *reference strategy* in Section 8.2 was based on zeroing the feedback error signal to the controller in the presence of surface defects. *Strategy A* in Section 8.3 is based on the same approach, but a repetitive filter, which provides a high attenuation of periodic disturbances, is included. *Strategy B* estimates the position of the focus point and the position of the information layer during a surface defect, such that the controller does not run in open loop. Finally, *strategy C* estimates the surface defects such that these can be removed from the feedback error signal. The controller runs also in closed loop. The simulation results of the strategies are included in Appendix A.3 and the experiments are presented in Section 8.6. The realized simulations and experiments indicate that the strategies *A*, *B* and *C* have a better performance against surface defects than the *reference strategy*. Finally the results are discussed in Section 8.7.

9

Conclusions and Future Work

This thesis considered different aspects related to the positioning control loops of the optical pickup in CD-players. Parameter estimation was studied and the results were used in connection with robust control. Fault diagnosis and fault-tolerant control were also treated. The main results are reviewed and summarized, and directions for further investigations are identified.

9.1 Conclusions

Theory and applications were combined in this thesis and all the proposed methods were implemented in the laboratory setup. Novel methods were developed in three fields: system identification, robust control and fault diagnosis/fault-tolerant control. The following conclusions are drawn based on the accomplishments of this thesis:

- Open loop system identification is shown to be possible by measuring the current through the coils of the optical pickup. While the suggested method is suitable for the identification of dynamics concerning the first resonance mode (<100[Hz]) of the treated CD-drives, closed loop method is preferred for higher frequencies.
- Parametric, complex and mixed uncertainty representations were employed to describe the dynamic behaviors of the CD-drives. The last one, based on an

"olympic stadium" (OS) shape-like geometric figure, proved to be the least conservative description. In order to fully exploit the OS properties, the synthesis algorithms which compute a robust controller should address the mixed uncertainties in a less conservative way, such as the (D,G)-K and (μ,D)-K-iteration.

- A method of general character was proposed for obtaining the nominal and uncertainty models appropriate for designing a robust controller. The models are generated based only on a measurement set of Nyquist points of the plants in question.

- Based on the OS uncertainty representation and on the Red Book specifications it was shown that it is possible to design a μ-controller which could be reduced to a third order controller and still satisfy the robust performance specifications. Hence a PID for a 1X CD-player applications can be regarded as an acceptable controller. However, for higher speed applications other controller structures should be considered.

- The high similarity between the simulated and measured output sensitivity plots of 12 CD-drives suggests that the approach employed to identify the parameters of the plants, described in Chapter 4, is reliable for simulation and control design purposes.

- An analysis realized on the possible faults which can occur in a CD-drive indicated that a fault diagnosis (and fault-tolerant control) strategy can be beneficial, increasing the tolerance against surface defects.

- Instead of considering the feedback error and sum signals separately, more information can be retrieved if the spanned space by the diode signals is considered. A subspace can be determined where the measurements of the diode signals should be located depending on the surface defects.

- A robust fault diagnosis filter to estimate the surface defects was designed and implemented based on the approach described in [Stoustrup *et al.*, 1997]. It was not a trivial task due to the number of constraints the filter was subjected to. Simulations showed that surface defects could be estimated to some extent.

- Simulations and measurements of a fault-tolerant control strategy, where the estimated surface defects were subtracted from the feedback error signals, showed that the strategy performed better than the considered *reference strategy* where the feedback error is zeroed on the presence of said surface defects. Two other strategies, one which estimates the disturbances and the position of the optical pickup during surface defects, and the other based on a repetitive control [Dötsch *et al.*, 1995], showed to have comparable performance in the realized simulations and measurements. While repetitive control is employed to attenuate

periodical disturbances, originated by the deviations of the disc, it is also documented in this thesis that such control technique has a significantly positive effect against surface defects.

What happened with the balloon?

In Section 2.6 the playability constraints were illustrated as a balloon, see Figure 9.1. The ideal (and utopian) case would be to have a single point where no parameter results in the degradation of playability. However, in practice, certain parameters influence the playability negatively, which is depicted by the length of the arrows. The longer the arrow, the more negative the playability is influenced by the parameter/disturbance in question. Hence the aim is to shrink the size of the balloon, avoiding pop-up effects and avoiding the translation of the balloon.

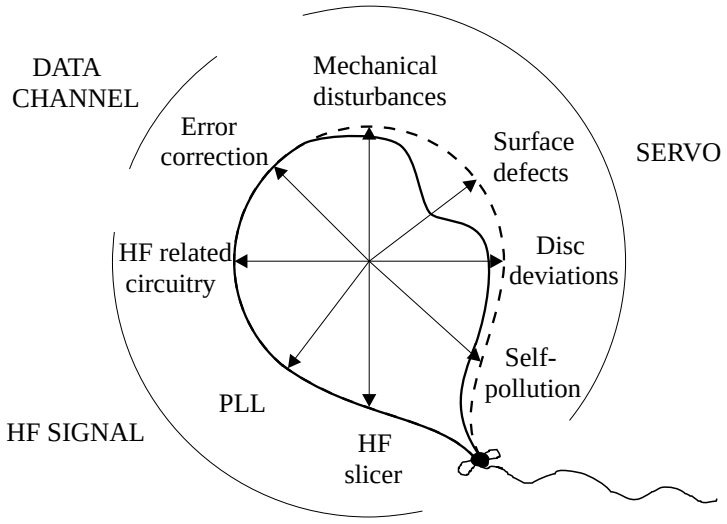

Figure 9.1: *Stylistic representation of playability improvements. The dashed balloon is the one presented in Section 2.6 with the* reference strategy *and the solid balloon shows the increased playability with the alternative fault-tolerant strategies explained in Chapter 8.*

Assuming that all disturbances can adequately be described with frequency weights, robust control theory yields a controller which meets the optimal trade-off for given requirements. Since it was shown that the PID structure is sufficient to meet relevant robustness requirements in 1X CD-players, it could be assumed that the positioning controllers in commercial CD-players are tuned such that they meet the optimal trade-off. A way to better handle this trade-off is to employ the *reference strategy*, since it increases the ability to cope with surface defects without deteriorating the ability to cope with

mechanical disturbances, self-pollution and disc deviations. The defect detector is only activated when a surface defect is present. This configuration can be considered as the reference playability, shown in Figure 9.1 with a dashed line. The realized simulations and experiments in the laboratory setup indicated that the other strategies (*A, B* and *C*) showed a better ability to cope with surface defects, and as for the *reference strategy*, performance against for example mechanical disturbances is not deteriorated. For this reason, it can be concluded that the playability arrow of surface defects would shrink as shown in Figure 9.1 with the strategies (*A, B* and *C*). Moreover, an improved immunity against surface defects allows to increase the bandwidth of the servos to better cope with other disturbances (disc deviations, self-pollution and mechanical disturbances). Therefore the balloon is also slightly shrunk in the directions of the last mentioned disturbances. The heuristic approaches used in the industry (see Section 2.6), could be employed to estimate how much the balloon is shrunk with the treated strategies in the thesis.

9.2 Future Work

Certain topics are not covered in the thesis. They are presented in the following, as the author believes that future investigation could be beneficial:

- One of the keys to successful simulation, design and implementation of a controller is to have an appropriate description of the plant dynamics therefore system identification was treated. The positioning loops were identified separately, however, it could be interesting to investigate to what extent the suggested method can be used to identify the cross-coupling between the positioning loops. Although the optical pickups in CD-players are designed such that the cross-coupling is minimized, with the constant advent of higher capacity optical discs, the requirements increase accordingly and the cross-coupling between the loops becomes more noticeable.
- As indicated in Chapter 7, fault diagnosis and fault-tolerant control can offer some benefits in order to better handle faults in the sledge which may affect the performance of the focus and especially the radial positioning loop. It could be interesting to investigate these potential benefits.
- The proposed method generates a nominal and uncertainty model based only on a measurement set of Nyquist points. No statistical knowledge is included in the method and consequently the designer should find a representative set of worst-case plants. These plants might not always be at hand and therefore it should be studied how to extrapolate the measurement set such that it can represent all the possible plants.
- A topic which should be analyzed in more details is the closed loop stability of the proposed strategy (*strategy C*) where the estimated surface defects are removed

from the feedback error signals. Instability in the loop results in a divergence of the signals from their normal trend. If such divergence is slow, it might be acceptable during the short time the surface defects are present.

- As also mentioned in Chapter 8 thorough playability tests should be realized in order to assess the performance of the presented fault-tolerant control strategies. It is a time-consuming activity where primarily the data channel, the control loops and the HF signal should be tested. It would be also interesting to investigate how to assess playability in an objective way. As it is now, the companies have their own heuristic approaches to test playability and the playability results between companies are therefore not comparable.

- It should also be investigated to what extent the proposed methods in the thesis can be applied to other optical disc players, such as for example DVD-players. Further research efforts should be realized in increasing the efficiency to handle disturbances with conflicting requirements, like surface defects and mechanical disturbances in CD-players and other higher capacity optical disc players.

- In the thesis the spanned space of the focus diode signals was treated. However all the signals from the photo diodes should be considered, which take values in a multi-dimensional space. Such space can be divided into different subspaces in order to have a detailed representation of the possible faults, hence offering a better possibility in a fault-tolerant control strategy to react against faults and disturbances. This topic has already attracted the attention of a Ph.D. project which forms part of a large research project, WAVES, (Wavelets in Audio/Visual Electronic Systems). In the Ph.D. project [Odgaard, to be submitted in 2004], wavelets are used as an identification tool to discern between the possible disturbances which affect the CD-drives. Another interesting aspect which also is treated in [Odgaard, to be submitted in 2004] is to combine time and frequency analysis in an optimal way such that a fast and reliable detection of disturbances is achieved.

- The author believes that a sensitive approach towards the design of positioning controllers in CD-players and other optical disc drives consists on designing controllers, robust to some given measures, such that a passive fault tolerance is ensured. Adaptivity schemes, like the AGC, can be employed to offer active fault tolerance against incipient faults. Fault-tolerant control should be used to achieved immunity to abrupt faults such as surface defects. Such fault-tolerant control strategy relaxes therefore the robustness requirements of the positioning controllers and performance can be increased. The results from this thesis indicate that fault diagnosis and fault-tolerant control offer some advantages in optical disc drives which are worth to investigate further.

A

Appendix

A.1 Parameter Estimation Results From Chapter 4

Tables A.1 and A.2 present the estimated parameters of 12 CD-drives. The estimated parameters are based on the methods explained in Chapter 4. The parameters R[Ω], b[N·s/m], k[N/m] and Bl[N/A] are estimated with the open loop method (see Subsection 4.3.1). The distribution between the following parameters is estimated with the closed loop method (see Subsection 4.3.2): m_1[Kg], m_2[Kg], k_1[N/m], k_2[N/m], b_1[N·s/m] and b_2[N·s/m]. Moreover, the inductance and resistance of the coils were measured and their values are included at the top of the tables.

The optical gains were estimated with the methods described in Section 4.4. Table A.3 presents the results of such estimations.

CD1-drive	**Focus**	**Radial**	**CD2-drive**	**Focus**	**Radial**
L_{meas} [H]	160e-6	115e-6	L_{meas} [H]	160e-6	115e-6
R_{meas} [Ω]	18.4	17.2	R_{meas} [Ω]	18.2	17.2
$\hat{R}$ [Ω](1%)	18.7	17.3	$\hat{R}$ [Ω](1%)	18.2	17.2
$\hat{Bl}$ [N/A](1%)	0.24	0.21	$\hat{Bl}$ [N/A](1%)	0.23	0.21
$\hat{k}$ [N/m](1%)	20.5	53.2	$\hat{k}$ [N/m](1%)	20.6	54.9
$\hat{b}$ [N·s/m](5%)	7.6e-3	12.5e-3	$\hat{b}$ [N·s/m](5%)	8.3e-3	13.5e-3
$\hat{k}_1$ [N/m]	23.6	57.4	$\hat{k}_1$ [N/m]	22.3	59.3
$\hat{k}_2$ [N/m]	157.4	717.9	$\hat{k}_2$ [N/m]	262.6	741.2
$\hat{b}_1$ [N·s/m]	7.25e-3	11.9e-3	$\hat{b}_1$ [N·s/m]	7.9e-3	12.85e-3
$\hat{b}_2$ [N·s/m]	0.35e-3	0.6e-3	$\hat{b}_2$ [N·s/m]	0.4e-3	0.65e-3
$\hat{m}_1$ [Kg]	0.543e-3	0.532e-3	$\hat{m}_1$ [Kg]	0.532e-3	0.536e-3
$\hat{m}_2$ [Kg]	0.017e-3	0.028e-3	$\hat{m}_2$ [Kg]	0.028e-3	0.024e-3
CD3-drive	**Focus**	**Radial**	**CD4-drive**	**Focus**	**Radial**
L_{meas} [H]	160e-6	115e-6	L_{meas} [H]	160e-6	110e-6
R_{meas} [Ω]	18.0	17.3	R_{meas} [Ω]	17.5	16.6
$\hat{R}$ [Ω](1%)	18.2	17.3	$\hat{R}$ [Ω](1%)	17.8	16.7
$\hat{Bl}$ [N/A](1%)	0.23	0.21	$\hat{Bl}$ [N/A](1%)	0.22	0.19
$\hat{k}$ [N/m](1%)	24.4	55.1	$\hat{k}$ [N/m](1%)	17.9	55.4
$\hat{b}$ [N·s/m](5%)	8.3e-3	12.5e-3	$\hat{b}$ [N·s/m](5%)	6.9e-3	12.6e-3
$\hat{k}_1$ [N/m]	27.2	59.0	$\hat{k}_1$ [N/m]	19.1	56.7
$\hat{k}_2$ [N/m]	230.7	842.9	$\hat{k}_2$ [N/m]	273.5	900.8
$\hat{b}_1$ [N·s/m]	7.9e-3	11.85e-3	$\hat{b}_1$ [N·s/m]	6.6e-3	12.0e-3
$\hat{b}_2$ [N·s/m]	0.4e-3	0.65e-3	$\hat{b}_2$ [N·s/m]	0.3-e3	0.6e-3
$\hat{m}_1$ [Kg]	0.538e-3	0.533e-3	$\hat{m}_1$ [Kg]	0.532e-3	0.532e-3
$\hat{m}_2$ [Kg]	0.022e-3	0.027e-3	$\hat{m}_2$ [Kg]	0.028e-3	0.028e-3
CD5-drive	**Focus**	**Radial**	**CD6-drive**	**Focus**	**Radial**
L_{meas} [H]	160e-6	115e-6	L_{meas} [H]	160e-6	115e-6
R_{meas} [Ω]	18.0	17.1	R_{meas} [Ω]	18.3	17.1
$\hat{R}$ [Ω](1%)	18.2	17.1	$\hat{R}$ [Ω](1%)	18.5	17.1
$\hat{Bl}$ [N/A](1%)	0.23	0.21	$\hat{Bl}$ [N/A](1%)	0.24	0.20
$\hat{k}$ [N/m](1%)	19.1	55.4	$\hat{k}$ [N/m](1%)	18.5	57.2
$\hat{b}$ [N·s/m](5%)	7.8e-3	12.7e-3	$\hat{b}$ [N·s/m](5%)	7.7e-3	12.9e-3
$\hat{k}_1$ [N/m]	20.6	59.6	$\hat{k}_1$ [N/m]	20.5	62.0
$\hat{k}_2$ [N/m]	257.8	794.3	$\hat{k}_2$ [N/m]	186.4	746.5
$\hat{b}_1$ [N·s/m]	7.4e-3	12.1e-3	$\hat{b}_1$ [N·s/m]	7.3e-3	12.3e-3
$\hat{b}_2$ [N·s/m]	0.4e-3	0.6e-3	$\hat{b}_2$ [N·s/m]	0.4e-3	0.6e-3
$\hat{m}_1$ [Kg]	0.532e-3	0.532e-3	$\hat{m}_1$ [Kg]	0.543e-3	0.532e-3
$\hat{m}_2$ [Kg]	0.028e-3	0.028e-3	$\hat{m}_2$ [Kg]	0.017e-3	0.028e-3

Table A.1: Estimated parameters of drives CD1. . .CD6.

CD7-drive	**Focus**	**Radial**	**CD8-drive**	**Focus**	**Radial**
L_{meas} [H]	160e-6	115e-6	L_{meas} [H]	160e-6	115e-6
R_{meas} [Ω]	18.1	17.6	R_{meas} [Ω]	16.1	16.9
$\hat{R}$ [Ω](1%)	18.2	17.5	$\hat{R}$ [Ω](1%)	16.3	16.8
$\hat{Bl}$ [N/A](1%)	0.23	0.21	$\hat{Bl}$ [N/A](1%)	0.24	0.21
$\hat{k}$ [N/m](1%)	21.9	58.7	$\hat{k}$ [N/m](1%)	20.5	56.9
$\hat{b}$ [N·s/m](5%)	8.2e-3	12.6e-3	$\hat{b}$ [N·s/m](5%)	7.9e-3	12.8e-3
$\hat{k}_1$ [N/m]	23.7	63.8	$\hat{k}_1$ [N/m]	22.6	61.7
$\hat{k}_2$ [N/m]	285.3	732.9	$\hat{k}_2$ [N/m]	226.0	726.2
$\hat{b}_1$ [N·s/m]	7.8e-3	12.0e-3	$\hat{b}_1$ [N·s/m]	7.5e-3	12.2e-3
$\hat{b}_2$ [N·s/m]	0.4e-3	0.6e-3	$\hat{b}_2$ [N·s/m]	0.4e-3	0.6e-3
$\hat{m}_1$ [Kg]	0.528e-3	0.532e-3	$\hat{m}_1$ [Kg]	0.532e-3	0.532e-3
$\hat{m}_2$ [Kg]	0.032e-3	0.028e-3	$\hat{m}_2$ [Kg]	0.028e-3	0.028e-3
CD9-drive	**Focus**	**Radial**	**CD10-drive**	**Focus**	**Radial**
L_{meas} [H]	160e-6	115e-6	L_{meas} [H]	160e-6	115e-6
R_{meas} [Ω]	18.1	17.2	R_{meas} [Ω]	16.9	17.8
$\hat{R}$ [Ω](1%)	18.4	17.2	$\hat{R}$ [Ω](1%)	16.8	17.6
$\hat{Bl}$ [N/A](1%)	0.21	0.20	$\hat{Bl}$ [N/A](1%)	0.23	0.21
$\hat{k}$ [N/m](1%)	19.7	53.1	$\hat{k}$ [N/m](1%)	20.8	54.2
$\hat{b}$ [N·s/m](5%)	7.4e-3	12.0e-3	$\hat{b}$ [N·s/m](5%)	7.6e-3	12.2e-3
$\hat{k}_1$ [N/m]	21.3	51.8	$\hat{k}_1$ [N/m]	22.7	58.3
$\hat{k}_2$ [N/m]	257.0	611.6	$\hat{k}_2$ [N/m]	239.3	776.7
$\hat{b}_1$ [N·s/m]	7.0e-3	11.4e-3	$\hat{b}_1$ [N·s/m]	7.35e-3	11.6e-3
$\hat{b}_2$ [N·s/m]	0.4e-3	0.6e-3	$\hat{b}_2$ [N·s/m]	0.35e-3	0.6e-3
$\hat{m}_1$ [Kg]	0.532e-3	0.538e-3	$\hat{m}_1$ [Kg]	0.537e-3	0.532e-3
$\hat{m}_2$ [Kg]	0.028e-3	0.022e-3	$\hat{m}_2$ [Kg]	0.023e-3	0.028e-3
CD11-drive	**Focus**	**Radial**	**CD12-drive**	**Focus**	**Radial**
L_{meas} [H]	160e-6	115e-6	L_{meas} [H]	160e-6	115e-6
R_{meas} [Ω]	18.5	17.2	R_{meas} [Ω]	18.1	17.5
$\hat{R}$ [Ω](1%)	18.6	17.3	$\hat{R}$ [Ω](1%)	18.2	17.6
$\hat{Bl}$ [N/A](1%)	0.23	0.21	$\hat{Bl}$ [N/A](1%)	0.23	0.20
$\hat{k}$ [N/m](1%)	21.1	57.7	$\hat{k}$ [N/m](1%)	19.3	56.5
$\hat{b}$ [N·s/m](5%)	8.0e-3	13.0e-3	$\hat{b}$ [N·s/m](5%)	7.3e-3	12.5e-3
$\hat{k}_1$ [N/m]	22.8	61.5	$\hat{k}_1$ [N/m]	21.1	61.2
$\hat{k}_2$ [N/m]	271.9	945.7	$\hat{k}_2$ [N/m]	222.5	736.8
$\hat{b}_1$ [N·s/m]	7.6e-3	12.35e-3	$\hat{b}_1$ [N·s/m]	6.95e-3	11.9e-3
$\hat{b}_2$ [N·s/m]	0.4e-3	0.65e-3	$\hat{b}_2$ [N·s/m]	0.35e-3	0.6e-3
$\hat{m}_1$ [Kg]	0.535e-3	0.532e-3	$\hat{m}_1$ [Kg]	0.535e-3	0.532e-3
$\hat{m}_2$ [Kg]	0.025e-3	0.028e-3	$\hat{m}_2$ [Kg]	0.025e-3	0.028e-3

Table A.2: Estimated parameters of drives CD7. . .CD12.

CD1-drive	**Opt. gain**	**CD2-drive**	**Opt. gain**
K_{optF}[V/m]	813	K_{optF}[V/m]	833
K_{optFn}[units/m]	260160	K_{optFn}[units/m]	278222
K_{optR}[V/m]	2512	K_{optR}[V/m]	2238
K_{optRn}[units/m]	1027408	K_{optRn}[units/m]	928770
CD3-drive	**Opt. gain**	**CD4-drive**	**Opt. gain**
K_{optF}[V/m]	1212	K_{optF}[V/m]	700
K_{optFn}[units/m]	313908	K_{optFn}[units/m]	228900
K_{optR}[V/m]	2274	K_{optR}[V/m]	1720
K_{optRn}[units/m]	1046040	K_{optRn}[units/m]	951160
CD5-drive	**Opt. gain**	**CD6-drive**	**Opt. gain**
K_{optF}[V/m]	1041	K_{optF}[V/m]	357
K_{optFn}[units/m]	254004	K_{optFn}[units/m]	259896
K_{optR}[V/m]	3068	K_{optR}[V/m]	2753
K_{optRn}[units/m]	1107548	K_{optRn}[units/m]	1026869
CD7-drive	**Opt. gain**	**CD8-drive**	**Opt. gain**
K_{optF}[V/m]	897	K_{optF}[V/m]	589
K_{optFn}[units/m]	330993	K_{optFn}[units/m]	325717
K_{optR}[V/m]	2438	K_{optR}[V/m]	1886
K_{optRn}[units/m]	1021522	K_{optRn}[units/m]	1052388
CD9-drive	**Opt. gain**	**CD10-drive**	**Opt. gain**
K_{optF}[V/m]	1073	K_{optF}[V/m]	820
K_{optFn}[units/m]	311170	K_{optFn}[units/m]	248460
K_{optR}[V/m]	2284	K_{optR}[V/m]	2372
K_{optRn}[units/m]	888476	K_{optRn}[units/m]	965404
CD11-drive	**Opt. gain**	**CD12-drive**	**Opt. gain**
K_{optF}[V/m]	933	K_{optF}[V/m]	719
K_{optFn}[units/m]	276168	K_{optFn}[units/m]	276815
K_{optR}[V/m]	2026	K_{optR}[V/m]	2434
K_{optRn}[units/m]	942090	K_{optRn}[units/m]	1000374

Table A.3: Estimated normalized and unnormalized optical gains of the 12 CD-drives.

A.2 Measured Gain Margins From Chapter 6

Table A.4 shows the results of the gain margin measurements with the nominal gain μ-PID controller for each CD-drive (see Subsection 6.3.3). The *gain margin* is understood in this context as the absolute value of the minimum allowable gain increase/decrease of the controller with respect to its nominal gain before instability is met. In practice, the focus loop was closed with the μ-PID controller and, after two seconds, the gain was gradually de/increased with 2[dB/sec] until the vicinity of instability was reached or until the saturation limits of the control signal was reached.

CD-drive	**gain margin [dB]**
CD1	15.7
CD2	15.5
CD3	16.4
CD4	15.0
CD5	15.2
CD6	13.1
CD7	15.4
CD8	15.8
CD9	15.0
CD10	15.8
CD11	14.3
CD12	15.1

Table A.4: Measured gain margin in each CD-drive.

A.3 Simulation Results From Chapter 8

In the following, the simulation results of the *reference strategy* are compared with the the other strategies, namely strategy *A*, *B* and *C*. The measurement results can be found in Section 8.6. All the simulations are structured in the same way. In the first second the *reference strategy* is active whilst either strategy *A*, *B* or *C* is engaged posteriorly. An unbalanced disc of 500[μm] and two scratches where included in the simulations. Furthermore a false detection is simulated.

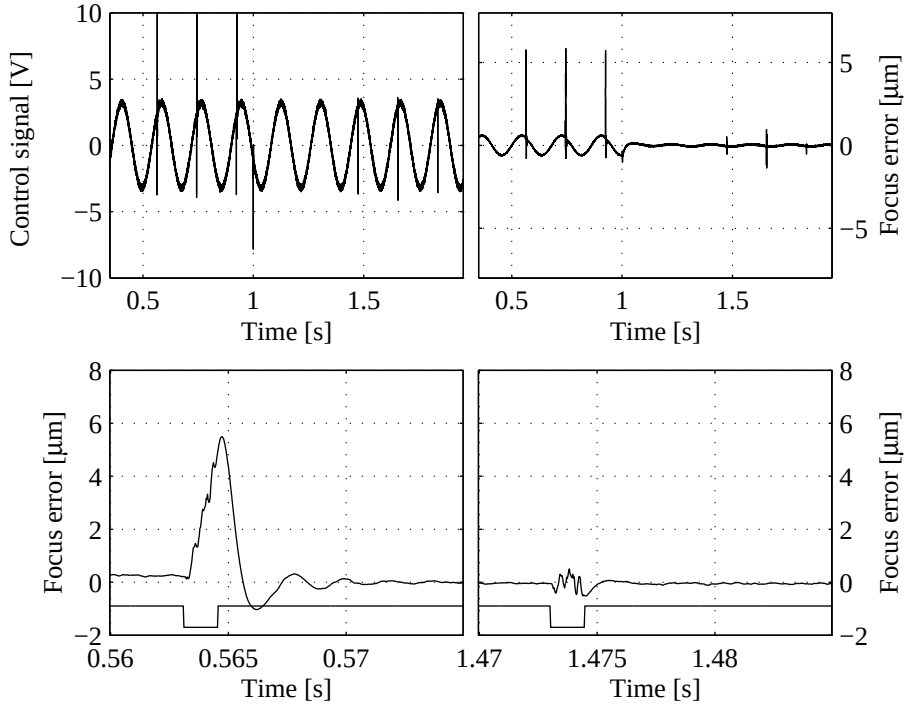

Figure A.1: *Simulation where the* reference strategy *is compared with* strategy A.

The upper left plots of Figures A.1, A.2 and A.3 show the control signal $u(t)$ where it can be appreciated that the spikes due to the scratches are reduced when either *strategy A*, *B* or *C* is engaged. The upper right plots show their corresponding measured focus errors. In *strategy A* and *B* it can be appreciated the efficacy against the periodical disturbance due to respectively the repetitive filter $REP(s)$ and the position estimator of the information layer. The square signals at the lower plots indicate the period where the surface defect is detected and for a better comparison of the focus error, their DC-offset

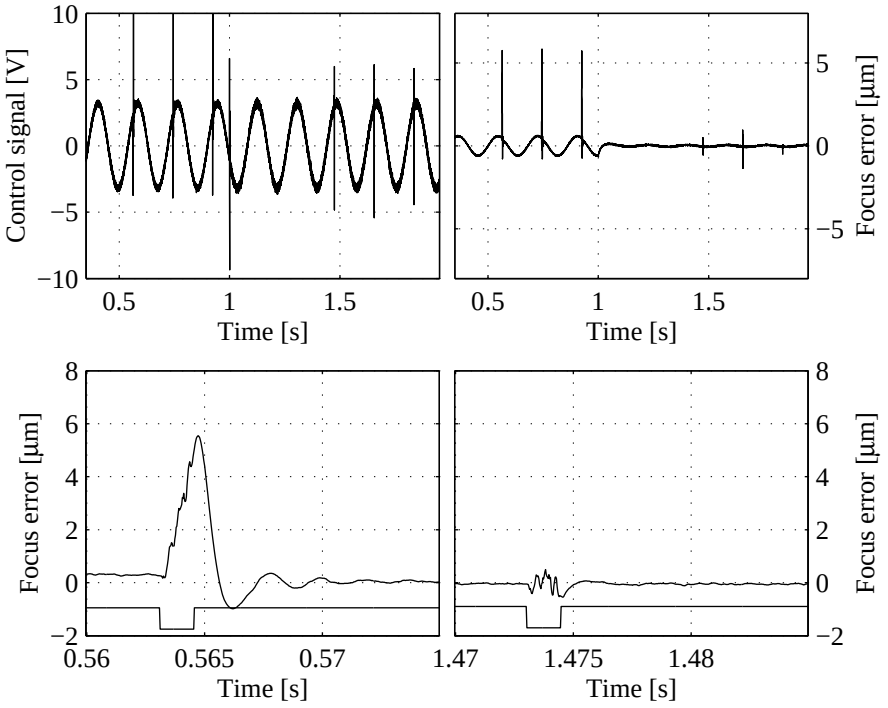

Figure A.2: *Simulation where the* reference strategy *is compared with* strategy B.

has been removed. Once the surface defect is passed, the controller is again enabled, and as it can be observed in the left plot with the *reference strategy*, the amplitude of the focus error experiences a sudden increase and decrease, followed by some oscillations. The spike on the focus error is reduced significantly with the other strategies which indicates that the excursion of the focus point from the information layer during the surface defect has been restricted. A fact that can be checked in the simulations but not in the measurements. In the laboratory, the focus error $e_x(s)$ is measured indirectly, by means of the photo diodes the so-called normalized focus error $f_{en}(s)$ is generated. However, in the simulations the focus error $e_x(s)$ can be computed, which gives the direct relation between the position of the focus point $x(s)$ and the position of the information layer $x_{cd}(s)$, since $e_x(s) = -x(s) + x_{cd}(s)$. Figures A.4, A.5 and A.6 display the results of such simulations. In all three cases it can be observed that the excursion of the focus point in the *reference strategy* is significantly larger than in the other strategies.

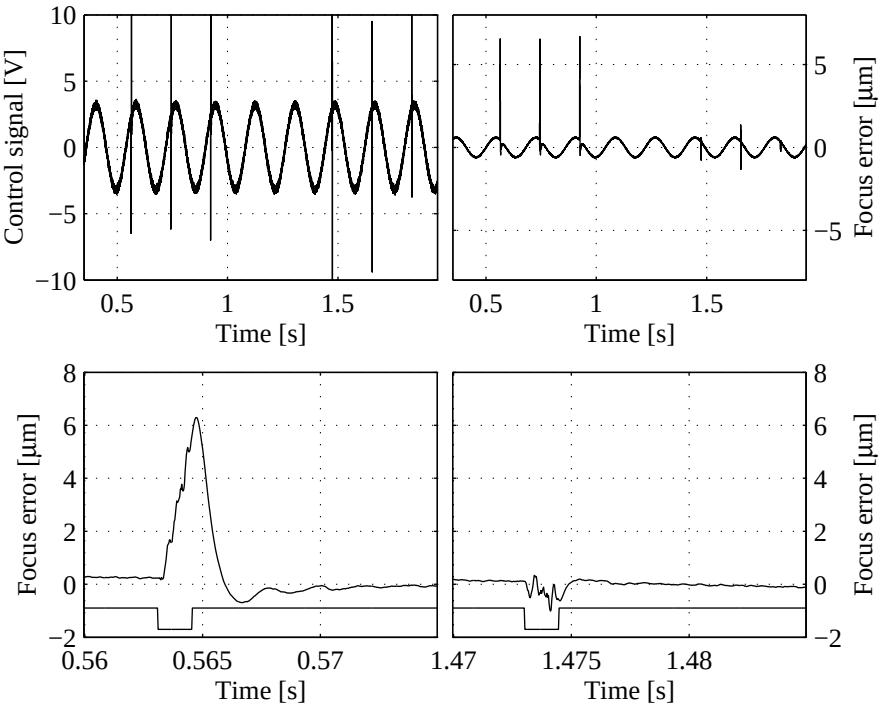

Figure A.3: *Simulation where the* reference strategy *is compared with* strategy C*.*

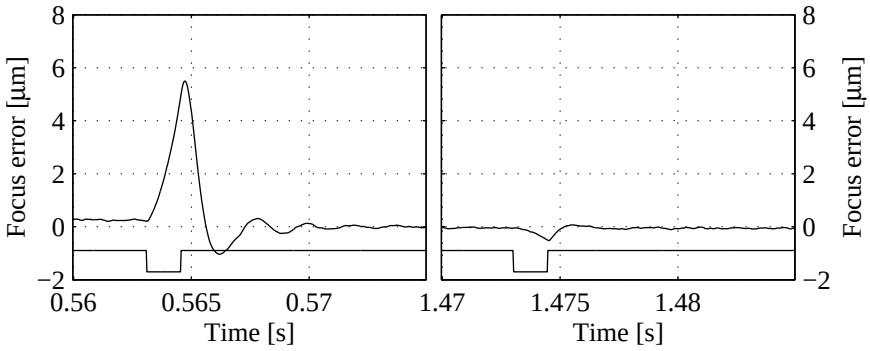

Figure A.4: *Simulation of the actual focus error* $e_x(s)$ *with the* reference strategy *(left) and* strategy A *(right).*

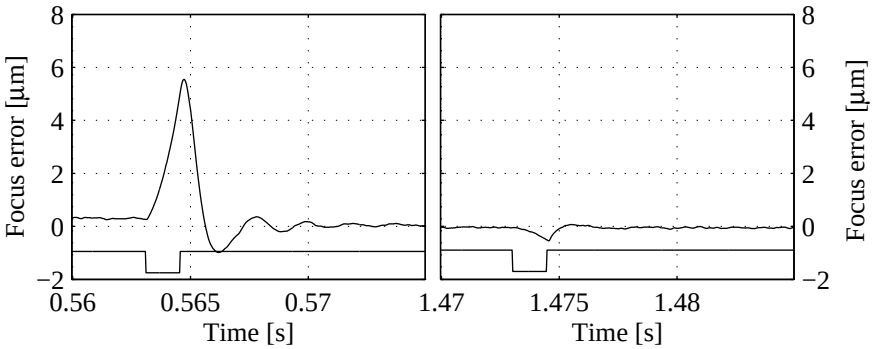

Figure A.5: *Simulation of the actual focus error $e_x(s)$ with the* reference strategy *(left) and* strategy B *(right).*

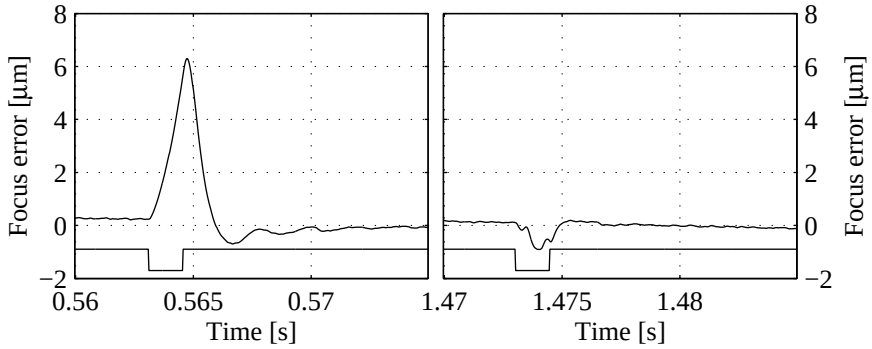

Figure A.6: *Simulation of the actual focus error $e_x(s)$ with the* reference strategy *(left) and* strategy C *(right).*

Bibliography

[Aangenent, 2002] W.H.T.M. Aangenent. The modeling and control of the sledge system in the beosound 3000. Technical report, Department of Control, Institute of Electronic Systems, Aalborg University, Fredrik Bajers vej 7, DK 9220 Aalborg Ø, Danmark, june 2002.

[Akkermans, 2001] Ton H.M. Akkermans. Digital control in optical disc drives. In *International Conference on Consumer Electronics*, june 2001.

[Andersen and Karlsson, 2000] B. Andersen and R. V. Karlsson. Regulering af optisk pickup i cd-afspiller. Master thesis, Department of Control, Institute of Electronic Systems, Aalborg University, Fredrik Bajers vej 7, DK 9220 Aalborg Ø, Danmark, june 2000.

[Åström and Wittenmark, 1995] K.J. Åström and B. Wittenmark. *Adaptive Control*. Addison-Wesley, 1995. Second Edition, ISBN: 0-201-55866-1.

[Balas *et al.*, 1993] G. J. Balas, J. C. Doyle, K. Glover, A. Packard, and R. Smith. μ-analysis and synthesis TOOLBOX. The mathworks inc., 1993.

[Beard, 1971] R.V. Beard. *Failure Accommodation in Linear System Through Self Reorganization*. PhD thesis, Massachusetts Institute of Technology, USA, 1971.

[Bierhoff, 1984] M.P.M. Bierhoff. Apparatus for optimally scanning a disc-shaped record carrier. United states. patent us 4471477, september 1984.

[Blanke *et al.*, 2003] M. Blanke, M. Kinnaert, J. Lunze, and M. Staroswiecki. *Diagnosis and Fault-Tolerant Control*. Springer Verlag, 2003. ISBN: 3-540-01056-4.

[Bouwhuis *et al.*, 1985] G. Bouwhuis, J. Braat, A. Huijser, J. Pasman, G. van Rosmalen, and K. Schouhamer Immink. *Principles of Optical Disc Systems*. Adam Hilger Ltd, 1985. ISBN: 0-85274-785-3.

[Braat *et al.*, 2002] J. Braat, P. Dirksen, and Augustus J.E.M. Janssen. *Diffractive readout of optical discs*. Springer, 2002.

[Braat, 1998] J.J.M. Braat. Differential time detection for radial tracking of optical disks. Applied optics, jaargang 37, 29, april 1998. ISSN: 00036935.

[Braatz *et al.*, 1994] R. P. Braatz, P. M. Young, J. C. Doyle, and M. Morari. Computational complexity of μ calculation. *IEEE Transactions on Automatic Control*, 39:1000–1002, 1994.

[Bros, 2002] Warner Bros. Dvd production: Factions debate hd-dvd. Press news: http://www.medialinenews.com/issues/2002/september/dvd_10.shtml, september 2002.

[Chait *et al.*, 1994] Y. Chait, M. Soo Park, and M. Steinbuch. Design and implementation of a qft controller for a compact disc player. In *Proceedings of the 1994 American Control Conference*, june 1994.

[Chen and Patton, 1999] J. Chen and R.J. Patton. *Robust Model-based Fault Diagnosis for Dynamic Systems*. Kluwer Academic Publishers, 1999. ISBN 0-7923-8411-3.

[Chow and Willsky, 1980] E.Y. Chow and A.S. Willsky. Issues in the development of a general algorithm for reliable failure detection. In *Proceedings of the 19th IEEE Conference on Decision and Control*, 1980.

[Clark *et al.*, 1975] R.N. Clark, D.C. Fosth, and V.M. Walton. Process fault detection based on modelling and estimation methods: A survey. *IEEE Transactions on Aeronautics and Electronic Systems*, 11:465–473, 1975.

[de Callafon *et al.*, 1993] R.A. de Callafon, P.M.J. Van den Hof, and M. Steinbuch. Control relevant identification of a compact disc pick-up mechanism. In *Proceedings of the 32nd IEEE Conference on Decision and Control*, 1993.

[Dettori *et al.*, 1999] M. Dettori, P. Valk, and C. W. Scherer. Digital implementation of a mixed objectives mimo controller for a compact disc player using a multiprocessor system. In *Proceedings of the 1999 American Control Conference*, june 1999.

[Dettori, 2001] M. Dettori. *LMI techniques for control with applications to a compact disc player mechanism*. PhD thesis, Delft University, The Netherlands, 2001.

[Ding and Frank, 1991] X. Ding and P.M. Frank. Frequency domain approach and threshold selector for robust model-based fault detection and isolation. *SAFEPROCESS'91*, 1:307–312, 1991.

[Doh *et al.*, 2002] T.Y. Doh, J.R. Tyoo, and M.J. Chung. Repetitive controller design for track-following servo system of an optical disk drive. In *Advanced Motion Control*, july 2002.

[Dötsch *et al.*, 1995] Hans G.M. Dötsch, Henk T. Smakman, Paul M.J. Van den Hof, and Maarten Steinbuch. Adaptive repetitive control of a compact disc mechanism. In *Proceedings of the 34th IEEE Conference on Decision and Control*, december 1995.

[Dötsch, 1998] H. Dötsch. *Identification for Control Design with Application to a Compact Disk Mechanism*. PhD thesis, 1998.

[Doyle *et al.*, 1989] J. Doyle, K. Glover, P. Khargonekar, and B.A. Francis. State-space solutions to standard $\mathcal{H}_2$ and $\mathcal{H}_\infty$ control problems. *IEEE Transactions on Automatic Control*, AC-34:831–847, 1989.

[Draijer *et al.*, 1992] W. Draijer, M. Steinbuch, and O.H. Bosgra. Adaptive control of the radial servo system of a compact disc player. *Automatica*, 28(3):455–462, may 1992.

[Dzanovic and Lauritsen, 2003] H. Dzanovic and K. Lauritsen. Modellering af slædesystemet i et cdm12 løbeværk. Technical report, Department of Control, Institute of Electronic Systems, Aalborg University, Fredrik Bajers vej 7, DK 9220 Aalborg Ø, Danmark, january 2003.

[ECMA, 2001] ECMA. Standard ecma-267: 120mm dvd read-only-disk. Standard, april 2001.

[Evans *et al.*, 1994] D. C. Evans, D. Rees, and D. L. Jones. Identifying linear models of systems suffering nonlinear distortions. In *CONTROL IEE*, march 1994.

[Fan *et al.*, 1991] M. K. H. Fan, A. L. Tits, and J. C. Doyle. Robustness in the presence of mixed parametric uncertainty and unmodeled dynamics. *IEEE Transactions on Automatic Control*, 36:25–38, 1991.

[Filardi *et al.*, 2002] G. Filardi, A. Besançon-Voda, O. Sename, and H.J. Schroeder. Modeling, identification and performance analysis of a dvd player. In *Proceedings of the IEEE International Conference on Control Applications*, june 2002.

[Filardi *et al.*, 2003] G. Filardi, O. Sename, A. Besaçon-Voda, and H.J. Schroeder. Robust $\mathcal{H}_\infty$ control of a dvd drive under parametric uncertainties. september 2003. To appear in European Control Conference.

[Forssell, 1999] U. Forssell. *Closed-loop Identification: Methods, Theory, and Applications*. PhD thesis, 1999.

[Franklin *et al.*, 1990] G.F. Franklin, J.D. Powel, and Abbas Emami-Naeini. *Feedback control of dynamic systems*. Addison-Wesley, 1990. Third Edition.

[Fujiyama *et al.*, 1998] K. Fujiyama, M. Tomizuka, and R. Katayama. Digital tracking controller design for cd player using disturbance observer. In *International Workshop on Advanced Motion Control*, june 1998.

[Hearns and Grimble, 1999] G. Hearns and M. J. Grimble. Limits of performance of an optical disk drive controller. In *Proceedings of the 1999 American Control Conference*, june 1999.

[Hitachi *et al.*, 2002] Ltd. Hitachi, LG Electronics Inc., Ltd. Matsushita Electric Industrial Co., Pioneer Corporation, Royal Philips Electronics, Ltd. Samsung Electronics Co., Sharp Corporation, Sony Corporation, and Thomson Multimedia. Large capacity optical disc video recording format "blu-ray disc" established. Technical report, february 2002. Press Release: http://www.sony.net/SonyInfo/News/Press/200202/02-0219E/.

[Huang *et al.*, 1999] Y. Huang, P. Mathur, and W. C. Messner. Robustness analysis on a high bandwidth disk drive servo system with an instrumented suspension. In *Proceedings of the 1999 American Control Conference*, june 1999.

[Isermann, 1984] R. Isermann. Process fault detection based on modelling and estimation methods: A survey. *Automatica*, 20(4):387–404, 1984.

[Knudsen, 1993] T. Knudsen. Systemidentifikation. Auc-proces-u-93-4008, Department of Control, Institute of Electronic Systems, Aalborg University, Fredrik Bajers vej 7, DK 9220 Aalborg Ø, Danmark, januar 1993.

[Lee, 1998] Chak Hong Lee. *Robust repetitive control and application to a CD player*. PhD thesis, Trinity Hall Cambridge, february 1998.

[Li and Tsao, 1999] J. Li and T-C. Tsao. Rejection of repeatable and non-repeatable disturbances for disk drive actuators. In *Proceedings of the 1999 American Control Conference*, june 1999.

[Ljung, 1987] L. Ljung. *System Identification, Theory for the User*. Prentice Hall, 1987. ISBN: 0-138-81640-9.

[Mangoubi *et al.*, 1992] R. Mangoubi, B.D. Appleby, and J.R. Farrell. Robust estimation in fault detection. In *Proceedings of the 31st IEEE Conference on Decision and Control*, 1992.

[Milster, 2003] Tom D. Milster. Hd-dvd prospects. Widescreen review. issue 73, 2003.

[Moon *et al.*, 1996] J. Moon, M. Lee, and M. Jin Chung. Track-following control for optical disk drives using an iterative learning scheme. *IEEE Transactions on Consumer Electronics*, 42(2):192–198, may 1996.

[Odgaard *et al.*, 2003] P.F. Odgaard, J. Stoustrup, P. Andersen, and H.F. Mikkelsen. Modelling of the optical detector system in a compact disc player. In *Proceedings of the 2003 American Control Conference*, june 2003.

[Odgaard, to be submitted in 2004] P. F. Odgaard. *Feature based control of Compact Disc Players*. PhD thesis, Aalborg University, Denmark, (to be submitted in 2004).

[OES and AOSRA, 2002] OES and AOSRA. OES, AOSRA develops blue laser HD-DVD format. Technical report, november 2002. Press News: http://www.eetasia.com/ART_8800289292_499481,499484.HTM.

[Packard and Pandey, 1993] A. Packard and P. Pandey. Continuity properties of the real/complex structured singular value. *IEEE Transactions on Automatic Control*, 38:415–428, 1993.

[Packard *et al.*, 1988] A. Packard, M. K. H. Fan, and J. Doyle. A power method for the structured singular value. In *CDC27*, december 1988.

[Patton and Chen, 1991] R.J. Patton and J. Chen. A review of parity space approaches to fault diagnosis. *SAFEPROCESS'91*, 1:239–255, 1991.

[Philips and Sony Corporation, 1991] N.V. Philips and Sony Corporation. *Compact Disc Digital Audio*. november 1991. Red Book.

[Pintelon *et al.*, 1992] R. Pintelon, P. Guillaume, Y. Rolain, and F. Verbeyst. Identification of linear systems captured in a feedback loop. *IEEE Transactions on Instrumentation and Measurement*, 41(6):14–20, december 1992.

[Reed and Solomon, 1960] I.S. Reed and G. Solomon. Polynomial codes over certain finite fields. *Journal of the Society for Industrial and Applied Mathematics*, june 1960.

[Ross, 1987] S. M. Ross. *Introduction to probability and statistics for engineers and scientists*. John Wiley & Sons, 1987. ISBN: 0-471-60815-7.

[Sadrnia *et al.*, 1996] M.A. Sadrnia, J. Chen, and R.J. Patton. Robust fault diagnosis observer design using $\mathcal{H}_\infty$-optimization and μ-synthesis. *Institution of Electrical Engineers*, 1996.

[Schønhoff, 2002] U. Schønhoff. *Practical Robust Control of Mechatronic Systems with Structural Flexibilites*. PhD thesis, Der Technischen Universität Darmstadt, 2002.

[Schoukens *et al.*, 1997] J. Schoukens, R. Pintelon, G. Vandersteen, and P. Guillaume. Frequency-domain system identification using non-parametric noise models estimated from a small number of data sets. *Automatica*, 33(6):1073–1086, 1997.

[Sharp, 2003] Sharp. General information about laser diodes and hologram lasers. Technical report, 2003. http://www.sharpsma.com/sma/products/opto/Laser_diodes/ld_info_e.pdf.

[Skogestad and Postlethwaite, 1997] S. Skogestad and I. Postlethwaite. *Multivariable Feedback Control (Analysis and Design)*. John Wiley & Sons, 1997. ISBN: 0-471-94330-4.

[Stan, 1998] Soring G. Stan. *The CD-ROM Drive, A Brief System Description*. Kluwer Academic Publishers, 1998.

[Stark and Woods, 1994] H. Stark and J. W. Woods. *Probability, Random Process and Estimation Theory for Engineers*. Prentice Hall, 1994. ISBN: 0-13-728791-7.

[Steinbuch and Norg, 1998] M. Steinbuch and M. L Norg. Advanced motion control: An industrial perspective. *European Journal of Control*, 4:278–293, 1998.

[Steinbuch *et al.*, 1992] M. Steinbuch, G. Schoostra, and O. H. Bosgra. Robust control of a compact disc player. In *Proceedings of the 31st IEEE Conference on Decision and Control*, december 1992.

[Steinbuch *et al.*, 1994a] M. Steinbuch, P. J.M. van Gross, G. Schooststra, and O. H. Bosgra. Multivariable control of a compact disc player using dsps. In *Proceedings of the 1994 American Control Conference*, june 1994.

[Steinbuch *et al.*, 1994b] M. Steinbuch, P. Wortelboer, P. J. M. van Groos, , and O. H. Bosgra. Limits of implementation: A cd player control case study. In *Proceedings of the 1994 American Control Conference*, june 1994.

[Stoustrup *et al.*, 1997] J. Stoustrup, M.J. Grimble, and H. Niemann. Design of integrated systems for the control and detection of actuator/sensor faults. *Sensor Review*, 17:138–149, 1997.

[Stoustrup *et al.*, 2000] J. Stoustrup, E. Vidal, P. Andersen, T.S. Pedersen, and H.F. Mikkelsen. Current feedback for shock disturbance attenuation in a compact disk player. In *Proceedings of the 2000 American Control Conference*, september 2000.

[Tøffner-Clausen *et al.*, 1995] S. Tøffner-Clausen, P. Andersen, J. Stoustrup, and H.H. Niemann. A new approach to μ-synthesis for mixed perturbation sets. In *Proceedings of the European Control Conference*, pages 147–152, september 1995.

[Tøffner-Claussen, 1995] S. Tøffner-Claussen. *System Identification and Robust Control: A Synergistic Approach*. PhD thesis, Aalborg University, Denmark, 1995.

[Toshiba and NEC, 2002] Toshiba and NEC. Toshiba and nec jointly propose next generation, high capacity, blue-laser dvd format. Press release: http://www.nec.co.jp/press/en/0208/2901.html, august 2002.

[van Donkelaar *et al.*, 1995] E. T. van Donkelaar, H.G.M. Dötsch, and P.M.J. Van den Hof. Identification of model uncertainty of a compact disc pick-up mechanism. In *Delft University Press*, december 1995.

[van Groos *et al.*, 1994] P. J. M. van Groos, M. Steinbuch, and O. H. Bosgra. Robust control of a compact disc player. *Journal A*, 35(1):57–62, 1994.

[van Helvoirt, 2002] J. van Helvoirt. Disc defect handling in optical disc drives. Master thesis, Eindhoven University of Technology, Faculty of Mechanical Engineering, Dynamics and Control Technology, august 2002.

[Vidal *et al.*, 1998] E. Vidal, H. C. Schøien, and J. Rasmussen. Focus control of the optical pick-up in a cd player. Master thesis, Department of Control, Institute of Electronic Systems, Aalborg University, Fredrik Bajers vej 7, DK 9220 Aalborg Ø, Danmark, june 1998.

[Vidal *et al.*, 2000] E. Vidal, B. Andersen, and R. V. Karlsson. Robust $\mathcal{H}_\infty$-control in cd players to suppress external disturbances and defects on the disc. In *Proceedings of the 2000 Control, Automation, Robotics & Vision Conference*, december 2000.

[Vidal *et al.*, 2001a] E. Vidal, P. Andersen, J. Stoustrup, and T. S. Pedersen. A study on the surface defects of a compact disk. In *Proceedings of the 2001 IEEE International Conference on Control Applications*, september 2001.

[Vidal *et al.*, 2001b] E. Vidal, K.G. Hansen, R.S. Andersen, K.B. Poulsen, J. Stoustrup, P. Andersen, and T.S. Pedersen. Linear quadratic controller with fault detection in compact disk players. In *Proceedings of the 2001 IEEE International Conference on Control Applications*, september 2001.

[Vidal *et al.*, 2001c] E. Vidal, J. Stoustrup, P. Andersen, and T. S. Pedersen. Method for improved reading of a digital data disc. International patent application, july 2001. PCT/DK01/00485.

[Vidal *et al.*, 2001d] E. Vidal, J. Stoustrup, P. Andersen, T.S. Pedersen, and H.F. Mikkelsen. Open and closed loop parametric system identification in compact disk players. In *Proceedings of the 2001 American Control Conference*, june 2001.

[Vidal *et al.*, 2002] E. Vidal, J. Stoustrup, P. Andersen, T.S. Pedersen, and H.F. Mikkelsen. Deterministic method for obtaining nominal and uncertainty models of cd drives. In *Proceedings of the IEEE International Conference on Control Applications*, september 2002.

[Vidal *et al.*, 2003] E. Vidal, J. Stoustrup, P. Andersen, and T.S. Pedersen. Parametric uncertainty with perturbations restricted to be real on 12 cd mechanisms. In *Proceedings of the 2003 American Control Conference*, june 2003.

[Wahlberg and Ljung, 1992] B. Wahlberg and L. Ljung. Hard frequency-domain model error bounds from least-squares like identification techniques. *IEEE Transactions on Automatic Control*, 37:900–912, 1992.

[Watkinson, 2001] John Watkinson. *The Art of Digital Audio*. Focal Press, 2001. ISBN: 0-240-51587-0.

[Weerasooriya and Phan, 1995] S. Weerasooriya and D. T. Phan. Discrete-time lqg/ltr design and modeling of a disk drive actuator tracking servo system. *IEEE Transactions on Industrial Electronics*, 42(3):240–247, june 1995.

[Yeh and Pan, 2000] Ting-Jen Yeh and Yi-Chuan Pan. Modeling and identification of opto-mechanical coupling and backlash nonlinearity in optical disk drives. *IEEE Transactions on Consumer Electronics*, 46(1):105–115, february 2000.

[Yen *et al.*, 1992] J-Y. Yen, C-S. Lin, C-H. Li, and Y-Y. Chen. Servo controller design for an optical disk drive ussing fuzzy control algorithm. In *IEEE International Conference on Fuzzy Systems*, march 1992.

[Yokoyama *et al.*, 1994] E. Yokoyama, M. Nagasawa, and T. Katayama. A disturbance suppression control system for car-mounted and portable optical disk drives. *IEEE Transactions on Consumer Electronics*, 40(2):92–99, may 1994.

[Young and Doyle, 1990a] P. M. Young and J. C. Doyle. Computation of μ with real and complex uncertainties. In *CDC29*, december 1990.

[Young and Doyle, 1990b] Peter M. Young and John C. Doyle. Computation of μ with real and complex uncertainties. In *Proceedings of the 29th Conference on Decision and Control*, pages 1230–1235, Honolulu, Hawaii, december 1990.

[Young *et al.*, 1992] Peter M. Young, Matthew P. Newlin, and John C. Doyle. Practical computation of the mixed μ problem. In *Proceedings of the American Control Conference*, pages 2190–2194, 1992.

[Zhou *et al.*, 1996] K. Zhou, J. C. Doyle, and K. Glover. *Robust and Optimal Control*. Prentice Hall, 1996. ISBN: 0-13-456567-3.

[Zhou *et al.*, 2002] Y. Zhou, M. Steinbuch, and D. Kostic. Estimator-based sliding mode control of an optical disc drive under shock and vibration. In *CCA02*, september 2002.